



HAL
open science

Empirical modeling of beach evolution combining cross-shore and longshore processes

Teddy Chataigner

► **To cite this version:**

Teddy Chataigner. Empirical modeling of beach evolution combining cross-shore and longshore processes. Environmental Engineering. École des Ponts ParisTech, 2021. English. NNT : 2021ENPC0028 . tel-03600745

HAL Id: tel-03600745

<https://pastel.hal.science/tel-03600745v1>

Submitted on 7 Mar 2022

HAL is a multi-disciplinary open access archive for the deposit and dissemination of scientific research documents, whether they are published or not. The documents may come from teaching and research institutions in France or abroad, or from public or private research centers.

L'archive ouverte pluridisciplinaire **HAL**, est destinée au dépôt et à la diffusion de documents scientifiques de niveau recherche, publiés ou non, émanant des établissements d'enseignement et de recherche français ou étrangers, des laboratoires publics ou privés.



École des Ponts
ParisTech



THÈSE DE DOCTORAT
de l'École des Ponts ParisTech

MODELISATION EMPIRIQUE DE L'EVOLUTION DES PLAGES INTEGRANT LES PROCESSUS CROSS-SHORE ET LONGSHORE

École Doctorale Sciences, Ingénierie et Environnement (SIE)

Science et Technique de l'Environnement

Thèse préparée au sein du Laboratoire d'Hydraulique Saint-Venant (LHSV)

Thèse soutenue le 6 Décembre 2021, par
Teddy CHATAIGNER

Composition du jury :

Éric, BARTHELEMY Professeur, Université Grenoble Alpes	<i>Président</i>
Giovanni, COCO Associate Professor, Auckland University	<i>Rapporteur</i>
Bruno, CASTELLE Directeur de Recherche, CNRS	<i>Rapporteur</i>
Imen, TURKI Professeure Associée, Université de Normandie	<i>Examineur</i>
Rafael, ALMAR Chargé de Recherche HDR, IRD LEGOS	<i>Examineur</i>
Marissa, YATES MICHELIN Chargée de Recherche HDR, CEREMA	<i>Directrice de thèse</i>
Nicolas, LE DANTEC Chargée de Recherche, CEREMA	<i>Invité</i>
Nicole, GOUTAL Directrice de Recherche, EDF R&D LHSV	<i>Invité</i>



**École Doctorale Sciences, Ingénierie et
Environnement (SIE)**

Laboratoire d'Hydraulique Saint-Venant (LHSV)

Thèse

Présentée pour l'obtention du grade de Docteur

de L'Ecole des Ponts ParisTech

par

Teddy Chataigner

**Modélisation empirique de l'évolution
des plages intégrant les processus
cross-shore et longshore**

Spécialité : Sciences et techniques de l'environnement

Soutenue le 6 Décembre 2021 devant un jury composé de :

Rapporteur	Bruno Castelle	(DR CNRS, EPOC)
Rapporteur	Giovanni Coco	(Associate Professor, Université d'Auckland)
Examineur	Rafael Almar	(CR HdR, IRD, LEGOS)
Examineur	Imen Turki	(Professeur Associé, Université de Normandie)
Directrice de thèse	Marissa Yates	(CR HdR, Cerema, LHSV)
Co-encadrant de thèse	Nicolas Le Dantec	(CR, Université de Bretagne Occidentale)
Président du jury	Eric Barthelemy	(Professeur, Université de Grenoble INP/ENSE3)
Invitée	Nicole Goutal	(DR EDF R&D)



Thèse effectuée au sein du **Laboratoire d'Hydraulique Saint-Venant**

de l'Université Paris-Est

6, quai Watier

BP 49

78401 Chatou cedex

France

Résumé

Les côtes sableuses sont des environnements très dynamiques soumis aux risques d'érosion et de submersion marine, constituant une menace pour les populations et les activités économiques côtières: ainsi des méthodes et des outils sont nécessaires pour répondre aux problématiques liées à ces risques côtiers, et notamment des modèles permettant de prédire l'évolution future du trait de côte aux échelles de temps saisonnières à décennales, et aux échelles spatiales allant d'une plage à une région.

Ce travail de thèse est axé sur l'amélioration des performances d'approches empiriques basées sur une représentation simplifiée des processus physiques dominants, notamment en couplant un modèle longshore "one-line" avec un modèle cross-shore d'équilibre.

L'objectif est d'améliorer les compétences de prédiction des modèles cross-shore pour de longues échelles de temps (de décennale à centennale) et d'étendre leur application à une plus grande diversité de configurations hydrodynamiques et géomorphologiques, y compris les côtes potentiellement plus dominées par les processus longshore.

Le modèle empirique d'équilibre de changement de la position du trait de côte de Yates et al. (2009), modifié par Lemos et al. (2018) est utilisé pour modéliser les processus cross-shore, et une approche simple one-line est utilisée pour modéliser les processus longshore. Le modèle couplé est mis en œuvre, validé et analysé sur la plage de Narrabeen (Australie) où de nombreuses études et données sont disponibles.

Une analyse de sensibilité aux erreurs dans les conditions de forçage des vagues est effectuée sur le modèle longshore, et une sensibilité importante aux biais dans la direction des vagues est mise en évidence. Une méthode est proposée pour corriger un comportement du modèle one-line déjà constaté précédemment, générant un changement dans l'orientation de la côte qui n'est pas présent dans les observations, en supposant qu'il est dû à des biais dans la direction du forçage par les vagues. En utilisant une approche de Monte Carlo, un set de biais de direction de vague relativement faible est trouvé, qui corrige la réorientation de la côte dans le modèle.

Ensuite, 7 modèles combinés, utilisant différentes manières de coupler le modèle cross-shore, le modèle longshore et un terme de tendance linéaire, sont mis en œuvre et testés sur la plage de Narrabeen pour évaluer la capacité du modèle à reproduire la position du trait de côte à différentes échelles temporelles. Trois critères sont utilisés pour cette intercomparaison, basés sur l'échelle de temps à laquelle la capacité du modèle à reproduire la variabilité du trait de côte est évaluée : aux échelles temporelles courtes (\approx mensuelle), moyenne (\approx saisonnière) et longue (\approx pluri-annuelle).

Enfin, dans l'objectif d'étendre l'échelle de temps des prévisions de changement du trait de côte en utilisant des modèles empiriques tels que le modèle couplé présenté ici, 3 méthodes existantes pour prédire le changement du trait de côte à long terme (de 10 à 100 ans) ont été testées sur la plage de Vougot (France) pour examiner les différences entre les méthodes existantes, ainsi que les incertitudes de ces prévisions. Ces travaux mettent en évidence les incertitudes importantes et la

complexité de générer des conditions de forçage à long terme, qui incluent l'impact potentiel du changement climatique, lors de la réalisation de prédictions à long terme. Ils soulignent également la nécessité d'améliorer les méthodes utilisées pour prendre en compte les changements de niveaux d'eau dans le modèle d'équilibre de changement du trait de côte.

Mots-clé:

Morphodynamique de plage, Modélisation empirique, Processus longshore, Processus cross-shore

**Empirical modeling of beach evolution
combining cross-shore and longshore
processes**

Abstract

Sandy coasts are highly dynamic environments subject to erosion and marine flooding hazards, which are a threat to populations and economical activities near the coastline: methods and tools are needed to address coastal challenges, including models to predict future shoreline evolution at seasonal to decadal time scales and at beach to regional spatial scales. This PhD work is focused on improving the performance of empirical approaches based on a simplified representation of the dominant physical processes, in particular by coupling a longshore one-line model with an equilibrium cross-shore model.

The goal is to improve the cross-shore model prediction skill for long (decadal to centennial) time scales including coasts potentially more dominated by longshore processes. The empirical equilibrium shoreline change model of Yates et al. (2009), modified by Lemos et al. (2018) is used to model cross-shore processes, and a simple one-line approach is used to model longshore processes.

The coupled model is implemented, validated and analyzed at the well-studied Narrabeen Beach (Australia). A sensitivity analysis is performed on the longshore model to errors in the forcing wave conditions, and an important sensitivity to errors in the wave direction is highlighted. Then, a method is proposed to correct a previously observed behavior of the one-line model generating a change in the coastline planform orientation that is not observed in the survey data, by assuming that it is due to biases in the forcing wave direction. Using a Monte Carlo approach, a set of relatively small wave angle biases is found to correct the model reorientation.

Then, 7 combined models, with different ways of coupling the cross-shore model, the longshore model and a linear trend term, are implemented and tested at Narrabeen Beach to evaluate the model performance at reproducing the shoreline position at different temporal scales. Three criteria are used for this inter-comparison, based on the time scale at which the model skill in reproducing shoreline variability is assessed: short (\approx monthly), medium (\approx seasonal) and long (\approx pluri-annual) temporal scales.

With the overall objective to extend the timescale of shoreline change predictions using empirical models such as the coupled model presented herein, 3 existing methods to predict long-term (from 10 to 100 years) shoreline change were tested at Vougot Beach (France) to examine the differences between existing methods, as well as the uncertainties of such long-term predictions. This work pointed out the uncertainties and the complexity of generating long term forcing conditions, including potential climate change impacts, when performing long-term predictions. It also highlights the necessity to improve the methods used to take into account changes in water levels in the equilibrium shoreline change model.

Keywords:

Beach morphodynamics, Empirical modeling, Longshore processes, Cross-shore processes

Remerciements

Faire une thèse, tout particulièrement en cette période, n'est clairement pas un long fleuve tranquille. Cependant, si elle s'achève finalement sur une note très positive, c'est grâce au soutien de nombreuses personnes qui ont, de façon passive ou très active, contribué à me faire avancer contre vent et marée (parfois littéralement) pendant ces 3 ans. Ainsi, cette section du manuscrit leur est dédiée.

Avant de remercier au cas par cas l'ensemble de ces contributeurs du quotidien, je me dois de remercier mes différents financeurs, sans qui cette thèse n'aurait pas eu lieu. Je remercie donc la DGA et le Cerema ainsi que l'ENPC pour avoir financé ma thèse.

Ensuite, je tiens à remercier tout particulièrement mon encadrement, Marissa, Nicolas et Nicole au début de ma thèse, pour leur quasi dévouement à ma cause (parfois un peu perdu) pendant ces 3 ans. Merci aussi Marissa pour le temps passé en discussion technique, parfois très longue (trop, tu me dirais) mais toujours très enrichissante et agréable.

Je voulais ensuite remercier l'ensemble de mes co-bureau qui ont défilé en I142 au cours de ma thèse, que ce soit des stagiaires (et même mes stagiaires), doctorants, post-doctorants ou visiteur externe de passage (et si Marina tu lis un jour ces lignes, sache que je t'ai battu parce que j'ai perdu le compte après le 15ème !). Ces personnes étaient quotidiennement en 1ère ligne de mon humeur et de mes sautes d'humeur et je pense donc que cela mérite vraiment des remerciements pour m'avoir soutenu et supporté.

Je remercie aussi pour leur soutien l'ensemble des doctorants et post-doctorants, qui furent ou sont actuellement au laboratoire, pour les moments passés en pause café ou au déjeuner (ou au bar !) à rire, à se plaindre d'un problème numérique, ou à prendre conscience de la complexité de nos propres travaux devant la difficulté de nos collègues à nous comprendre! Tout cela fait un bien fou, et est, je pense, nécessaire au bon déroulement d'une thèse. C'est donc malheureux que le covid nous en est privé pour une partie de ces 2 dernières années... Courage à ceux qui restent !

Je remercie les membres permanents du LHSV et du LNHE pour leur accueil, les discussions que l'on a pu avoir, et les conseils souvent très avisés obtenus au détour d'un café.

Enfin, je remercie mes amis et ma famille pour leur soutien et leur intérêt envers ma thèse (même si clairement, il ne faut pas leur demander trop en détail le sujet). Pour terminer, je voudrais remercier tout particulièrement ma chérie, qui m'a supportée quelque soit les difficultés ou la complexité de la situation (et il y en a eu ! Confinement et télétravail oblige) et grâce à qui j'ai pu achever cette thèse !

Je voulais aussi remercier, au passage, un certain arbre, pour m'avoir fait devenir célèbre sur l'ensemble du site (presque autant que le renard).

Contents

General introduction	1
I State of the art	7
I.1 Coastal morphodynamics	8
I.1.1 Beach morphodynamic systems	9
I.1.2 Beach morphodynamic classification	11
I.1.3 Coastal hydrodynamics	13
I.2 Beach morphological modeling	17
I.2.1 Overview of existing approaches	17
I.2.2 Empirical equilibrium cross-shore models	19
I.2.3 Longshore modeling	22
I.2.4 Combined cross-shore and longshore models	25
I.3 Conclusion	29
II Study site	30
II.1 Vougot Beach	31
II.1.1 Beach geomorphology	31
II.1.2 Hydrodynamic conditions	33
II.1.3 Data and beach morphodynamical behavior	33
II.2 Narrabeen-Collaroy Beach	36
II.2.1 Beach geomorphology	36
II.2.2 Hydrodynamic conditions	37
II.2.3 Data and beach morphodynamical behavior	38
III Cross-shore modeling	41

III.1	Empirical cross-shore equilibrium model	42
III.1.1	Model formulation and hypothesis	42
III.1.2	Model limitations	45
III.2	Empirical cross-shore model optimisation	46
III.3	Model application at Vougot Beach	50
III.3.1	Data processing and model configuration	50
III.3.2	Results of the model application	54
III.3.3	Discussion	60
IV	Longshore modeling	64
IV.1	Longshore one-line model	65
IV.1.1	Model formulation and numerical implementation	66
IV.1.2	Model validation with synthetic test cases	69
IV.1.3	K parameter value	72
IV.2	Longshore model application to Narrabeen	74
V	Combined modeling	89
V.1	Introduction to combined modeling	90
V.2	Model combinations	91
V.2.1	Cross-shore model with a linear term	94
V.2.2	Hybrid models	97
V.2.3	Coupled models	98
V.3	Model performance at Narrabeen Beach	103
V.3.1	Model configuration at Narrabeen Beach	104
V.3.2	Model performance	105
V.3.3	Model optimization	107
V.3.4	Comparison of model performance	109
V.3.5	Analysis and discussion of model performance	116
V.3.6	Conclusion	121
VI	Long term modeling	123
VI.1	Introduction	124
VI.2	Generation of future wave time series	126

VI.3 Existing methods for long term shoreline change predictions	128
VI.3.1 Bruun rule	128
VI.3.2 Linear extrapolation	131
VI.3.3 Empirical cross-shore model	132
Bibliography	141

List of Figures

1	Global distribution of sandy shorelines, from Luijendijk et al. (2018), with percent of sandy shoreline expressed in color and percentage of sandy beach represented for each continent and as a function of latitude and longitude.	2
2	Coastal erosion rates (m/yr) in France (in 1994) from Chamley (2002), indicating that a large part of the soft coastline (sandy and muddy) presents an important erosion trend.	4
I	State of the art	7
I.1	Temporal and spatial scales of coastal morphological processes.	8
I.2	Temporal and spatial scales of coastal hydrodynamical processes.	9
I.3	Conceptual schematic of a morphological system including the impacts of the hydrodynamics on the morphological changes and the associated feedback on the hydrodynamic conditions.	10
I.4	Beach profile zonation, identifying the important geomorphological features, from the US Shore Protection Manual (USACE 1984).	10
I.5	Dune zonation from Valentini et al. (2020).	11
I.6	Sandy beach morphodynamic classification by Masselink & Short (1993)	12
I.7	Synthesis of nearshore hydrodynamics, from Stépanian (2002)	13
I.8	Zone division in the nearshore region based on hydrodynamic processes (Horikawa 1988).	14
I.9	Equilibrium beach profile theory (Dean 1977), conceptual scheme from Yates (2009).	19
I.10	Conceptual scheme of the CEM cellular longshore model (Ashton & Murray 2006)	23
I.11	Conceptual schematic of shoreline rotation on pocket beach, from (Turki et al. 2013).	25
I.12	Cosmos-Coast framework and model equation from (Vitousek et al. 2017)	26
I.13	LX-Shore model showing the (a) global framework and (b) cellular conceptual scheme, from (Robinet et al. 2020).	28

II	Study site	30
II.1	Vougot location: (a) map of France and the Finistère indicating the study site location shown in (b) (graphic adapted from Suanez et al. (2015)), (b) Vougot Beach, showing the location of the 6 cross-shore profile transects (PF1, PF2, PF3, PF4, PF5, and PF6).	32
II.2	Vougot Beach aerial view: Vougot Beach aerial photography seen from the eastern extremity, with the addition of the location of the 6 cross-shore profiles (named PF1, PF2, PF3, PF4, PF5, and PF6). <i>credit: Serge Suanez and géosAEL</i>	34
II.3	Vougot Beach hydrodynamics and morphodynamics: (a) H_s from 7km north-westward offshore HOMERE node (Boudière et al. 2013), (b),(e) Contour elevation position time series from the dune to the intertidal zone of profile 1 and profile 5, respectively (with certain contour elevation time series highlight in black and associate elevation value indicate on the right side), (c)(d) Envelope of Profile 5 and 1, respectively, with the mean profile position for the observed time (solid black line).	35
II.4	Narrabeen-Collaroy beach: (a) map of Australia indicating the zoom shown in (b), (b) satellite image around Narrabeen Beach, showing the location of Sydney and the offshore wave buoy, and (c) aerial photograph of Narrabeen Beach showing the location of the 5 surveyed cross-shore profiles (named PF1, PF2, PF4, PF6, and PF8) and the 5 locations of wave condition estimates (WP1, WP2, WP4, WP6, and WP8). The bathymetry contours are shown every 5 meters (in grey).	36
II.5	Wave roses in 10 m water depth offshore of each profile and in 80 m water depth 11km offshore at the Sydney wave buoy. The black line indicates the respective profile transect orientation (from Turner et al. (2016)).	38
II.6	Conceptual model of the 3 different planform rotation modes observed in (Harley et al. 2015). The red/green arrows represent the direction and magnitude of the offshore wave climate associated with the respective red/green embayed beach planform, while the grey arrows represent the magnitude and direction of sediment transport (scheme from Harley et al. (2015))	40
III	Cross-shore modeling	41
III.1	Global framework of the empirical cross-shore shoreline change model	43
III.2	Scheme of the adaptation of Lemos et al. (2018) of the equilibrium model to account for water level η depending on a threshold based on the wave height H_s	44
III.3	Impact of $Ntmax$ on the cost function value for 10 repetitions of the optimisation algorithm at profile 6 with the same parameters for (a) a well reproduced contour position time series ($R^2 > 0.5$, see eq. III.5) and (b) a badly reproduced contour position time series ($R^2 < 0.3$), showing the mean value, minimum value, and standard deviation of the cost function for both cases.	47

III.4	Effect of changing $CoeffT$ on the cost function value for 10 realizations of the model optimisation at profile 6 for a well-reproduced contour position time series ($R^2 > 0.5$) showing the mean value, the standard deviation and the minimum value of the cost function and on a badly reproduced contour position time series ($R^2 < 0.3$)	48
III.5	Homere database domain extent (a) database output node locations, (b) bathymetry used in the wave model.	51
III.6	Position of the different Homere database nodes used to select the wave forcing time series	52
III.7	Roses of Homere wave direction, with color based on the wave height occurrence, at 4 different nodes located on Fig. III.7.	53
III.8	Modeled contour position S_{mod} (blue), versus observations S_{obs} (black) for profile 1 at three elevations: (a) Upper Beach ($Z=5$ m NGF), (b) \approx Mean High Water Neap ($Z=2.0$ m NGF), and (c) Mean Sea Level ($Z=0.5$ m NGF).	55
III.9	Model contour position S_{mod} (blue), versus observation S_{obs} (black) for profile 3 at three elevations: (a) Upper Beach altitude (5 m NGF), (b) \approx Mean High Water Neap altitude (2.0 m NGF), and (c) Mean Sea Level (0.5 m NGF).	55
III.10	Model contour position S_{mod} (blue), versus observation S_{obs} (black) for profile 5 at three elevations: (a) Upper Beach altitude ($Z=5$ m NGF), (b) \approx Mean High Water Neap altitude ($z=2.0$ m NGF), and (c) Mean Sea Level ($z=0.5$ m NGF).	56
III.11	Optimized model coefficients as a function of altitude for profile 1 (brown), 2 (purple), and 3 (light blue) for (a) coefficient a , (b) coefficient b , (c) coefficient C^+ , (d) coefficient C^-	57
III.12	Model optimum coefficients at every applied altitude for profile 4 (green), 5 (red) and 6 (blue), (a) coefficient a , (b) coefficient b , (c) coefficient C^+ , (d) coefficient C^-	58
III.13	Model statistics for profiles 1, 2, and 3, as a function of altitude at Vougot Beach: (a) R^2 , (b) Brier Skill Score (BSS), and (c) $RMSE$	59
III.14	Model statistics for profile 4, 5 and 6 at different altitude of Vougot Beach: (a) R^2 , (b) Brier Skill Score (BSS), and (c) $RMSE$	59
III.15	Model statistics for profile 6 at Vougot Beach as a function of the elevation along the intertidal profile when using wave energy or wave power as the forcing wave condition: (a) R^2 , (b) Brier Skill Score (BSS), and (c) $RMSE$	61
III.16	Optimum model coefficients as a function of altitude along profile 6 using wave energy (a-d) or wave power (e-h) to force the model for: a (a,e), b (b,f), C^+ (c,g), and C^- (d,h).	62

IV.1	One-line longshore model conceptual functioning	66
IV.2	Schematic representation of the model setup for three cross-shore transects (index n), showing the shoreline position S , the relative wave angle α (eq. IV.4), the along-shore sediment flux Q , and the local reference frame (X, Y)	68
IV.3	No evolution test case: (a) Shoreline position evolution, (b) longshore sediment flux Q in time and space showing a null value.	70
IV.4	No flux test case: (a) Shoreline position evolution, (b) longshore sediment flux Q in time and space showing a constant and uniform flux value.	70
IV.5	Accretion test case: (a) Shoreline position evolution from initial position (light blue) to final position (blue line), (b) longshore sediment flux Q evolution.	71
IV.6	Diffusion test case, as in Vitousek & Barnard (2015), where the initial sinusoidal shoreline (light blue) is progressively diffused by the longshore model to tend toward a straight coastline (blue) perpendicular to the wave forcing conditions. The model coastline evolution (in colors) is compared to the analytical solution of the diffusion equation (eq. IV.10) (in black). Here the model and the analytical solution are well superimposed at each represented intermediate state.	72
V	Combined modeling	89
V.1	Comparison of the linear term integration effects on model behavior for 2 different amplitudes of (a) positive linear trend, (b) negative linear trend. With S_{CSL} : model version with sum of the 2 independent components, and S_{CSLEEF} : model with the integration of the linear term in the equilibrium equation.	96
V.2	Scheme of the weakly coupled model (W) functioning with illustration of the difference with the fully coupled approach (F). The text color refers to the cross-shore component in red, the longshore component in green, and the coupled model aspects in blue.	100
V.3	Synthetic test case to illustrate the effects of the weak coupling between the longshore and cross-shore models: (a) model x, y position at $t=0$, $t=15h$ and $t=1000$ for W model and H model. (b-c) Model shoreline position for the W model S_W (red) and H model S_H (blue) at 2 locations, and (d) longshore model shoreline position S_{LS} in the W model in time at each transect position.	101
V.4	Synthetic test case to illustrate the difference between the weakly coupled W and the fully coupled F models: (a) model x, y position at $t=0$, $t=15h$ and $t=1000$. (b-c) Model shoreline positions S_W (red) and S_F (light blue) at 2 locations, (d) longshore model shoreline position S_{LS} in the F model, and (e) cross-shore model shoreline position S_{CS} in the F model as a function of time at each transect position.	103

V.5	Narrabeen model configuration showing the 15 cross-shore transects (green lines) used to discretize the model, with the initial shoreline position indicated for each transect (black squares) and cross-shore profile (red circles).	104
V.6	Short term criterion conceptual scheme representing the observations and the model variations and their respective sign (+ or -) between 2 consecutive observations, with both signs in green indicating agreement between the model and observations, and in red indicating disagreement.	105
V.7	Medium term criterion conceptual scheme representing the <i>BSS</i> calculation with the observations, the model, and the linear regression of the model (the baseline). The blue area corresponds to the model improvement compared to the baseline, assumed here mainly to account for the reproduced seasonal and intra-annual scales.	106
V.8	Long term criterion conceptual scheme representing the observations, the model shoreline position, and their respective linear regressions in black and red, highlighting the difference in slope between the 2 regressions used as criteria.	106
V.9	Optimized values of (a) <i>trd</i> (linear trend term) and (b) <i>K</i> (longshore model coefficient, constant for all profiles) at Narrabeen Beach for each model formulation.	108
V.10	Observed (black dashed line) and modeled (colored lines, see legend to identify each model) shoreline position time series for PF1 at Narrabeen Beach.	109
V.11	Shoreline position time series for PF2 at Narrabeen Beach (same legend as Fig. V.10).	110
V.12	Shoreline position time series for PF4 at Narrabeen Beach (same legend as Fig. V.10)	111
V.13	Shoreline position time series for PF6 at Narrabeen Beach (same legend as Fig. V.10)	112
V.14	Shoreline position time series for PF8 at Narrabeen Beach (same legend as Fig. V.10)	113
V.15	Criteria value for every model at short term, medium term and long term for the 5 profile and mean value over all profile, and RMSE	114
V.16	Normalized Criteria for every model for short term, medium term, long term and RMSE based on mean value other all profile criteria and normalized using the lower and higher mean criteria value	115
V.17	Fully coupled model, <i>FL</i> shoreline position time series at PF2 and PF8 with the cross-shore S_{CS} , longshore S_{LS} and linear trend term component contribution.	120
VI	Long term modeling	123
VI.1	Calculation of the wave height distribution following the Banno & Kuriyama (2014) approach to account for RCP scenarios impacts.	127
VI.2	Bruun rule conceptual scheme, from Ranasinghe et al. (2012).	129

VI.3	Bruun rule application: (a) sea level elevation used in the Bruun rule application at Vougot Beach, and (b) shoreline retreat estimated with the Bruun rule using 2 sea level rise estimates.	130
VI.4	Sobol indices for Bruun rule at profile 6 (Cailler 2019) representing the contribution of each parameter to the variance of R with or without accounting for the interaction and compensation effect between the parameter (figure from Cailler (2019)).	130
VI.5	Linear extrapolation method applied to profile 6 at Vougot Beach: (a) Example calculated linear regression (in red) of the shoreline position observations (blue points) at MHWN elevation. (b) Linear extrapolation of the shoreline position at MSL, MHWN and MHWS elevations from the present to the year 2100 (figure from Cailler (2019)).	132
VI.6	Empirical cross-shore model application at Profile 6 of Vougot Beach at MSL ($z=0.5\text{m}$) from 2011 to 2100, using the projected wave time series from different RCP scenarios generated following the approach of Banno & Kuriyama (2014). The shaded red zone indicates the model calibration period.	133
VI.7	Empirical cross-shore model application at profile 6 of Vougot Beach at MSL ($z=0.5\text{m}$), using the projected wave time series from different RCP scenarios generate following the approach of Banno & Kuriyama (2014) (same color legend as Fig. VI.6): zooms of (a) the first 10 years (showing the calibration period in the shaded red zone) and (b) the last 10 years of the simulation period.	133

General introduction

Les territoires littoraux sont très attractifs et fortement anthropisés, mais ils sont soumis aux aléas d'érosion et de submersion marine. Pour répondre à la problématique de la gestion de ces risques côtiers, des outils sont nécessaires notamment pour prédire l'évolution future des littoraux. Dans le monde, les côtes sableuses représentent un tiers des zones côtières. Ce sont des environnements extrêmement dynamiques et complexes. Outre les aménités qu'ils offrent aux touristes comme aux résidents, les côtes sableuses fournissent aussi une protection naturelle contre les événements de submersion. Cependant, la modélisation numérique de l'évolution des côtes sableuses est particulièrement difficile du fait des changements morphologiques se produisant à des échelles spatio-temporelles très différentes allant de la seconde à plusieurs années et agissant de l'échelle du grain de sable à l'ensemble d'une cellule hydro-sédimentaire. Il est particulièrement complexe de représenter l'ensemble de ces échelles avec des modèles physiques du fait du coût de calcul et de l'accumulation des incertitudes sur le long terme. Aussi des modèles simplifiés basés sur la reproduction d'un ensemble de processus hydro-sédimentaire, par exemple, le transport sédimentaire cross-shore, ont été développés et sont une alternative efficace du fait de leur faible coût de calcul et de leur capacité à reproduire l'évolution côtière après calibration. L'objectif de cette thèse est d'améliorer la capacité de ces modèles en intégrant la prise en compte des processus hydro-sédimentaire longshore dans un modèle basé sur les processus et reproduisant l'évolution cross-shore du trait de côte. L'objectif est d'avoir un outil applicable sur le plus long terme (e.g. 10-100 ans) où les processus longshore peuvent devenir dominants, ainsi que sur un plus grand nombre de sites où les variations du trait de côte sont expliquées par les processus longshore.

General Introduction

Context

The exact definition of the coastal zone varies depending of the domain of application, already exhibiting the complexity of this environment. Nevertheless, its definition can be summarized as the strip of land that separates the ocean from the continent.

However, depending of the considered spatial scale, this strip can either account for a large area a few kilometers long in both the seaward and landward directions, or only designate the intertidal zone.

Coastal areas are among the most dynamic and developed zones in the world with an important and growing population density, strategic and essential infrastructure but also an important ecosystem diversity. The trend of intense coastal migration, population and occupation is predicted to increase in the coming years (Neumann et al. 2015).

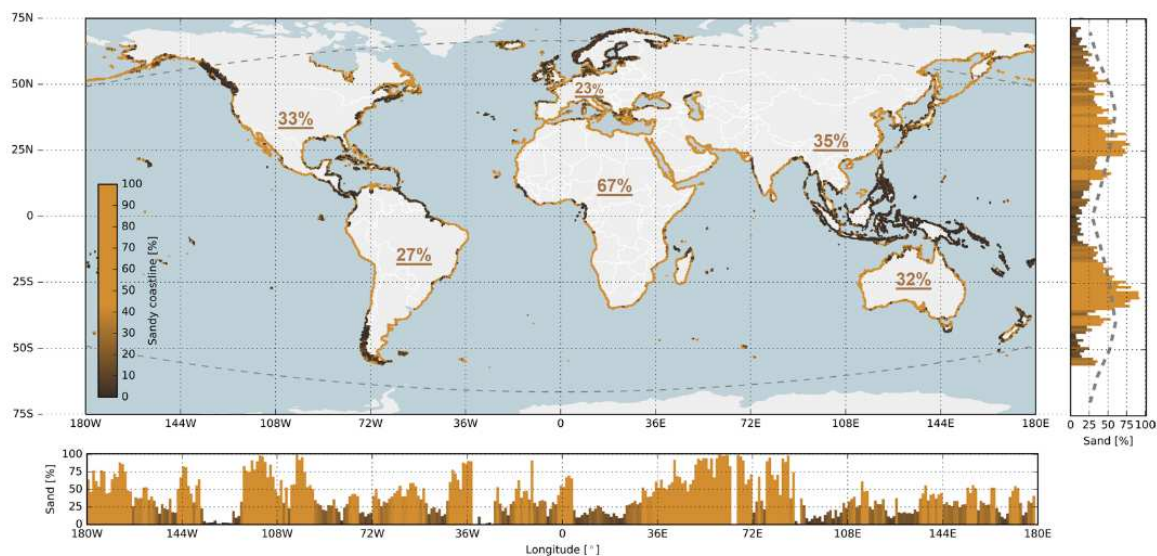


Figure 1: Global distribution of sandy shorelines, from Lujendijk et al. (2018), with percent of sandy shoreline expressed in color and percentage of sandy beach represented for each continent and as a function of latitude and longitude.

Approximately one-third of the world's coastlines consist of sandy beaches (Lujendijk et al. 2018) (Fig. 1) and the rest is rocky or muddy coasts. This environment has an important socio-economic value due to its exploitation for tourism and recreational activities, but also in the ecosystem services it offers. Beaches are a natural protection for coastal areas that can prevent marine flooding during storms in these zones (Kamphuis 2000). Nonetheless, this environment is highly dynamic and complex with morphological processes generated by hydrodynamical processes occurring on a large range of time scales, from the turbulence induced by a single wave breaking to decadal-scale

changes in mean sea level that can induce coastal erosion or marine flooding risks. Therefore, the morphological and hydrodynamical functioning of sandy beaches is still a largely open domain of research due to the difficulty to observe, understand and model all the physical processes at all the spatial and temporal scale.

The improvement of the knowledge of the spatio-temporal evolution of this system is ensured by the increase of morphological evolution and hydrodynamical forcing measurements due to the multiplication of the measurement sources (video-camera, satellites data) and monitoring programs (e.g. [Turner et al. 2016](#)), which, when analyzed, enable understanding the dominant physical processes.

In France, coastal areas are also highly attractive, with 1 inhabitant out of 10 living in the coastal zone that corresponds to 4% of the territory. Approximately 25% of the coastline is estimated to be retreating ([Chamley 2002](#)) (Fig. 2), including mostly sandy or gravel beaches that represent one third of the french coastline, and the projection including the sea level rise from the global warming indicates that this value will likely increase, thus potentially increasing the threat to coastal cities and infrastructure.

Recent storm impacts have emphasized the sensitivity of the coastal area to the risks of erosion and marine flooding, for example the energetic winter of 2013-2014 ([Masselink et al. 2016](#)). Furthermore, with the recent evaluation of global warming and its effects on mean sea level and the wave climate, including storm frequency and intensity, the necessity to understand their effects on future shoreline evolution is progressively growing. Thus, tools to predict shoreline evolution in response to hydrodynamic forcing and to evaluate these risks at pluri-annual to decadal time scales are becoming a priority for most countries ([IPCC 2014](#)).

Challenge

Beach shoreline evolution is highly dependent on the past wave conditions and the sequences of storms and less energetic conditions. Thus, existing seasonal variation of wave conditions results in an important seasonal variability of the beach shoreline position.

Numerical physics-based models represent the most physical process possible solving the whole hydrodynamics of the beach and its effect on the beach morphology (e.g., Delft3D ([Roelvink & Banning 1995](#)), and XBeach ([Roelvink et al. 2009](#))). However, this type of model encounters large difficulties in reproducing the morphological response of beaches at longer time scales than storm events due to high computational costs and the growth in time of numerical errors ([French et al. 2016](#), [Murray 2007](#), [Ranasinghe R. 2013](#)).

Another family of models, empirical equilibrium cross-shore models, are an alternative to physics-based models. They are well-adapted to predict beach profile evolution for medium to long temporal scales, corresponding to seasonal to pluri-annual period, and on spatial scales of a beach to a whole region ([Davidson et al. 2013](#), [Miller & Dean 2004](#), [Yates et al. 2009](#)). This large spatio-temporal scale of applications is explained by their relative simplicity that generate a really cheap computational

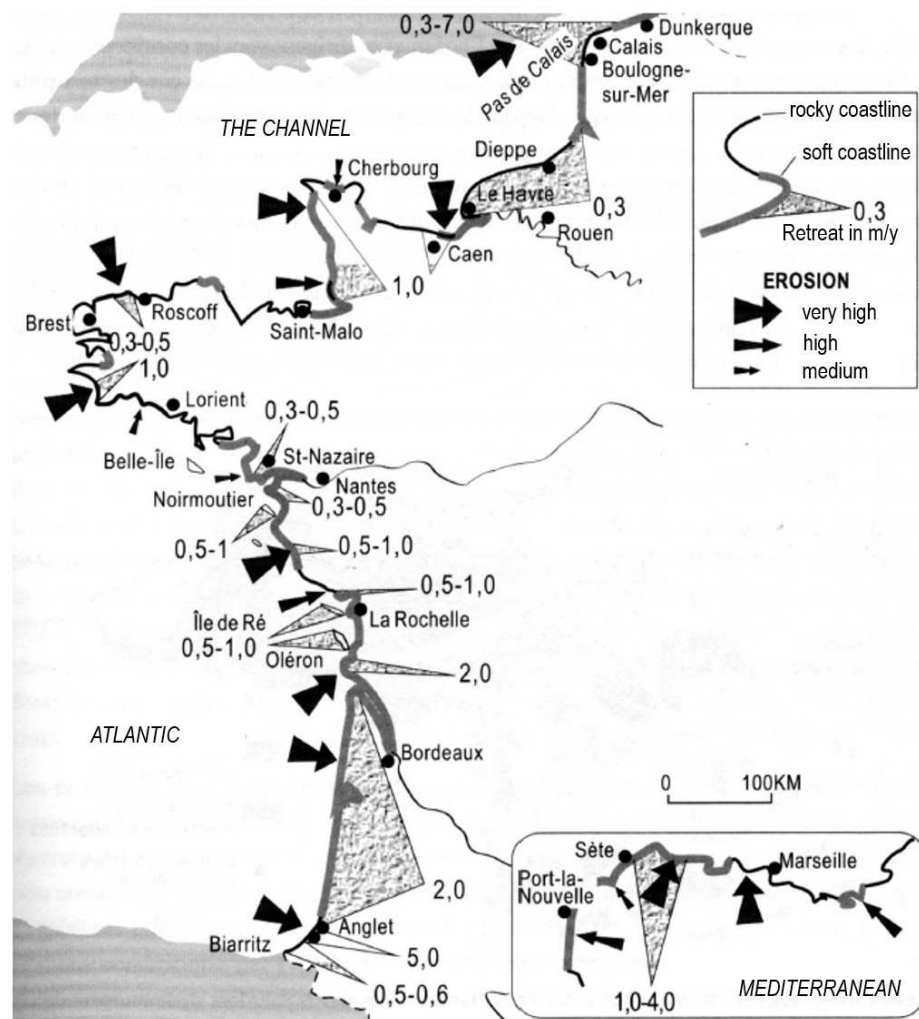


Figure 2: Coastal erosion rates (m/yr) in France (in 1994) from Chamley (2002), indicating that a large part of the soft coastline (sandy and muddy) presents an important erosion trend.

cost. These empirical approaches use coefficients that need to be calibrated with observations. However, they then show good performance when applied at these spatio-temporal scales (Castelle et al. 2014, Splinter et al. 2014).

As their name suggests, empirical equilibrium cross-shore models only account for cross-shore processes. However, for long term applications (from pluri-annual to decadal and longer time scales), or at sites with high wave incidence angle conditions, the relative importance of longshore processes in the total shoreline variability can increase and even become dominant (Ashton & Murray 2006). Thus, representing both cross-shore and longshore processes is essential for tools designed to predict accurately long-term shoreline evolution.

The overall goal of this thesis work is to improve shoreline change modeling tools by extending an existing equilibrium shoreline change model with the integration of longshore processes, the

evaluation of the improvement in the model performance, and the quantification of the new model uncertainties.

This thesis work should provide answers to the following questions emerging when concerned with how to improve equilibrium shoreline change models:

An initial interrogation is on evaluating empirical equilibrium cross-shore model skill and limitations. For example, what are the performance and limitations in complex macrotidal environments influenced by longshore processes? Also, what are the difficulties and the limitations when applying these approaches at long time scales to account for climate change impacts?

Then, concerning longshore processes: using a one-line model to account for these processes to remain efficient at operational time scales, jointly with empirical equilibrium cross-shore models, what are the expected uncertainties of the longshore approach? How can cross-shore and longshore modeling approaches be combined? How do the coupled models perform at different temporal scales of application?

Thesis organization

The first chapter presents, in an initial part, a state of the art of beach morphodynamics, including the different beach morphologies observed and the hydrodynamical processes that are shaping them. The second part presents the existing models developed to reproduce coastal morphodynamics, and a focus is made on empirical process-based approaches, with a synthesis of cross-shore, longshore, and combined approaches.

The second chapter characterizes the 2 study sites involved in this thesis work: Vougot Beach (in Brittany, France) and the Narrabeen-Collaroy embayment (in New-South-Wales, Australia), with a presentation of the morphological and hydrodynamical setting of the 2 beaches and a synthesis of the current knowledge of the beach morphological behavior from the literature.

The third chapter describes the chosen cross-shore empirical shoreline change model, including its hypotheses, advantages, and limitations. The analysis of the observations, the model calibration approach, and the model results are presented. Then, the model is applied at Vougot Beach to explore and analyze the model performance in a macrotidal environment with a complex nearshore bathymetry. Finally, the results are discussed to identify the limitations of the cross-shore model at this beach and the potential model improvement.

The fourth chapter presents the longshore model implemented during this thesis work to account for longshore processes not represent in the cross-shore model. The model formulation, hypotheses, and numerical implementation are defined and the model is applied to synthetic and analytical validation cases. Then, the model is applied at Narrabeen Beach to validate its performance, and the longshore model predicts a long-term trend in the evolution of coastline that is not present in the observations. A method is proposed to evaluate the model sensitivity to biases in the wave angle, and this work is the subject of a paper accepted in Coastal Engineering.

The fifth chapter details the combination of the cross-shore and longshore approaches presented in the previous chapters, with the formulations and hypotheses of the different approaches to combined or coupled the models. Then the combined models are applied at Narrabeen Beach, and their performance are analyzed using 3 criteria to evaluate the model performance at different times scales. Finally, each combined model performance is discussed considering their formulations and hypotheses.

The sixth chapter is devoted to challenges rising when predicting long-term shoreline changes using both existing simple approaches and morphodynamic predictions using process-based models, using an existing method that take into account the effects of climate change to predict future wave characteristics.

Chapter I

State of the art

Ce chapitre introduit la morphodynamique côtière, en particulier, la morphodynamique des plages sableuses. Ainsi, la description géomorphologique du système, les différentes morphologies, et les classifications existantes sont décrites ainsi que les principaux agents hydrodynamiques morphogènes: les vagues gravitaires, la marée et les courants qui en résultent. Puis un état de l'art des modèles permettant de reproduire la morphodynamique de ces environnements est dressé. L'accent est mis sur les modèles reproduisant de manière simplifiée les processus dominants avec des approches empiriques. Parmi les approches existantes, les modèles d'équilibre reproduisent l'évolution cross-shore du profil de plage et permettent des applications opérationnelles sur des échelles de temps allant de quelques mois à plusieurs dizaines années, et des échelles spatiales allant d'une plage à une façade littorale du fait de leur simplicité. L'approche "one-line" permet de reproduire les évolutions morphologiques associées aux processus longshore de manière simplifiée en tenant compte des gradients dans le flux sédimentaire le long de la côte. Récemment, des approches combinant ces modèles basés sur la reproduction des processus dominants ont été développées pour améliorer la capacité de ces approches dans des environnements mixtes, en intégrant à la fois les composantes cross-shore et longshore.

Chapter I

State of the art

I.1 Coastal morphodynamics

Coasts are among the most dynamic natural systems since they form the interface between oceanic and continental environments, and are thus exposed to numerous forcing processes like hydrodynamics, eustatics, or tectonics that act and shape the coast at different spatial and temporal scales. For example, the short term variation of the coast (at a period lower than a few years) is a function of the local meteorology, like the wind and storm occurrence, and the hydrodynamic conditions, with the tide and waves characteristics. However, at longer time scales, for example at geological time scales, shoreline changes are controlled by eustatic (Chapell 1974, Peltier 1998) and tectonic processes (IPCC 2014, Warrick & Mertes 2009).

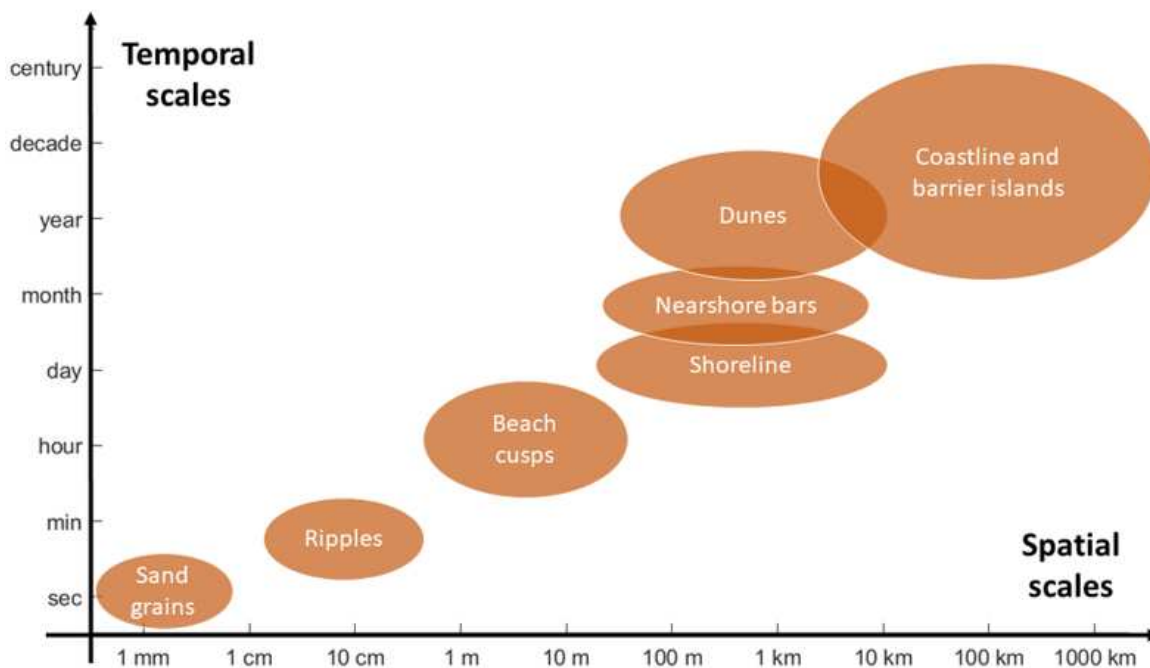


Figure I.1: Temporal and spatial scales of coastal morphological processes.

Thus, understanding coastal morphodynamics requires accounting for the complex links and interactions between every morphological and hydrodynamical processes at all the considered times scales.

This also highlights the importance of the spatio-temporal framework definition that determines the processes that should be taken into account (Fig. I.1 and Fig. I.2).

The feedback between the hydrodynamic and morphodynamic processes associated with sediment transport can be either positive (self organization) or negative (self regulation) (Cowell et al. 1995). A positive feedback corresponds to an increase in the disequilibrium, while a negative feedback corresponds to processes that compensate for each other, bringing the system back to an equilibrium state.

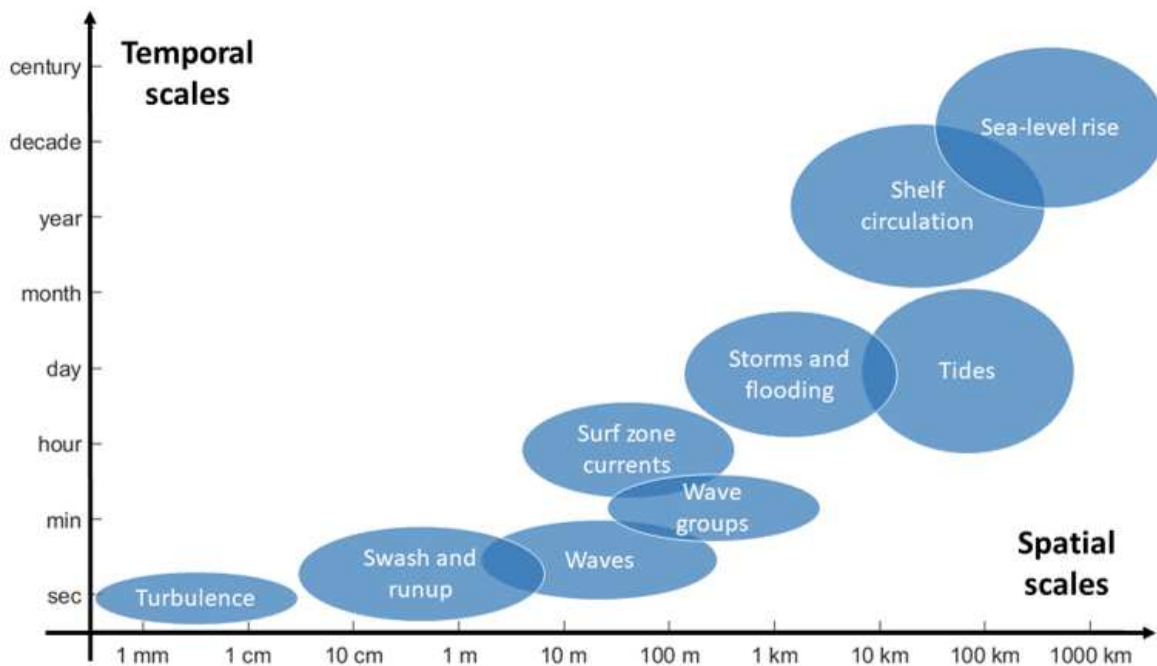


Figure I.2: Temporal and spatial scales of coastal hydrodynamical processes.

I.1.1 Beach morphodynamic systems

Beaches are detritic accumulations located in the coastal area that are composed of variable sediments from fine sand to large pebbles (Guilcher 1954), depending on the local environment, that were either transported from the shelf during the last marine invasion, inherit from the continental rivers discharged, or the erosion product of calcium carbonate compound such as coral or shellfish.

Beach morphodynamics consists of studying the effects and feedbacks of the forcing hydrodynamic on the beach morphology (Fig. I.3). In case of a theoretically constant hydrodynamical forcing, the coastal system can reach a state of “morphological equilibrium,” which is defined as a state where the coast remains unchanged in time (Kraus 2001).

However, the natural instability and variability of the hydrodynamic forcing conditions leads to a succession of morphological changes from one unstable morphological equilibrium to another. Thus the concept of “morphological equilibrium” can only be examined for long time series of observations that enable defining a more stable shape within this permanent oscillation.

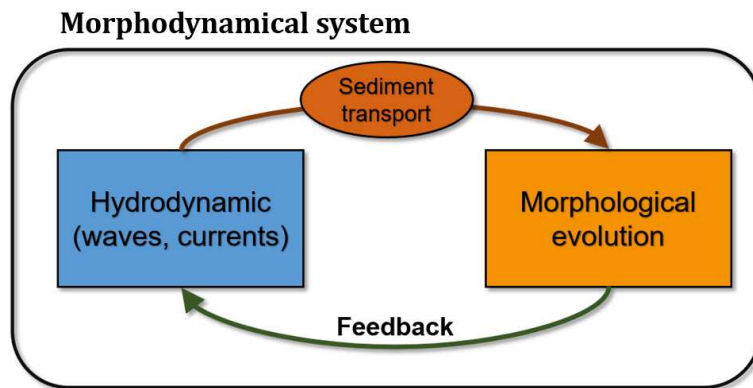


Figure I.3: Conceptual schematic of a morphological system including the impacts of the hydrodynamics on the morphological changes and the associated feedback on the hydrodynamic conditions.

The cross-shore profile of a beach is shaped by the sedimentary flux induced by the local hydrodynamics. Beach profiles may have a concave shape from the dune to the ocean but often also include some additional morphological features, like sand bars or a berm, as represented in Fig. I.4.

Beaches can have different slopes, which are primarily determined by the beach sediment grain size (Bascom 1951) and the wave conditions. The beach slope has an important effect on the beach morphodynamics since it controls the waves dynamics, in particular the non-linear interactions between wave propagation, dissipation, and reflection (Battjes 1974, Elgar & Guza 1985, Hasselmann 1962).

A beach profile can be divided in different areas based on the water level (Fig. I.4).

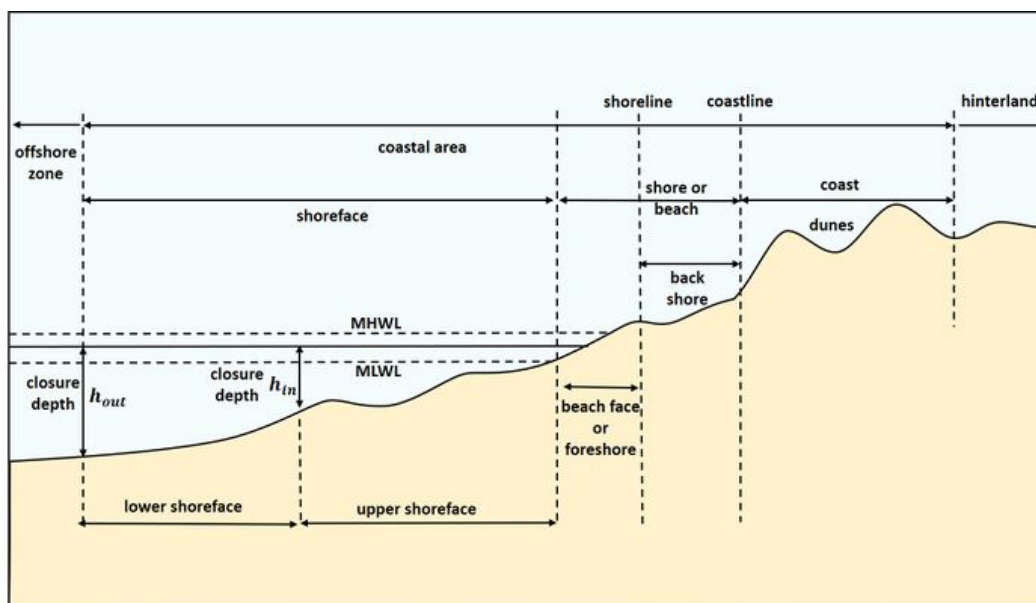


Figure I.4: Beach profile zonation, identifying the important geomorphological features, from the US Shore Protection Manual (USACE 1984).

Three zones are defined: the subtidal (offshore + shoreface zone), intertidal (foreshore zone), and supratidal (backshore + dune) zones that correspond respectively to the area located beneath the lowest tide level, between the lowest and highest tide level, and above the highest tide level (Fig. I.4).

The subtidal zone is the part of the beach submerged by water and thus is exposed continuously to tidal and wave action. The intertidal zone has a length depending on the tide amplitude and the beach slope, and is the most dynamic zone of the beach. The supratidal zone corresponds to the upper part of the beach, including the foredune and dune (Fig. I.5).

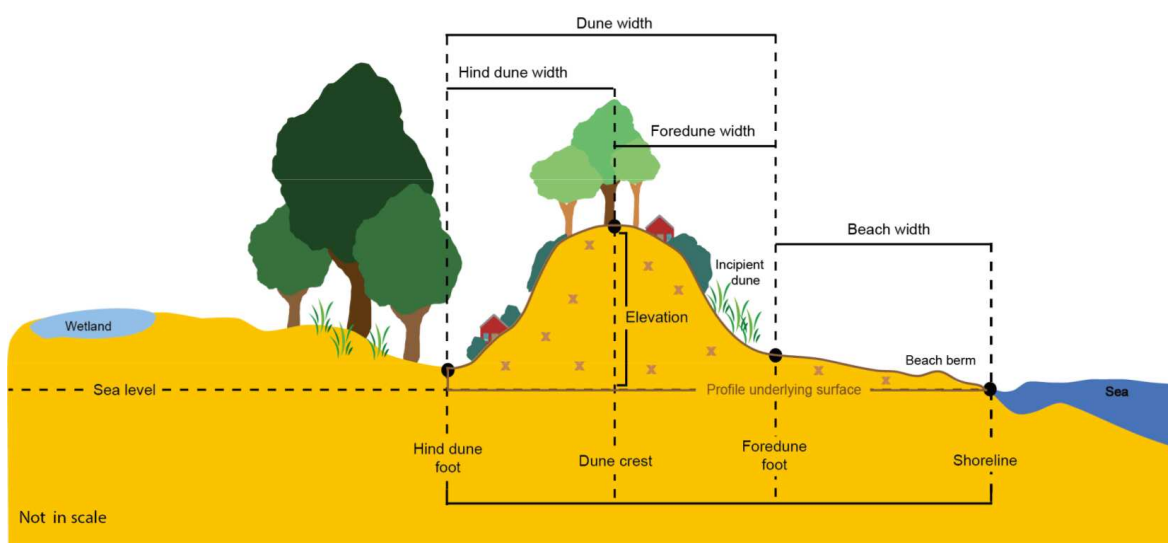


Figure I.5: Dune zonation from [Valentini et al. \(2020\)](#).

The morphological dynamics in this zone are controlled by the wind and are strongly impacted by vegetation: the sand is transported inland from the dry beach by the wind, but it can be trapped by the vegetation on the foredune and dune (Fig. I.4 and Fig. I.5), thus the vegetation stabilizes and encourages dune growth ([Hesp 1989](#), [Keijsers et al. 2015](#)).

I.1.2 Beach morphodynamic classification

Beach morphological observations and the comparison of their characteristics have highlighted some patterns that enable the creation of beach classifications.

Classifications are an effective tool to characterize and compare different beaches and to obtain some rapid understanding of their potential evolution. Environmental parameters used are combining hydrodynamic variables with morphological characteristics like the beach slope, wave height, or tide amplitude, which can be easily obtained or estimated for a site.

A classification was proposed by [Wright & Short \(1984\)](#) for different beach profile morphologies in

microtidal environments. They used the Dean number Ω

$$\Omega = \frac{H_b}{Tw_s} \tag{I.1}$$

to classify Australian beaches, with H_b the wave height at the breaking point, T the wave period, and w_s the sediment fall velocity.

The value of Ω indicates if the beach profile shape is either reflective, with a steep slope, small H_b and large sediment grain size, for $\Omega < 1$, or dissipative, with a smaller beach slope, fine sediment grain size, more important H_b , and a large surf zone, for $\Omega > 5$.

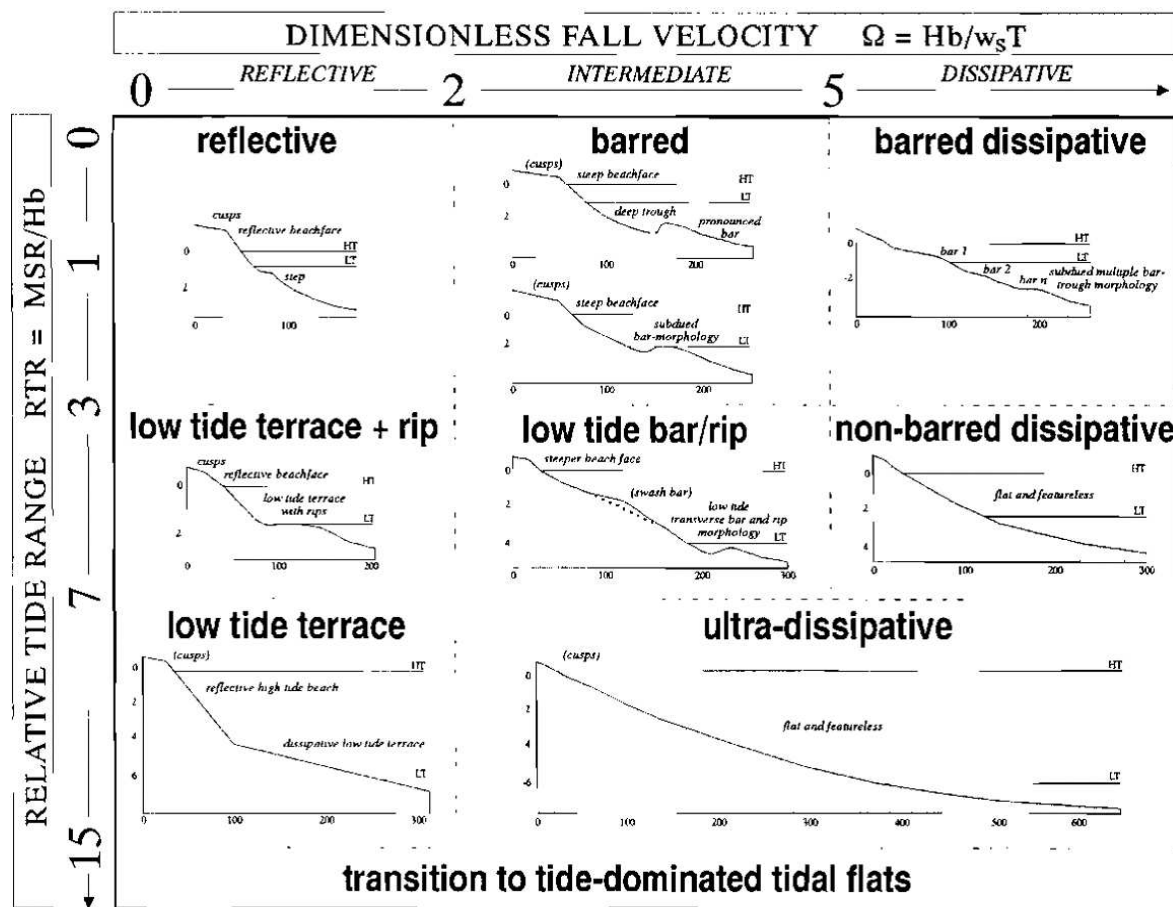


Figure I.6: Sandy beach morphodynamic classification by Masselink & Short (1993)

Masselink & Short (1993) proposed an extension for mesotidal and macrotidal beaches (Fig. I.6) by integrating an additional parameter: the Relative Tidal Range RTR , which compares the relative importance of the incoming wave amplitude with the tidal range:

$$RTR = \frac{MSR}{H_b} \tag{I.2}$$

where MSR is the Mean Spring tide Range. This classification proposed 8 different types of beach profiles (Fig. I.6), ranging from reflective to dissipative, depending on Ω (left to right), and including the relative importance of the tide, ranging from microtidal to macrotidal, to the transition to tide-dominated tidal flats (top to bottom). More complex classifications exist that integrates the different types of sand bars and the associated changes in the morphology.

I.1.3 Coastal hydrodynamics

Coastal morphodynamics are forced by a large array of hydrodynamic processes (Fig. I.7) that result from the effects of atmospheric forcing on the ocean (e.g. surface waves generated by the wind) or from the effects of astronomical gravitational forces (e.g. tides). These physical processes occur at a wide range of temporal and spatial scales, ranging from the scales of a few seconds and a few centimeters, to scales of centuries and hundreds of kilometers (Fig. I.2).

In this section, the main hydrodynamic processes that are generating currents responsible for adaptations of the coast and in particular changes of the beach morphology are presented.

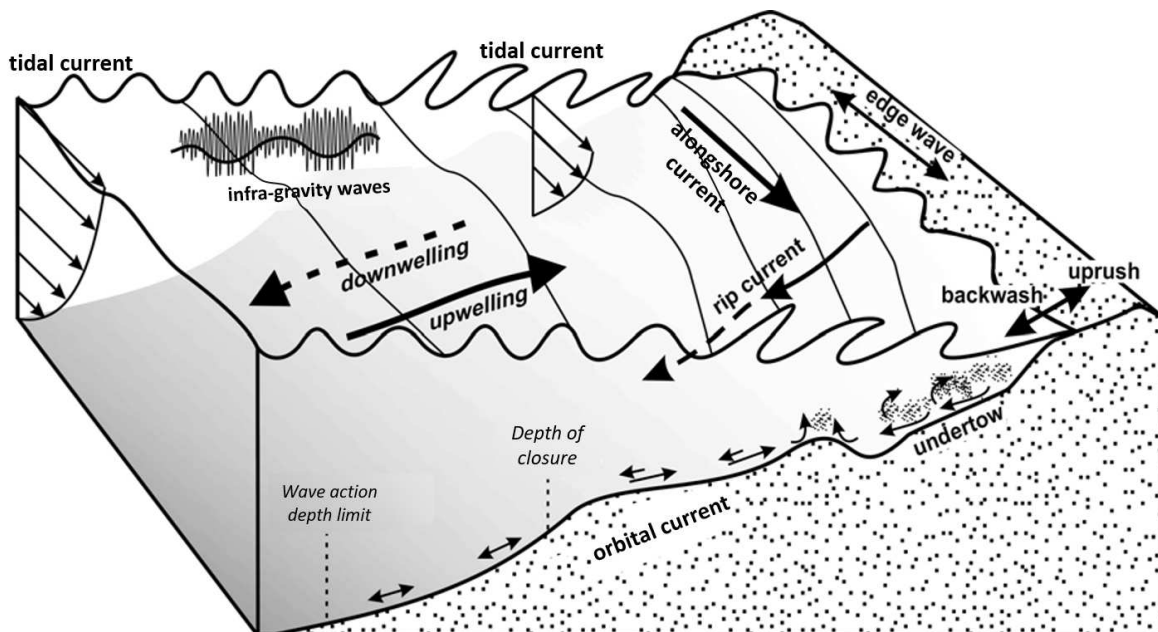


Figure I.7: Synthesis of nearshore hydrodynamics, from Stépanian (2002)

Surface gravity wave action

Here, the main attention will be on surface ocean waves, in particular gravity waves that are the main hydrodynamical factor responsible of beach evolution at short to medium time scales (Fig. I.2), thus internal waves won't be considered.

Gravity waves are the commonly observed oscillations at the ocean free surface and are divided into 2 categories: swell and wind waves. The term gravity wave comes from the gravity force being the

restoring force that creates a pressure gradient maintaining the wave propagation.

Surface gravity waves are generated by the friction force applied by the wind at the ocean surface generating an agitation that grows into ripples propagating at the water surface. The length of the spatial zone of formation by the wind is called "fetch", and this determines the difference between wind waves and swell, since swell waves propagate outside of their zone of formation, while wind waves are locally generated waves propagating within the zone of formation.

Gravity waves can be defined, like all waves, by their characteristics: amplitude, period, and wave length. These characteristics are determined by the fetch and the intensity and duration of the wind. In coastal areas, the sea state is often a mix of locally generated wind waves and swell formed farther offshore.

When propagating in deep water, waves are often more symmetrical, since they are not affected by the seabed, but when they arrive in shallower water (e.g. near the coast), they start interacting with the bottom bathymetry. This area where the waves are affected by the seabed is divided in several zones (Fig. I.8).

In the nearshore zone, corresponding to the region that extends from the landward limit associated with storm-wave phenomena (e.g., swash or overwash processes) to a seaward boundary located farther offshore than the point where incident waves break (Horikawa 1988), wave interactions with the bathymetry slow them down, which increases their amplitude and reduces their wave length due to energy conservation. This phenomenon is called shoaling and it occurs in the shoaling zone (Fig. I.8).

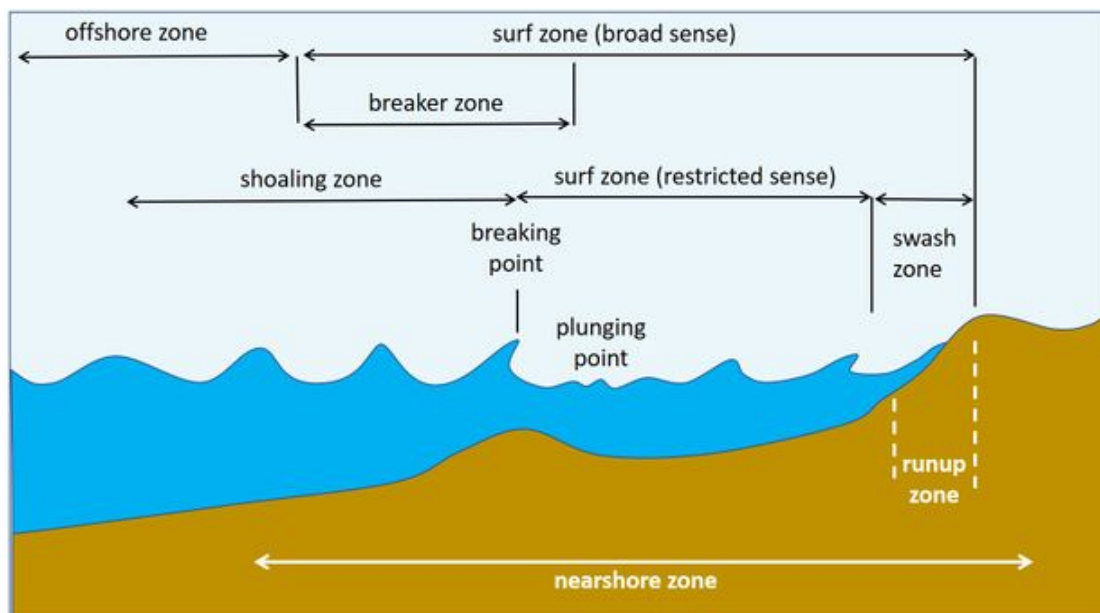


Figure I.8: Zone division in the nearshore region based on hydrodynamic processes (Horikawa 1988).

Waves change shape when propagating toward the coast, into shallower water, with an increasing vertical and horizontal asymmetry of the wave by shoaling and dissipation processes.

This asymmetry can lead to wave breaking, when the speed of the wave crest exceeds that of the wave face, due to bottom friction affecting more the lower part of the wave. The area where it happens is called the breaker zone (Fig. I.8).

Then, the breaking wave continues to propagate toward the coast as a bore in the surf zone, which is defined as the area between the breaker zone, as the offshore limit, and the high turbulence zone created by the encounter of the back-rushing water from the previous wave and the incoming bore waves (Horikawa 1988) (Fig. I.8). The contact area between the exposed beach and the breaking wave is called the swash zone, which extends to the highest point of the beach reached by waves and is alternatively covered and uncovered by incoming waves.

In the coastal area, interactions with the bathymetry and obstacles can generate wave refraction, diffraction and reflection. Wave refraction consists of the progressive alignment of the wave front with the isobaths as waves propagate in decreasing water depth. This occurs due to the wave speed decreasing with decreasing water depth, causing the waves to turn. Wave diffraction happens when waves encounter an obstacle or propagate through a small gap that has dimensions on the same order of magnitude of their wave length. It results in a spreading of the direction of wave propagation and in a decrease of the wave front amplitude due to the geometrical spreading. Finally, wave reflection occurs when waves encounter a sharp decrease in the water depth, for example, a sea wall or a cliff. The amplitude of reflection is a function of the wave characteristics (wave length, period) and the obstacle characteristics (slope, porosity, ...).

Waves are responsible for sediment suspension generated by the wave orbital velocity and induced turbulence at the breaking point and in the surf zone. The waves create currents in the breaking and surf zones transporting the suspended sediment, the main currents are: rip currents, undertow, and alongshore currents (Fig. I.8).

Rip currents are currents directed offshore, originating at the beach and flowing toward the offshore zone. They are often located periodically along the coastline inside channels, and they compensate for the water flux at the coast induced by wave propagation and breaking (van Rijn 1998). Undertow is also an offshore-directed current that is located in the breaking zone and is generated by the horizontal pressure gradient induced by breaking waves.

Finally, alongshore currents are generated by wave breaking with an angle between the wave front and the coastline, caused by an alongshore gradient of the wave height or the wave incidence angle. These currents are oriented parallel to the isobaths. Alongshore current intensity is maximum in the breaking zone and decreases toward the coast and offshore (Komar & Inman 1970). Their intensity is proportional to the angle between the wave front and the coastline at the breaking point and the wave height. Alongshore currents are responsible for longshore sediment transport also called littoral drift.

Tide influence

The tide is a water level oscillation generated primarily by the gravitational attraction of the sun and the moon, and the earth's rotation. This generates a wave propagating around point called an amphidromic point, or tidal node, defined as the location where the harmonics composing the tidal signal have a null amplitude. In coastal areas, the amplitude and phase of the tide is determined by the astronomical alignment of the sun and the moon, the coastal geometry (shape and bathymetry), and the location of the closest amphidromic point.

Based on the above environmental conditions, the oscillation frequency and amplitude (tidal range) of the water level from the tide can vary with 3 different patterns: a diurnal tide with one high water level (high tide) and one low water level (low tide) per day, a semi-diurnal tide with 2 almost identical high water levels and low water levels per day, and a mixed tide, with 2 high water levels and low water levels per day with different amplitudes.

Tidal amplitudes vary in time due to changes between the moon and sun axes. When they are in phase, the attraction effect is enhanced and the tidal range increases (spring tide), while when they are in quadrature, the tide amplitude decreases (neap tide) (Simon 2007).

The amplitude of the tidal range during spring tide conditions has been used to classify the coastal environment (Davies 1964): microtidal for a tidal range inferior to 2 m, mesotidal for a tidal range between 2 m and 4 m and macrotidal for a tidal range above 4 m. More recently, more uncommon environments with a tidal range greater than 8 m were classified as megatidal.

On the beach, the tide generates a fluctuation of the water level thus justifying the definition of reference tide levels. The Mean Sea Level (MSL) is the mean level reached by the water in time that is also affected by wave action (wave setup). The Mean High Water Spring (MHWS) and Mean Low Water Spring (MLWS) are the mean of the 2 highest and lowest levels reached by the water during the day of a spring tide. The Mean High Water Neap (MHWN) and Mean Low Water Neap (MLWN) are the mean of the 2 highest and lowest levels reached by the water during the day of a neap tide (Simon 2007).

The tide influences the morphodynamics of the beach by the tidal currents that, added to the wave currents, mostly participate in the transport of the sediment suspended by the waves (Aagaard et al. 1997, Masselink & Short 1993). The tide also modulates the beach area submerged by water and thus subject to the wave action. Furthermore, the tide interacts with waves through tidal currents. Lastly, by modifying the water level and thus the characteristics of the surf zone, the tide indirectly changes the length and the slopes of the surf zone as well as the bathymetry over which the wave propagate, thus impacting the propagated wave characteristics at the coast.

Consequently, the characterization of the tide relative importance in coastal area is determinant, since the tide potentially increases the complexity of the system, thus properly taking into account its effect is essential as tides interact with a large variety of processes responsible for beach morphological evolution.

I.2 Beach morphological modeling

To represent, understand, and predict the complex evolution of a natural environment such as beaches, numerical modeling, coupled with observations, is a commonly used tool. Thus, over time, a large variety of models with different levels of complexity have been developed.

I.2.1 Overview of existing approaches

This section will make a short review of the different kinds of models used to reproduce the beach evolution. As presented before, the coastal environment is extremely dynamic, with processes at various spatio-temporal scales. This aspect of the beach and the different challenges leads to the development and use of a wide variety of approaches depending on the spatio-temporal context and goals of the model application.

Thus, 3 families of models can be identified and are defined in the following section: physics-based models, data-based models and process-based models.

Physics-based approaches

This category of models resolve as many physical processes as possible, often by coupling computationally expensive 2D or 3D hydrodynamic models that resolve the wave propagation and currents, with a sediment transport model that estimates the sediment flux by calculating currents and the bottom shear stress. Then the morphology of the beach is modified using a conservation law such as the Exner equation.

$$\frac{d\eta}{dt} = -\frac{1}{(1-\lambda)} \nabla \cdot q \quad (\text{I.3})$$

where η is the bed position, q the sediment flux and λ is the sediment porosity.

In coastal areas, the hydrodynamic model component can be coupled with or forced by a spectral (e.g. SWAN (Booij et al. 1999) or WaveWatchIII (Tolman 2009)) or a phase-resolving (e.g. Non linear shallow water equation model like SWASH Zijlema et al. (2011), Boussinesq type model or potential flow model) wave model to propagate the offshore wave energy to the coast. Examples of such models are MIKE21 (Warren & Bach 1992), Delft3D (Roelvink & Banning 1995), and XBeach (Roelvink et al. 2009).

The computational cost of these approaches increases quickly from the necessity of fine spatial and temporal discretization to solve correctly the processes at a wide range of scales. For example, to resolve swash processes that cover a small surface of the beach and happen in a few seconds, the model needs to have a spatial discretization of the beach of a few centimeters, and a time step on the order of less than a second.

Thus, even with increased computational capacity from the growth and multiplication of powerful computers, the long-term application of this kind of model is still challenging as small numerical

errors or physical approximations of unresolved processes, made at each time step, then accumulate over a large number of time steps.

Thus, this type of model is mainly used at the scale of a beach or a section of a beach, and for the duration of a few days, to reproduce, for example, the impact of a storm on a beach/dune system.

Data-based approaches

With the increasing amount of measurements and data sources coming from new methods of observation providing high spatial and/or frequency observations, such as video cameras or altimetric satellites, machine learning and statistical modeling approaches are becoming optimal tools to reproduce efficiently beach morphological changes (e.g., Regression Trees (De'ath & Fabricius 2000), Genetic Algorithm (Holland et al. 1992) and Genetic programming (Koza & Koza 1992), Bayesian Network (Charniak 1991), or Artificial Neural Network approaches (see LeCun et al. 2015)).

These methods only require all the available data of a site, to get an accurate result by resolving numerical methods or optimization processes, but often without incorporating physical assumptions.

A recent review of different machine learning applications in the field of coastal morphodynamics was produced by Goldstein et al. (2018), where they summarized the different applications of machine learning approaches in the prediction of coastal evolution, or as part of "machine learning hybrid methods" that combine machine learning algorithms with existing morphodynamic models.

Process-based approaches

To achieve accurate results at a less expensive computational cost than physics-based models, approaches using simplified processes have been developed. These approaches only resolve the main physical processes of a complex dynamic system at a given spatio-temporal scale with the use of empirical parameters, which are calibrated using observations.

For example, models were developed reproducing the effect of cross-shore hydro-sedimentary processes using equilibrium concept (e.g. Miller & Dean 2004, Splinter et al. 2014, Yates et al. 2009), or from longshore hydro-sedimentary processes (e.g. Ashton & Murray 2006, Pelnard-Considére 1956), or combining in one model several of these approaches (e.g. Robinet et al. 2018, Vitousek et al. 2017). Thus, the numerical cost of these process-based approaches is usually small, and these models can be applied on large spatio-temporal scales and can often still run quickly, even on a personal computer.

These approaches are the most efficient for engineering applications or for coastal management purposes that involve large spatial domains (e.g., beach, littoral zone, regional or national coastline) and long temporal scales (e.g. pluri-annual to decadal or longer time scales) of morphological evolution since they provide relatively reliable predictions, once calibrated, at a low computational cost.

The work described in this thesis is focused on using, understanding the limitations, and im-

proving one of these models. Thus a summary of the different developed process-based approaches is made in the following section, differentiating approaches reproducing cross-shore and longshore processes.

I.2.2 Empirical equilibrium cross-shore models

Based on the equilibrium beach profile theory (Dean 1977), it is assumed that for a given wave energy there exists an associated equilibrium beach profile for which this wave energy generates no morphological change on the profile, thus a wave energy higher or lower than this equilibrium energy causes an adaptation of the beach profile, which is a function of the actual state of the profile and the difference between the incoming and the equilibrium wave energy (Fig. I.9).

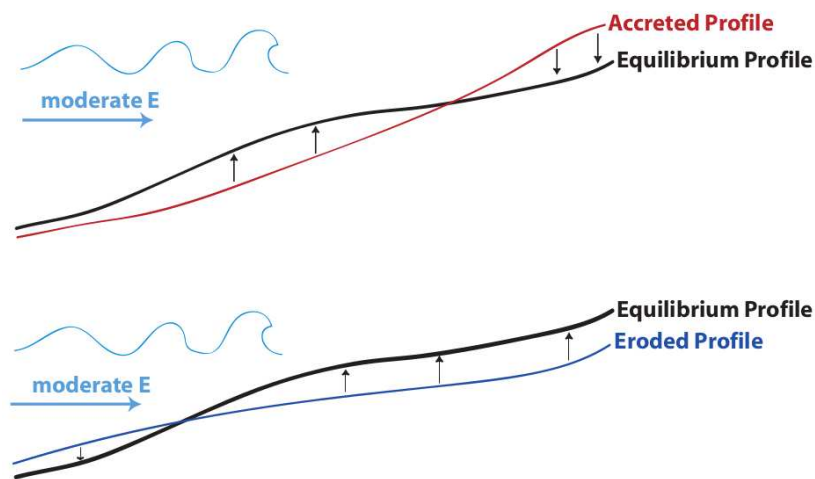


Figure I.9: Equilibrium beach profile theory (Dean 1977), conceptual scheme from Yates (2009).

Using this theory, several empirical models have been created. These models relate the beach evolution to the waves forcing and to beach characteristics using a "relaxation type equation", these equations describe how the beach evolves due to a perturbation and then return to an equilibrium. These models estimate the shoreline evolution made by the cross-shore sediment transport only.

Here, 3 existing approaches are described: the Miller & Dean (2004) model, the ShoreFor model of Davidson & Turner (2009) and generalized by Splinter et al. (2014), and the Yates et al. (2009) model. Each model differs in the manner used to define the equilibrium and to relate the cross-shore evolution of the beach to the wave and beach characteristics.

Miller & Dean (2004) model

Miller & Dean (2004) proposed a shoreline change model that uses a linear equilibrium relaxation equation based on the pioneer work of Kriebel & Dean (1993). This equation enables approaching the equilibrium position exponentially in time when subjected to constant wave forcing. They

integrated a time-dependent wave and water level variation as forcing.

$$\frac{dS(t)}{dt} = k(S_{eq}(t) - S(t)) \quad (I.4)$$

where k is a constant governing the rate of the model to converge to the equilibrium or was try setting dependent of the beach characteristics, S_{eq} is the equilibrium shoreline position and $S(t)$ the shoreline position at time t . The value of S_{eq} is approximate using the [Dean & Dalrymple \(1991\)](#) formulation, based on equilibrium beach profile theory, and a Bruun-type conservation of volume argument.

They applied the model to 10 different study sites, representing a wide variety of beach states. They show that the model results are promising and highlight the need to gather high quality observations to improve the model performance.

They also point out that their model performs better at seasonal scale than at shorter time scales, and that it could be attributed to the lack of high frequency data. Their model is able to represent correctly (at 57% on average) the sign of shoreline changes (erosion/accretion), but globally underestimates the amplitude ([Miller & Dean 2004](#)).

ShoreFor model

The ShoreFor model, developed by [Davidson & Turner \(2009\)](#), improved in [Davidson et al. \(2013\)](#) and generalized by [Splinter et al. \(2014\)](#), is a cross-shore shoreline change model that uses the instantaneous value of the dimensionless fall velocity parameter $\Omega = H/w_sT$ to simulate erosion or accretion on the shoreline. The model uses the following relation to simulate changes in the cross-shore position S of a given beach altitude (e.g. MSL):

$$\frac{dS}{dt} = C^\pm P^{1/2} (\Omega_{eq}(t) - \Omega(t)) + trd \quad (I.5)$$

where P is the incident wave power, Ω_{eq} is the equilibrium dimensionless fall velocity (or Dean number), C^\pm are 2 free parameters defining the accretion or erosion rate depending of the sign of the disequilibrium ($\Omega_{eq} - \Omega$), and trd is a linear change rate, accounting for the missing physical processes.

[Splinter et al. \(2014\)](#) proposed an extension of [Davidson et al. \(2013\)](#) of the form:

$$\frac{dS}{dt} = c(F^+ + rF^-) + trd \quad (I.6)$$

where c and trd are calibration parameters and F is the forcing term defined as:

$$F = P^{1/2} \frac{\Delta\Omega}{\sigma_{\Delta\Omega}} \quad (I.7)$$

where $\Delta\Omega$ is the disequilibrium dimensionless fall velocity, and $\sigma_{\Delta\Omega}$ is the standard deviation of $\Delta\Omega$. The sign of the forcing term F is to differentiate erosion and accretion. r is the erosion ratio numerically evaluated in the model as:

$$r = \left| \frac{\int_{i=0}^n \langle F_i^- \rangle}{\int_{i=0}^n \langle F_i^+ \rangle} \right| \quad (\text{I.8})$$

where $||$ is the absolute value, $\langle \rangle$ design an operation removing the linear trend while preserving the observation mean value (Splinter et al. 2014), and n the length of the observations.

Splinter et al. (2014) applied this approach at 12 study sites, and then evaluated the calibrated model parameters obtained to propose a relation between the site characteristics (e.g. Ω) and the expected values of the free parameters.

Yates et al. (2009) model

This cross-shore model relates the change in the cross-shore position of a given altitude dS/dt to the disequilibrium ΔE between the instantaneous and equilibrium wave energy with the following relation:

$$\frac{dS}{dt} = C^\pm E^{1/2} \Delta E \quad (\text{I.9})$$

where C^\pm are two free parameters specifying the accretion C^+ and erosion C^- rates depending of the sign of the energy disequilibrium $\Delta E(S) = E - E_{eq}(S)$.

E is the instantaneous wave energy (in 10 m water depth), and $E_{eq}(S)$ is the equilibrium energy defined as a linear function of the shoreline position $E_{eq}(S) = aS + b$, based on observations. This line is a mathematical representation of the equilibrium position of the shoreline for a given wave energy and beach state.

The four coefficients a , b , C^- and C^+ are obtained using an optimization method, simulated annealing (Kirkpatrick et al. 1983), with observations from topographic surveys and estimates of the local wave energy.

A fifth coefficient d was added by Castelle et al. (2014) to account for uncertainties coming from the choice of the initial cross-shore position in the optimization process and to lessen the weight of the first shoreline position used.

As a shoreline change model, this approach is applied at a chosen elevation, treating each altitude independently. This model was developed and tested, at first, on microtidal beaches in Southern California. To apply this shoreline change approach in mesotidal environments, where the definition of the shoreline position is less distinct, Castelle et al. (2014) applied the model at several altitudes of the profile at the Truc Vert Beach, as performed by Yates et al. (2011) at the microtidal environment of Ocean beach, showing that this model can efficiently reproduce beach morphological changes at different positions of the cross-shore profile. It should be note that the same process could be used for the 2 other cross-shore shoreline change model presented.

More recently, [Lemos et al. \(2018\)](#) applied an extended version of the model at the macrotidal beach of Porsmilin, adding a binary threshold to account for water level variations.

This model will be further discussed in Chapter III.

I.2.3 Longshore modeling

The One-line concept

The one-line concept is a simple approach representing longshore processes. The theory was first introduced and mathematically presented by [Pelnaud-Considère \(1956\)](#). The one-line approach relies on the assumption that at long temporal scales, longshore processes dominate and that the beach profile maintains an equilibrium profile shape. Then this equilibrium profile is simply shifted landward or seaward depending of the alongshore divergence or convergence of the longshore sediment flux ([Hanson 1989](#)).

An important review of the development of the model from 1956 to 1990 from this theory was made by [Hanson \(1989\)](#) while introducing the complete *GENESIS* model. Previously, [Hanson & Kraus \(1985\)](#) and [Hanson et al. \(1988\)](#) had already presented an application of this approach in a model developed as an engineering tool to estimate coastal infrastructure impacts on shoreline evolution.

The one-line approach has been widely employed in engineering applications ([Delft Hydraulics 1994](#), [Hanson et al. 1988](#)) and is still used and implemented in the more recent approaches developed to account for longshore processes, ([Antolínez et al. 2019](#), [Vitousek et al. 2017](#)).

Numerous modifications and improvements of the method have been proposed to try correcting some flaws of the concept, for example the model management of high angle wave incidence or accounting for high planform curvature shoreline areas in the transect discretization, they are summarized in the following section.

Formulation of longshore sediment flux estimation

Several different approaches for estimating the beach longshore sediment flux have been proposed in the literature. Overall, they rely on offshore wave conditions or breaking wave conditions with empirical coefficients and sometimes integrating beach characteristics like the sediment grain size or the beach slope ([Kamphuis 1991](#), [Komar & Inman 1970](#), [Ozasa & Brampton 1980](#)). For example, the CERC formula ([USACE 1984](#)):

$$Q_0 = \frac{\rho K H_b^{2.5} \sqrt{g/\gamma_b}}{16(\rho_s - \rho)\lambda}, \quad (\text{I.10})$$

where, K is a dimensionless empirical parameter (the typical range of values is discussed in Chapter IV), H_b is the breaking wave height, g is the gravitational acceleration, γ_b is the breaker index ratio, and ρ and ρ_s are the water and sediment density.

The one-line model formulation and the longshore sediment flux calculation will be described further in the Chapter IV, focused on longshore modeling.

CEM : Coastal Evolution Model by Ashton et al. (2001) and Ashton & Murray (2006)

Wave angle reaching the coast at a larger angle than the angle maximizing the longshore transport are responsible of development of the high angle wave instabilities (HAWI) (Ashton et al. 2001). To account for HAWI that lead to the formation of longshore morphological features like sand spits, cusps, or longshore sand-waves, Ashton & Murray (2006) developed a novel approach, using a 2D cellular method, to describe beach morphological changes estimated using the one-line equation with a new numerical scheme and a shoreline diffusivity term that account for the wave angle and became negative generating instability. It allows the model to remain stable for wave angles relative to the coast higher than 45 degrees.

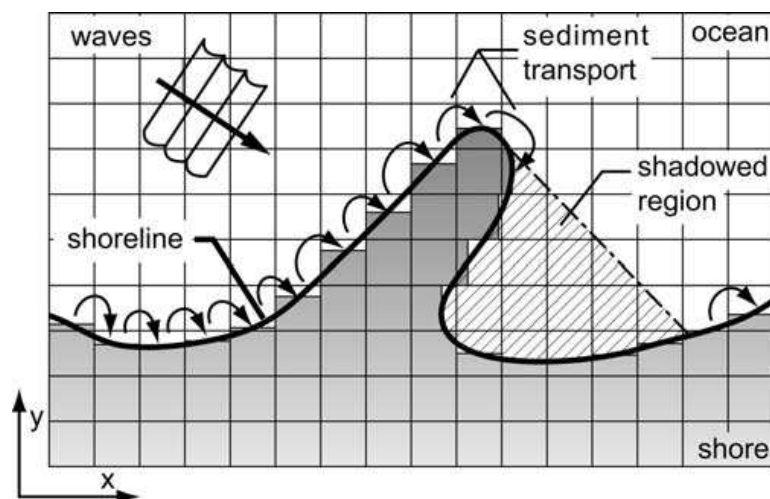


Figure I.10: Conceptual scheme of the CEM cellular longshore model (Ashton & Murray 2006)

CEMSWAN model by Limber et al. (2017)

To efficiently account for the offshore wave transformation and wave propagation to the coast, which have an important role in the longshore sediment flux estimation in particular for the HAWI reproduction, and also in the longshore model uncertainty, Limber et al. (2017) improved the CEM approach of Ashton & Murray (2006) by coupling this longshore cellular approach with the spectral wave model SWAN.

They show that using the spectral model to propagate the wave to the coast and updating the bathymetry accordingly with the shoreline evolution impact the formation of shoreline instabilities.

The vector approach of Hurst et al. (2015)

Hurst et al. (2015) presented a new vector based approach (COVE model) based on the one-line model that ensures correct mass conservation and avoids cells covering in high planform curvature shoreline areas. It allows, for example, to represent correctly the evolution of crenulate bays by using irregularly shaped cells. Thus the coastline cell can either be trapezoidal for a low planform curvature shoreline or polygonal/triangular for a high planform curvature shoreline.

They applied their model to reproduce the evolution of a bay located between two headlands and showed that this model is able to produce a realistic equilibrium bay shape with the right wave forcing.

The waves are propagated from the offshore using linear wave theory like in the CEM model of Ashton & Murray (2006), and they added simple rules for diffraction and refraction to account for propagation in high planform curvature areas (for example areas shadowed from incident waves).

Shoreline rotation models

Analysis of shoreline spatio-temporal variability, (e.g. *EOF* analysis) point out that beach rotation is the second main mode of movement on embayed and pocket beaches (Harley et al. 2010), and this mode is associated with a change in the longshore sediment transport direction from one extremity of the beach to the other (Turki et al. 2013). It causes accretion at one beach extremity and erosion at the other, and vice versa (Fig. I.11).

To reproduce this process, models have been developed using equilibrium concepts and a semi-empirical formulation (similar to the equilibrium cross-shore model) to link the shoreline rotation rate to the alongshore component of the wave energy flux (Turki et al. 2013).

$$\frac{dS}{dt} = \omega \cdot (S_{\infty} - S(t)) \quad (\text{I.11})$$

where S is the shoreline position, ω is the rate of beach change, $S(t)$ is the instantaneous shoreline position whereas S_{∞} is the long term equilibrium position define using the equilibrium planform of the shoreline (see Turki et al. 2013, for more details).

More recently, Jaramillo et al. (2021) proposed a new equilibrium-based shoreline rotation model that assumes that the beach rotation is generated by the forcing wave power and wave direction.

$$\frac{d\alpha}{dt} = L^{\pm} P(\alpha - \alpha_{eq}) \quad (\text{I.12})$$

here, α and α_{eq} are respectively the shoreline orientation and the equilibrium shoreline orientation and L^{\pm} are proportionality constants that accounts for a clockwise shoreline rotation L^+ , or a counterclockwise rotation L^- .

In this model, the beach orientation α evolves toward an equilibrium angle α_{eq} that is associated

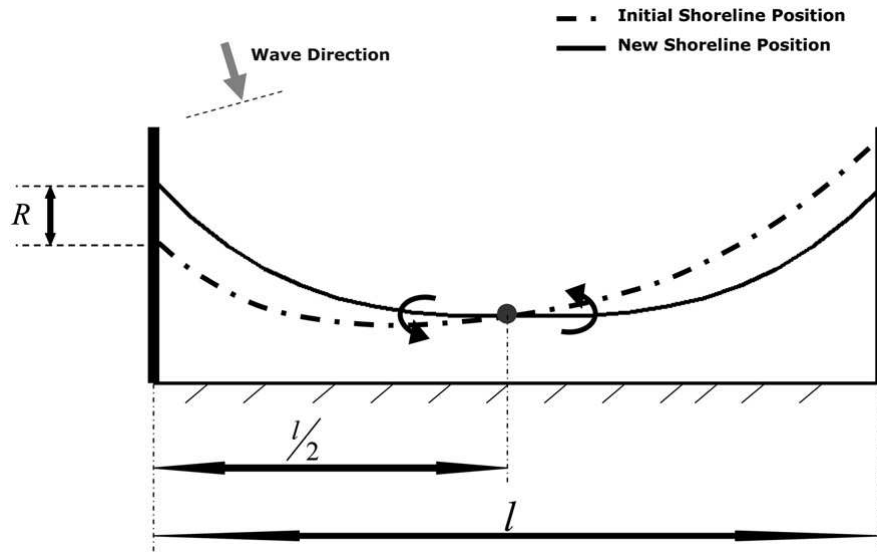


Figure I.11: Conceptual schematic of shoreline rotation on pocket beach, from (Turki et al. 2013).

with an equilibrium wave direction function, defined from a linear relation between the incident wave direction θ and the shoreline orientation.

$$\alpha_{eq} = \frac{\theta - b}{a} \quad (\text{I.13})$$

where a and b are empirical parameters. The empirical shoreline rotation model was applied on 2 sites showing the model performance to reproduced the observed shoreline orientation.

I.2.4 Combined cross-shore and longshore models

This section describes 5 models that take into account both longshore and cross-shore processes, ranging from complex approaches more physics-based, incorporating hydrodynamic models or spectral wave models, to simple approaches, process-based mixing equilibrium cross-shore model with one-line approach.

Q2D-Morpho model of Van Den Berg et al. (2011)

This combined model is a non linear quasi-2D morphodynamic model based on the linear model of Falqués & Calvete (2005). The model configuration is a 2D grid model in which offshore wave conditions are propagated using a wave ray model over a bathymetry that is updated during the simulation by the morphodynamic model.

The model estimates sediment transport in cross-shore and longshore directions so that the morphological evolution of the beach is modeled by updating the bathymetry with the effect of gradients in longshore sediment fluxes generating sediment convergence and divergence like in a classical one-line approach.

The shoreline change rate is calculated, first using a formulation of a cross-shore integrated long-shore sediment flux rate with the CERC formula (Komar & Inman 1970) using the second term of Ozasa & Brampton (1980) to include the contribution of the alongshore gradients in wave height in the sediment flux.

Then they distribute this rate along the profile by multiplying the flux with a cross shore distribution function based on the cross-shore profile of the longshore current. However, in this model they made an important simplification with the parameterization of cross-shore sediment processes as a diffusive process, assuming that, at long time scales, cross-shore processes lead to an equilibrium profile.

CoSMoS-COAST model of Vitousek et al. (2017)

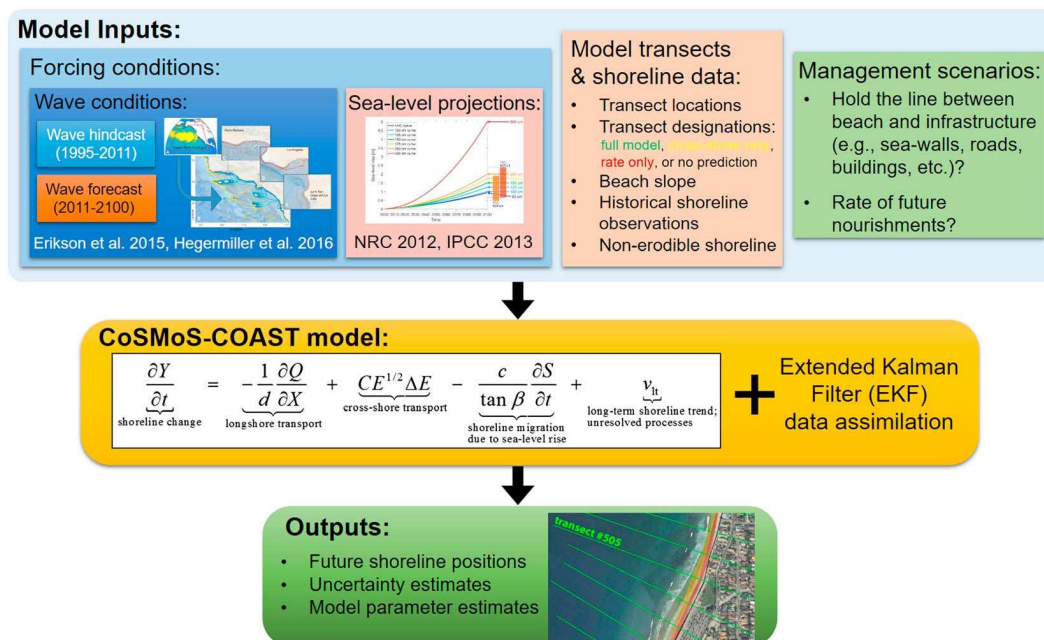


Figure I.12: Cosmos-Coast framework and model equation from (Vitousek et al. 2017)

This combined model, CoSMoS-COAST, uses a simplified version of the cross-shore model of Yates et al. (2009), considering only one coefficient C for both the erosion and accretion rates, with a one-line approach for the longshore component (Vitousek & Barnard 2015), the "Bruun rule" formulation to account for a geometrical retreat of the shoreline due to sea level rise (Bruun 1962), and a linear trend component to take into account all unresolved processes (see model equation in CoSMoS-COAST model section of Fig. I.12).

The model discretization is based on transects perpendicular to the coastline so that the shoreline position moves landward/seaward, like on a rail (Vitousek & Barnard 2015), thus this approach can't represent shoreline instability development such as sand spits.

They applied this model to over 500km coastline of the US West coast, with shore normal tran-

sects, using data assimilation with a Kalman Filter to estimate the model coefficients a , b , C , K and a long term trend v_{lt} at each transect.

They looked at the model results for long term shoreline change (up to year 2100) for different scenarios of sea level rise, then they identified the relative importance of each component contribution depending of the time period showing that during the 15 year of hindcast the cross-shore component explained the majority of the reproduced shoreline variability ($\approx 90\%$) whereas in the forecast period of 2010 to 2100, the Bruun rule term is dominant (explained 70%).

LX-Shore model of [Robinet et al. \(2018\)](#)

LX-Shore is a model combining an adaptation of the ShoreFor model of [Davidson et al. \(2013\)](#) and [Splinter et al. \(2014\)](#) for the cross-shore part with the CEMSWAN approach of [Limber et al. \(2017\)](#) to estimate the longshore component. Thus the model discretization is 2D cellular-based, allowing the reproduction of alongshore instability morphologies such as sand spits and accounting for non-erodible area.

The model can be coupled with the spectral wave model SWAN to propagate waves nearshore and to estimate the wave characteristics at breaking, like in [Limber et al. \(2017\)](#). The model also uses an adaptation of the method of [Kaergaard & Fredsoe \(2013\)](#) to account for the feedback between morphological changes and the nearshore bathymetry in the SWAN wave propagation model by updating the bathymetry (Fig. I.13). The breaking wave condition can be either extracted from SWAN output or obtained from nearshore wave condition using the formula of [Larson et al. \(2010\)](#).

COCOONED model of [Antolínez et al. \(2019\)](#)

[Antolínez et al. \(2019\)](#) proposed a combined approach that integrates a one-line model approach for longshore processes, a cross-shore empirical model that accounts for both waves and water level effects based on a modified version of the [Miller & Dean \(2004\)](#) model, and a foredune evolution model that accounts for waves and water level action based on the [Kriebel & Dean \(1993\)](#) model.

An additional term is added to integrate in the shoreline evolution the influence of cross-shore or longshore sediment supply in the profile adjustment as an additional flux to the one-line model estimate longshore sediment flux.

The model estimates nearshore wave conditions using a hybrid downscaling method ([Camus et al. 2011](#)) of a deep water sea state representative subset that includes the hourly significant wave height, the peak period, and the mean wave direction. However, the model doesn't consider variations of the wave conditions at local scales, for example propagating close to jetties. Furthermore, the model discretization is based on shore normal transects (as in the CoSMoS-COAST model of [Vitousek et al. \(2017\)](#)), thus, the model can't reproduce shoreline evolution creating important coastline curvature (like sand spits) that would cause double values of the shoreline position along one transect.

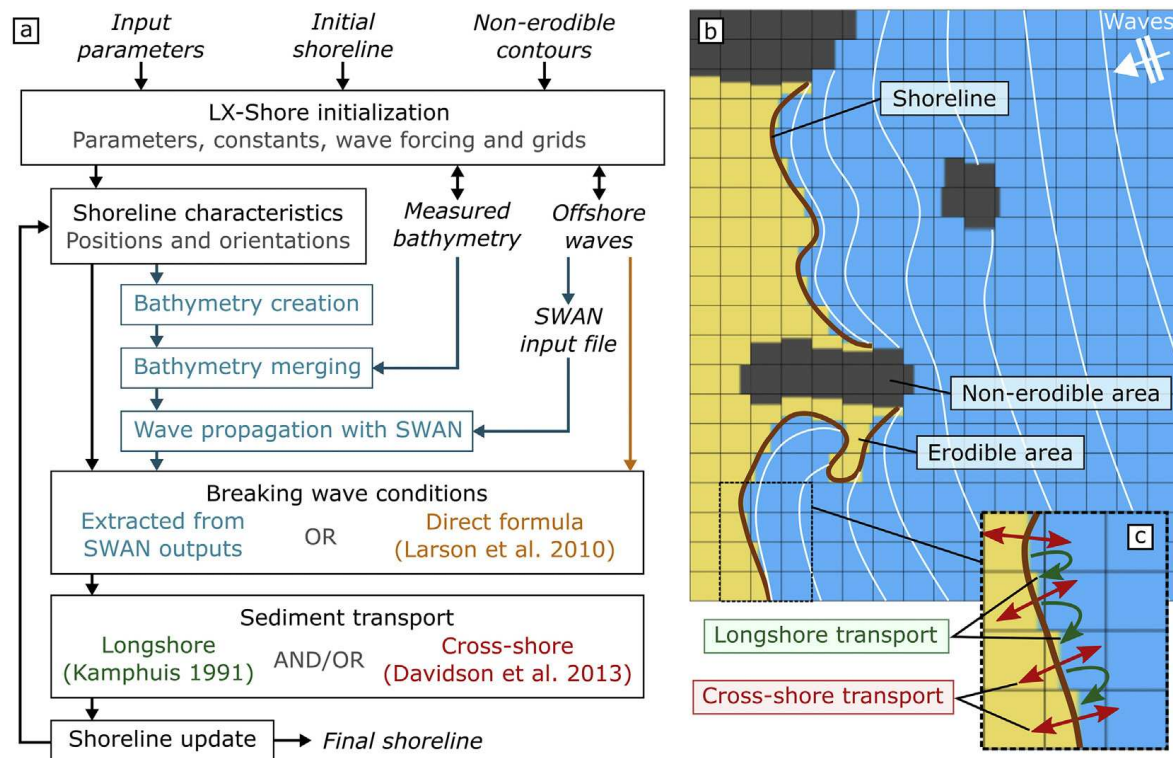


Figure I.13: LX-Shore model showing the (a) global framework and (b) cellular conceptual scheme, from (Robinet et al. 2020).

Combined model of Tran & Barthélemy (2020)

The combined model of Tran & Barthélemy (2020) consists of the ShoreFor cross-shore model of Splinter et al. (2014) and a modified one-line longshore model. The modified longshore model is obtained by decomposing the wave forcing into the average and the fluctuations to then relate the wave direction and amplitude to variations in the beach orientation. These fluctuations from the mean wave direction are used to calculate the longshore contribution (Tran & Barthélemy 2020).

The derivation of the longshore model made several hypotheses: that an embayed beach is a closed system bounded by non-erodible features, that the fluctuations of the shoreline angle are small compared to the fluctuation of the wave angles, and that the derivatives of wave parameters with respect to the alongshore direction are constant in time on a given transect (Tran & Barthélemy 2020).

It results in a semi-empirical formulation with 2 free parameters a , b that account for the alongshore gradient of wave incidence angle and wave height. Furthermore, since this model assumes that the beach orientation fluctuations are negligible, it can't reproduce unstable features such as spits or longshore sediment retained by a groin. Another limitation is that this combined model doesn't account for the water level variations.

I.3 Conclusion

In this chapter, the beach morphodynamical system, and the existing approach to model its evolution in particular the process-based models, were introduced.

In the general introduction, the existing risks and the necessity to develop tools to predict coastal evolution at medium to long temporal scales and on spatial scales of a beach to a region was highlighted. Then, existing morphological modeling approaches were summarized, and it was pointed out, from the beginning, that physics-based approaches are still too computationally expensive or showing numerical errors too large to apply at these spatio-temporal scales (Ranasinghe R. 2013). Empirical process-based approaches are an optimal approach since they are efficient in reproducing morphological changes at these spatio-temporal scales and they can represent well morphological changes once calibrated with observations (French et al. 2016).

Thus, since the end of the XXth century, a variety of empirical process-based approaches were developed with cross-shore models based on equilibrium theory (Davidson et al. 2010, Miller & Dean 2004, Splinter et al. 2014, Yates et al. 2009) showing good results in reproducing shoreline changes at inter-annual scales. For long term simulations (e.g. decadal), longshore models based on the simple one-line approach (Ashton & Murray 2006, Hurst et al. 2015, Limber et al. 2017, Pelnard-Considére 1956) were developed and are used actively.

Recently, an increasing number of models combining empirical cross-shore and longshore approaches have been developed (Antolínez et al. 2019, Robinet et al. 2018, Tran & Barthélemy 2020, Vitousek et al. 2017), highlighting the importance of accounting for both processes to reproduce accurately shoreline changes over a large range of spatio-temporal scales and environments. However, the quantification of the respective contributions of each process is difficult to evaluate in observations, which complicates the validation and calibration of these combined approaches. Furthermore, assuming a particular spatio-temporal scale of relevance for the cross-shore or longshore process can be questionable depending on the site of application. This will be discussed in Chapter V.

Combined models may also include an additional term to account for climate change effects such as changes in sea level (e.g. Antolínez et al. 2019, Vitousek et al. 2017), or other unresolved processes, with the goal of developing accurate operational tools for long term predictions.

Thus, this thesis work is focused first on evaluating the performance, sensitivity, and limitations of the Yates et al. (2009) cross-shore model (pursuing the recent work of Lemos et al. (2018) on a macrotidal beach) and a simple one-line longshore model, including the data required and an evaluation of the model performance. This is achieved by applying the models at 2 study sites, Vougot Beach and Narrabeen Beach, for which high quality, long-term morphological observations and hydrodynamic estimates are available. Then, the different possibilities of combinations of these two approaches are described, implemented, and applied at Narrabeen Beach, and three criteria are used to analyze and compare the model performance at different time scales, to evaluate the advantages and limitations of each combined approach.

Chapter II

Study site

Ce chapitre présente les 2 plages étudiées dans le cadre de ces travaux de thèse : la plage du Vougot, située sur la commune de Guissény dans le Finistère, en France, et la plage de Narrabeen, au nord-est de Sydney, en Australie. Sont réalisés pour chaque site : une description géomorphologique, une synthèse des observations sur les évolutions morphologiques, et un résumé des données morphologiques et hydrodynamiques exploitées. La plage du Vougot s'étend sur 2 km d'Est en Ouest et est composée de 2 anses séparées par un tombolo. Le site est macrotidal et possède une bathymétrie d'avant-côte complexe, comportant des hauts-fonds rocheux et de nombreux îlots qui influencent la propagation des vagues. De plus, la dynamique hydro-sédimentaire du site est influencée par un épis qui constitue la limite est de la plage et qui modifie le transport longshore. Sur ce site, 6 profils cross-shore ont été définis pour être suivis mensuellement par levé DGPS, depuis 2004 pour les 3 profils à l'Est et depuis 2011 pour les 3 profils à l'Ouest. La plage de Narrabeen est une plage macrotidale s'étendant sur 3.5km dans la direction Nord - Sud, et délimitée à ces 2 extrémités par 2 éperons rocheux. La présence de ces éperons, en particulier celui à l'extrémité Sud, influence la propagation des vagues dans la baie, et génère un gradient du Nord au Sud dans la taille des vagues à la côte, avec une partie Nord plus exposée que la partie Sud. L'évolution morphologique de ce site est suivie mensuellement depuis 1976 via 5 profils cross-shore répartis le long de la plage. De plus, des données de conditions de vagues à 10m de profondeur sont disponibles, obtenues par propagation numérique à partir des conditions au large en face de chaque profil.

Chapter II

Study site

In this chapter, the morphological and hydrodynamical setting of the two beaches used during this thesis work, Vougot Beach and the Narrabeen-Collaroy embayment, are described. This description is followed by a synthesis of the data used and a description of the current understanding of the beach morphodynamic behavior, for each site, based on the literature.

These 2 beaches were chosen firstly for their important morphological and hydrodynamical dataset available covering both a wide spatial and temporal extend.

II.1 Vougot Beach

II.1.1 Beach geomorphology

Vougot Beach is located in the 2000 inhabitants municipality of Guissény, situated on the northern coast of Finistère in Brittany (France). Vougot is formed by a dune system, stretching from 200m to 400m wide, anchored to the Zorn abandoned cliff, in the southwest, and which extends over 2km in the northeast direction. The dunes reach an altitude of 13m above sea level (NGF, *Nivellement Général de la France*, i.e. french reference system).

The morphological setting of the area, corresponding to the submerged part of the Leon plateau, presents complex bathymetry composed of shallow rocky platforms, deeper incised channels located farther offshore, and scattered, large rocky outcrops. The rocky platform creates a zone of nearly constant shallow water depth (with depth from 6m to 10m below MLWS) that extends up to 2km offshore in front of the western part of the beach and around 4km in front of the eastern part (SCAN littoral from Data.SHOM¹).

This offshore morphological setting of the beach generates complex hydrodynamics with wave refraction and diffraction around the outcrops. Vougot Beach formed 2 bights: this shape is due to the formation of a tombolo, generated by a rocky outcrop located in front of the beach (in the center of Fig. II.1b and Fig. II.2 in the alignment of the profile 4).

The eastern part of the beach is longer (~ 1.3 km long) and more west facing than the western part (~ 600 m long), which faces more to the north and is more concave (Fig. II.1b). The north-east extremity of the beach is delimited by a 300 m-long jetty that connects the coast to an offshore rocky island, thus isolating Vougot Beach from the Centre Nautique beach cell situated on the other side of the jetty (Fig. II.1b) (Suanez et al. 2010).

Vougot Beach is a semi-diurnal macrotidal environment, with a tidal range of around 7m be-

¹https://services.data.shom.fr/geonetwork/srv/fre/catalog.search#/metadata/CARTO_SCAN_LITTO.xml

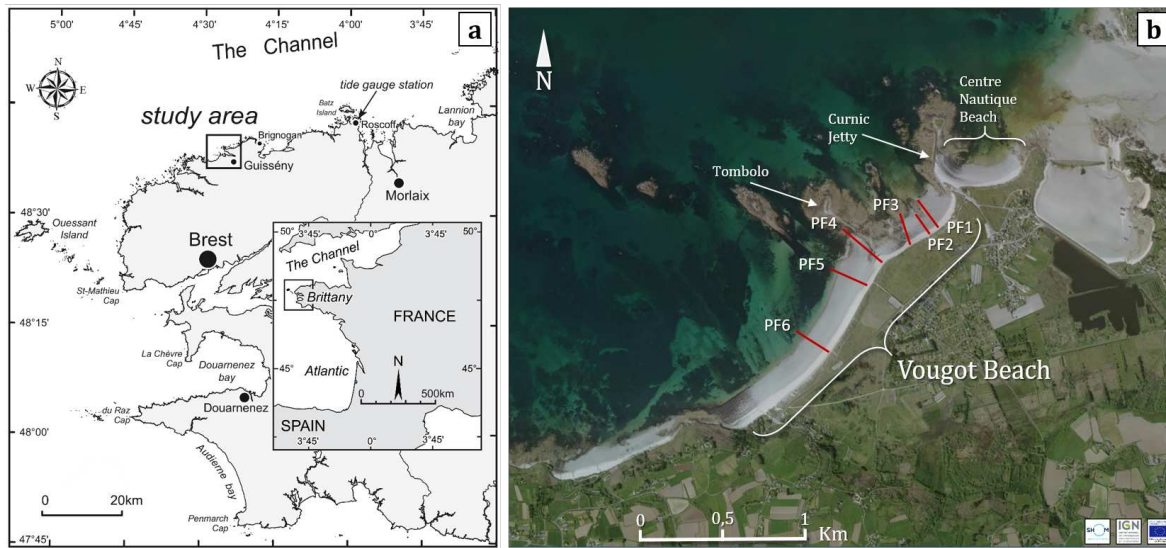


Figure II.1: Vougot location: (a) map of France and the Finistère indicating the study site location shown in (b) (graphic adapted from [Suanez et al. \(2015\)](#)), (b) Vougot Beach, showing the location of the 6 cross-shore profile transects (PF1, PF2, PF3, PF4, PF5, and PF6).

tween the MHWS and MLWS. Based on estimation of the 2 parameters (the relative tide range and the dimensionless fall velocity) used for the beach state classification of [Masselink & Short \(1993\)](#), Vougot is a non-barred dissipative beach. However, the beach profiles present 2 different slopes with an inflection point of the beach slope located around 3.0m NGF, between the MHWS and the MHWN (situated respectively at 3.9m and 2.1m NGF).

Therefore, along the upper part of the beach profile, the beach slope is steeper $\tan\beta \approx 0.1$ while along the lower part of the beach profile, the beach slope is more gentle $\tan\beta \approx 0.02$.

Thus, the upper part of the beach profile is characterized by intermediate to reflective conditions while the lower part of the beach profile corresponds to a dissipative environment, similar to a low-tide terrace beach (Fig. II.3d,e). This change in the beach slope with the elevation of the beach creates a variable morphodynamic response that depends on the tide level.

At Vougot Beach, the sediment grain size varies from the dune to the intertidal area with a coarser sediment grain size on the beach with $D_{50,beach} = 0.25 - 0.32\text{mm}$ than on the dune where $D_{50,dune} = 0.2\text{mm}$. After erosive events in the winter, Pleistocene/Holocene pebbles and gravel may be exposed at the eastern end of the beach, and peat layers from periglacial deposits can also be found at some altitudes of the intertidal zone, but no precise cartography or measurement of the thickness nor the extent of those layers exists. Once this "hard bottom" limit is exposed, this reduces the sand potentially available on the beach, which may have important impacts on numerical modeling of the site.

II.1.2 Hydrodynamic conditions

The 30km offshore deep water wave conditions obtained from the Wavewatch III spectral wave model from 1979 to 2002 show that the incident waves are mostly coming from the west-northwest direction (292°N), with average wave height of 2.2m and mean peak period of 10.6s (Suanez et al. 2012).

During this thesis work, wave data closer to the beach were used from the HOMERE wave database of IFREMER (Boudière et al. 2013). The HOMERE database consists of the integral wave parameters describing the sea states main characteristics and their evolution in time in an area covering the English Channel and the Bay of Biscay (from 43° N to 53° N and from -7° E to 4° E). The database was created using the WAVEWATCH III spectral model, with an unstructured grid with cell sizes ranging from 10km offshore to 200m in the coastal area. Thus the seas state characteristics are available at the 110000 nodes of the domain. This wave data spans the period from 1994 to 2016.

The node extracted is located approximately 7km offshore of the beach in the north-west direction, in approximately 40m water depth (below MLWS). At this location, the wave direction is slightly more northwest oriented than the the wave direction from the 30km offshore point. Due to the complex setting of the nearshore beach area, a comparison of the wave characteristics at different nodes located in front of the beach is made in Chapter III to evaluate the quality of the waves characteristics propagate by the wave model in this environment.

The tide data used in this thesis work are hourly predicted tide levels calculated by the SHOM (French Navy's Hydrographic and Oceanographic Department) at Brignogan Harbor located 10km east of Vougot (Fig. II.1a).

II.1.3 Data and beach morphodynamical behavior

The beach sand levels of the beach has been recorded since 2004 by the LETG Brest laboratory (Suanez et al. 2010), with 3 profiles defined in the eastern part (PF1, PF2 and PF3) that were surveyed monthly, using DGPS, from the top of the dune to the MLWN. Then, 3 other profiles (PF4, PF5 and PF6), located farther west, were also surveyed starting in 2011. (Fig. II.1b and Fig. II.2). This monitoring was started in order to evaluate the submersion risk of the area because of observations of dune retreat (Suanez et al. 2007). Thus the previous studies completed at this beach are mainly focused on the dune evolution (Suanez et al. 2015, 2012, 2010).

However, some studies (Suanez et al. 2010) have also considered the intertidal part of the beach and highlight that the eastern part of the beach, corresponding to profiles 1 to 3, shows an important long term erosion trend. This intense erosion of the eastern beach-dune system of Vougot was identified as resulting from the construction, at the eastern extremity of the site, of the Curnic jetty in 1974 (Fig. II.1b) that interrupts the westward longshore sand drift. The jetty impact was demonstrated using aerial photography from 1952 to 2014 (Suanez et al. 2010) that illustrated the change



Figure II.2: Vougot Beach aerial view: Vougot Beach aerial photography seen from the eastern extremity, with the addition of the location of the 6 cross-shore profiles (named PF1, PF2, PF3, PF4, PF5, and PF6). *crédit: Serge Suanez and géosAEL*

in the Centre Nautique beach morphology and the progressive sand depletion on the western side of the jetty facing Vougot Beach (intertidal zone from 2004 to 2010 in Fig. II.3b). These observations are supported by the comparison between the volume of sand accumulated on the eastern side of the jetty and lost on the western side of the jetty along the beach between profiles 1 to 3 (Suanez et al. 2010). The estimation of the erosion rate following the jetty construction showed a maximum retreat rate of -0.6m/y over the 1978-2000 period and an increase to -1.5m/y in the 2000-2009 period due to the 2008 storm event at the dune toe elevation. The 2009-2013 period showed slow recovery of the front dune system (Fig. II.3b), however the energetic winter of 2014 induced significant erosion of the dune (almost -15m retreat of the dune toe position in 3 energetic winter storms), thus the eastern part of the beach showed a -0.7m/y erosion rate during the 2008-2014 period (Suanez et al. 2015). The recent data from 2014-2019 showed a new slow recovery phase of the eroded dune with the observed growing of vegetation as well as sand accumulating at the dune toe (embryo dune development).

Because of the 7m tidal range, the phase between the high tide (and even more spring high tide) and energetic storm events is crucial in the beach response to the event, as it changes the altitudes that are potentially reached and affected by the wave run-up as well as extent of the active surf zone where sediment transport processes are most active. As a result, the wave effects on the dune during

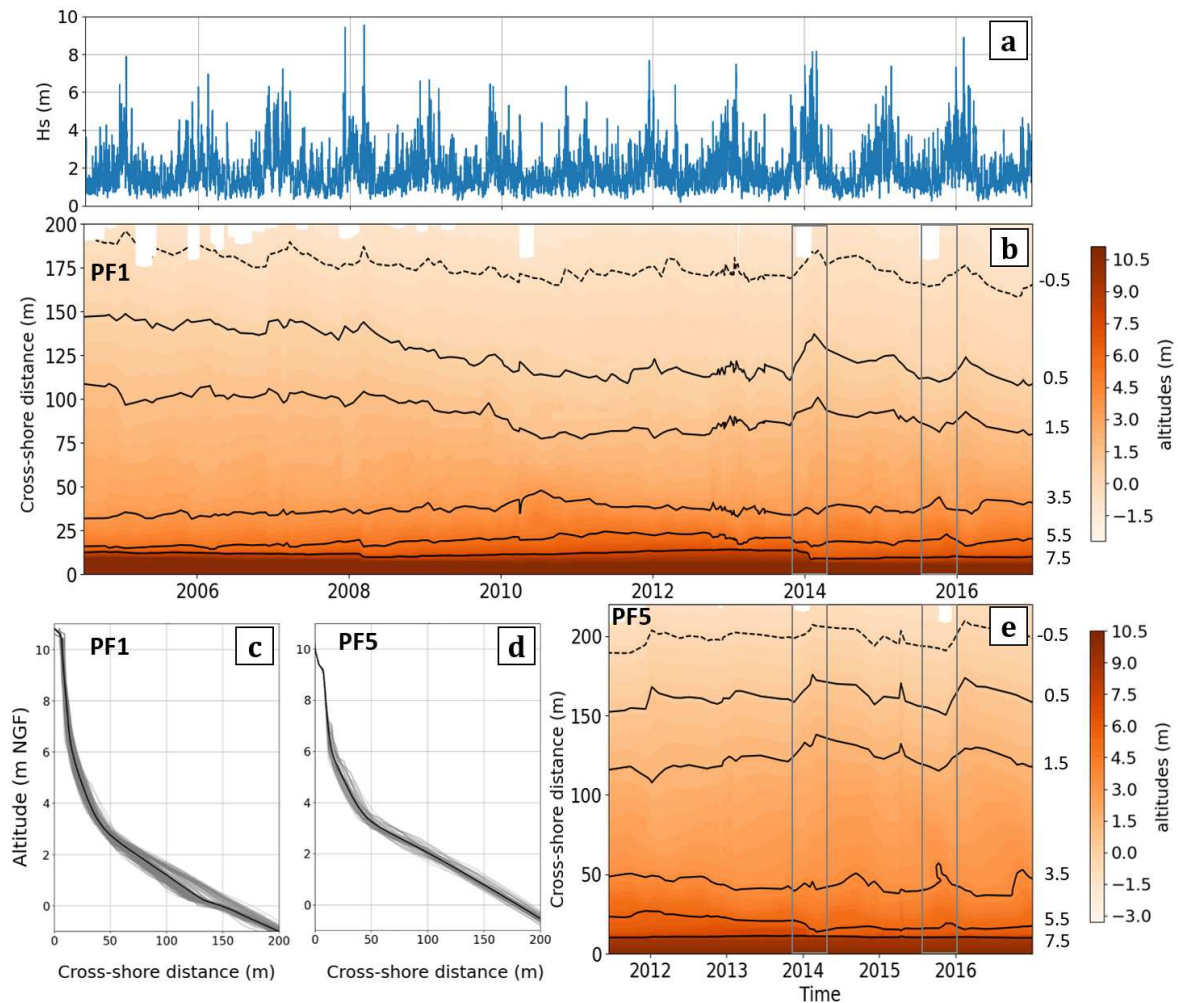


Figure II.3: Vougot Beach hydrodynamics and morphodynamics: (a) H_s from 7km northwestward offshore HOMERE node (Bouidière et al. 2013), (b),(e) Contour elevation position time series from the dune to the intertidal zone of profile 1 and profile 5, respectively (with certain contour elevation time series highlight in black and associate elevation value indicate on the right side), (c)(d) Envelope of Profile 5 and 1, respectively, with the mean profile position for the observed time (solid black line).

a particular event, are highly linked to the phase of the tide. Thus a storm occurring at spring high tide would strongly affect the dune system, like the 3 major storms of the 2014 winter cluster (the storms Petra, Ulla and Christine, on the 05/02/14, 14/02/14 and 03/03/14 respectively) (Blaise et al. 2015). However, observations show that the first storm effectively impacted and eroded the dune, but it also flattened the beach profile forming a more dissipative shape, such that the 2 subsequent storms didn't eroded the dune with the same intensity.

The observations show cross-shore exchanges of sediment between the lower and upper part of the intertidal zone at inter-annual time scales, with accretion at lower altitudes during energetic events while the upper part is eroded, and the inverse in calmer conditions (Fig. II.3a,b,e event of winter 2014 and 2016 for example in the grey box).

II.2 Narrabeen-Collaroy Beach

II.2.1 Beach geomorphology

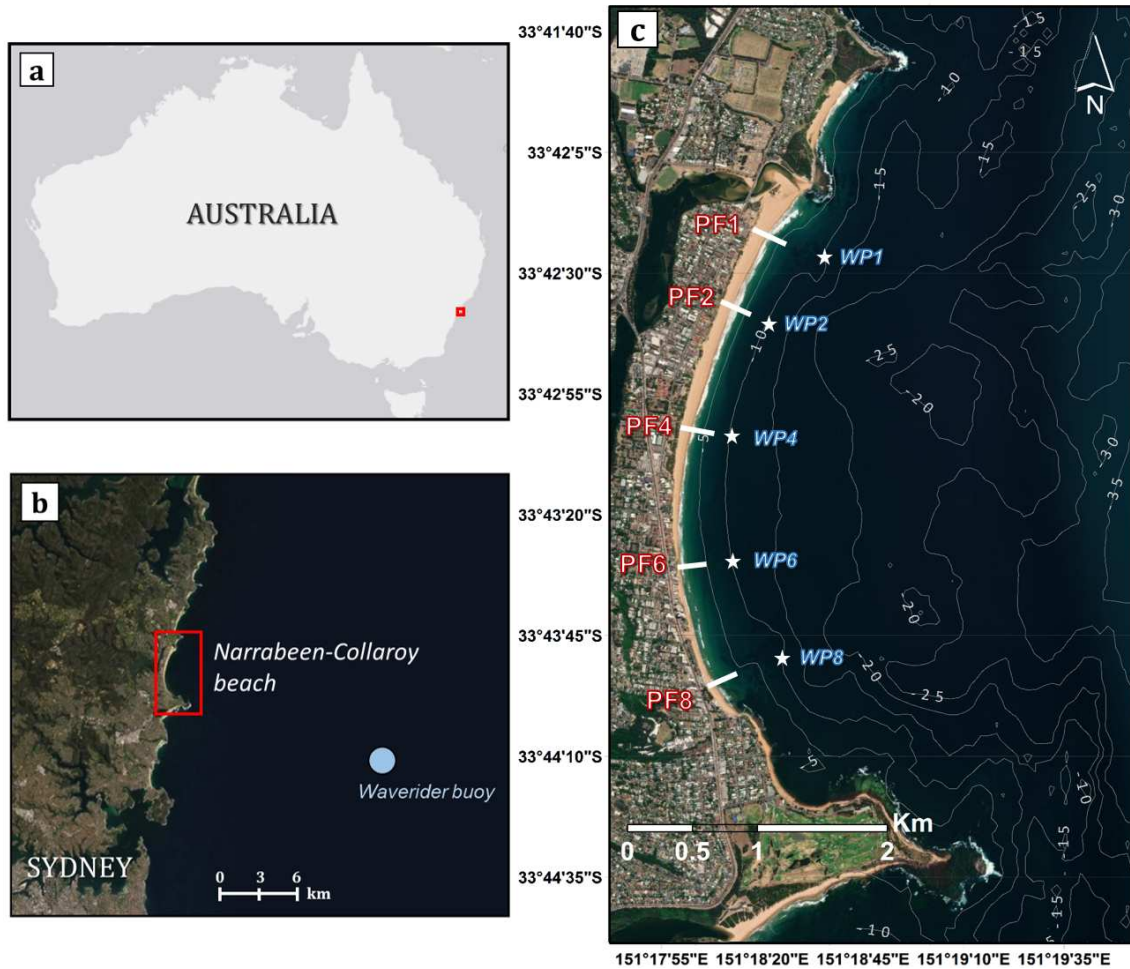


Figure II.4: Narrabeen-Collaroy beach: (a) map of Australia indicating the zoom shown in (b), (b) satellite image around Narrabeen Beach, showing the location of Sydney and the offshore wave buoy, and (c) aerial photograph of Narrabeen Beach showing the location of the 5 surveyed cross-shore profiles (named PF1, PF2, PF4, PF6, and PF8) and the 5 locations of wave condition estimates (WP1, WP2, WP4, WP6, and WP8). The bathymetry contours are shown every 5 meters (in grey).

The Narrabeen-Collaroy embayment is a 3.6km-long sandy beach situated in southeast Australia, to the north of Sydney (Fig. II.4). The embayment consists of Narrabeen Beach at the northern end and Collaroy Beach at the southern end, and is hereafter referred to as Narrabeen Beach for simplicity. The southeastern coast of Australia contains more than 700 embayed beaches (of on average 1.3 km length) that are delimited by rocky headlands, with sediments filling local bays deposited progressively in the mid-Holocene as a regressive barrier at a position located landward compare to the actual shoreline (around 300m) (Short 2007).

Like the other embayed beaches on this coastline, Narrabeen is bordered by two rocky headlands at

the northern and southern extremities, with rocky substrate extending underwater to approximately 60 m depth.

Reefs are also present from 5 m to 10 m water depth in front of both extremities of the beach (as can be seen partially in the satellite image in Fig. II.4c in front of cross-shore profiles PF1 and PF8). The beach is backed by a vegetated foredune (up to 9m above sea level) at the northern end, the dune height decreases to reach around 3 to 4m at the southern end where it's backed by a seawall. At the northern extremity, the beach is also backed by a lagoon that is connected to the ocean by a shallow and narrow inlet that opens and closes intermittently. Thus, the mouth of the lagoon breaches the dune occasionally north of PF1 and can act as a source or sink of sediment for the beach (Harley et al. 2011).

Narrabeen Beach is characterized by fine to medium quartz sand ($D_{50} \approx 0.3$ mm) that is nearly uniform alongshore (Turner et al. 2016) with $\approx 30\%$ carbonate fragments.

The headlands at the extremities of the beach and the curvature of the bay generate alongshore gradients in wave energy caused by wave refraction over nearshore bathymetry, reefs and shoals (Fig. II.4c). The effects of wave sheltering are more dominant at the southern end of the beach owing to the presence of the 1.5 km-long rocky headland and the predominantly southeasterly incident waves, but sheltering effects also exist at the northern end of the beach for less-frequent northerly incident waves (Fig. II.5). This differences in the wave exposure generates alongshore differences in the morphodynamic beach state as defined by Wright & Short (1984): it changes from a higher energy, longshore-bar trough beach state in the north to a lower energy, low tide terrace/reflective beach state in the south (Harley et al. 2011).

II.2.2 Hydrodynamic conditions

Narrabeen Beach is a semi-diurnal, micro-tidal environment with a mean spring tide of less than 1.5 m. The Sydney waverider buoy, located 11 km offshore in 80 m water depth (Fig. II.4b), has recorded directional wave conditions since 1992, which are supplemented by hourly hindcast waves from WAVEWATCHIII model (Tolman 2009) set up by the Centre for Australian Weather and Climate Research (Durrant T. & C. 2014) to fill data gaps due to buoy maintenance/dysfunction.

The offshore wave climate ranges from moderate to high wave energy (mean $H_s \simeq 1.6$ m and $T_p \simeq 10$ s), with dominant long-period swell waves impacting the beach from the south-south-east (SSE) direction. In addition, storm waves (defined as $H_s > 3$ m) are generated by tropical cyclones to the northeast, east-coast lows from the east, and cyclones from the south (Turner et al. 2016).

Nearshore, the mean H_s ranges from 1.15 m at the northern end of the beach to 0.76 m at the southern end of the beach due to sheltering effects (colorbar in Fig. II.5 WP1 and WP8). The nearshore bathymetry (Fig. II.4c) induced wave refraction, thus the mean wave direction are more southern in the northern part of the beach and become more westerly oriented at the southern extremity (roses in Fig. II.5 from WP1 to WP8).

The regional wave climate induces a seasonal cycle with change in wave direction and with higher energy conditions in the austral winter and lower energy conditions in the austral summer (Ranasinghe et al. 2004).

In addition, the beach is influenced by the El Niño-Southern Oscillation (ENSO) at interannual timescales (approximately 3 to 7 years), resulting in more energetic and easterly waves impacting Narrabeen Beach during la Niña periods and less energetic and more southern waves during El Niño periods (Harley et al. 2010).

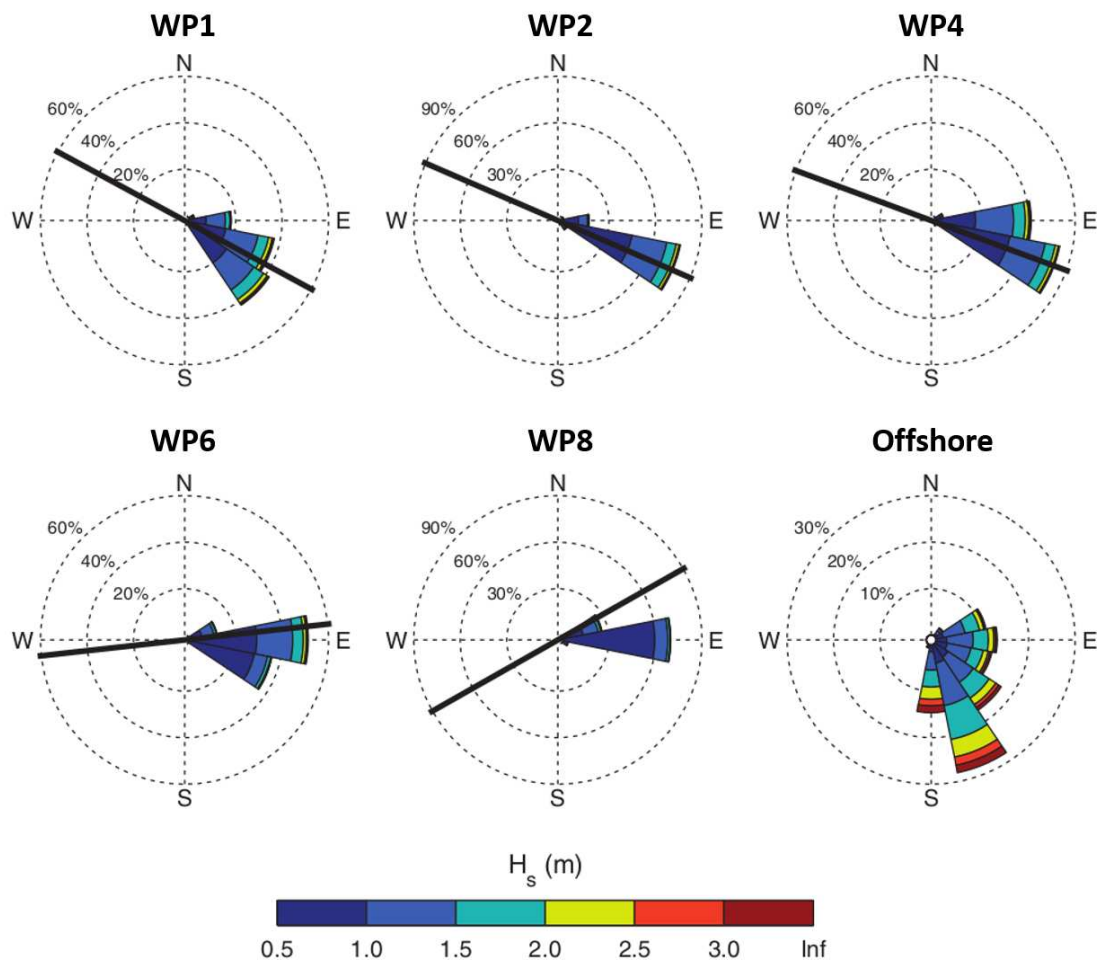


Figure II.5: Wave roses in 10 m water depth offshore of each profile and in 80 m water depth 11km offshore at the Sydney wave buoy. The black line indicates the respective profile transect orientation (from Turner et al. (2016)).

II.2.3 Data and beach morphodynamical behavior

Beach sand levels have been measured along 5 historical profiles (PF1, PF2, PF4, PF6, and PF8, as shown in Fig. II.4c) at approximately monthly intervals since 1976. The surveys were completed by

the members of the Coastal study unit of the University of Sydney using, from 1976 to 2004, a simple Emery-based method, and then from 2004 onward, more modern DGPS surveys. The surveyed profiles extend from the landward benchmark to the limit of water (at low tide).

The offshore wave data from the wave buoy are transformed into wave conditions along the 10 m depth contour in front of each profile (WP1 to WP8 in Fig. II.4c and Fig. II.5) using a look-up table generated with a series of hundreds of SWAN spectral model runs (Turner et al. 2016).

This high spatial and temporal resolution dataset consisting of topographic measurements and hourly wave conditions at 5 cross-shore profiles along Narrabeen Beach (described in detail by Turner et al. (2016)) is freely available at <http://narrabeen.wrl.unsw.edu.au> and is the principal reason for the choice of this particular site.

The observed morphological changes at the 5 cross-shore profiles show limited long-term changes in shoreline position estimated as the cross-shore location of the $z=0$ m altitude (for example, the maximum linear trend rate over all profiles is obtained at PF4 with a rate of $\approx -0.5\text{m/yr}$ for the 35 years of observations, Harley et al. (2011)). However, significant seasonal, annual, and inter annual variability is observed, with a mean value of 71 m for the overall range (min/max) of variability of the shoreline cross-shore position, estimated across all profiles.

Seasonal variations in shoreline position show primarily accretion during the austral summer and erosion during the austral winter due to the variation in the hydrodynamic conditions.

Using 30 years of the profile observations, Harley et al. (2011) show that the beach rotation signal observed at Narrabeen results not only from alongshore sediment transport but also from alongshore gradients in cross-shore sediment transport, which has an important role at Narrabeen (e.g. the mean wave height is greater in the northern end than in the southern extremity (color variation between WP1 and WP8 in Fig. II.5)).

Harley et al. (2015) completed an EOF (empirical orthogonal function) analysis of 5 years of extensive 2D surveys of the beach topography, the analysis results are summarized in a conceptual model of the three different physical processes that were identified to cause planform rotation (Fig. II.6). They identified: the planform rotation due to alongshore variability in wave exposure (explaining 55% of overall variability), the planform rotation due to reversing alongshore currents and the planform rotation due to differences in sandbar processes between the two embayment extremities (both explaining 22% of overall variability).

The second mode is driven by longshore sediment flux as seen in classic rotation approach but the modes 1 and 3 are controlled by the alongshore variability of the cross-shore sediment fluxes. The first process, corresponding to cross-shore migration, is an onshore-offshore sediment exchange, and its intensity is controlled by the wave height at breaking (Fig. II.6 (1)).

Thus, due to alongshore gradients in breaking wave height, this process generates a rotation of the beach planform that is not associated with longshore sediment transport processes. The second component is associated with longshore sediment transport processes caused by both the incident wave angle and alongshore gradients in wave conditions, as described above (Fig. II.6 (2)).

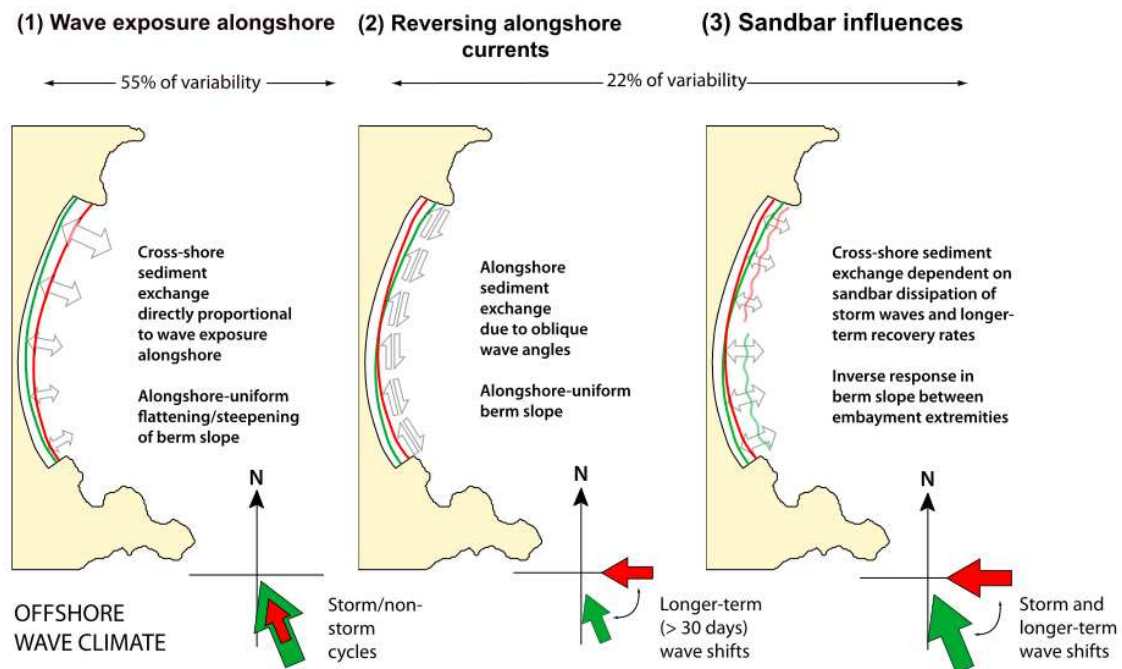


Figure II.6: Conceptual model of the 3 different planform rotation modes observed in (Harley et al. 2015). The red/green arrows represent the direction and magnitude of the offshore wave climate associated with the respective red/green embayed beach planform, while the grey arrows represent the magnitude and direction of sediment transport (scheme from Harley et al. (2015))

They point out that these 3 modes of shoreline rotation correspond to 3 different time scales of wave forcing with increasing time scale from mode 1 to mode 3 (see wave climate description at the bottom of Fig. II.6).

Their study validates that the center of the beach acts as a pivot point for the variation in intensity of the alongshore sediment transport, the "classical" rotation mode. But they also highlight that this area is a morphological transition zone for the cross-shore sediment rate intensity between the northern exposed and southern more sheltered part of the embayment (Fig. II.6 (1) and (3)).

Chapter III

Cross-shore modeling

Ce chapitre s'intéresse à la modélisation des processus cross-shore utilisant le modèle d'équilibre de la position du trait de côte de Yates et al, (2009). Ce modèle empirique est basé sur le concept d'équilibre du profil de plage pour reproduire l'évolution de la position du trait de côte sous l'action des vagues. Il utilise 4 coefficients qui sont calibrés à partir des observations. Les hypothèses et les limitations du modèle sont discutées, puis la méthode d'optimisation des coefficients du modèle, le recuit simulé, est décrite, et enfin une analyse de sensibilité des paramètres de cette méthode est réalisée pour quantifier l'effet de ces paramètres sur la convergence de l'optimisation. Le modèle cross-shore est ensuite appliqué au site du Vougot pour évaluer sa capacité modèle sur un site mixte où les processus longshore contribuent à l'évolution morphologique. Le modèle est appliqué à différentes altitudes le long du profil de plage pour évaluer les variations des performances du modèle dans la zone intertidale et le haut de plage. L'analyse des résultats montre que la performance du modèle empirique est variable à la fois le long d'un profil et dans la direction longshore. Le long du profil de plage, le modèle reproduit bien les contours situés dans la zone intertidale et devant le pied de la dune, mais il montre une moins bonne capacité autour du niveau de marée haute de morte-eaux, correspondant à la zone de transition entre les parties réfléchives et dissipatives du profil. La dynamique dans cette zone de la plage est trop complexe pour être représentée avec un simple modèle empirique d'évolution de la position du trait de côte, puisque cette dynamique est dépendante de la forme de l'ensemble du profil. Dans la direction longshore, le modèle montre de meilleures performances à l'extrémité Ouest de la plage qu'à l'extrémité Est, où l'influence des processus longshore semble être plus importante dans l'évolution morphologique de la plage. Lorsque des tendances à long terme existent dans l'évolution de la position du trait de côte, l'algorithme d'optimisation identifie et sélectionne des minima correspondant à des sets de coefficients qui permettent au modèle cross-shore de reproduire de telles tendances à long terme, aux dépens de la qualité dans la reproduction de la variabilité saisonnière. Ce résultat met en évidence le potentiel d'amélioration du modèle avec l'intégration des processus responsables de ces tendances à long terme.

Chapter III

Cross-shore modeling

This chapter presents the empirical cross-shore equilibrium model used during this thesis work, including its formulation, the conceptual limitations, and the calibration method used to determine the model free parameters, completed using an optimisation algorithm. Then, the next section consists of the application of this model to the complex, macrotidal Vougot Beach to analyze and discuss the cross-shore model performance and limitations in this environment.

III.1 Empirical cross-shore equilibrium model

III.1.1 Model formulation and hypothesis

The empirical cross-shore model used is based on the equilibrium shoreline change model developed by Yates et al. (2009). This kind of empirical model is based on the beach equilibrium profile hypothesis (Dean 1977), as described in Chapter I. Thus, the approach makes the assumption that the shoreline position tends toward an equilibrium position when exposed to a constant wave energy. This constant wave energy will be called the equilibrium energy, E_{eq} .

The estimated E_{eq} can be compared to the instantaneous incident wave energy $E(t)$, if this incident energy is different from the equilibrium energy, the beach profile will adjust by either accreting or eroding depending of the considered part of the profile and the sign of disequilibrium in wave energy. This results in a change in the shoreline position of the beach.

This model was developed and initially applied to simulate the shoreline position in microtidal environments, but it has been tested and extended to be applied at all altitudes of the beach profile. Thus, the beach contour change is proportional to the energy disequilibrium, ΔE , between the incident energy and the equilibrium energy.

Yates et al. (2009) proposed a cross-shore shoreline change model composed of a single differential equation:

$$\frac{dS}{dt} = C^{\pm} E^{1/2} \Delta E \quad (\text{III.1})$$

that relates the cross-shore evolution in time of the contour position at a given altitude of the beach, $S(z, t)$ to the incident wave height \sqrt{E} and to the energy disequilibrium ΔE , with a coefficient representing the erosion or accretion change rate C^{\pm} . The term \sqrt{E} is mean to assure that there's no morphological change happening when the incident energy tends to 0. The sign of the coefficient C^+ or C^- is determined by the sign of the energy disequilibrium. The energy disequilibrium ΔE is calculated as :

$$\Delta E(S, t) = E(t) - E_{eq}(S), \quad (\text{III.2})$$

where E_{eq} is the equilibrium energy that is assumed to be a linear function of S :

$$E_{eq}(S, t) = aS(t) + b, \tag{III.3}$$

with a and b the slope and the intercept of the linear relation between the wave energy and the observed contour position. This line is a mathematical representation that expresses, for a given altitude of the beach profile, the equilibrium energy associated with the contour position in regard with the equilibrium profile position.

The four coefficients a , b , C^+ and C^- are obtained by calibrating the model results with morphological observations using an optimisation algorithm described in section III.2. The conceptual framework of the model used in this thesis work is presented in Fig. III.1.

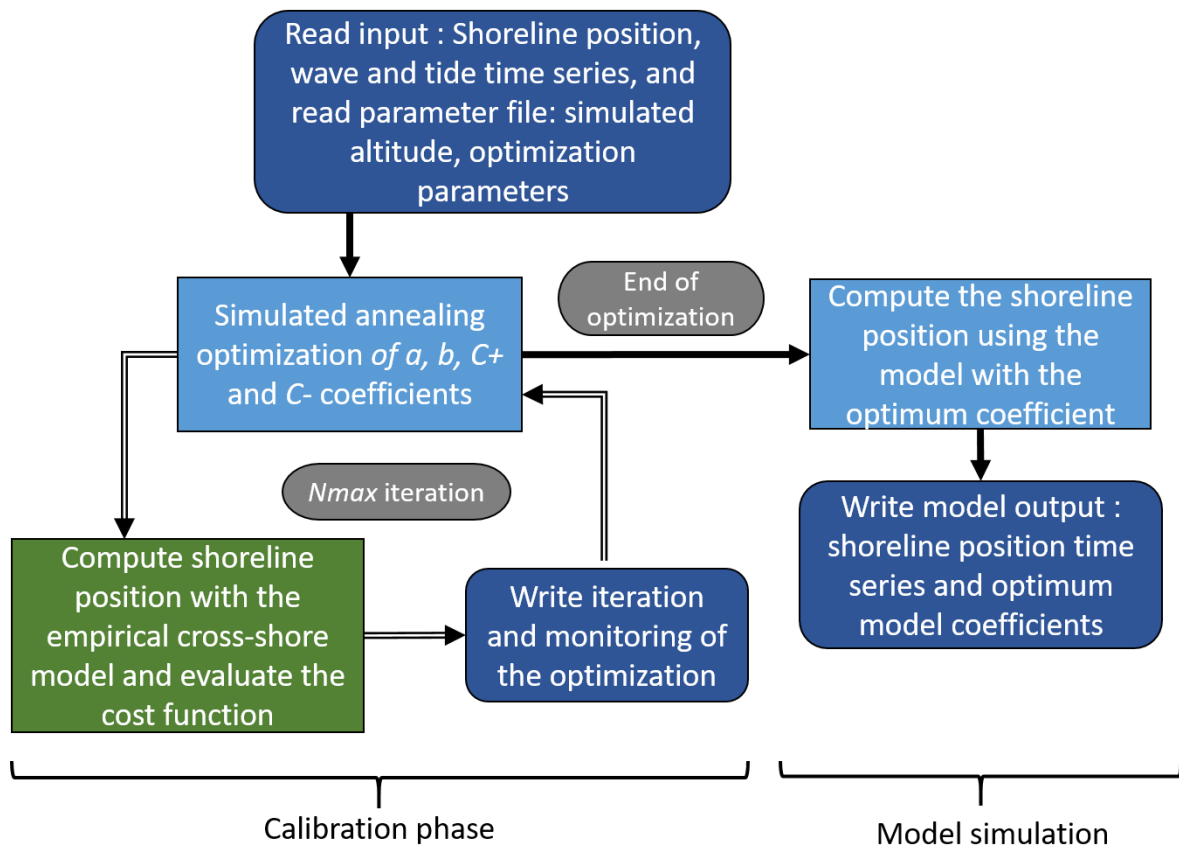


Figure III.1: Global framework of the empirical cross-shore shoreline change model

The original model was modified by [Castelle et al. \(2014\)](#), who added an additional parameter, d , that corresponds to a potential change of the initial position of the model contour position to lessen the model dependency on the initial position used.

However, this parameter is not considered in this thesis work since it has a minimal impact of the initial contour position and the use of the observation for this position. Then, as performed on the microtidal beach of Ocean Beach by [Yates et al. \(2011\)](#) by looking at the model skill at the

Mean Higher High Water level, [Castelle et al. \(2014\)](#) also applied the model at different altitudes of a mesotidal beach and not only at the Mean Sea Level used as reference level for the microtidal environment for initial model application ([Yates et al. 2009](#)). Thus it shows the model skill at reproducing contour position changes at different elevations in a different type of tidal environment.

Finally, [Lemos et al. \(2018\)](#) applied the model at the macrotidal beach of Porsmilin (Brittany, France) at a range of beach elevations along the intertidal beach profile to assess the capacity of the model as a function of the position in the intertidal zone. They also modified the model to account for the impacts of the water level on the cross-shore evolution of the contour position.

The approach they implemented consists of the application of a binary function to activate the model (or not) depending on a water depth threshold that integrates the instantaneous tide level ($\eta(t)$) at each given beach altitude Z . The water depth threshold is based on defining the active surf zone using an empirical cutoff that is a function of the instantaneous wave height $H_s(t)$ (Fig. III.2). This approach enables representing the covering and uncovering of the beach by the tide, applying two hypotheses:

- First, for a given moment of the tide, the beach profile part located at an altitude above the position reached by the run-up undergoes no changes by the wave action (Fig. III.2).
- Second, the profile region located deeper than a certain water depth (here, lower than the breaking zone water depth) is not significantly impacted by the wave action (Fig. III.2).

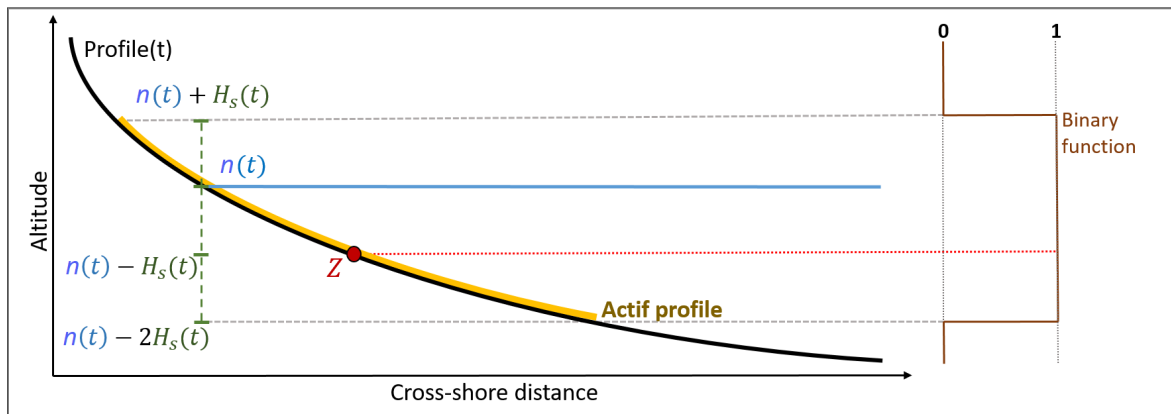


Figure III.2: Scheme of the adaptation of [Lemos et al. \(2018\)](#) of the equilibrium model to account for water level η depending on a threshold based on the wave height H_s

If the considered contour altitude is within the region where the binary function is equal to 1 (Fig. III.2) at a given time step, the cross-shore model is applied normally, otherwise the contour position is not modified during this time step. These vertical thresholds were estimated by [Lemos et al. \(2018\)](#) for a given altitude of the tide $\eta(t)$ as $\eta(t) + 1H_s$ for vertical extent of the wave runup, and $\eta(t) - 2H_s$ for the water depth limiting the breaking zone. A more detailed representation of the modification made by [Lemos et al. \(2018\)](#) is presented in Fig. III.2 that incorporates the water level modification.

III.1.2 Model limitations

The cross-shore model as presented has several limitations. First, accounting only for cross-shore processes is insufficient on most beaches when considering increasing time scales (i.e. toward long timescale) where the relative importance of other processes, such as longshore processes or Mean Sea Level change, increases.

The second important limitation of this approach is that, due to the empirical coefficients in the model, this approach needs observational data at sufficient frequency and duration for the calibration. [Yates et al. \(2009\)](#) highlighted that the model RMSE increased when the length of data used for the calibration phase decreased, with an increase of the RMSE of 30% when using only 1 year as opposed to 4 years of monthly observations at Torrey Pines Beach (California).

The generalization of the model coefficients, for this kind of approach, can lessen the dependency on data availability. However, it requires an important database of model applications (and associated coefficients) for a wide variety of beaches to assess the link between beach morphological characteristics and model coefficient values.

When applied at different beach elevations as proposed in [Castelle et al. \(2014\)](#) or [Lemos et al. \(2018\)](#), this approach can effectively reproduce cross-shore contour position changes due to wave action at different elevations of the beach. However, from the model conception, the contour positions estimated at one altitude are independent of the contour position estimates at other altitudes. Thus, if the model is used to try to reproduce beach profiles, the profile reconstruction at a given instant can potentially present non-physical behavior where a given contour position is more seaward than a contour position located at a lower altitude, which is an unstable situation.

Furthermore, when using this approach at several altitudes, the independency of each altitude implies that this approach is non conservative of the beach sediment volume, this should be kept in mind when looking at cross-shore sediment exchanges between the lower and upper intertidal zone.

Finally, this model is formulated from the equilibrium theory, which implies that the contour position evolves around a constant equilibrium position. Thus, this approach, as described here, shouldn't reproduce long term trends for example, due to shoreline retreat from sea level rise, or from anthropic actions causing changes in beach sediment supply, but only from long term trends existing in the wave forcing conditions.

III.2 Empirical cross-shore model optimisation

The coefficients of the cross-shore model require a calibration phase using the observations to find the best set that minimize the RMSE error between the model contour position and the observations during the calibration period. The optimisation process is achieved by using the simulated annealing probabilistic optimisation method from Kirkpatrick et al. (1983) and Černý (1985).

This optimisation approach has the advantage of being less affected by local minimum as compared to simpler methods (e.g. hill climbing method). Its mathematical functioning is based on the Markov Chain principle. The Markov chain is a stochastic model describing a succession of feasible events where the probability of each of them depends solely on the state attained in the previous event. In simulated annealing, the Markov chain is used as a basis in a Markov chain Monte Carlo method, which is here used for sampling from complex probability distributions of the transition state.

Simulated annealing is specifically inspired from the thermodynamic process of the slow cooling of a heated solid. The interest of such an approach is that it is based on statistical mechanics explaining that if the cooling is slow enough, the solid will end in the lowest thermodynamic free energy configuration. By analogy, this state corresponds to the global minimum of the cost function in an optimization. Here, the cost function for the equilibrium shoreline model is taken as the sum of the error between the observed and the modeled contour position.

A simulated annealing algorithm is used to determine the 4 free coefficients a, b, C^+ and C^- in the model, but this optimisation method is itself controlled by several parameters that need to be defined:

- total number of iterations: $Nmax$,
- initial temperature: T_0 ,
- temperature decrease coefficient: $CoeffT$, which varies between 0 and 1, and
- number of “exploration” iterations between each temperature drop: $Ntmax$.

In each iteration, the simulated annealing algorithm is considering some neighboring state of the current state (here, the state corresponds to the set of values of the model coefficients), then the method probabilistically chooses between staying in the actual state or moving to the neighboring state. This probability of acceptance is evolving with the decreasing temperature coefficient $CoeffT$, to lead the algorithm toward the global minimum of the cost function.

In case of non improvement of the cost function value after considering several (here $Ntmax$) neighboring states, the algorithm return to its previous optimum state and restarts explore neighboring states until the number of iterations reaches $Nmax$.

The effects of these parameters in the optimisation algorithm on the coefficients and model results has been investigated to identify the values that produce the optimum set of model free parameters with the highest repeatability.

Preliminary tests at Vougot Beach showed important differences in the model free coefficients when optimized when using identical optimisation parameters, resulting in large variability in the empirical model results.

These tests were performed using profile observations at Vougot Beach, in particular for profile 6, using contour position every 0.1 m at elevation 1 m to 1.5 m, where a suspiciously large variability of model performance from one elevation to another were observed during the preliminary application of the model.

Thus the model was applied at these 5 elevations to evaluate the repeatability of the optimization results by varying the simulated annealing parameter values and then performing 10 repetitions of the optimization process using identical parameters. These 10 repetitions allow analyzing the variability of the optimum coefficients and the resulting equilibrium model skill. In particular, a large range of $Ntmax$ values, $CoeffT$ values and associated $Nmax$ values were tested.

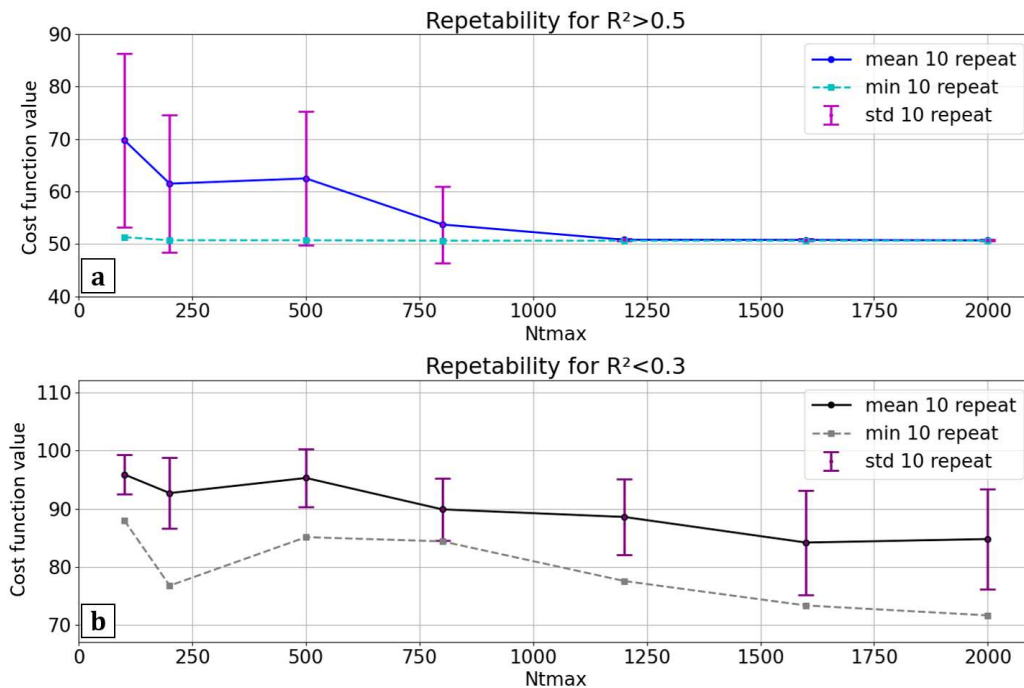


Figure III.3: Impact of $Ntmax$ on the cost function value for 10 repetitions of the optimisation algorithm at profile 6 with the same parameters for (a) a well reproduced contour position time series ($R^2 > 0.5$, see eq. III.5) and (b) a badly reproduced contour position time series ($R^2 < 0.3$), showing the mean value, minimum value, and standard deviation of the cost function for both cases.

The tests performed allowed identifying that the differences in the coefficients obtained from identical repetitions of the optimisation process were most strongly controlled by the $Ntmax$ parameter. This parameter corresponds to the number of iterations before returning to the optimal solution. Thus, the number of tests at each “temperature” is highly important, and increasing this parameter allows enhancing the optimisation quality and repeatability of the algorithm by increasing the probability of finding the true minimum of the cost function (Fig. III.3a).

However, increasing $Ntmax$ requires also increasing the total number of iterations $Nmax$ to allow the system to reduce progressively the search radius. The method's principle goal is to decrease the temperature to reach the global minimum of the cost function, thus if the temperature is not low enough at the end of $Nmax$ iterations, the optimal result has not necessarily been identified.

The parameter $Nmax$ can be set to a higher value, but increasing $Nmax$ increases the calculation time of the optimisation, however this is not a limiting factor as the optimization is effectuated only once. To limit the value of $Nmax$, the $CoeffT$ parameter can be decreased. This parameter controls the geometric rate of temperature drop of the system of $T * CoeffT$ every $Ntmax$ iterations. Yet, the method implies that the temperature should decrease slowly enough to maintain the system stability, and thus this parameter should remain close to 1.

The results obtained for different values of $CoeffT$, ranging from 0.8 to 0.99 show that the repeatability decreases and the optimum value of the cost function increases rapidly when the value of $CoeffT$ decreases (Fig. III.3).

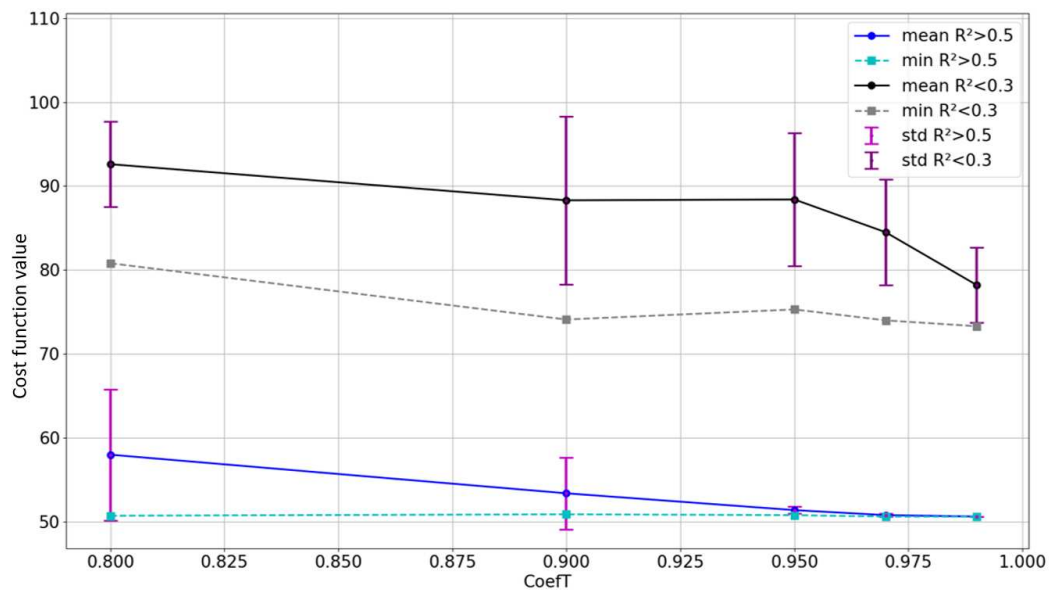


Figure III.4: Effect of changing $CoeffT$ on the cost function value for 10 realizations of the model optimisation at profile 6 for a well-reproduced contour position time series ($R^2 > 0.5$) showing the mean value, the standard deviation and the minimum value of the cost function and on a badly reproduced contour position time series ($R^2 < 0.3$)

The completed tests allow defining a range of acceptable values for the different optimisation parameters, and estimating the associated uncertainties in the cross-shore model results. For example, the tests highlight that the method sensitivity to a decrease in $CoeffT$ requires to set the value $CoeffT > 0.98$ based on the observed uncertainty in the minimum cost function.

The test also highlights that the repeatability of the simulated annealing optimisation is affected by the model performance. This is shown in Fig. III.3 and Fig. III.4, where the standard deviation of the cost function doesn't decrease for the case where the optimum model skill has a low corre-

lation with the observations, $R^2 < 0.3$, compared to the case where $R^2 > 0.5$, which shows a clear convergence.

This behavior for the case where observation and model agreement is low ($R^2 < 0.3$) is hypothesized to be due to the empirical model not being able to reproduce well the contour position as it results in no true minimum existing. Thus, the important residual error is reached by a larger range of coefficients.

III.3 Model application at Vougot Beach

III.3.1 Data processing and model configuration

The cross-shore model is applied at Vougot Beach at the 6 profiles (shown in Fig II.2) at different altitudes along the intertidal beach profile ranging from the beach front dune, at approximately +6m NGF, to the lowest altitude where observations were available, ~ 0 m to -1 m NGF, with a chosen spacing of 0.5 m.

Morphological data processing

The contour position $S_{obs}(t, Z)$ is computed from the (x, y, Z, t) position of each DGPS survey defining the origin of the profile at the top of the dune as the reference position (x_0, y_0) , corresponding to $S_{obs} = 0$ m.

The distance between each DGPS position and the reference position is calculated. Then, the time series of the contour position for a given beach altitude Z is obtained by interpolation of the $S_{obs}(t, Z)$ at the defined altitudes, for example at the Mean Sea Level, here located at 0.5m NGF (see Fig II.3).

Model evaluation criteria

These contour position time series are used for the model calibration and to evaluate the model skill. The model skill is analyzed using 3 different statistics, the *RMSE*:

$$RMSE(Z) = \sqrt{\frac{\sum_{t_i=1}^N (S_{obs}(t, Z) - S_m(t, Z))^2}{N}}, \quad (\text{III.4})$$

where S_{obs} and S_m are respectively the observation and the model contour position.

This statistic quantifies the contour position residual (in m), and thus is a measure of the model accuracy.

The coefficient of determination R^2 , represents the square of the correlation between the model and observations, or the proportion of variance explained by the model,

$$R^2(Z) = Cor(S_{obs}(Z), S_m(Z))^2. \quad (\text{III.5})$$

Finally, the Brier Skill Score (*BSS*) assesses how well the model reproduces the observed variance compared to a baseline:

$$BSS(Z) = 1 - \frac{\sum_{i=1}^n (S_{obs}(t, Z) - S_m(t, Z))^2}{\sum_{i=1}^n (S_{obs}(t, Z) - S_b(t, Z))^2}, \quad (\text{III.6})$$

where S_b is the baseline, which is defined here as the linear regression of the observed contour position, and n the number of observations.

The choice of the baseline here is to account for the improvement of the model reproduced contour position compare to a simple linear regression of the observations.

The *BSS* value ranges from negative values to 1, and a positive value indicates an improvement compared to the baseline. Typical values greater than 0.0, 0.3, 0.6 and 0.8 are qualified as ‘poor’, ‘fair’, ‘good’, and ‘excellent’, respectively, in the literature (Sutherland et al. 2004, van Rijn et al. 2003)

Hydrodynamic data

The model is run from 2005 to 2017 for profiles 1 to 3 and from 2011 to 2017 for profiles 4 to 6 using an hourly time step. The tide data are predicted tide levels calculated by the SHOM (French naval army) for the Brignogan harbour located 10km east of Vougot Beach.

Wave forcing selection

For the model forcing wave time series, the Homere wave database (Bouidière et al. 2013) was used. The Homere database is composed of sea states generated by the WAVEWATCH III model (version 4.1) on an unstructured grid that covers the French Atlantic coast from the Bay of Biscay to the English Channel.

The global model output parameters are available at $\approx 110,000$ nodes (Fig. III.5a) over the 23-year period from 1994 to 2016 (that continues to be updated to the present).

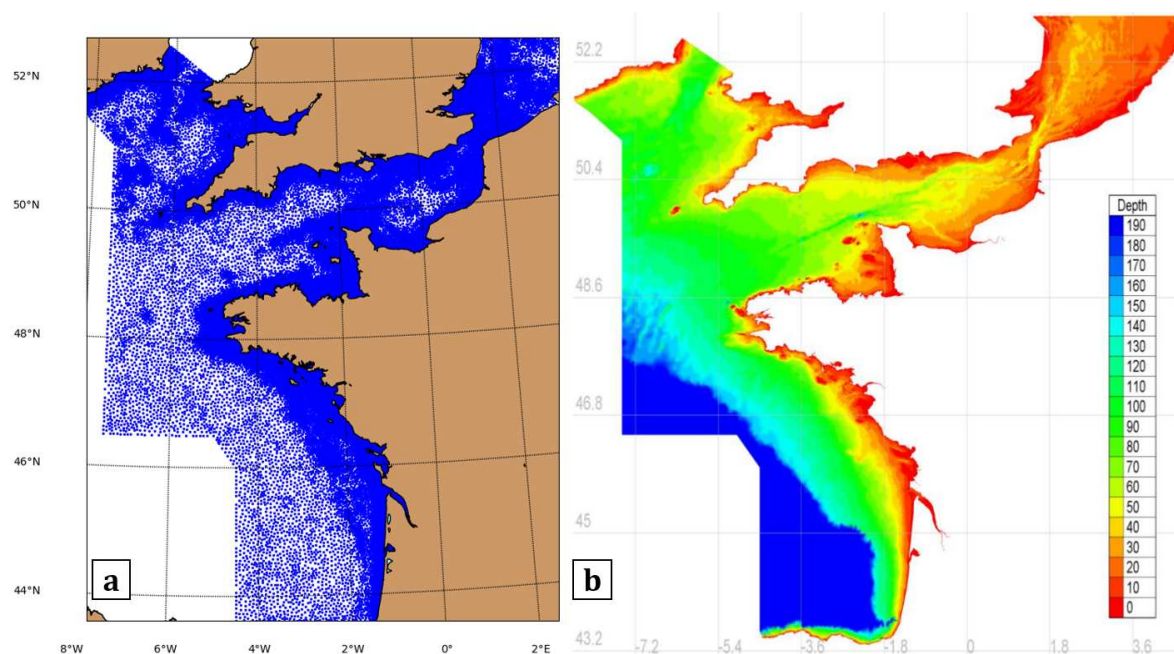


Figure III.5: Homere database domain extent (a) database output node locations, (b) bathymetry used in the wave model.

An analysis was performed on the choice of node used to force the morphological model and the

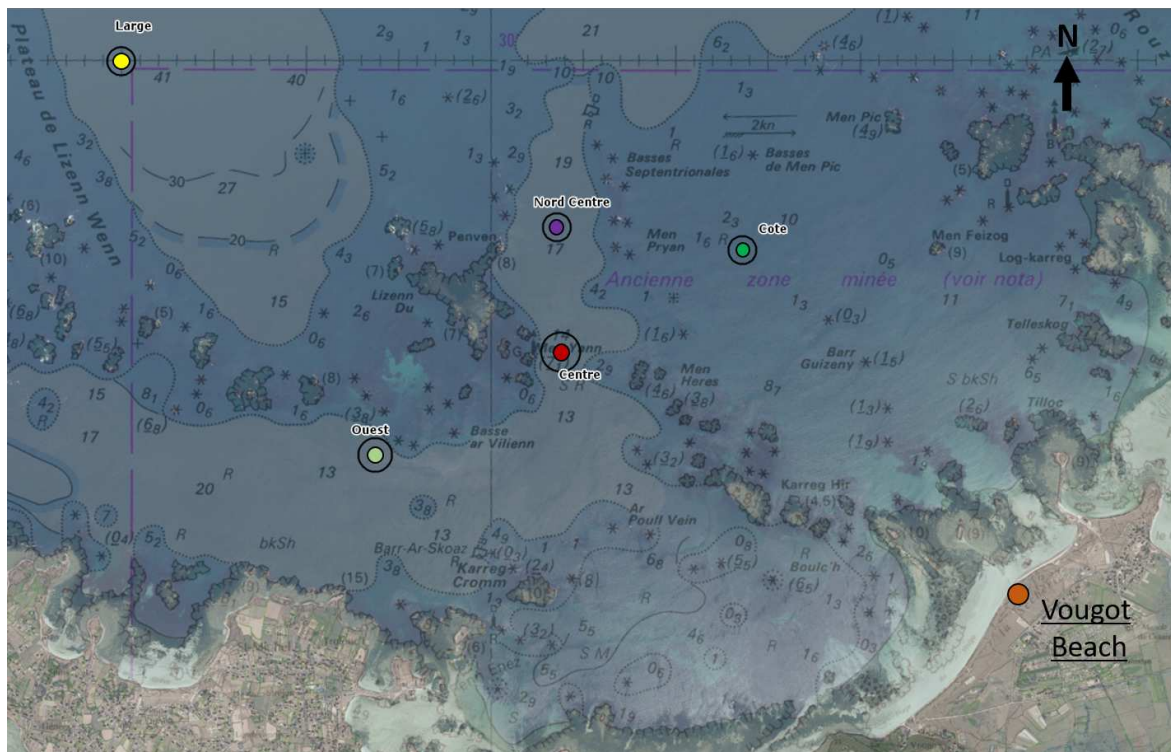


Figure III.6: Position of the different Homere database nodes used to select the wave forcing time series

associated effects on the model performance. The nearshore node selection was made to ensure that the chosen forcing wave conditions are representative of the waves impacting the beach. The difficulty in using the Homere wave database for this purpose is that the coastal bathymetry resolution is relatively coarse ($\geq 200\text{m}$ resolution) (Fig. III.5a).

In the case of a complex bathymetry like at Vougot Beach, this lack of resolution smooths or completely neglects important bathymetric variations, including some of the small rocky outcrops and even a small island, that may highly influence the nearshore wave propagation, and in particular, wave diffraction. This was evaluated by comparing the distribution of the wave direction at several nearshore positions located in the shadow of a small island (point "Ouest" and "Centre" in Fig. III.6 and Fig. III.7).

These 2 points show no difference in the wave direction compared to nodes not located the shadow of the island, thus suggesting that nodes located in the nearshore do not account fully for nearshore wave transformation processes (Fig. III.7). Unfortunately, nearshore wave observations were not available at this site, preventing the validation or estimation of errors associated with the wave data.

Furthermore, there's a large rocky platform located in shallow water (less than 10m water depth) in front of the eastern part of the beach that is also not taken into account in the spectral wave model (point "Cote" in Fig. III.6 and Fig. III.7).

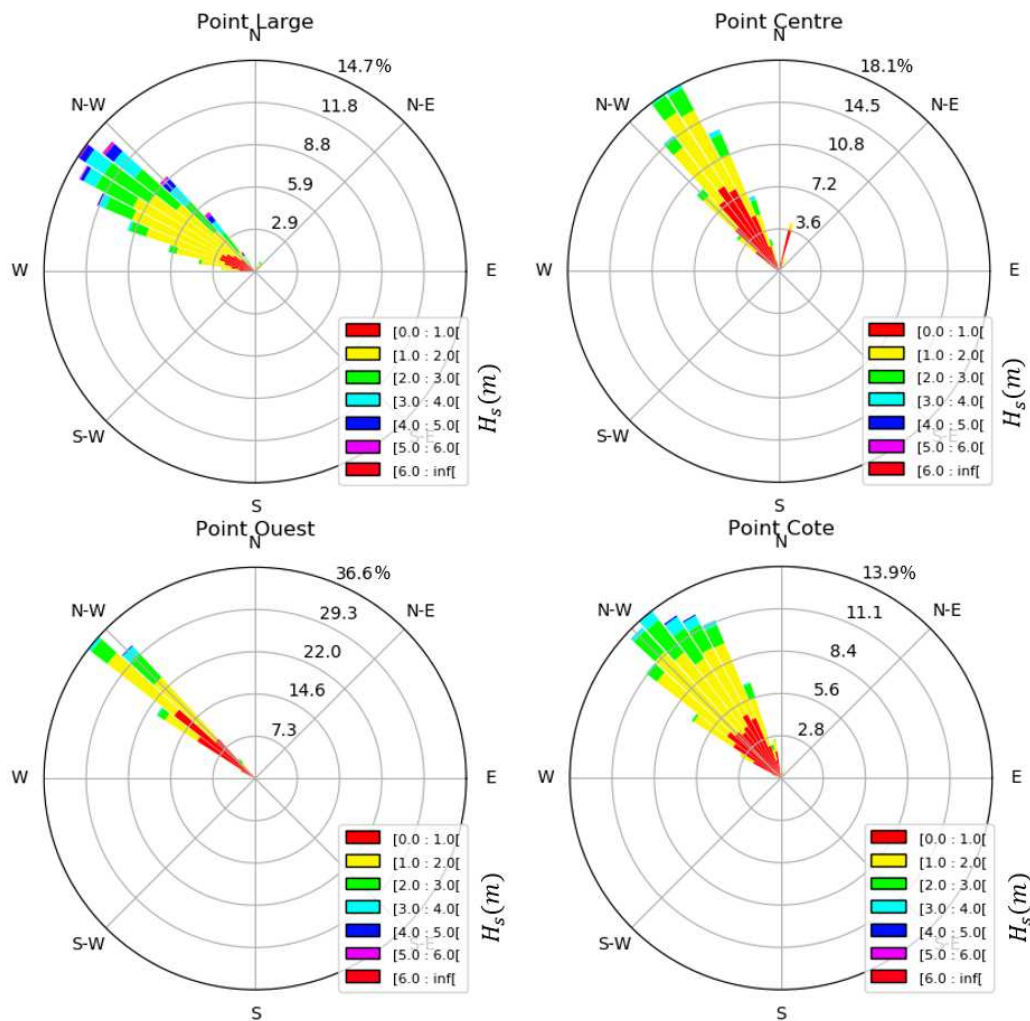


Figure III.7: Roses of Homere wave direction, with color based on the wave height occurrence, at 4 different nodes located on Fig. III.7.

Likewise, the point "Nord Centre" (Fig. III.6) was not selected since the comparison with the more offshore point "Large" shows that the wave direction distribution almost does not change despite the shallow rocky platform between these 2 points (Fig. III.7). Furthermore, it suggests that the dissipation observed in the wave height between these 2 points is then potentially incorrect.

Thus, the wave forcing conditions were finally chosen more offshore of the beach (in ≈ 40 m water depth) to ensure that the spectral model correctly represented the wave transformation offshore of this position (point "Large" in Fig. III.6). This output point is also located close to the WaveWatch III NORGAS-UG grid point used in previous studies (e.g. [Suanez et al. 2015](#)) at this beach.

III.3.2 Results of the model application

Modeled contour position

The shoreline model was applied from the lower intertidal zone (down to -1m NGF) to the upper beach and the dune toe (up to 6.5m NGF), and the coefficients were optimized using the observed contour time series extracted at each elevation (see Fig II.3).

The modeled contour position S_{mod} is compared with the observations S_{obs} and illustrated here at 3 elevations: on the upper beach at 5 m NGF, at 2.0 m NGF at approximately the Mean High Water Neap (2.1 m NGF), and at the Mean Sea Level (0.5 m NGF), for 3 profiles : 1 located in the western part of the beach (profiles 5, Fig. III.10), and 2 located in the eastern part, (profiles 1 and 3, Fig. III.8 and Fig. III.9, respectively).

For each contour time series, the associated model R^2 and BSS is shown in the legend to indicate the model skill.

For profiles 1, 2 and 3, a long term trend of erosion is observed in the contour position in the lower intertidal zone (below 3 m NGF). During the period 2004-2018, this trend reached a mean annual value of -4 m/y on profile 3 and -3 m/y on profiles 1 and 2.

On the contrary, at higher elevations, between 3 m and 6.5 m, the long term trend shows accretion of approximately $+0.3$ m/y. Thus this area is globally losing sand and is subject to an increasing sediment depletion.

At these profiles, the cross-shore model reproduced the contour position long term trend (e.g. Fig. III.8 and Fig. III.9), but was unable to represent the observed inter-annual and seasonal variations in the lower intertidal zone (e.g. up to 30 m variability on profile 3) for the given set of optimal model parameters.

Profile 4 shows long term erosion trends at all altitudes, while profile 5 experiences erosion along the upper beach, accretion from 3 m to 1 m NGF, and then slight erosion in the lower intertidal zone. Overall, the model reproduced well the contour position evolution at profile 5 (e.g. Fig. III.10a,c), with exception of altitudes located near ≈ 3 m NGF where the model reproduced only the long term trend of the observations (e.g. Fig. III.10b).

The contour position at profile 6 shows a long term trend of accretion at all elevations along the intertidal beach (not shown here). Similar to profile 5, the model reproduced well the contour variations but more the slight trend near ≈ 3 m NGF.

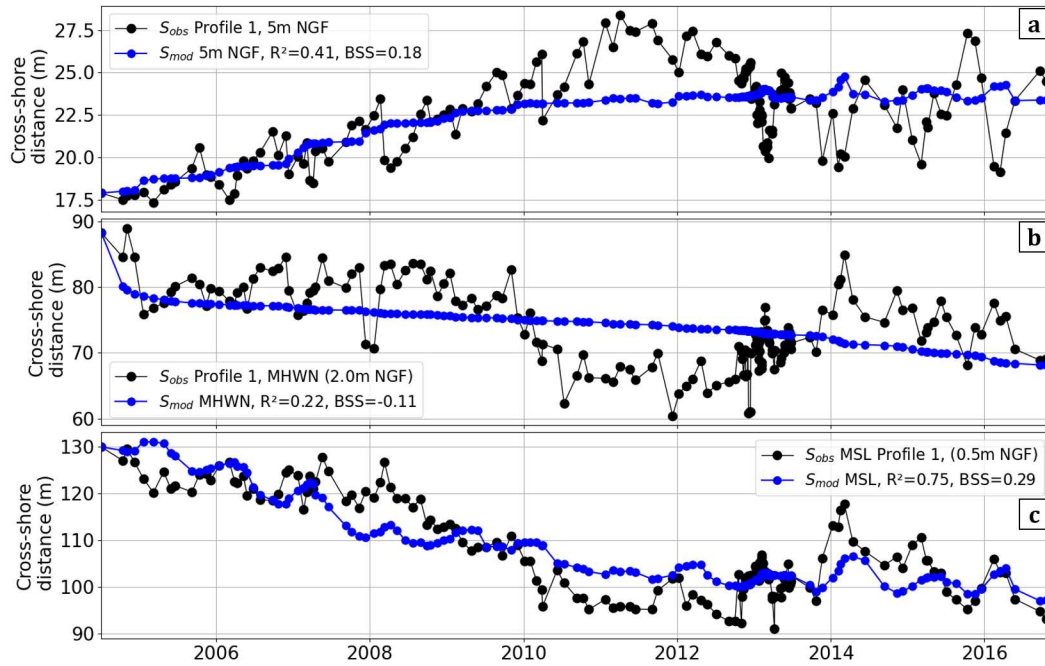


Figure III.8: Modeled contour position S_{mod} (blue), versus observations S_{obs} (black) for profile 1 at three elevations: (a) Upper Beach ($Z=5$ m NGF), (b) \approx Mean High Water Neap ($Z=2.0$ m NGF), and (c) Mean Sea Level ($Z=0.5$ m NGF).

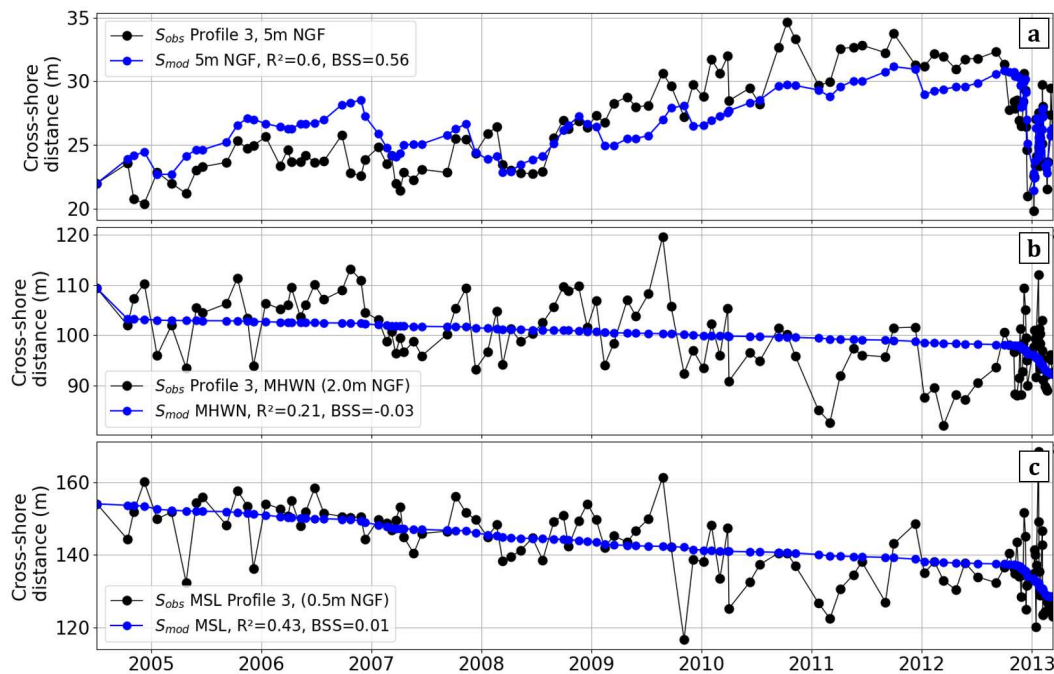


Figure III.9: Model contour position S_{mod} (blue), versus observation S_{obs} (black) for profile 3 at three elevations: (a) Upper Beach altitude (5 m NGF), (b) \approx Mean High Water Neap altitude (2.0 m NGF), and (c) Mean Sea Level (0.5 m NGF).

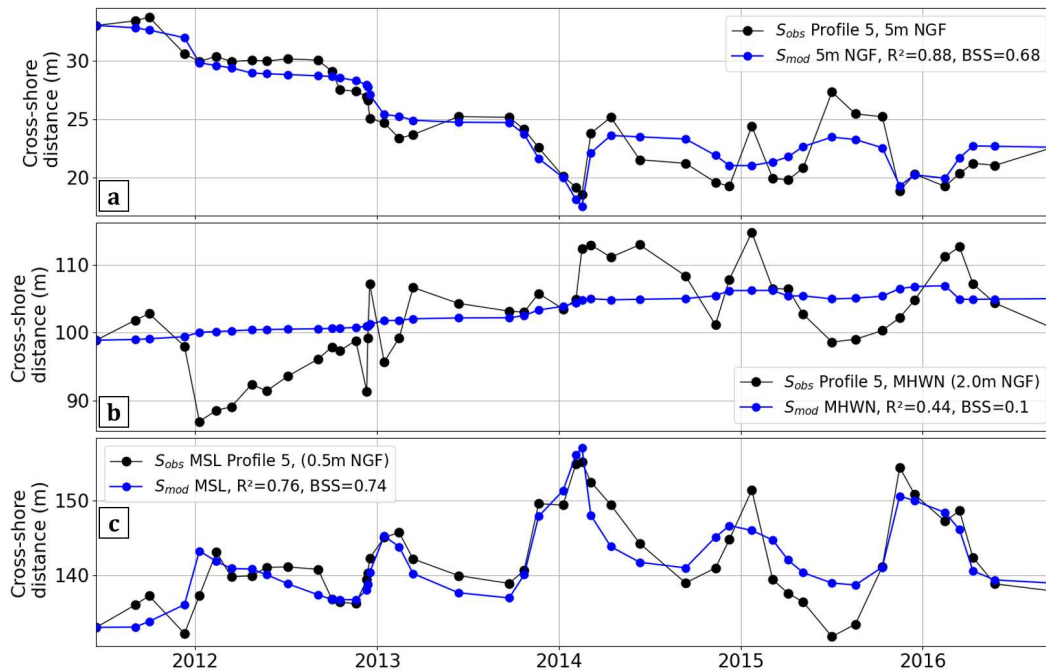


Figure III.10: Model contour position S_{mod} (blue), versus observation S_{obs} (black) for profile 5 at three elevations: (a) Upper Beach altitude ($Z=5$ m NGF), (b) \approx Mean High Water Neap altitude ($z=2.0$ m NGF), and (c) Mean Sea Level ($z=0.5$ m NGF).

Model optimum coefficients

The optimum coefficients obtained during the calibration phase for each profile at every altitude are presented for profiles 1, 2, and 3 (Fig. III.11) and for profiles 4, 5, and 6 (Fig. III.12).

The results show variations in the model coefficients depending on the altitude with, for example, changes in the sign of the coefficients within the intertidal zone, around the transition zone. A clearer trend as a function of elevation is observed in the coefficients a and C^- than for the coefficient C^+ , with an associated change in sign occurring at different altitudes for both profiles 1, 2, and 3 (Fig. III.11a,c) and profiles 4, 5 and 6 (Fig. III.12a,c).

Changes in the sign of a correspond to changes in the model response to the wave forcing in the form of an inversion of the sign of the energy disequilibrium causing erosion instead of accretion, for example. For profiles 4, 5, and 6, the lower and upper parts of the beach have optimal a coefficients of a different sign, meaning that for an event more energetic than the equilibrium energy ($E > E_{eq}$), the lower part of the beach accretes while the upper part (\approx above MHW) erodes. This is coherent with the observed morphological behavior changing between the lower intertidal zone more dissipative and the higher part of the beach profile being more reflective.

The C^+ coefficient varies between -20 and +20, with no clear patterns between the different profiles, and coefficients with different signs are even observed at the same altitude for different profiles, in particular at elevations where the model reproduces the long term trend of the observa-

tion rather than the seasonal variations. However, a small confidence is attributed to the coefficient value generating this behavior and further work is needed to evaluate the cross-shore coefficient while accounting for this long term trend with an additional component.

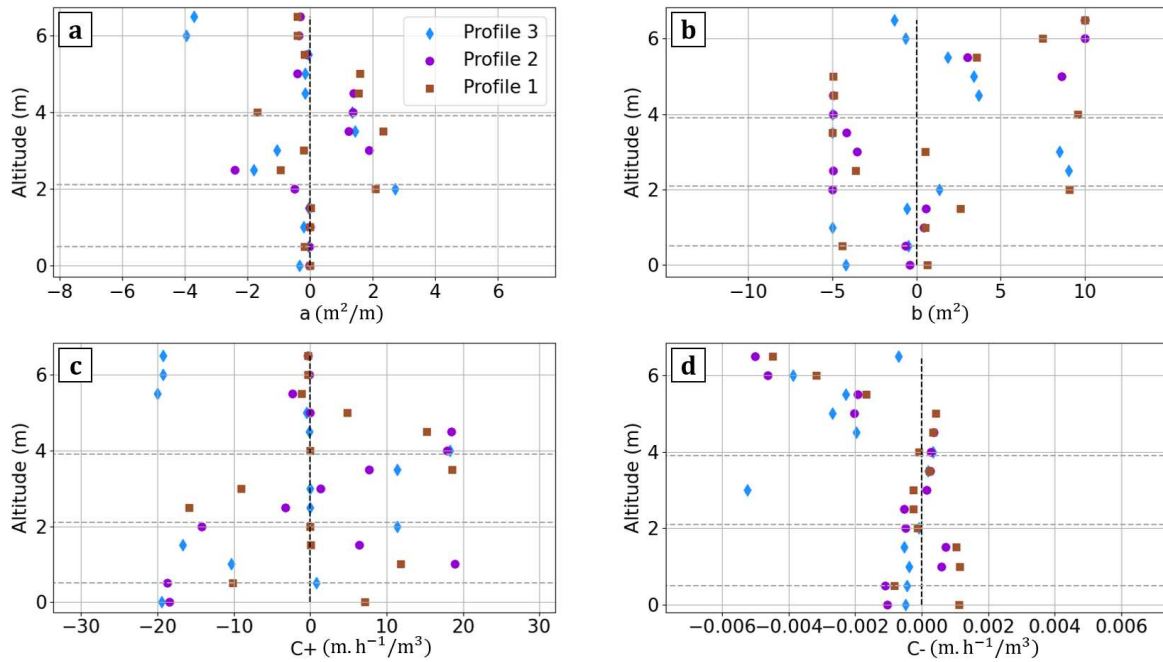


Figure III.11: Optimized model coefficients as a function of altitude for profile 1 (brown), 2 (purple), and 3 (light blue) for (a) coefficient a , (b) coefficient b , (c) coefficient C^+ , (d) coefficient C^- .

The coefficient b varies between -5m and 10m for the different profiles and altitudes, and no clear pattern is observed for this coefficient, as expected. This coefficient defines the equilibrium energy E_{eq} (eq. III.3) and the associated equilibrium contour position S_{eq} and thus determines around which equilibrium contour position the model evolves.

Hence, the b value is not expected to be correlated with the altitude, but rather with the mean contour position and also the possible trend in the contour position that affects the demeaned contour position values. The b value also depends on the time period over which the mean is calculated since the observed trend also varies as a function of the time period.

The differences in C^- and C^+ are explained by the C^+ coefficient typically being used in the model during the low energy events (for $E < E_{eq}$), while C^- is used during more energetic events (for $E > E_{eq}$). Thus, the value of the contour position change is impacted by the value of the disequilibrium ΔE and by the value of the \sqrt{E} that is smaller for low energy events.

Furthermore, this difference represents physically the fact that accretion, for the upper beach, is a slow process acting over all calm conditions whereas erosion events occur for shorter periods of time, on the time scale of a single storm event.

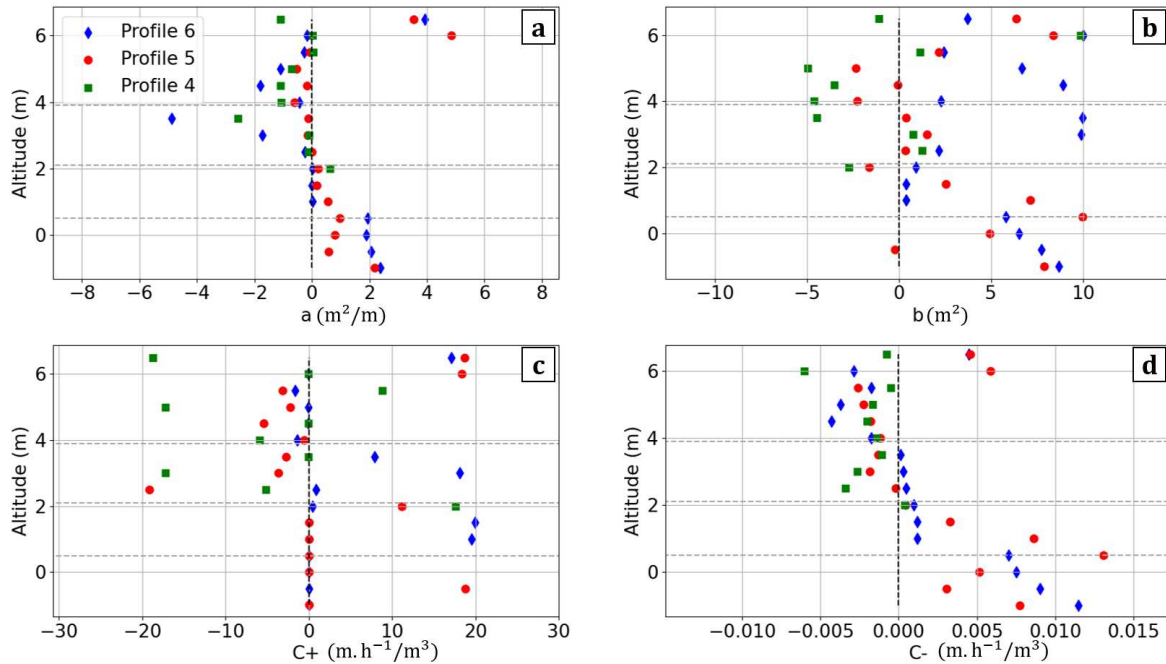


Figure III.12: Model optimum coefficients at every applied altitude for profile 4 (green), 5 (red) and 6 (blue), (a) coefficient a , (b) coefficient b , (c) coefficient C^+ , (d) coefficient C^-

Model skill score

The model performance is evaluated at all applied altitudes and for all profiles using the $RMSE$, the BSS and the R^2 (Fig. III.13 and Fig. III.14).

For profiles 1, 2 and 3, Fig. III.13a shows that, going from the upper beach to the lower intertidal zone, the model R^2 is first relatively high ($R^2 > 0.5$), then decreases, with a minimum located between the MHWN and the MHSW where $R^2 < 0.2$. Then, it increases again below the MHWN to reach a maximum of $R^2 = 0.7 - 0.8$ for profiles 1 and 2, but only $R^2 = 0.4$ for profile 3.

For profiles 4, 5, and 6, Fig. III.14a presents a similar pattern from the upper beach to the MHWN as profiles 1, 2 and 3, but here, the increase in the R^2 is less important in the lower intertidal zone for the profile 6. Profile 5 shows a decrease of the R^2 below MSL. For profile 4, consistent observations don't exist below 2m NGF due to a non erodible rocky substrate in this elevation range, so the model is only applied for elevations greater than 2m NGF.

The BSS , calculated using the linear regression of the observations as the baseline, is used here to verify if the model is capable of reproducing the seasonal and interannual variability of the beach, and not only the long term trend.

When important long term trends exist in the contour position and are better reproduced by the model in comparison with shorter term variations (e.g., seasonal), the calculated R^2 can be relatively high, while the model only reproduced the trend, which is not its expected behavior, thus potentially miss important accretion and erosion event (as in Fig. III.9b, c, or Fig. III.8a, and b, or Fig. III.10b).

Fig. III.13b and Fig. III.14b show that, similar to the R^2 , the BSS decreases for all profiles from the upper beach (where globally $BSS > 0.5$) to the MHWN (where $BSS < 0.25$). However, at lower altitudes, the behavior differs, with $BSS < 0.4$ for profiles 1, 2, and 3, and $BSS > 0.5$ for profiles 5 and 6.

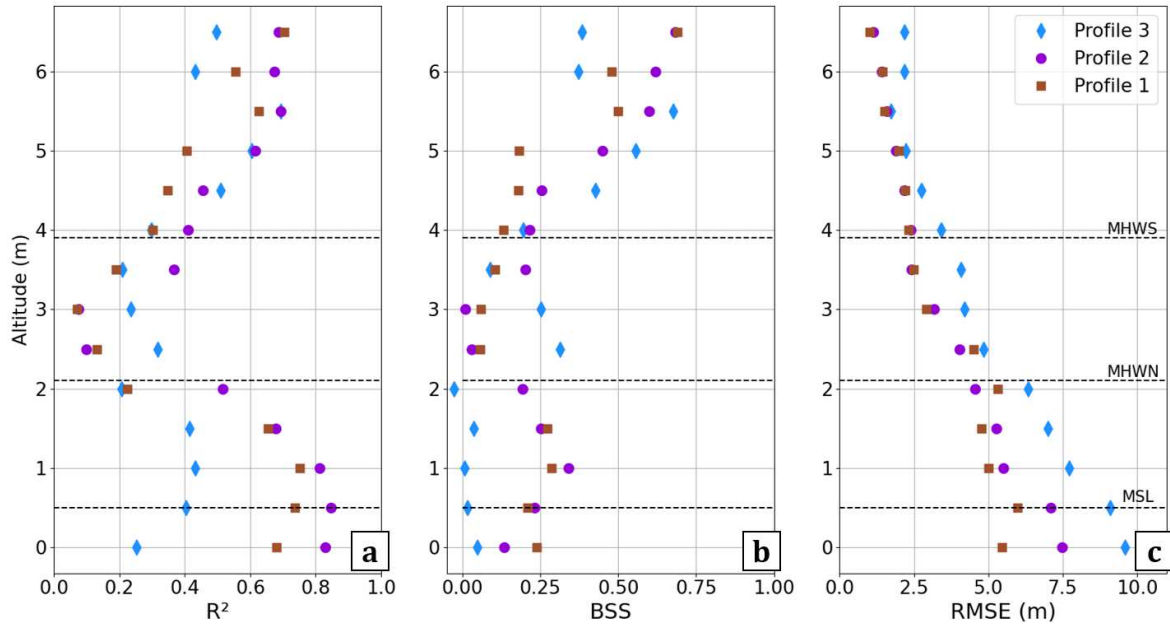


Figure III.13: Model statistics for profiles 1, 2, and 3, as a function of altitude at Vougot Beach: (a) R^2 , (b) Brier Skill Score (BSS), and (c) $RMSE$.

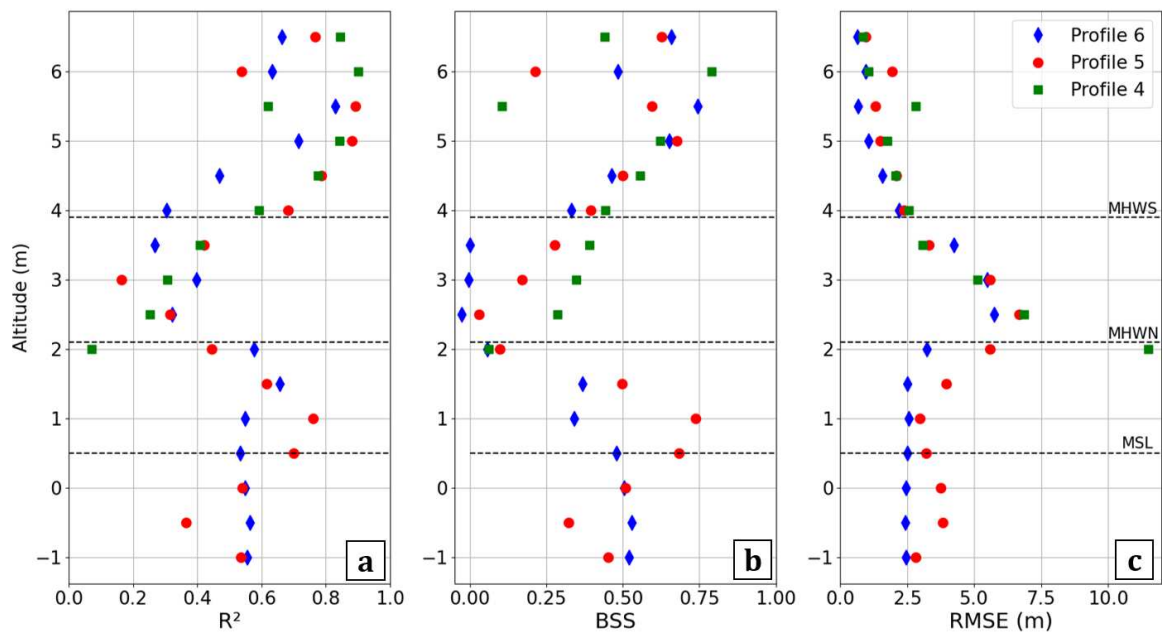


Figure III.14: Model statistics for profile 4, 5 and 6 at different altitude of Vougot Beach: (a) R^2 , (b) Brier Skill Score (BSS), and (c) $RMSE$.

The model $RMSE$ presented in Fig. III.14c for profile 1, 2, and 3 shows that the $RMSE$ increases at lower altitudes for the 3 profiles, with $RMSE < 2.5 m$ above 5 m elevation and $RMSE > 5 m$ at MSL for profile 1 and up to $RMSE > 9 m$ for profile 3.

For profiles 4, 5 and 6, the $RMSE$ is small along the upper beach and in the lower intertidal zone, with $RMSE < 3 m$ for these 3 profiles in the upper part, and $RMSE < 4 m$ for profiles 5 and 6 in the lower part. However, for the 3 profiles, the $RMSE$ increases between MHWN and MHWS, with $RMSE \approx 3 m$ at 2.5m elevation.

III.3.3 Discussion

Synthesis of model performance

The application of the model to Vougot Beach shows that the model skill varies both alongshore and as a function of the beach elevation. In the western part of the beach, the model reproduced well the contour position changes along the lower and upper intertidal zone based on the BSS and the R^2 , while in the eastern part, the BSS highlighted that the model skill is poor below the MHWS for all 3 profiles, since the model only reproduced long term trend.

Here, profile 4 is ignored due to the impact of the tombolo located in the alignment of the profile, and the associate hard ground that influences the model results, preventing its application below 2.5m NGF.

Thus, the results of the application of this simple cross-shore model highlight that the western part of the beach (profiles 5 and 6) is globally better reproduced than the eastern part of the beach (profiles 1, 2 and 3).

This is coherent with current knowledge (Suanez et al. 2010) of this beach behavior that the western part is more cross-shore dominated compared to the eastern part, where important changes in the shoreline position and sediment budget have been attributed to longshore processes, and in particular, to longshore sediment transport interruption by the jetty construction (Suanez et al. 2010).

The beach altitude where a decrease in the model performance is observed for profiles 5 and 6 (around 3 m NGF) (Fig. III.14a,b,c) is identified as the inflexion zone of this low tide terrace beach that separates the upper, reflective part of the intertidal profile and the lower, more dissipative part of the intertidal profile.

The inflexion point also demarcates how the beach responds to a single event generating accretion or erosion. For example, an erosion event that happens above this zone causes accretion below, and vice versa.

The physical processes that are responsible for sediment transport processes near the inflexion zone are complex and are not resolved by this simple shoreline change model since the contour position changes in this zone appear highly dependant of the adjacent altitude evolution.

This inflexion zone can also be identified in the pattern of the model coefficients along profiles 5

and 6 (Fig. III.12a,c), since the $\approx 3\text{ m}$ altitude corresponds to the change in the sign of the optimum coefficient a , which is coherent with the observed change of beach response above and below this transition zone (see inversion of contour position response between Fig. III.10a and c or in Fig. III.10a and c).

Wave forcing sensitivity

Following the observations made by Lemos et al. (2018) on the macrotidal beach of Porsmilin (Brittany, France), located $\approx 40\text{ km}$ south of Vougot Beach, the cross-shore model was applied using wave energy and wave power, computed as $P(t) = E(t) * Tp(t)$, where $Tp(t)$ is the instantaneous wave peak period.

At Porsmilin Beach, Lemos et al. (2018) showed that using the wave power to force the model instead of the wave energy increased the model skill with R^2 increasing from 0.4 to 0.7 in the lower part of the intertidal zone (between 0.5 m and -1 m NGF).

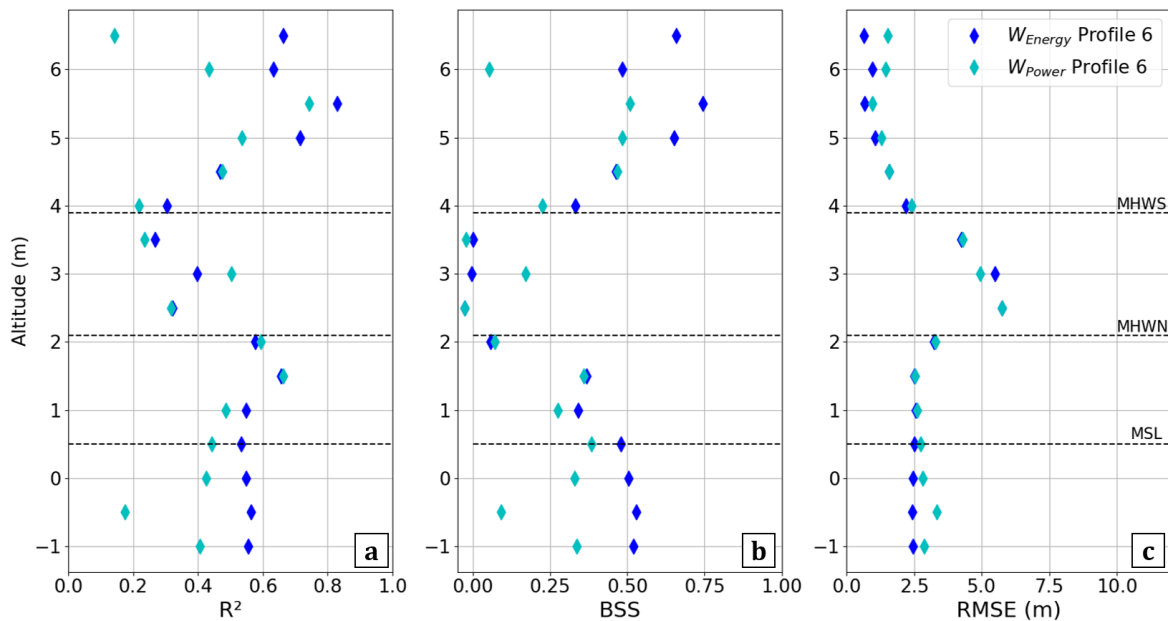


Figure III.15: Model statistics for profile 6 at Vougot Beach as a function of the elevation along the intertidal profile when using wave energy or wave power as the forcing wave condition: (a) R^2 , (b) Brier Skill Score (BSS), and (c) $RMSE$.

The wave power was used to force the cross-shore model at profile 6, and the statistics were compare with those obtained when the model was forced with the wave energy (Fig. III.15).

The 3 statistics show that the wave power doesn't increase the model skill at this profile at Vougot Beach, thus indicating that the influence of the wave period is less important on this beach.

The optimum cross-shore model coefficients obtained using the wave power are shown in Fig. III.16 in comparison to those obtained using the wave energy to illustrate the effect of changing the forcing variable.

The comparison shows that the amplitude of a increases, while the amplitude of C^- clearly decreases with the wave power which is expected, since the wave power has a larger amplitude, thus the $C^{+/-}$ coefficients should be smaller, moreover the equilibrium curves associate to the wave power would likely has a steeper slope explaining the a increase. This behavior was also observed by Lemos et al. (2018) at Porsmilin beach.

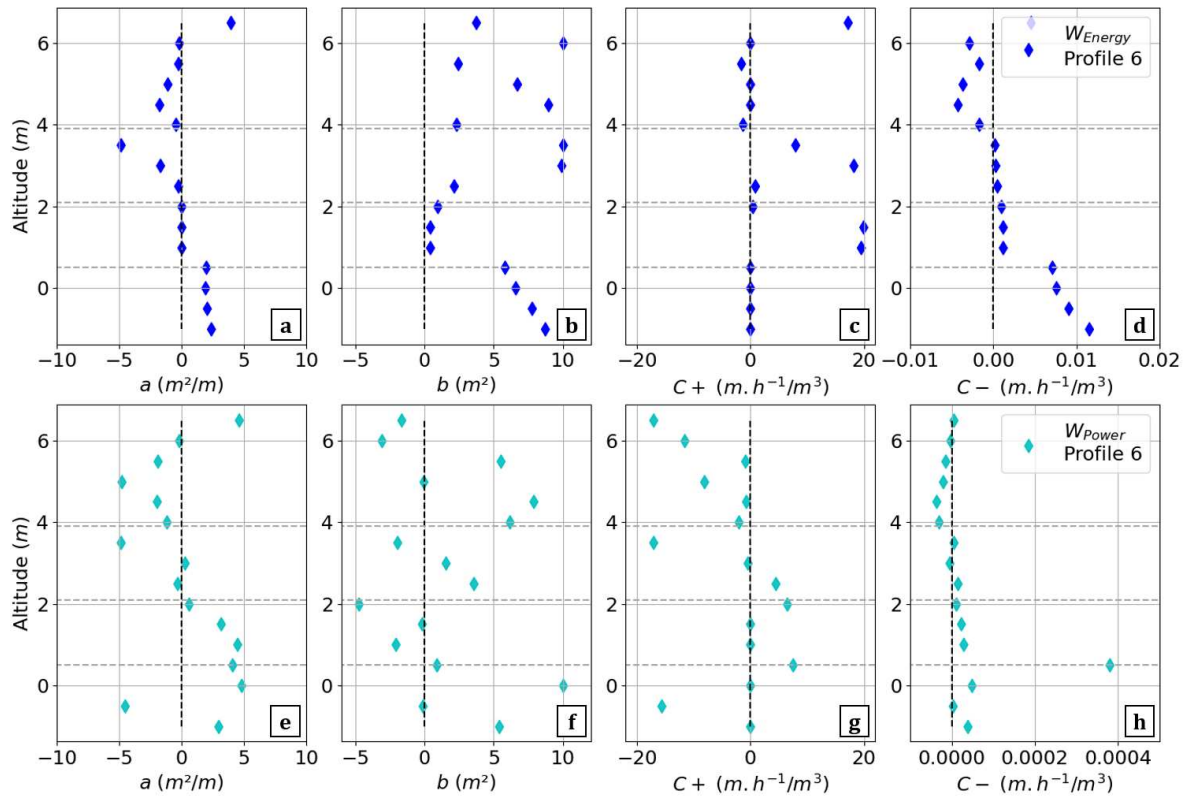


Figure III.16: Optimum model coefficients as a function of altitude along profile 6 using wave energy (a-d) or wave power (e-h) to force the model for: a (a,e), b (b,f), C^+ (c,g), and C^- (d,h).

Cross-shore model limits on Vougot Beach

The analysis of the model results highlights several limitations of the cross-shore empirical shoreline change model skill when applied at Vougot Beach.

The first is the model’s inability to reproduce well the contour position variations along profiles 1, 2, and 3 due to the important trend in the observations that is assumed to be generated by long-shore processes that are not represented in the model.

It also shows that when a trend in the observations exists, the optimisation algorithm may find a set of coefficients that can force the equilibrium-based model to generate a long term trend. However, this set of coefficients is then unable to reproduce seasonal and inter-annual contour position variations (see model behavior in Fig. III.9b,c, Fig. III.8b or Fig. III.10b).

This behavior has been identified in synthetic test cases, as being generated by high ratio between

the optimized value of C^+ and C^- which are also observed here on some profile where C^+ have a value up to three order of magnitude bigger than C^- . This behavior is also impact by the a value that modify the response time of the equilibrium model but a sensitivity analysis to both a and C^+/C^- ratio is still to be done.

These tests with the cross-shore only model point out the importance of accounting for the processes that are responsible for the observed long term trends, such as longshore processes.

The second limitation is that this model considers contour variations at each altitude independently. At this macrotidal beach, the model is applied at a range of altitudes, following [Castelle et al. \(2014\)](#) and [Lemos et al. \(2018\)](#), however the model doesn't account for the impacts of changes in adjacent contours/elevations along the beach profile.

The independence of $S(z)$ leads to the incapacity of the model to represent cross-shore dynamics controlled by changes occurring at the whole profile scale. For example, here the results show a decrease in the model performance at the altitude of the inflexion point, where the morphodynamics are governed by the respective adjustment of the dissipative and reflective parts of the beach profile. In the last chapter, a suggestion of a model modification that could correct for this model limitation is presented as a perspective for future work.

Another limitation, highlighted by the lack of data below 2m at profile 4, is that the model doesn't account for non-erodible substrate or sediment depletion when gravel or peat layers have been observed (but not mapped) at this beach.

The modeled contour position could be heavily modified by the restriction of the contour position movement caused by non-erodible substrate if they were taken into account.

Chapter IV

Longshore modeling

Ce chapitre présente le modèle longshore implémenté au cours de ce travail de thèse pour prendre en compte les processus longshore non représentés dans le modèle cross-shore. C'est un modèle one-line qui est utilisé, par ailleurs très largement employé comme outil opérationnel ou pour l'ingénierie en raison de sa simplicité et de son faible coût de calcul. Cependant, la simplicité de cette approche est également critiquée, en particulier concernant l'évaluation et la calibration du flux sédimentaire longshore. La formulation du modèle, les hypothèses et l'implémentation numérique sont présentées, et le modèle est appliqué à des cas de validation synthétique et analytiques. Puis, le modèle est appliqué à la plage de Narrabeen, décrite dans le chapitre 2, pour valider ses performances. De précédentes applications du modèle one-line à la plage de Narrabeen réalisées par d'autres chercheurs, tout comme la présente application du modèle dans ce travail de thèse, montrent que le modèle one-line génère un réajustement de l'orientation du trait de côte à long terme, qui n'est pas constatée dans les observations. Une analyse de sensibilité a été menée sur les effets de l'existence de biais dans la hauteur et la direction des vagues, montrant que de faibles biais dans la direction des vagues peuvent avoir un impact significatif sur la position du trait de côte modélisé. En supposant que la réorientation non-observée de la côte est générée par des biais dans la direction des vagues forçant le modèle, une méthode est proposée, basée sur une approche de Monte-Carlo, qui corrige efficacement les changements d'orientation du trait de côte modélisé. Ce travail fait l'objet d'un article, publié dans le journal Coastal Engineering, qui est présenté dans ce chapitre.

Chapter IV

Longshore modeling

This chapter introduces the longshore model implemented during this thesis work, including the mathematical formulation and numerical implementation, as well as several validation cases. Then, in a second part, the model is applied at Narrabeen Beach, and the model sensitivity to the wave forcing conditions is explored. A method is proposed to correct a change in the coastline orientation generated by the model that does not exist in the observations. This work has been published in Coastal Engineering, and the paper manuscript is presented in section IV.2.

IV.1 Longshore one-line model

In the previous chapter, a cross-shore empirical equilibrium contour position change model was presented and applied at Vougot Beach. The model results showed that on a complex beach, the cross-shore model can reproduce an important part of the shoreline variability (up to 80% on the western part of the beach along the upper intertidal zone).

However, the application at Vougot Beach also highlights that, on the eastern part of the beach, the empirical cross-shore model skill is lower ($BSS < 0.4$ in the intertidal zone) since the model doesn't account for shoreline variability associated with longshore processes in its actual formulation.

Thus, to account for longshore processes, a simple longshore model, based on the one-line approach (Pelnard-Considére 1956), has been implemented during this thesis work.

As presented in Chapter I.2.3, the one-line approach was developed with several strong hypotheses. This concept is based on the assumption that the beach cross-shore profile shape remains constant, thus assuming that the profile maintains an equilibrium shape, based on the hypothesis that cross-shore processes can be neglected at long temporal scales. Therefore, gradients in longshore sediment fluxes generate landward or seaward shifts in the equilibrium profile (Hanson 1989).

Furthermore, the one-line approach considers constant vertical shoreward and landward limit of the profile corresponding to the coastline elevation of model application and the depth of closure, respectively. Finally the model used a cross-shore uniform estimation of the alongshore sediment flux distribution thus ignoring the structure of the nearshore circulation.

The implemented one-line model framework is described in Fig. IV.1, which summarizes the main steps of the model calculation. From the initiation of the model loading the parameter and the model input to the description of the step effectuated for each time step: Calculate the shoreline angle, then calculate the angle between the wave and the coastline, use this angle to estimate the magnitude of the longshore sediment flux and updating the shoreline position.

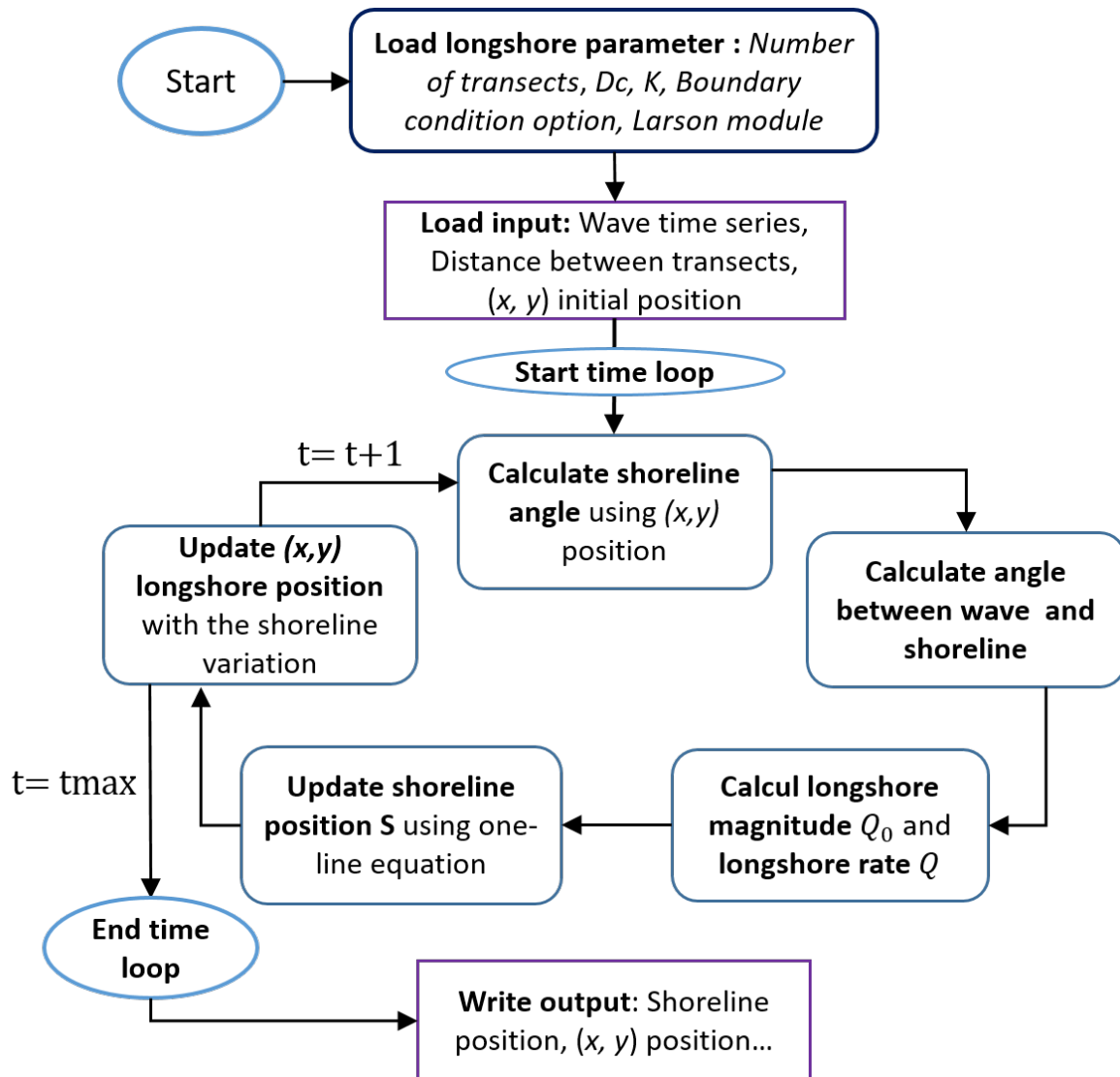


Figure IV.1: One-line longshore model conceptual functioning

IV.1.1 Model formulation and numerical implementation

The one-line model computes changes in the cross-shore location of the shoreline position S generated by alongshore gradients in the alongshore sediment flux Q :

$$\frac{\partial S}{\partial t} = -\frac{1}{Dc} \frac{\partial Q}{\partial x}, \quad (\text{IV.1})$$

where Dc is the depth of closure, and x is the alongshore coordinate. The longshore sediment flux Q is defined as:

$$Q = Q_0 \sin(2\alpha), \quad (\text{IV.2})$$

where

$$Q_0 = \frac{\rho K H_b^{2.5} \sqrt{g/\gamma_b}}{16(\rho_s - \rho)\lambda}, \quad (\text{IV.3})$$

and

$$\alpha = \alpha_b - \alpha_{shore}. \quad (\text{IV.4})$$

Here, K is a dimensionless empirical parameter (the typical range of values is discussed in section IV.1.3), H_b is the breaking wave height, g is the gravitational acceleration, γ_b is the breaker index ratio, ρ and ρ_s are the water and sediment density, respectively, λ is the sediment porosity, and α_b and α_{shore} are the breaking wave angle and the shoreline angle (Fig. IV.2), respectively.

The shoreline angle is calculated as:

$$\alpha_{shore} = \arctan\left(\frac{\partial S}{\partial x}\right). \quad (\text{IV.5})$$

Equation (IV.1) thus can be rewritten as:

$$\frac{\partial S}{\partial t} = -\frac{1}{Dc} \frac{K \sqrt{g/\gamma_b}}{16(\rho_s - \rho)\lambda} \frac{\partial}{\partial x} \left[H_b^{2.5} \sin\left(2\left(\alpha_b - \arctan\frac{\partial S}{\partial x}\right)\right) \right]. \quad (\text{IV.6})$$

The mathematical model is discretized at predefined transects spaced uniformly along the coast (Fig. IV.2), and first-order, centered finite difference schemes are used to calculate all spatial derivatives in the longshore direction:

$$\frac{S_n^{i+1} - S_n^i}{\Delta t} = -\frac{1}{Dc} \frac{Q_{n+1/2} - Q_{n-1/2}}{\Delta X_n}. \quad (\text{IV.7})$$

As shown in Fig. IV.2, n is the transect index, X_n is the alongshore distance between adjacent transects, and i is the time index. The time integration scheme is explicit.

Thus the discretized flux is written as:

$$Q_{n+1/2} = K_2 H_{b,n+1/2}^{2.5} \sin\left(2\left(\alpha_{b,n+1/2} - \arctan\frac{S_{n+1}^i - S_n^i}{\Delta X_n}\right)\right), \quad (\text{IV.8})$$

where K_2 the alongshore constant part of Q_0 :

$$K_2 = \frac{K \sqrt{g/\gamma_b}}{16(\rho_s - \rho)\lambda}. \quad (\text{IV.9})$$

By assuming that the wave angle is constant in time, and that $\sin(\alpha) \approx \alpha$ and $\arctan(\alpha) \approx \alpha$, which is valid for small angles, then equation (IV.6) can be written as an alongshore diffusion equation of the form:

$$\frac{\partial S}{\partial t} = \nu \frac{\partial^2 S}{\partial x^2}, \tag{IV.10}$$

where the diffusion coefficient $\nu = 2 \frac{Q_0}{D_c}$. This form shows that the coastline reaches an equilibrium position when exposed to constant wave forcing.

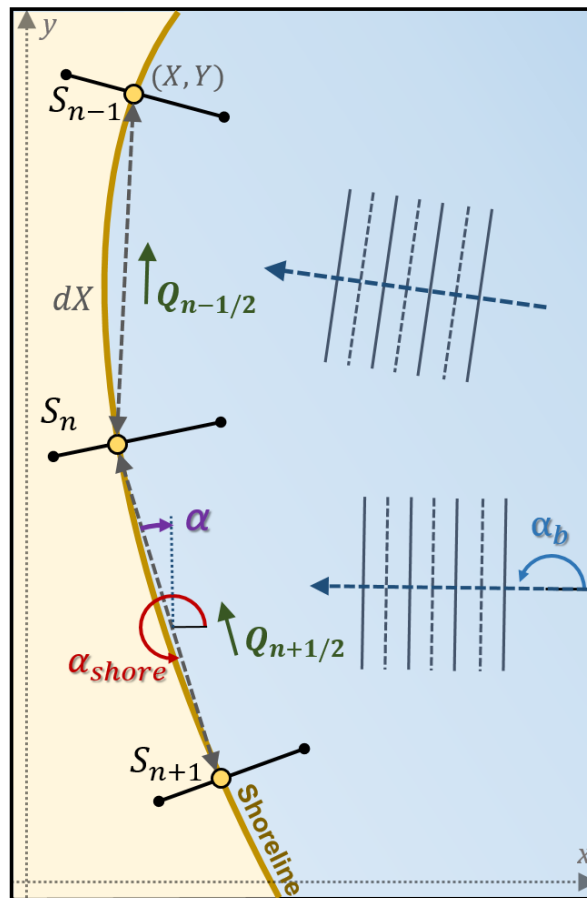


Figure IV.2: Schematic representation of the model setup for three cross-shore transects (index n), showing the shoreline position S , the relative wave angle α (eq. IV.4), the alongshore sediment flux Q , and the local reference frame (X, Y) .

The one-line model behavior is heavily impact by the choice of boundary conditions, and in the implemented model, 3 different options are available:

- a Dirichlet boundary condition where the 2 lateral boundary longshore fluxes Q are set to a prescribed value, for example the particular case $Q=0 \text{ m}^3/\text{s}$ for simulating a closed system such as an enclosed beach.

- a Neumann boundary condition where the lateral boundary sediment flux gradient $\frac{\partial Q}{\partial x}$ is set to a specified value, for example, $\frac{\partial Q}{\partial x} = 0$ fixes the shoreline position and can be used to account for non erodible boundaries such as a cliff or a sea wall, because the one-line model generate shoreline change from gradient of longshore sediment flux.
- a cyclic boundary condition, which is a particular case of a Dirichlet boundary condition, where the lateral incoming/outgoing sediment flux Q is set to the value of the sediment flux leaving/entering the opposite extremity of the beach. This boundary condition conserves the total sediment volume of the beach.

The longshore model uses input wave conditions potentially located offshore of the breaking zone due to the difficulty to access wave data propagated to the breaking point.

Thus, the model is completed by an additional module using the [Larson et al. \(2010\)](#) method to propagate the wave characteristics, here the wave direction and wave height, from the nearshore position where wave data are available (e.g. the buoy position or a large scale wave model output point) to the breaking point.

IV.1.2 Model validation with synthetic test cases

This part describes 4 different simple synthetic test cases used to validate the model implementation. The first 2 tests case uses constant wave direction conditions to validate the correct model behavior when no shoreline evolution is expected, whereas the third test evaluate the model capacity to converge toward a new equilibrium position by generating shoreline change in case of a sediment flux set to zero at the boundary and wave with a constant incidence angle. The last test compares the model results for a particular configuration to an analytical solution of the linear diffusion equation (as in [Vitousek & Barnard 2015](#)).

No evolution test cases

In this first validation case, a simple straight linear coastline of 4 km length is considered with a constant, cross-shore oriented wave direction ($\alpha = 0$) and with a uniform breaking wave height $H_b = 1$ m. The coastline is discretized into 80 transects with $\Delta x = 50$. The lateral boundary conditions are set to $Q = 0$ and the simulation for a one year time period with an hourly time step. Under such conditions, no shoreline changes should be observed (as correctly represent in [Fig. IV.3a](#) with no change of the initial shoreline position) since the longshore sediment flux $Q = 0$ due to $\sin(2\alpha) = 0$ at all transects during all the simulations (as verified in [Fig. IV.3b](#)).

A second test, based on the same beach configuration, is made but now using waves with a constant alongshore uniform angle $\alpha = 45^\circ$, and zero flux gradient $dQ/dx = 0$ boundary conditions. The model longshore sediment flux Q is not zero ([Fig. IV.4.b](#)), the flux gradient $dQ/dx = 0$ causing no shoreline change, as observed in [Fig. IV.4.a](#).

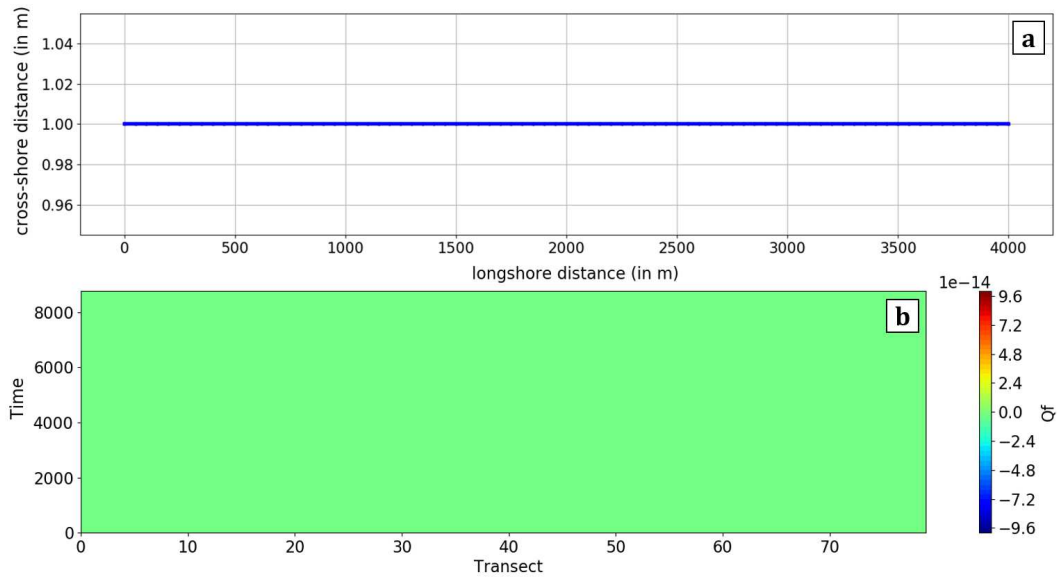


Figure IV.3: No evolution test case: (a) Shoreline position evolution, (b) longshore sediment flux Q in time and space showing a null value.

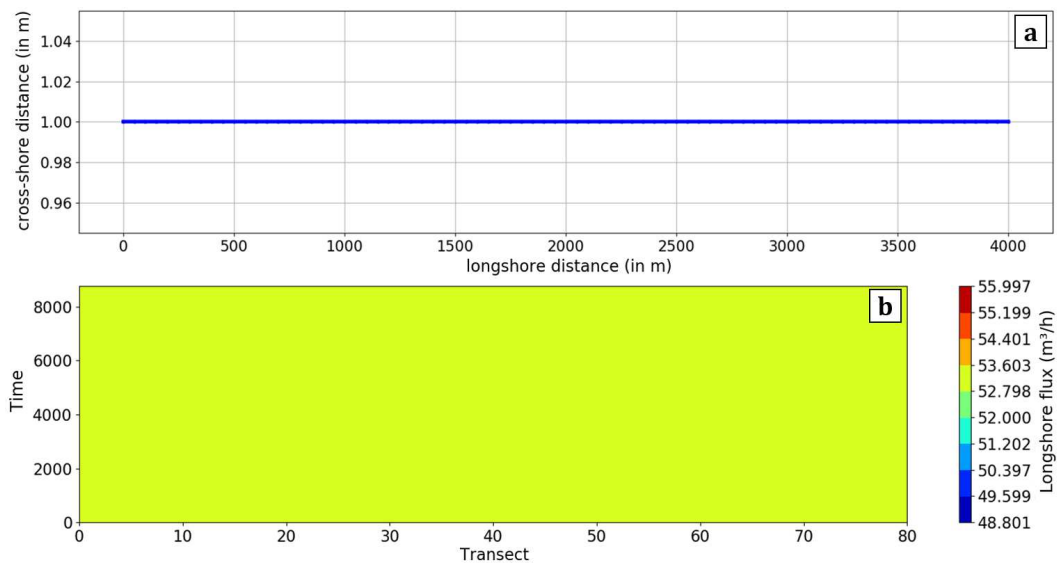


Figure IV.4: No flux test case: (a) Shoreline position evolution, (b) longshore sediment flux Q in time and space showing a constant and uniform flux value.

Accretion test case

Finally, a third test is carried out with the same model configuration using a constant alongshore uniform wave angle $\alpha = 45^\circ$, but here the Larson module is activated to calculate the breaking condition from offshore wave conditions arbitrary specified in a depth of 20m, and the lateral boundary conditions are set to $Q = 0$.

The results show that in the one-year period of simulation the coastline orientation changed (Fig. IV.5.a), with erosion at one boundary and accretion at the other boundary due to the $Q = 0$ boundary condition that generates a sediment flux gradient (Fig. IV.5.b).

These gradients gradually disappear as the shoreline orientation evolves, approaching the wave direction, forming a new equilibrium coastline orientation approximately 20° shifted from the initial orientation (correctly reproduced in Fig. IV.5).

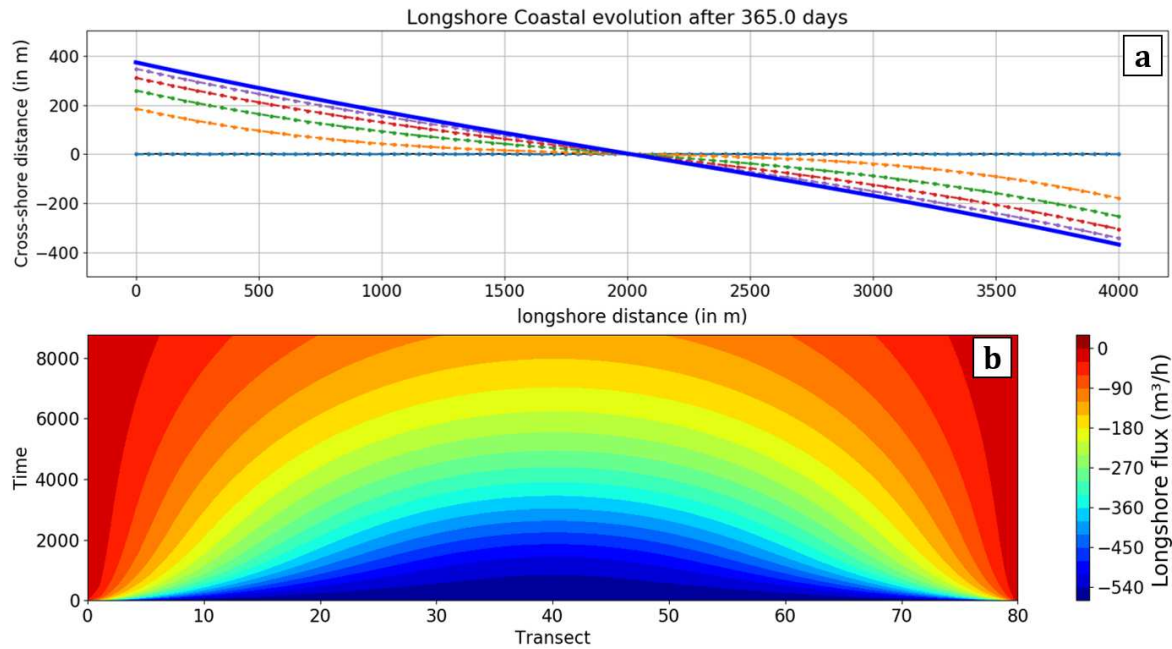


Figure IV.5: Accretion test case: (a) Shoreline position evolution from initial position (light blue) to final position (blue line), (b) longshore sediment flux Q evolution.

Diffusion test case

The second type of validation test case consists of comparing the model shoreline position in time and space with an analytical solution of the linear diffusion equation (eq. IV.10), as presented in Vitousek & Barnard (2015).

The initial shoreline configuration is a sinusoidal function $S = a \cos(kx)$, where a is the shoreline perturbation amplitude, k is the sand wave alongshore wave number $k = 4\pi/L$, and $L = 5km$ is the length of the model domain (Fig. IV.6). The solution of the eq. IV.10 is $S = a \exp(-\nu k^2 t) \cos(kx)$, where ν is the diffusion coefficient $\nu = 2Q_0/Dc$.

For this test, the coastline is discretized by 101 transects spaced by $\Delta x = 50$, the transport rate Q_0 is set to a constant value of $1 \text{ m}^3/\text{s}$, and $Dc = 1 \text{ m}$. The wave direction is set to a constant, alongshore uniform angle $\alpha_{wave} = 0$, and the boundary conditions are set to no flux, $Q = 0$.

The model is run during a period $T = 3 \cdot 10^5 \text{ s}$ with a time step of $dt = 625 \text{ s}$, and the results are compared with the analytical solution (dashed black line) in Fig. IV.6 every $T/5$. The results show

that the model (in color) reproduces well the analytical solution, since they are superimposed.

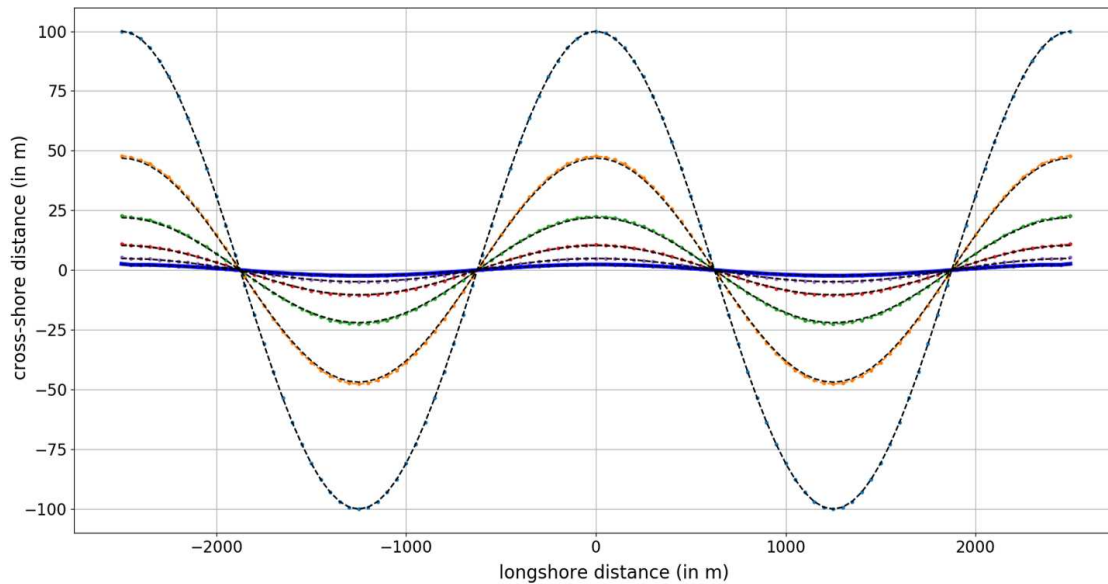


Figure IV.6: Diffusion test case, as in Vitousek & Barnard (2015), where the initial sinusoidal shoreline (light blue) is progressively diffused by the longshore model to tend toward a straight coastline (blue) perpendicular to the wave forcing conditions. The model coastline evolution (in colors) is compared to the analytical solution of the diffusion equation (eq. IV.10) (in black). Here the model and the analytical solution are well superimposed at each represented intermediate state.

IV.1.3 K parameter value

Literature review of K

The first estimation of the parameter K was made by Komar & Inman (1970) when they measured the longshore sediment drift volume at 2 beaches showing different hydrodynamics. They found that a coefficient of $K=0.77$ was needed to best fit the sediment drift volume measured with their mathematical formulation (which is similar to what is now known as the CERC formula (USACE 1984)). Then they assumed that this value is valid for all beaches. This is the beginning of a long and complex history of the use and re-estimation of the K parameter (see Table IV.1).

Not much later, Bodge & Kraus (1991) pointed out that K values can range from 0.014 to 1.6 using existing measurements from multiple field studies.

These studies suggest that a universal K value of 0.77, first proposed by Komar & Inman (1970) is not valid. However, this value can still be found in some coastal engineering manuals as a guideline to estimate the longshore sediment transport volume. However, the large range of values presented in the literature (from $K \approx 0.01$ to $K > 2$, see Table IV.1) can be attributed to the large uncertainties in the process of estimating the longshore sediment transport volume.

In their 2002 critical paper, Pilkey & Cooper (2002) assess the different origins of this uncertainty

in the measures used to estimate K , which potentially lead to errors of more than one order of magnitude.

First, the uncertainties in measuring the sediment volume are large: as pointed out by [Pilkey & Cooper \(2002\)](#). The volume estimation is usually made based on experiments lasting only a couple of hours, at one position along the beach (or at several position when the tide amplitude is uncovering a sufficiently wide section of the beach), using approaches with large errors (e.g. fluorescent tracer or sediment trap). Furthermore, the hydrodynamic conditions during these short experiments (often during fair-weather conditions) are assumed to be representative and are therefore applied to model longshore transport over years or even decades.

Second, there are potentially errors in the volume calculation formula where K appears (CERC, eq. [IV.1.1 USACE \(1984\)](#)), since this formula attributes the longshore sediment transport to the wave forcing, while studies have shown that, for example, local wind-induced currents have first-order impacts on the longshore sediment transport.

Table IV.1: Range of K values (eq. [IV.1.1](#)) encountered in literature for the longshore flux calculation and the origin of the value.

K value in literature		
Reference paper	$K[-]$ (flux in m^3/s)	Value origin
Komar & Inman (1970)	0.77	Observations at 2 sites: El Moreno Beach (US Gulf) and Silver Strand Beach (South West coast US) (14 four-hour experiments)
CERC (USACE 1984)	0.39	Observations of a beach nourishment in the Outer Banks, North Carolina
Wright et al. (1987)	0.2 to 1.0	Beach near Oregon Inlet
Bodge & Kraus (1991)	Varies from 0.014 to 1.6	Measurements from multiple field studies
Schoonees & Theron (1993) , Schoonees & Theron (1996)	0.2	Best fit of multiple existing field studies
Wang et al. (1998)	0.08	Best fit for observations a on low energy site in the south eastern US (with 3-5 min sediment trap survey)
Pilkey & Cooper (2002)	from 0.014 to 2.32	Review of the existing values
Vitousek & Barnard (2015)	0.04	Model application: Ocean Beach (USA)
Vitousek et al. (2017)	from $5 \cdot 10^{-3}$ to 0.0025	One-Line Model calibration along the US West Coast
Arriaga et al. (2017)	from 0.2 to 1.6	CERC formula calibration
Antolínez et al. (2019)	from 0.03 to 0.36	One-Line Model calibration

Finally, the errors from both the measurements and the mathematical volume calculation could be significant independently, and when combined, this may lead to a K value that is already questionable at the measurement site during the calibration period. Thus, extending the use of this

calibrated parameter becomes highly doubtful when the value is generalized for all hydrodynamic conditions and is exported to other beaches.

In conclusion, the K parameter should be handled carefully since its precise value is uncertain, while its effect on the model results can be significant. Thus, the large range of field values (2 orders of magnitude) found in the literature and the uncertainties described above, should be kept in mind while interpreting the optimized value of this parameter for a given site.

IV.2 Longshore model application to Narrabeen

In this section, the longshore one-line model described in this chapter is applied to the well studied Narrabeen Beach for validation of the model skill on a natural site.

This site was selected due to the large morphological and hydrodynamical dataset available freely online, in particular, the availability of 10m depth wave conditions at 5 alongshore locations of the beach for more than 40 year is the main reason justifying the choice of Narrabeen Beach over Vougot Beach.

There, a sensitivity analysis to the forcing wave height and direction is performed, pointing out the model sensitivity to biases in the forcing wave direction. Furthermore, a method is proposed to correct a commonly observed behavior of the one-line model in the form of a modification of the modeled coastline planform orientation that is not present in the observations.

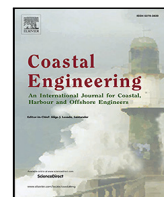
The approach assumes this behavior is due to bias in wave direction. Thus using a Monte-Carlo approach, a set of bias values is obtained correcting the model planform reorientation.

This work is described in the following article accepted for publication in “Coastal Engineering” and was achieved in collaboration with M. Yates, N. Le Dantec, M. Harley, K. Splinter and N. Goutal.



Contents lists available at ScienceDirect

Coastal Engineering

journal homepage: www.elsevier.com/locate/coastaleng

Sensitivity of a one-line longshore shoreline change model to the mean wave direction

T. Chataigner^{a,*}, M.L. Yates^a, N. Le Dantec^b, M.D. Harley^c, K.D. Splinter^c, N. Goutal^a

^a LHSV, Ecole des Ponts, Cerema, EDF R&D, Chatou, France

^b Geoscience Ocean Laboratory, University of Western Brittany, IUEM, Plouzané, France

^c Water Research Laboratory, School of Civil and Environmental Engineering, UNSW Sydney, Sydney, Australia

ARTICLE INFO

Keywords:

Beach morphodynamics
One-line model
Longshore transport
Shoreline change
Sensitivity analysis
Wave angle bias

ABSTRACT

The sensitivity of a one-line longshore shoreline change model to the incident wave direction is evaluated at Narrabeen Beach (Australia). As previously observed, the application of the one-line model using wave conditions generated along the 10-m depth contour produces a long-term reorientation of the coastline, with an initial transition period and then a new stable equilibrium during the 10-year period from 2005 to 2015. However, this coastline change in shoreline planform shape is not observed in the shoreline position measurements. The source of this error is investigated by assuming that it is caused by biases in the incident wave direction and by using a Monte Carlo approach to search for the optimal set of wave angle bias corrections to apply at each cross-shore transect. The obtained optimal values enable the one-line model to reproduce accurately the shoreline planform, and they are coherent with estimates of the wave breaking angle obtained independently using a nearshore wave propagation model. Then, using the corrected wave angle time series as a reference, a second Monte Carlo analysis is completed to investigate the sensitivity of the model to errors in the mean wave direction drawn from Gaussian distributions with varying standard deviations. The analysis shows the range of expected errors in shoreline position for an estimated range of errors in the mean wave direction at Narrabeen beach. This work highlights the importance of considering the sensitivity of one-line longshore model simulations to errors in the incident wave angle, which can be relatively large given the uncertainties in spectral wave model estimates of wave direction, in wave buoy observations, and in wave propagation methods or input bathymetry used to estimate wave breaking conditions.

1. Introduction

The littoral zone is a complex environment. It is both a physically dynamic interface, as well as a highly important social and economic zone, given the dense population and high concentration of human activities. In addition, the littoral zone and surrounding coastal areas are highly sensitive to marine flooding and erosion hazards, including shoreline retreat. Thus, it is essential to be able to understand and predict shoreline evolution, in particular at spatial scales of a beach and at medium to long temporal scales, as well as during extreme events.

To achieve this goal, a wide variety of morphological evolution models exist, ranging in complexity from three-dimensional, physics-based models (e.g. MIKE21 Warren and Bach, 1992, Delft3D Roelvink and Banning, 1995, XBeach Roelvink et al., 2009) to one-line models representing only cross-shore (e.g. Miller and Dean, 2004; Yates et al., 2009; Davidson et al., 2013) or longshore (e.g. Ashton and Murray, 2006; Turki et al., 2013; Bouchette et al., 2014) processes. The choice

of an appropriate model thus depends on the dominant physical processes that must be represented or parameterized at the spatial and temporal scales of interest, and predicting coastal evolution at seasonal to decadal or longer timescales remains a significant challenge (Safak et al., 2017; Davidson et al., 2017; Montaña et al., 2020). Given the limits of numerical models at these temporal and spatial scales, empirical, process-based models may be an optimal alternative to physics-based models (Murray, 2007; Ranasinghe and Callaghan, 2013; French et al., 2016). This family of models allows simulating shoreline evolution at these temporal and spatial scales given their numerical simplicity, low computational cost, and accuracy once calibrated.

At short (e.g. storm) to seasonal timescales, cross-shore processes are often dominant, while over longer timescales (e.g. interannual to decadal), longshore processes may become increasingly important. To reproduce shoreline changes at these scales, both cross-shore and

* Corresponding author.

E-mail addresses: teddy.chataigner@enpc.fr (T. Chataigner), marissa.yates@cerema.fr (M. Yates), nicolas.ledantec@univ-brest.fr (N. Le Dantec), m.harley@unsw.edu.au (M. Harley), k.splinter@unsw.edu.au (K. Splinter), nicole.goutal@edf.fr (N. Goutal).

<https://doi.org/10.1016/j.coastaleng.2021.104025>

Received 15 April 2021; Received in revised form 30 July 2021; Accepted 25 September 2021
Available online 17 November 2021

longshore processes must be taken into account. Recent work has thus focused on developing “hybrid” models that incorporate both cross-shore and longshore processes, including CoSMoS-COAST of Vitousek et al. (2017), LX-Shore of Robinet et al. (2018), COCOONED of Antolínez et al. (2019), and the combined model of Tran and Barthélemy (2020). These models are forced by hydrodynamic conditions (e.g. waves) and typically have several free parameters that must be calibrated for each study site.

In hybrid approaches, the one-line longshore transport model is the most commonly used approach to account for longshore processes (e.g., Vitousek et al., 2017; Robinet et al., 2018; Antolínez et al., 2019). For embayed beaches, additional approaches have been developed to simulate longshore processes, including semi-empirical approaches based on decomposing the mean and fluctuating components of the wave field (e.g. Tran and Barthélemy, 2020, which is then combined with a cross-shore model), or by modeling directly the beach orientation using an equilibrium approach (Turki et al., 2013; Jaramillo et al., 2021).

Here, the focus is on the classical one-line model, which was first introduced by Pelnaud-Considére (1956). It assumes that at long timescales, beach cross-shore profiles maintain an equilibrium shape in balance with the incoming wave field. The beach thus responds to perturbations by restoring the equilibrium shape. Therefore, gradients in longshore sediment fluxes cause landward or seaward shifts in the equilibrium profile, based on the hypothesis that cross-shore processes can be neglected at long temporal scales (Hanson, 1989). The longshore sediment flux can be estimated using different formulae (e.g. CERC, US-ACE, 1984; Kamphuis, Kamphuis et al., 1986) that empirically relate the hydrodynamic conditions (e.g. breaking wave height and direction) and the beach geological characteristics (e.g. sediment porosity or grain size) to the longshore sediment flux. This simple approach depends on the quality of both the input data and the choice of model free parameters.

Recently, several studies have focused on identifying and evaluating sources of uncertainties in coastal morphological models. For example, Davidson et al. (2017) tested the sensitivity of the cross-shore empirical model ShoreFor (Davidson et al., 2013; Splinter et al., 2014) to variations in the potential future wave climate. D’Anna et al. (2020) went one step further using the hybrid LX-Shore model (where cross-shore changes are based on the ShoreFor model) by estimating the contribution of different input parameters to the total model uncertainty in a test case applied at Truc Vert beach. In addition, recent studies have also quantified uncertainties related to climate change impacts (Toimil et al., 2020), in particular focusing on the importance of changes in the mean water level on long-term shoreline change (Le Cozannet et al., 2019; Athanasiou et al., 2020).

The one-line longshore model is a simple and therefore widely used model (Larson et al., 1997). It is thus important to study the uncertainties associated with this approach, and several recent studies have investigated the sensitivity of the model to a series of different assumptions and input parameters. Ruggiero et al. (2010) illustrated the relative importance of the wave climate (wave height, peak period and wave direction) and sediment supply (by varying the model sediment flux at the boundary) in simulations with the Unibest model (Delft Hydraulics, 1994) by evaluating the model skill in reproducing observed shoreline changes. They showed that altering the offshore mean wave angle generated an important increase in the model error. Kroon et al. (2020) analyzed the relative contribution of errors in different model parameters and wave climate variability to the total model uncertainties as a function of the considered timescales. The model sensitivity to the wave climate is also demonstrated in George et al. (2019), where the longshore flux uncertainties are estimated by incorporating errors in the input wave height and direction. Previous studies have highlighted the sensitivity of the one-line model to wave climate uncertainties, including uncertainties in the wave direction, without directly quantifying the impacts on the modeled shoreline position.

Depending on the inherent complexity of the study site and the quality of the input data, the one-line longshore model may generate changes in the beach planform (e.g. reorientation) that are different from observations. For example, this was observed recently using hybrid models when modeling shoreline changes in the North Beach Sub-cell of the Columbia River Littoral Cell (Washington, USA, Antolínez et al., 2019), and the highly studied Narrabeen Beach (Australia, Robinet et al., 2020).

The reorientation “artifact” is corrected for in Antolínez et al. (2019) by replacing the initial shoreline position with the computation of a new long-term average shoreline. This long-term average shoreline is generated by running their hindcast wave climate for 500 years, following Anderson et al. (2018). The authors assume that using the long-term average shoreline as the baseline should correct problems inherited from the wave climate, such as a wave direction bias in the offshore wave conditions or errors in the nearshore wave propagation.

Similarly, in Robinet et al. (2020), the beach reorientation observed in a 5-year-long simulation at Narrabeen Beach is corrected by running the model in two steps. First, the model simulates the 5-year period, and then the final shoreline position at the end of the first simulation is used as the initial shoreline position in the second simulation. The authors assume that the shoreline changes and not the shoreline position simulated in the second step are more accurate. Finally, the simulation results are corrected to account for the difference in the initial shoreline position in order to compare to the observations. Despite applying this two-step method, changes in the shoreline planform shape are still observed in the first year of the second simulation, and this time period is thus excluded from the remainder of their analysis.

These two studies (Antolínez et al., 2019; Robinet et al., 2020) used pre- and post-processing methods to manage the change in the coastline orientation introduced by the one-line longshore model. The authors suggest that the errors are potentially caused by errors in wave direction and/or nearshore propagation. However, they do not attempt to demonstrate this in their work. The current study is focused on understanding the source of the coastline reorientation simulated by the one-line model, as well as applying a simple approach to correct for this error. This work therefore aims to study the overall sensitivity of the one-line modeling approach to biases or errors in the wave conditions. The epistemic uncertainties introduced by the longshore one-line model have two potential sources: the model formulation or the input wave conditions. In this study, it is assumed that the formulation of the one-line model is accurate, and the input wave direction is studied as a potential source of model uncertainties.

Previous studies have used Monte Carlo-based approaches in applications of the one-line model by generating variations in the wave climate based on existing wave distributions (Wang and Reeve, 2010; Bergillos et al., 2018) or from measured wave statistics (Reeve et al., 2014; Kroon et al., 2020). Here, two Monte Carlo approaches are used to evaluate the sensitivity of a one-line longshore model to the mean wave direction and wave height at Narrabeen Beach.

In the first analysis, a spatially variable, random bias is added to the wave angle time series at each cross-shore transect to find the optimal values minimizing the difference between the simulated and observed shoreline position. Then, the second analysis aims to test the sensitivity of the shoreline model to spatially variable random biases drawn from specified Gaussian distributions. Here, it is assumed that the distribution of potential errors in measured (e.g. wave buoy observations) or modeled (e.g. large-scale spectral wave models) wave direction are Gaussian. Although this study is conducted using the data from Narrabeen beach, the results can be generalized to other sites.

In the following, the characteristics of the study site are presented (Section 2) before describing the one-line longshore model (Section 3) and the Monte Carlo approach applied in the analysis (Section 4). The optimal bias values and the sensitivity of the model to the input wave angle and wave height are then evaluated (Section 5), before discussing the hypotheses and limitations of this study, and the generalization of the approach to other sites (Section 6). Finally, a synthesis of the results, as well as perspectives for future studies (Section 7) are presented.

2. Study site

The Narrabeen-Collaroy embayment is a 3.6 km-long sandy beach located in southeast Australia, to the north of Sydney (Fig. 1). The embayment consists of Narrabeen beach at the northern end and Collaroy beach at the southern end, and is hereafter referred to as Narrabeen beach for simplicity. The beach is bordered by two rocky headlands at the northern and southern extremities, and the rocky substrate extends underwater to approximately 60 m depth. Reefs are also present from 5 m to 10 m water depth in front of both beach extremities (as can be seen partially in the satellite image in Fig. 1d in front of cross-shore profiles PF1 and PF8). The beach is backed by low dunes at the northern end and by a seawall at the southern end. An estuary forms a lagoon landward of the beach at the northern extremity, and the mouth of the estuary breaches the dune intermittently.

The beach is characterized by fine to medium quartz sand ($D_{50} \approx 0.3$ mm) that is nearly uniform alongshore (Turner et al., 2016). The headlands at the extremities of the beach and the curvature of the bay generate alongshore gradients in wave energy caused by wave sheltering and refraction processes. The effects of wave sheltering are more dominant at the southern end of the beach owing to the presence of the 1.5 km-long rocky headland and the predominantly southeasterly incident waves, but wave sheltering also occurs at the northern end of the beach for less-frequent northerly incident waves. Differences in the wave exposure cause differences in the morphodynamic beach state, changing from a higher-energy, longshore-bar trough beach state in the north to a lower energy, low tide terrace/reflective beach state in the south (Wright and Short, 1984; Harley et al., 2011).

Narrabeen beach is a semi-diurnal, micro-tidal environment with a mean spring tide of less than 1.5 m. The Sydney waverider buoy, located 11 km offshore in 80 m water depth (Fig. 1b), has recorded directional wave conditions since 1992, which are supplemented by hourly hindcast waves from the Centre for Australian Weather and Climate Research (Durrant et al., 2014) to fill data gaps due to buoy maintenance/dysfunction. The offshore wave climate ranges from moderate to high wave energy (mean $H_s \approx 1.6$ m and $T_p \approx 10$ s), with dominant long-period swell waves impacting the beach from the south–south–east (SSE) direction. In addition, storm waves (defined as $H_s > 3$ m) are generated from tropical cyclones from the northeast, east-coast lows from the east, and cyclones from the south (Turner et al., 2016). The regional wave climate induces a relatively subtle seasonal cycle with higher energy conditions in the austral winter and lower energy conditions in the austral summer. Furthermore, the beach is influenced by the El Niño-Southern Oscillation (ENSO) at interannual timescales (approximately 3 to 7 years), resulting in more energetic and easterly waves impacting Narrabeen beach during La Niña periods and less energetic and more southerly waves during El Niño periods (Harley et al., 2010). Overall, nearshore currents dynamics are primarily driven by waves, given the generally mild wind conditions and microtidal regime.

Beach sand levels have been measured along 5 historical profiles (PF1, PF2, PF4, PF6, and PF8, as shown in Fig. 1d) at approximately monthly intervals since 1976. The offshore wave data is transformed into wave conditions along the 10 m depth contour in front of each profile (Fig. 2c–e) using a look-up table generated with a series of hundreds of SWAN spectral model runs (Turner et al., 2016). This high spatial and temporal resolution dataset consisting of topographic measurements and hourly wave conditions at 5 cross-shore profiles along Narrabeen beach (described in detail by Turner et al. (2016)) is freely available at <http://narrabeen.wrl.unsw.edu.au>.

Observed morphological changes at the 5 cross-shore profiles show limited long-term changes (maximum linear trend = -0.54 m/yr at PF4) in shoreline position (estimated as the cross-shore location of the $z=0$ m altitude, Harley et al., 2011). However, significant seasonal, annual, and interannual variability is observed, with a mean value of 71 m for the overall range (min/max) of variability of the shoreline position,

estimated across all profiles (e.g. PF4 and PF8, Fig. 2a,b). Seasonal variations in shoreline position show primarily accretion during the austral summer and erosion during the austral winter. Offshore of the 10 m depth contour, bathymetric variations are nearly negligible, whereas in the surf zone, observed bathymetric variations are on the order of 1 m, and thus may influence nearshore wave refraction.

The alongshore differences in wave conditions show more northerly waves and larger wave heights at PF4 than at PF8 (Fig. 2c,e comparing the WP4 and WP8). The peak period (T_p , Fig. 2d) is assumed to be homogeneous along the 10 m depth contour for the 5 alongshore profiles since it is taken as equal to the offshore value (Turner et al., 2016). Fig. 2e also highlights the seasonal dependence of the variability in the wave direction, with reduced variability in wave direction during the austral winter.

3. Model and sensitivity test description

3.1. Mathematical model

In this study, alongshore sediment transport processes are modeled using a simple one-line approach based on the work of Pelnard-Considére (1956). The one-line model estimates changes in the shoreline position S generated by alongshore gradients in the alongshore sediment flux Q :

$$\frac{\partial S}{\partial t} = -\frac{1}{Dc} \frac{\partial Q}{\partial x}, \quad (1)$$

where Dc is the depth of closure. The longshore sediment flux Q is defined as:

$$Q = Q_0 \sin(2\alpha), \quad (2)$$

where

$$Q_0 = \frac{\rho K H_b^{2.5} \sqrt{g/\gamma_b}}{16(\rho_s - \rho)\lambda}, \quad (3)$$

and

$$\alpha = \alpha_b - \alpha_{shore}. \quad (4)$$

Here, K is a dimensionless empirical parameter, H_b is the breaking wave height, g is the gravitational acceleration, γ_b is the breaker index ratio, ρ and ρ_s are the water and sediment density, respectively, λ is the sediment porosity, and α_b and α_{shore} are the breaking wave angle and the shoreline angle (Fig. 3), respectively. The shoreline angle is calculated as:

$$\alpha_{shore} = \arctan\left(\frac{\partial S}{\partial x}\right). \quad (5)$$

Eq. (1) thus can be rewritten as:

$$\frac{\partial S}{\partial t} = -\frac{1}{Dc} \frac{K \sqrt{g/\gamma_b}}{16(\rho_s - \rho)\lambda} \frac{\partial}{\partial x} \left[H_b^{2.5} \sin\left(2\left(\alpha_b - \arctan\left(\frac{\partial S}{\partial x}\right)\right)\right) \right]. \quad (6)$$

The mathematical model is discretized at predefined transects along the coast (Fig. 3), and first-order, centered finite difference schemes are used:

$$\frac{S_n^{i+1} + S_n^i}{\Delta t} = -\frac{1}{Dc} \frac{Q_{n+1/2} - Q_{n-1/2}}{\Delta X_n}. \quad (7)$$

As shown in Fig. 3, n is the transect index, X_n is the alongshore distance between adjacent transects, and i is the time index.

The wave characteristics at breaking (e.g. H_b , α_b , and γ_b) are calculated by numerically refracting and transforming the wave conditions from 10 m water depth (e.g. WP points shown in Fig. 1d) using the method of Larson et al. (2010). The limitations and hypotheses of this empirical approach are discussed in Section 6.

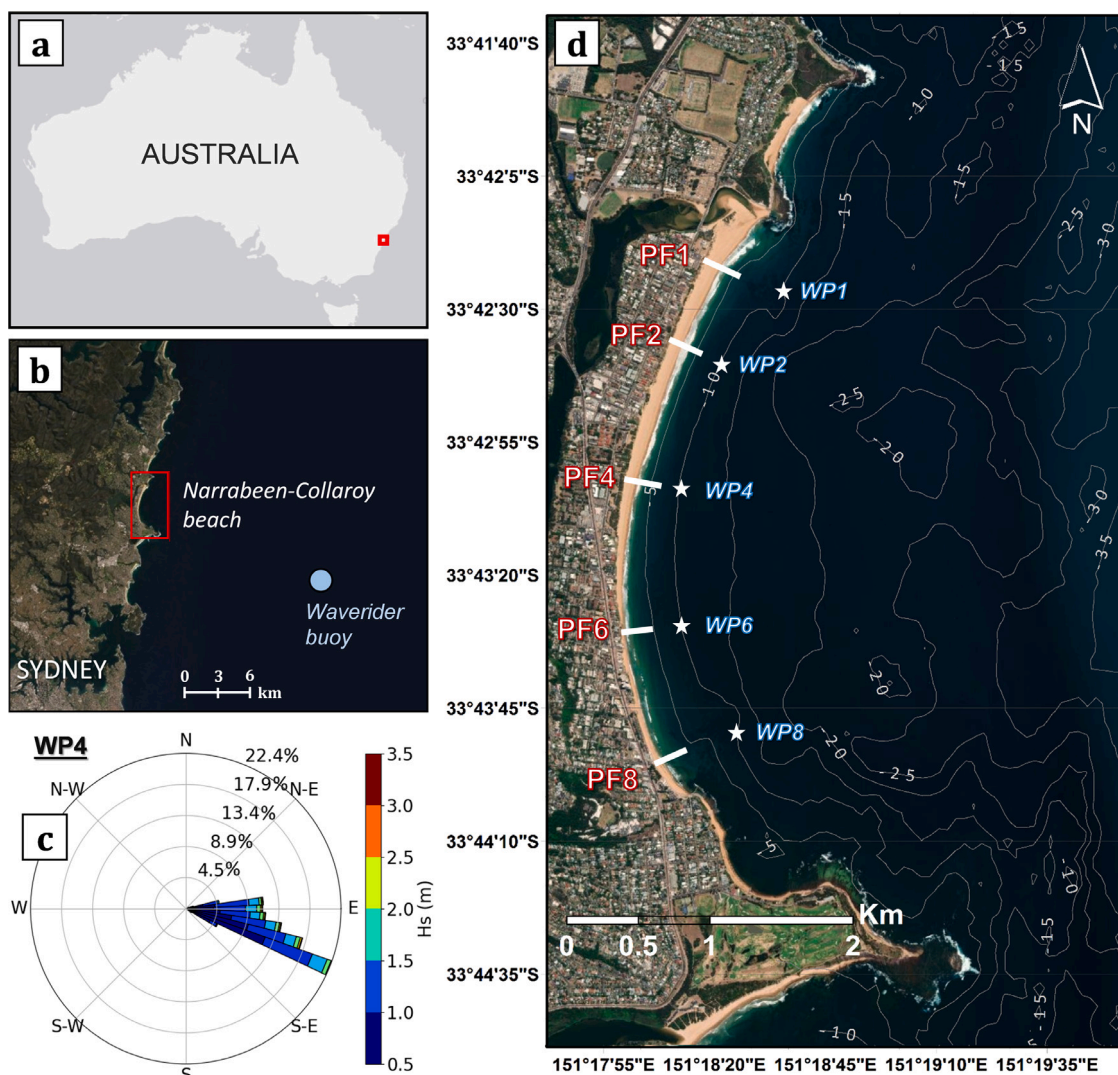


Fig. 1. Study site location and wave characteristics: (a) map of Australia indicating the zoom shown in (b), (b) the area around Narrabeen beach, showing the location of Sydney and the offshore wave buoy. (c) The wave rose indicates the percent occurrence of each wave height (colorbar) and wave direction bin (between 1979–2015), and (d) a satellite image of Narrabeen-Collaroy Beach showing the location of the 5 surveyed cross-shore profiles (named PF1, PF2, PF4, PF6, and PF8) and the 5 locations where wave conditions are available (WP1, WP2, WP4, WP6, and WP8). The bathymetry contours are shown at 5 meter depth intervals (in gray). (For interpretation of the references to color in this figure legend, the reader is referred to the web version of this article.)

3.2. Model application at Narrabeen beach

The one-line longshore model is applied at Narrabeen beach at 15 cross-shore transects distributed uniformly alongshore ($\Delta X = 250$ m). Wave conditions along the 10 m depth contour were interpolated from the time series provided at the 5 cross-shore profiles. Wave time series are unavailable at the 2 boundary transects, so the wave conditions at these locations are initially assumed to be the same as those of the adjacent profiles.

Although measurements of sediment fluxes at the domain boundaries are unavailable, given the presence of the rocky outcrops limiting alongshore sediment transport, they are assumed to be small, and zero-flux conditions are applied at the boundaries. This hypothesis will be discussed further in Section 6.

The K parameter is set to 0.02 for all transects based on qualitative comparisons of the amplitude of simulated and observed shoreline position variability. This parameter is often difficult to determine, and typical values in the literature range between 0.014 and 2.3 (Pilkey and Cooper, 2002). The relative contribution of the K parameter in this study will be discussed further in Section 6. The depth of closure D_c is estimated using the formula proposed by Hallermeier (1983), and

an alongshore mean value of 12 m is used for all transects in agreement with the bathymetric observations of Turner et al. (2016).

The one-line model is applied for a 10-year time period, from 2005 to 2015, to simulate shoreline changes caused by longshore processes using a hourly time step. Cross-shore processes are neglected by assuming that they are dominant at interannual timescales and do not contribute significantly to observed trends at pluriannual timescales. Harley et al. (2015) completed an EOF (empirical orthogonal function) analysis of 5 years of extensive 2D topographic surveys, identifying two principal modes of shoreline variability: cross-shore migration and beach rotation, explaining 55% and 22% of the variance, respectively. Beach rotation is typically attributed to longshore sediment processes, but the authors suggested that alongshore variability in cross-shore processes and differences in sandbar dynamics may also contribute. However, the contributions of these processes are not able to be quantified, and the temporal mode of the beach rotation EOF shows seasonal oscillations and no significant long-term trends.

Thus to compare the observations and the model, the mean annual shoreline position $\bar{S}(t)$, where the overline indicates the mean over a 12-month period, is calculated to focus predominantly on longshore processes and to evaluate the long-term trends in shoreline position.

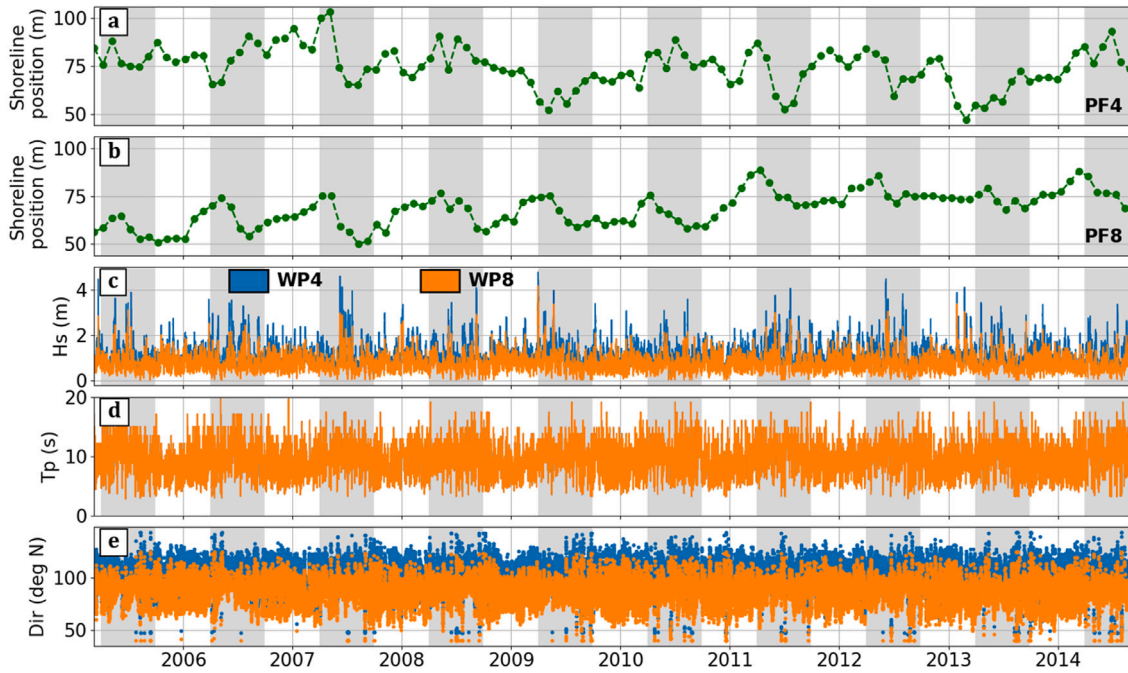


Fig. 2. Observations of the shoreline position ($z=0$ m altitude) at (a) PF4 and (b) PF8, and the corresponding wave conditions at WP4 (blue) and WP8 (orange) showing the: (c) significant wave height (H_s), (d) peak wave period (T_p), and (e) wave direction. The gray-shaded areas indicate austral winters. (For interpretation of the references to color in this figure legend, the reader is referred to the web version of this article.)

The simulation shows that, when forced with the wave time series along the 10 m depth contour, the one-line model causes a change in the shoreline planform shape, as seen in (Fig. 4b), where the final annual mean simulated ($\bar{S}_{f,mod}$) and observed ($\bar{S}_{f,obs}$) shoreline position are compared.

In comparison to the observed shoreline position at the end of the simulated time period, the simulated coastline shows significant erosion at the southern end (around 150 m at PF8), nearly no difference in the middle of the beach (with a pivot point near PF6), and accretion at the northern end (between +30 m to +60 m between PF1 and PF4)(Fig. 4b). Similar results producing large changes in the beach planform shape were also observed by Robinet et al. (2020) (as discussed previously) with the LX-Shore hybrid model over the 5-year time period from 2005 to 2010.

The beach reorientation simulated by the one-line model is caused by a disequilibrium between the coastline orientation and the incident wave direction. For a simplified case with a constant wave incidence angle, the one-line model is equivalent to a diffusion equation, bringing the shoreline position toward an equilibrium state. This equilibrium is reached when the coastline orientation is perpendicular to the incident wave direction. When the one-line model is applied at a natural site with temporal variations in the wave direction, the same response is achieved if the mean incident wave direction does not vary significantly in time. Thus, assuming that the one-line model concept is correct, the simulated beach reorientation observed here is hypothesized to be caused by errors in the model input variables or parameters, and in particular by biases in the incident wave direction. The potential contribution of bias errors in the wave height will be also discussed in Section 6.

4. Methods: wave angle bias assessment

To evaluate the sensitivity of the model to the incident wave angle, two different analyses are completed by: (1) first searching for the optimal set of bias values that minimize the differences between the simulated and observed shoreline evolution, and then (2) systematically testing the sensitivity of the model to sets of random wave angle biases

generated from specified Gaussian distributions. For both analyses, Monte Carlo simulations are completed to evaluate the impacts of the wave angle biases on the simulated shoreline position and resultant coastline orientation.

In this analysis, it is important to distinguish between a wave angle bias and a wave angle error. A wave angle bias is variable in space but constant in time (systematic error), whereas a wave angle error is variable in both space and time (non-systematic or random error). In this study, wave angle biases are examined because in the long term, random wave angle errors were observed to compensate for each other in time (not show here) and did not generate long-term coastline reorientation in the one-line longshore model, as will be discussed further in Section 6.4.

4.1. Wave angle bias estimation

In the first analysis, the impact of wave angle biases in the input wave time series at 10 m depth is evaluated with a 3-step method.

First, at each position between adjacent transects, a random wave angle bias (τ) that is constant in time, is drawn from a uniform, univariate distribution using a Monte Carlo approach. The uncorrelated random wave angle biases ($\tau_{n+1/2}$) are then added to the wave direction time-series at each position $n + 1/2$ such that the new wave angle $\tilde{\alpha}_{w,n+1/2}(t)$ in 10 m water depth is:

$$\tilde{\alpha}_{w,n+1/2}(t) = \alpha_{w,n+1/2}(t) + \tau_{n+1/2}. \quad (8)$$

Then, the one-line longshore model is run using the modified wave direction time series $\tilde{\alpha}_{w,n+1/2}(t)$, while the input wave height $H_{s,10}$ and wave period $T_{p,10}$ remain unchanged.

Lastly, the normalized root mean square error (NRMSE) is computed to quantify the difference between the observed and simulated shoreline position. The root mean square error (RMSE) is computed as:

$$RMSE = \sqrt{\sum_{n=1}^N \sum_{t=1}^T (\bar{S}_{mod,n}(t) - \bar{S}_{obs,n}(t))^2} \quad (9)$$

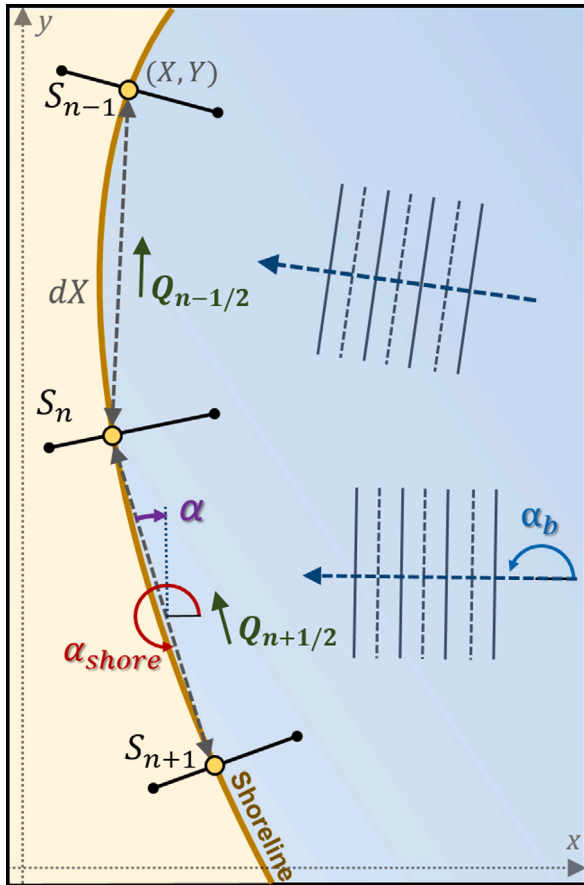


Fig. 3. Schematic representation of the model setup for cross-shore transects (index n), showing the shoreline position S , the relative wave angle α (Eq. (4)), the alongshore sediment flux Q , and the local reference frame (x, y) .

with \bar{S}_{obs} the annual moving average observation (to remove the seasonal variability) computed every month and \bar{S}_{mod} the simulated shoreline position at the corresponding time, summed over all observations times T and all transects N .

The NRMSE is calculated as the RMSE normalized by the minimum of all the RMSE values after the Monte Carlo process. This method is applied twice, in a nested approach. A first set of 15,000 Monte Carlo realizations of wave angle biases is generated, allowing τ to vary from -30° to $+30^\circ$, following a uniform univariate distribution. The results are then used to define smaller angle intervals for each transect $n+1/2$ (as shown by the vertical cyan bars in Fig. 5a), and a second set of 10,000 Monte Carlo realizations were completed to determine the set of wave angle biases $\tau_{n+1/2}$ yielding the minimum NRMSE.

Since morphological observations are not available at the domain boundaries during the simulated period, the existing 2D survey data, which spans part of the simulated period, are used to estimate the long-term trends at the two boundary transects. No trends are observed, thus it is assumed shoreline position remains unchanged for the 10-year period.

4.2. Model sensitivity analyses

In order to test the sensitivity of the model to the magnitude of the wave angle bias, the wave angle time series $\tilde{\alpha}_{w,n+1/2}(t)$ are corrected using the optimal set of biases obtained in the previous analysis. These new time series are then used as the reference simulation in the sensitivity analyses. Then, new randomly generated wave angle biases $\tau'_{n+1/2}$ are drawn from Gaussian distributions with specified standard

Table 1

Approximate optimum set of τ values for each cross-shore profile that minimize the NRMSE between the simulated and observed shoreline changes.

Profile	PF1	PF2	PF4	PF6	PF8
Optimum τ	-0.5°	4.8°	4.5°	-13.2°	-19.9°

deviations and are added to each cross-shore transect. The new wave angle time series $\alpha'_{w,n+1/2}(t)$ at each cross-shore transect are thus defined as:

$$\alpha'_{w,n+1/2}(t) = \tilde{\alpha}_{w,n+1/2}(t) + \tau'_{n+1/2}. \quad (10)$$

For each test, the $\tau'_{n+1/2}$ values are drawn from independent Gaussian distributions with a specified standard deviation $\sigma_{\tau'}$. Six different tests with 1000 Monte Carlo realizations were carried out for $\sigma_{\tau'}$ ranging from 1° to 6° .

A second sensitivity analysis testing the relative importance of biases in the wave height is carried out for comparison. The same approach is used, and the wave height time series are adjusted by a bias β' that is a percentage of the wave height, such that:

$$H'_{s,n+1/2}(t) = (1 + \beta'_{n+1/2})H_{s,n+1/2}(t). \quad (11)$$

For each test, the $\beta'_{n+1/2}$ values are drawn from independent Gaussian distributions with a specified standard deviation $\sigma_{\beta'}$. Four different tests with 1000 Monte Carlo realizations were carried out for $\sigma_{\beta'}$ ranging from 5% to 30%.

Finally, the associated error is quantified as the difference between the final, simulated annual mean shoreline position for each realization with a specified $\sigma_{\tau'}$ or $\sigma_{\beta'}$ and for the reference simulation.

The distribution of the differences is obtained for each value of $\sigma_{\tau'}$ or $\sigma_{\beta'}$, which is then characterized by its standard deviation $\sigma_{\Delta S}$. The standard deviation serves as a metric to estimate the order of magnitude of shoreline position errors for a given distribution of wave angle bias errors.

5. Results

5.1. Optimal wave angle analysis

In Fig. 5a, the 50 best Monte Carlo realizations with a NRMSE within 30% of the minimum value vary within a range of up to 10° for each transect and show generally positive values of τ in the north (with two exceptions just north of PF2 and PF4), and then increasingly negative values south of PF4. The optimum set of τ values (purple curve, Fig. 5a) between PF1 to PF8 ranges from 10° to -20° (Table 1).

It is important to note that the model depends not only on $\tau_{n+1/2}$, but also on alongshore gradients in $\tau_{n+1/2}$. In the one-line longshore model, changes in the shoreline position are caused by alongshore gradients in the sediment flux, which are calculated from alongshore gradients in the wave angle α_b and in the wave height H_b , as shown in Eq. (7). The alongshore gradients in $\tau_{n+1/2}$ for the 50 best realizations (Fig. 5b) have a similar, concave shape with the highest values at the extremities of the beach.

The optimal τ values correct for the potential wave angle bias at breaking, caused either by biases in the 10 m depth wave time series or by wave refraction occurring between the 10 m depth contour and the wave breaking point. The large values of $\tau_{n+1/2}$ obtained near the boundary transects (Fig. 5a) may also be attributed to two additional sources that impact more significantly the transects at or near the domain boundaries. They correct for errors induced by extrapolating the wave conditions from the WP points to the domain boundaries, likely generating the largest errors at these transects. They also correct for the assumption that there are no sediment fluxes at the boundaries.

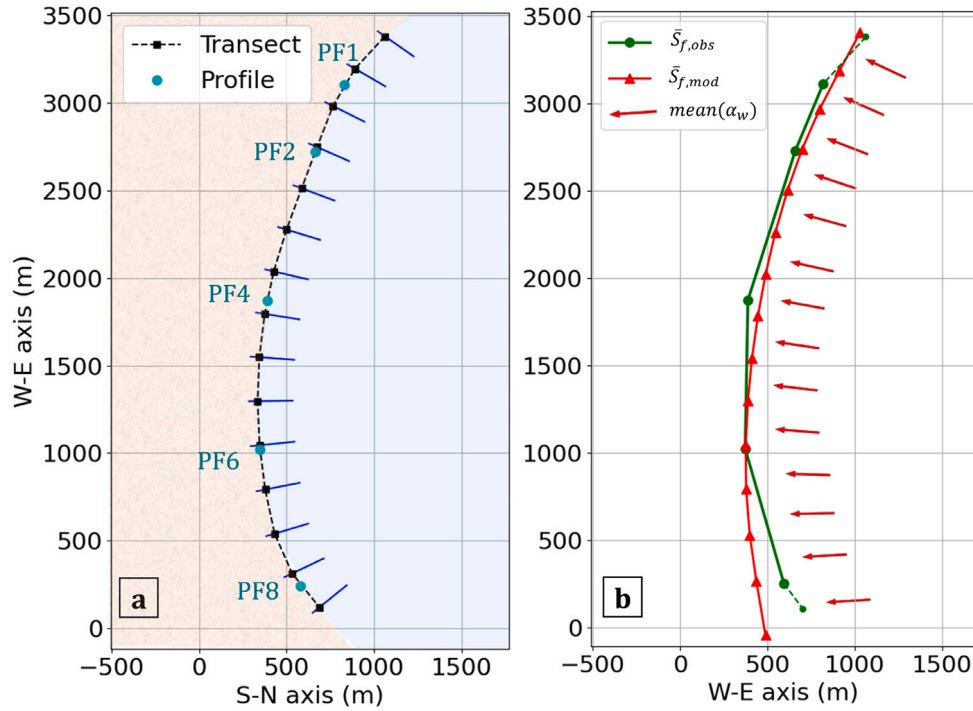


Fig. 4. (a) Longshore model setup at Narrabeen beach, showing the 15 defined cross-shore transects. (b) Observed (green line) and simulated (red line) annual mean shoreline position at the end of the 10-year simulation. For each cross-shore transect, the red arrow indicates the temporal mean wave angle (α_w) at 10 m water depth. (For interpretation of the references to color in this figure legend, the reader is referred to the web version of this article.)

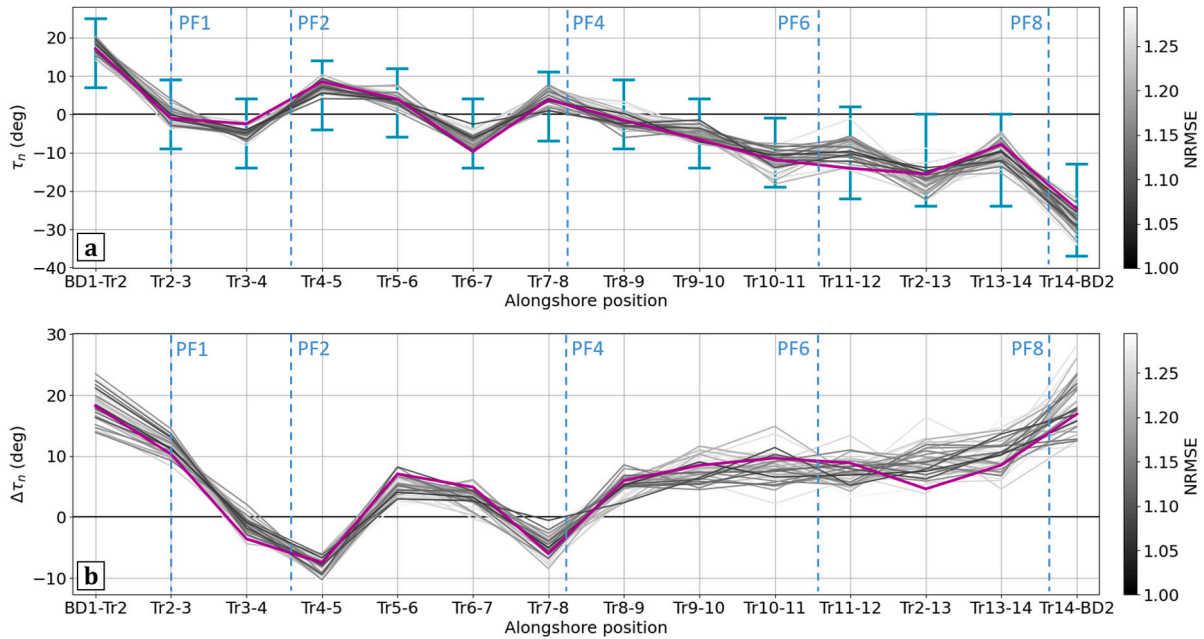


Fig. 5. Wave angle bias tests: (a) wave angle bias correction ($\tau_{n+1/2}$) and (b) gradient in wave angle bias correction between adjacent transects plotted for the 50 best Monte Carlo realizations. The vertical cyan bars indicate the range of values used to define the second set of refined Monte Carlo realizations. The color of each curve indicates the NRMSE (gray color scale ranging from 1.0 to 1.3), and the optimal set of $\tau_{n+1/2}$ values are shown in magenta. (For interpretation of the references to color in this figure legend, the reader is referred to the web version of this article.)

5.2. Optimal wave angle bias values

Using the optimal set of $\tau_{n+1/2}$ values in the one-line longshore model reproduces a simulated coastline shape similar to the observed coastline shape (Fig. 6a). The wave angle time series are corrected with small changes in the mean wave angle (e.g. Table 1 for PF1–PF8) relative to the original mean wave angle (Fig. 6a), except close to the

domain boundaries at the extremities of the beach. The difference between the annual mean initial, observed and final, observed or modeled shoreline position is calculated as: $\Delta \bar{S} = \bar{S}_f - \bar{S}_i$. The difference $\Delta \bar{S}$ calculated for the corrected wave time series is similar to the observed changes $\Delta \bar{S}_{obs}$ (Fig. 6b).

The simulated shoreline position changes using the original wave angle time series ($\alpha_{w,n+1/2}$ red triangles in Fig. 6b) are generally larger

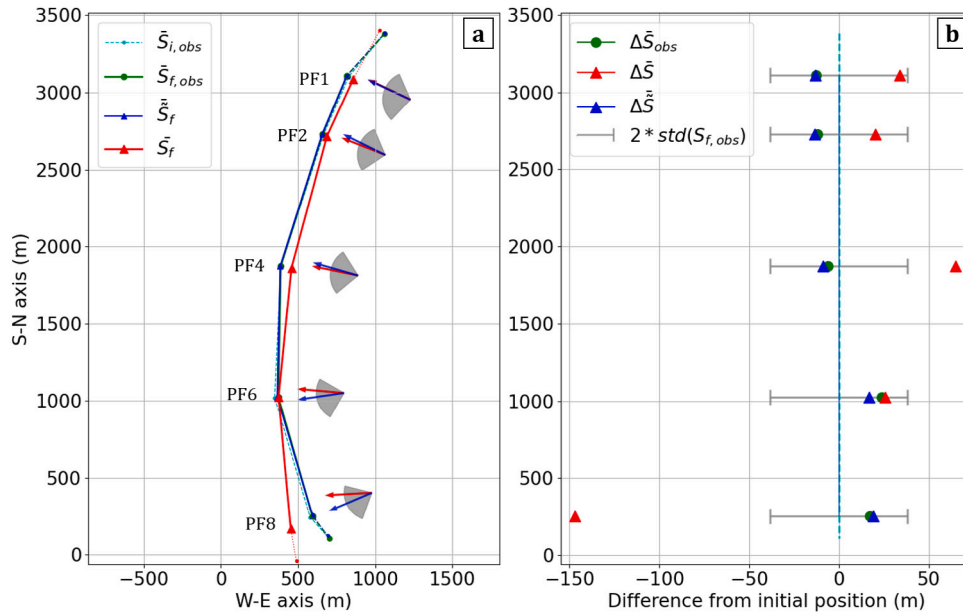


Fig. 6. Comparison of the observed and simulated shoreline position: (a) aerial view of the observed initial $\bar{S}_{i,obs}$ (cyan) and final $\bar{S}_{f,obs}$ (green) shoreline position and the simulated final shoreline position for the original \bar{S}_f (red) and corrected \bar{S}_f (blue) wave angle time series. Also shown are the temporal mean wave direction of the original α_w (red arrow) and corrected $\bar{\alpha}_w$ (blue arrow) time series and the wave direction envelop (gray shading) in 10 m water depth. (b) Difference in the shoreline position relative to the initial observations (cyan) for: the final observed ($\Delta\bar{S}_{obs}$, green) and simulated shoreline position for the original ($\Delta\bar{S}$, red) and corrected ($\Delta\bar{S}$, blue) wave angle time series, and beach shoreline position variance ($2 * std(S_{f,obs})$, gray). (For interpretation of the references to color in this figure legend, the reader is referred to the web version of this article.)

than or of the same order of magnitude as the seasonal variability over the 10-year period (Fig. 6b, gray bars). However, the simulated shoreline position changes using the corrected wave time series are smaller than the observed seasonal variability (Fig. 6b, gray bars) and agree more closely with the observations. Finally, this simple analysis demonstrates how a relatively small bias in the input wave angle can cause significant changes in the shoreline planform shape that are different from the observations.

5.3. Model sensitivity analyses

Using the wave angle time series $\bar{\alpha}_w$ corrected with the optimal set of bias values $\tau_{n+1/2}$ as the reference case, a sensitivity analysis is completed to evaluate the impacts of randomly distributed wave angle biases on the simulated shoreline position.

Six different tests of 1000 Monte Carlo realizations were carried out for σ_{τ} ranging from 1° to 6° , and the model error is quantified as the standard deviation $\sigma_{\Delta S}$ of a Gaussian distribution fit to the distribution of the estimated shoreline position differences (e.g. Fig. 7a,c, for $\sigma_{\tau} = 5^\circ$). The standard deviation of shoreline position errors $\sigma_{\Delta S}$ increases approximately linearly as a function of the standard deviation of the wave angle biases σ_{τ} (Fig. 7b). Shoreline position errors are on the order of 5 m for wave angle biases as small as 1° , and increase to more than 30 m for wave angle biases of only $5-6^\circ$.

With respect to the sensitivity of the model to a bias in the wave height, with $\sigma_{\beta} = 5\%$, 10% , 20% , 30% , the associated shoreline position errors $\sigma_{\Delta S}$ are approximately one order of magnitude smaller than for the wave angle bias tests (comparing Fig. 7d, e and f). For example, shoreline position errors are typically less than 1 m for wave height biases of 5% and reach only 3 m for wave height biases as large as 30%.

6. Discussion

6.1. One-line model limitations

The one-line longshore model is a simple approach for estimating large-scale longshore sediment transport that has several important

conceptual limitations (see Pilkey and Cooper, 2002). Two potential sources of error can be distinguished: the conceptual framework of the one-line model and the longshore flux estimation.

In the conceptual model, one limitation is the estimation of the depth of closure D_c , which determines the active profile length. The assumption that a well-defined depth of closure exists remains controversial, and it is difficult to identify this limit *in situ*. While a physical, cross-shore limit to the active profile (zone within which wave-breaking induced sediment transport occurs) likely exists, this limit varies in time as a function of the wave characteristics and sediment characteristics and availability, and depends on the considered time period (Valiente et al., 2019). Therefore, assuming a constant value in time and in space (e.g. for a beach) is convenient for modeling purposes but may contribute to intrinsic errors in one-line models (D'Anna et al., 2021). A second limitation is the assumption of a constant equilibrium profile and a uniform cross-shore distribution of the longshore sediment flux (Bayram et al., 2001). In addition, factors like the instantaneous tide level, which would be more important on a meso- or macrotidal beach, or total water depth likely impact the cross-shore distribution of sediments.

In estimating the longshore sediment flux, a second potential source of errors in the one-line model is the choice or calibration of the K parameter in the CERC formula. This free parameter determines the longshore flux magnitude, and its magnitude and even use are highly controversial (see Pilkey and Cooper, 2002). However, in this study the value of K does not impact the estimation of τ since K is constant for all transects and thus the one-line model can be simplified to a diffusion equation. Therefore, in long-term simulations where the coastline reaches a new equilibrium shape, the K value primarily impacts the value of the diffusion coefficient, which controls the coastline adjustment timescale to changes in the wave direction, but does not impact the coastline shape.

Finally, the one-line model conserves sediment, and therefore the choice of boundary conditions may have strong impacts on the simulated shoreline changes. In this study, it is assumed that there are no sediment fluxes at the boundaries since the beach is bounded by rocky outcrops. The only likely sediment sources or sinks are associated with the lagoon mouth at the northern end of the beach. However,

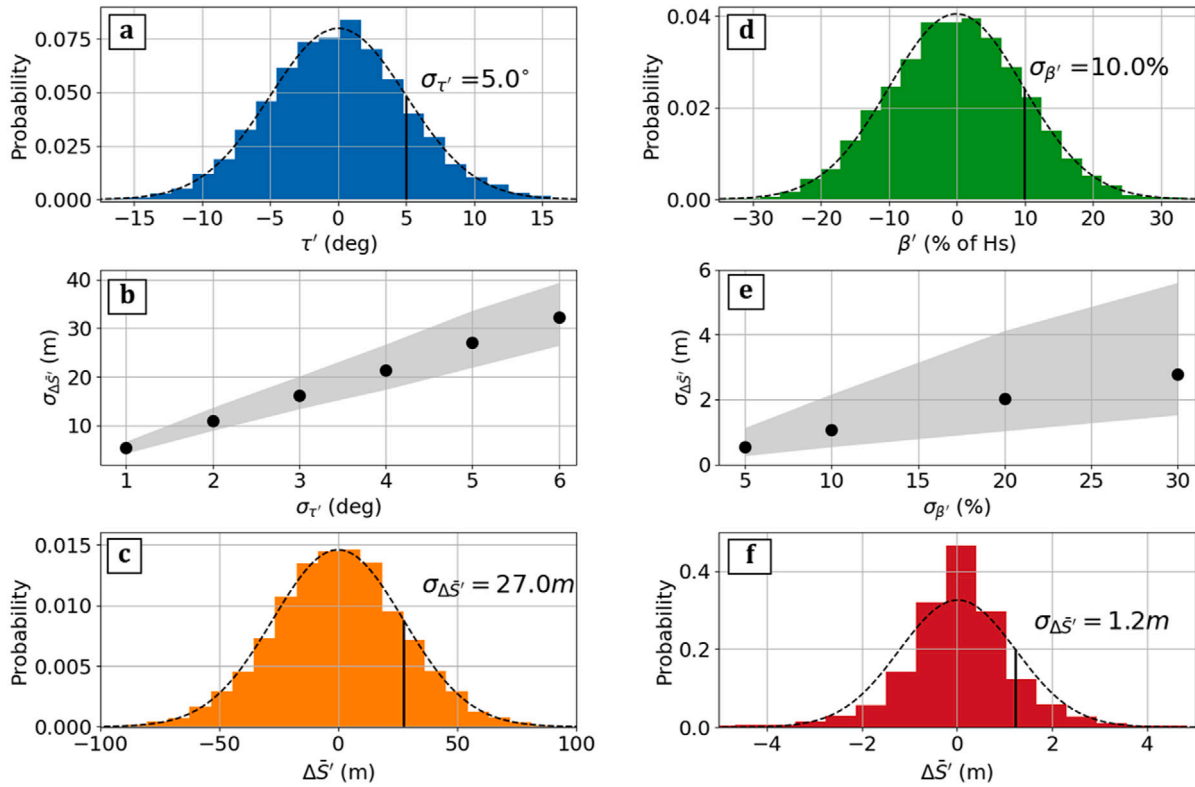


Fig. 7. Wave angle bias sensitivity analysis: (a) wave angle bias distribution for $\sigma_{\tau'} = 5^\circ$, (b) standard deviation of shoreline position differences ($\sigma_{\Delta S'}$) as a function of $\sigma_{\tau'}$, showing the mean (black points) and envelope (range of minimum and maximum values) over all transects (gray shading) (c) shoreline position difference (in comparison to the reference case) distribution for all transects for $\sigma_{\tau'} = 5^\circ$, (d) β' distribution for $\sigma_{\beta'} = 10\%$, (e) standard deviation of shoreline position differences ($\sigma_{\Delta S'}$) as a function of $\sigma_{\beta'}$, showing the mean (black points) and envelope (range of minimum and maximum values) over all transects (gray shading), and (f) shoreline position difference distribution for all transects for $\sigma_{\beta'} = 10\%$. (For interpretation of the references to color in this figure legend, the reader is referred to the web version of this article.)

the corresponding fluxes are unable to be quantified accurately and are assumed to be negligible in comparison to the estimated longshore fluxes (Harley et al., 2011), so they are not considered in the model.

6.2. Wave bias analysis assumptions and limits

In this study, several assumptions are made in applying a Monte Carlo approach to finding the optimal set of wave angle bias corrections and then in completing sensitivity analyses to randomly generated wave angle and wave height bias errors. Firstly, it is assumed that the errors observed in the one-line model simulation (e.g. reorientation of the coastline) are caused by errors in the input wave angle time series and not in the general model formulation.

This study focuses on evaluating the effects of random wave angle biases rather than random, time-variable errors because in preliminary tests (not shown here), the effects of random wave angle errors compensated for each other in time over the 10-year period, causing no long-term trends in shoreline position changes. Time-variable errors induce short-term shoreline changes, at timescales of the model time-step, which are affected by the K parameter. Thus, the sensitivity of the model to time-variable errors is linked intrinsically to the estimation of K , and therefore these two issues should be addressed simultaneously (as in Kroon et al., 2020).

Secondly, a Monte Carlo approach is chosen to generate the random wave angle biases $\tau_{n+1/2}$. A simpler hypothesis would be to consider an alongshore homogeneous τ , assuming that the wave angle bias originates at the wave buoy and remains constant as the waves propagate to the 10 m depth contour. In this case, the corrected wave angle time series would become:

$$\alpha_{w,n+1/2}^*(t) = \alpha_{w,n+1/2}(t) + \tau. \quad (12)$$

The effects of adding an alongshore homogeneous τ (ranging from $-30^\circ \leq \tau \leq 30^\circ$) show that it is insufficient to correct changes in the shoreline planform shape because it induces different responses at different alongshore locations. For example, an alongshore homogeneous change in mean wave direction is able to correct the shoreline position changes at PF8 with $\tau \approx -10^\circ$ (Fig. 8b), but it is unable to do so at PF4 (Fig. 8a). At PF4, adding a spatially homogeneous τ value does not allow reproducing the observed shoreline changes since all of the simulations predicted significant long-term trends that were not observed.

At Narrabeen beach, local wave refraction contributes to alongshore gradients in wave angle. Alongshore variable biases thus allow to correct for errors associated with local wave refraction that varies alongshore owing to the curvature of the coastline and the alongshore variable bathymetry. In particular, these errors may become large at the extremities of the beach near PF1 and PF8 where reefs located in -5 to -10 m water depth likely have significant impacts on wave refraction.

Extending this work beyond Narrabeen beach, this analysis emphasizes the importance in representing well not only the wave angle time series, but also alongshore gradients in the wave angle time series used to force one-line longshore models.

6.3. Planform beach orientation

To evaluate the capacity of the one-line model to accurately reproduce the beach orientation and its evolution in time, the Beach Orientation BO and Beach Orientation Index BOI were calculated following Harley et al. (2014) and Jaramillo et al. (2021). The BO and BOI are calculated using the observed shoreline position S_{obs} and both the original S and corrected \bar{S} simulated shoreline positions at the 5

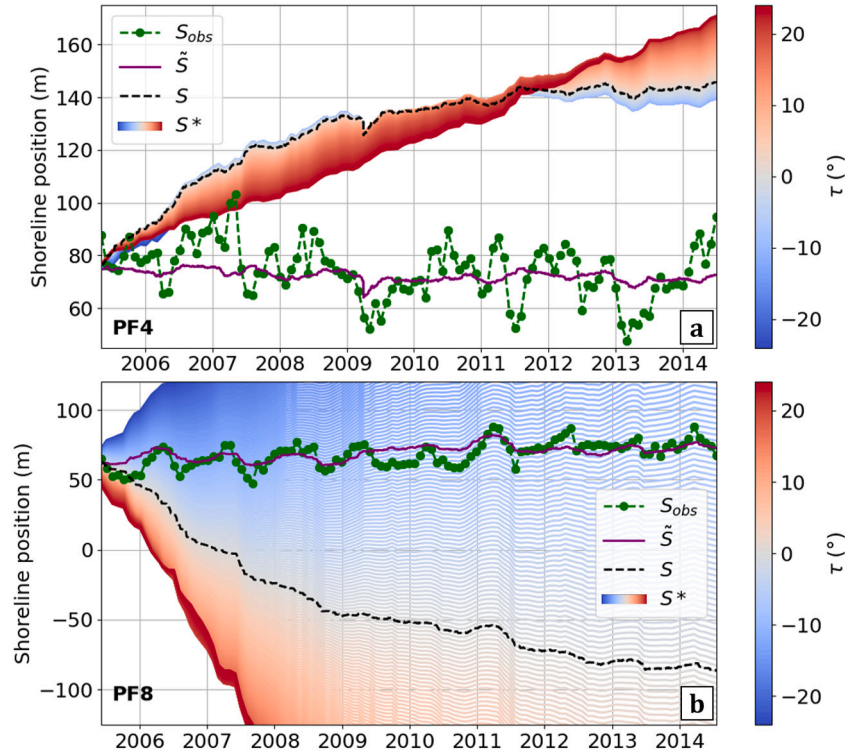


Fig. 8. Sensitivity analysis with alongshore homogeneous τ showing the shoreline position evolution from observations S_{obs} (green), the original model simulation S (black), the model simulation forced with the corrected wave angle time series \tilde{S} (purple), and the model simulations S^* forced with wave angle time series adjusted with alongshore homogeneous τ ranging from -30° to 30° (blue–red colorbar). (For interpretation of the references to color in this figure legend, the reader is referred to the web version of this article.)

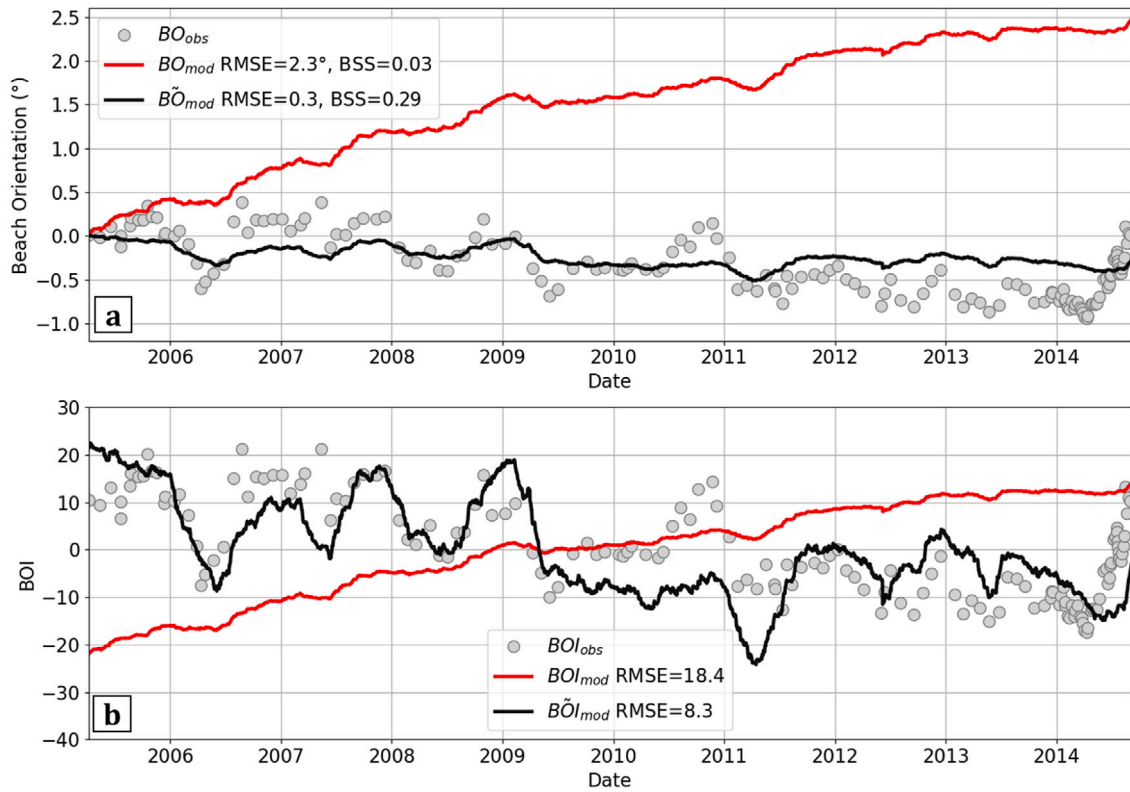


Fig. 9. Comparison of (a) Beach Orientation (BO) and (b) Beach Orientation Index (BOI) for shoreline observation (gray dotted), original model simulation (red) and model simulation forced with correct wave angle time series (black). (For interpretation of the references to color in this figure legend, the reader is referred to the web version of this article.)

cross-shore transects PF1–8 (Fig. 9a, b). During the simulated period, the observed beach orientation BO_{obs} and beach orientation index BOI_{obs} show slightly negative trends and small seasonal oscillations (gray circles, Fig. 9). In comparison, beach orientation BO_{mod} and beach orientation index BOI_{mod} calculated from the simulations with the original wave angle time series (red curves, Fig. 9) shows significant differences with the observations. After correcting the wave angle time series with the optimal set of biases, the agreement between the observed and simulated beach orientation \tilde{BO}_{mod} and beach orientation index \tilde{BOI}_{mod} (black curves, Fig. 9) increases significantly. Jaramillo et al. (2021) also modeled shoreline changes at Narrabeen beach with an equilibrium-based shoreline rotation model, quantifying their model performance with the $RMSE$ between the simulated and observed BO and BOI time series. The results presented here (using only a one-line longshore model) obtain $RMSE$ of the same order of magnitude as their study (which covered a longer time period).

6.4. One-line model sensitivity to biases in the wave height and direction

Assuming that the one-line model is conceptually correct, this work shows that correcting a small wave angle bias (approximately 5–10°) has significant impacts on simulated long-term shoreline change trends. The comparison of the observed and corrected simulations of shoreline changes highlights that this approach allows improving long-term (10-year) simulations of shoreline evolution (\tilde{S} , purple line compared to S_{obs} , the dashed black line in Fig. 8). As expected, the corrected mean wave angles in Fig. 6a are more perpendicular to the coastline orientation. However, the difference between the mean wave and shoreline angles is not reduced to zero, which would result in no longshore sediment fluxes.

The sensitivity analyses quantified the impacts of a Gaussian distribution of wave angle biases in wave direction and wave height. The wave angle sensitivity analysis showed significantly larger impacts on the modeled final shoreline position than the wave height sensitivity analysis. For wave angle biases τ' drawn from a Gaussian distribution with a standard deviation of $\sigma_{\tau'}$, the associated alongshore gradients in wave direction are even larger, following a Gaussian distribution with a standard deviation of $\sqrt{2}\sigma_{\tau'}$. The observed increases in $\sigma_{\Delta\tilde{S}}$ are thus a result of the importance of alongshore gradients in wave angle and wave height in the one-line model, as well as the uncorrelated sampling method used to obtain each Monte Carlo realization. These gradients thus cause large gradients in alongshore sediment fluxes, resulting in significant shoreline position changes (e.g. on the order of 5 m to 30 m for wave angle biases ranging from 1° to 6°).

In this study, the set of optimal τ values (Section 5.1) are the same order of magnitude as the uncertainties estimated by Turner et al. (2016) for transects PF1, 2, 4, and 6. The higher τ values obtained at PF8 and near the boundary transects BD1 and BD2 are likely caused by other factors, as suggested in Section 5.1. One such contribution is the assumption that the wave conditions at BD1 and BD2 are the same as those at adjacent transects, even though the coastline angle changes. Secondly, the presence of reefs in the nearshore zone may cause wave refraction between the 10 m depth contour and the location of wave breaking that is not taken into account in the Larson et al. (2010) wave refraction approach used here. Finally, the assumption of no sediment fluxes at the boundaries forces the longshore model to conserve sediment, although the sediment budget is not necessarily strictly closed if sediment either bypasses the rocky outcrop at the southern end of the beach or is gained or lost at the lagoon mouth at the northern end of beach.

Finally, biases in the wave height have significantly smaller impacts on the resultant shoreline changes than biases in the wave angle (Fig. 7b,e), causing shoreline position changes on the order of 3 m for wave height biases as large as 30%. When generating wave conditions from wind-forced wave models, Komen et al. (1996) estimated that a 10% error in the surface wind speed can cause a 10%–20% error

in the wave height. Thus, similar to George et al. (2019), the range of wave height bias errors β' tested in this study ranged from 5% to 30%, representing a potentially common range of errors encountered at sites with limited wave data. However, these biases are significantly larger than the expected values at Narrabeen beach, where Turner et al. (2016) estimated wave height biases on the order of only 3%–4%.

6.5. Comparison of corrected and SWAN model breaking wave angles

To investigate the cause of the wave bias and the validity of the wave angle corrections $\tau_{n+1/2}$ proposed here, the corrected mean wave direction at the breaking point $\tilde{\alpha}_{b,n+1/2}$ obtained in this analysis (after using the Larson et al. (2010) method to propagate $\tilde{\alpha}_{w,n+1/2}$ to the breaking point) is compared to the breaking wave direction derived independently from a high resolution SWAN model (Harley et al., 2011) (Fig. 10b). These data are produced using a look-up table similar to that described in Turner et al. (2016), after extending it from producing wave conditions at 10 m water depth to the break point (thereby taking into account the additional refraction caused by nearshore reefs). The SWAN simulations were run using a single directional spreading value (30°) and were calibrated using nearshore wave data, showing a high correlation for the wave height and a slightly lower correlation for the wave direction (approximately 0.9 and 0.7, respectively Turner et al., 2016). While the SWAN model succeeds overall in reproducing the nearshore wave conditions, a deterministic wave model such as XBeach may be able to reproduce better the breaking wave conditions for this complex bathymetry. Before comparing the wave angles at the breaking point, it is important to note that the refraction calculated by the Larson et al. (2010) method between 10 m depth and the breaking point is small, ranging from 0° in the north to approximately –7° in the south (Fig. 10a). The estimated refraction effects are even smaller for the corrected wave angles $\tilde{\alpha}_{w,n+1/2}$ since on average the difference between the offshore wave angle and the coastline orientation decreased.

The comparison of the optimal breaking wave angles obtained in this analysis ($\tilde{\alpha}_b$) with the SWAN breaking wave angle ($\alpha_{b,SWAN}$) shows good overall agreement (Fig. 10b), supporting the hypothesis that the errors generated by the one-line model are caused by biases in the input wave angle. The corrected breaking wave angles are in general close to the SWAN breaking wave angles. The largest differences are observed at PF1, which is close to the model boundary, and PF6, where the wave angle bias is overestimated in comparison to the SWAN model look-up table. The largest change (nearly 20°) between the original (α_b) and corrected ($\tilde{\alpha}_b$) wave angle time series occurred at PF8, where $\tilde{\alpha}_b$ now agrees well with $\alpha_{b,SWAN}$. It is assumed that the optimal wave angle bias at this location primarily corrects for the underestimation of local wave refraction caused by a nearshore reef.

6.6. Wave data uncertainties

Morphological evolution models are forced with wave conditions derived from observations (e.g. wave buoys) and model outputs (e.g. spectral wave models). This study shows the sensitivity of a one-line longshore model to errors in the input wave direction, which then propagate through the modeling chain to cause errors in the predicted morphological changes. This is an important result because it is well known that the wave direction is difficult to estimate accurately with spectral wave models, often showing large uncertainties (e.g. Ardhuin and Roland, 2013; Cavaleri et al., 2018), and that wave buoy observations also have errors in measured wave angles (e.g. Barstow et al., 2005). Even if the input wave conditions are known with high accuracy from one of these sources, wave conditions are often obtained at an offshore location and then must be propagated to the breaking point to be input in the one-line model flux calculation. Therefore, at the breaking point, it is often difficult to have highly accurate knowledge of the wave conditions, and in particular the incident wave angle, especially in areas where refraction over complex bathymetry may be

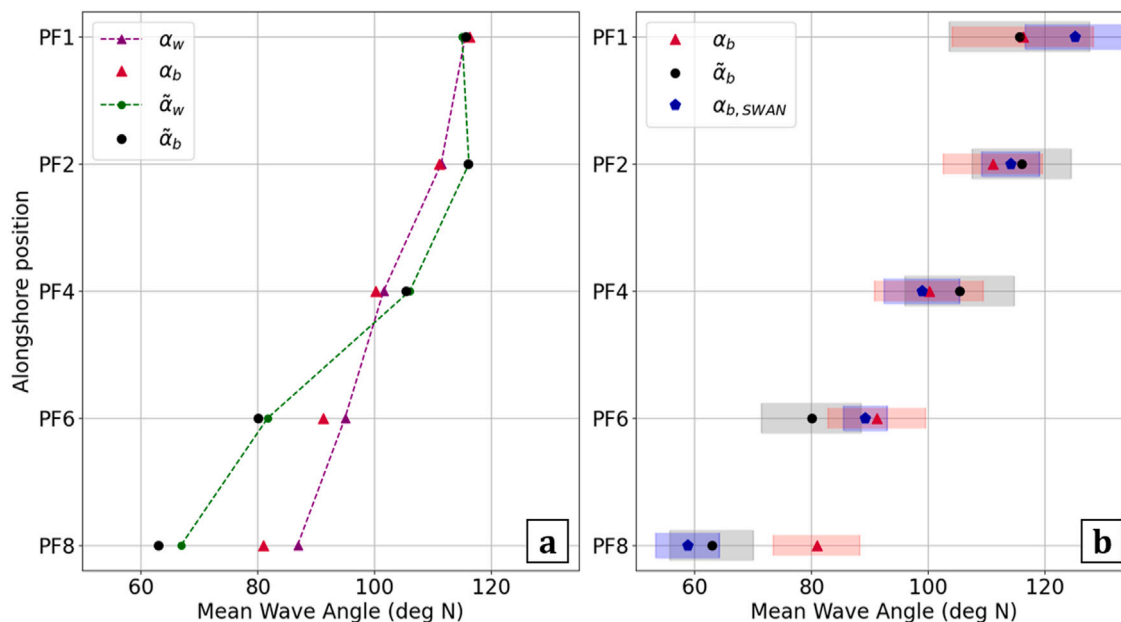


Fig. 10. Temporal mean input and breaking wave angles: (a) Comparison between the mean original α_w (purple triangles) and corrected $\tilde{\alpha}_w$ (green points) 10 m depth wave angles, and the original α_b (red triangles) and corrected $\tilde{\alpha}_b$ (black points) breaking wave angles propagated using the Larson et al. (2010) method. (b) Comparison between the mean original (red triangles), corrected (black points), and SWAN (blue points) breaking wave angles, where the shaded zones indicate the standard deviation. (For interpretation of the references to color in this figure legend, the reader is referred to the web version of this article.)

significant and not necessarily represented well when using simple wave transformation approaches. An additional limitation in one-line longshore models is that bulk wave parameters are used to force the model, and thus the potential complexity of the full spectra is neglected (e.g. existence of secondary swells, bimodal spectra, or high wave angle spreading).

This study highlights the importance of propagating accurately offshore wave conditions to the nearshore zone to force morphological evolution models. One-line longshore models are particularly sensitive to the input wave angle, and even more so, to alongshore gradients in the input wave angle. In addition, this work also demonstrates that having high-quality estimates of nearshore wave conditions at 10 m depth may not be sufficient in particular cases where there is significant refraction shoreward of this location up to the breaking point (e.g. for embayed beach or beaches with complex nearshore bathymetry such as Narrabeen). However, it is not common to have access to high-quality, high-resolution, long-term estimates of wave conditions at the wave breaking point due to the high computational costs associated with nearshore wave propagation models. This emphasizes the need for further developments in nearshore in situ hydrodynamics monitoring and accurate and efficient nearshore wave propagation models, as well as the necessity to take into account uncertainties in morphological evolution studies.

7. Conclusions

In this study, the sensitivity of a commonly used one-line longshore sediment transport model to the input wave angle is evaluated using a statistical approach. The study is carried out at Narrabeen beach for the 10-year period from 2005 to 2015, where the model, forced with an available dataset of wave conditions at the 10 m depth contour, simulated a change in the shoreline planform orientation that was different from that of the observations. The objective of the current work is to study the source of this error and to understand the sensitivity of the one-line longshore model to the input wave angle by using a Monte Carlo approach to correct the wave angle time series by adding randomly generated biases (spatially variable but temporally constant). The model sensitivity is further quantified by comparing the simulated

shoreline position at the end of the 10-year period to the observations and to the reference test case corresponding to the optimal wave bias correction.

The results of the first analysis show that by correcting the wave angle time series with the optimal set of biases (in the range of -20° to 5°), the simulated shoreline planform orientation agrees well with the observations. The shoreline position error distributions resulting from the wave angle and wave height bias sensitivity analyses demonstrate that the one-line longshore model is highly sensitive to biases in the wave angle. For example, the standard deviation of the shoreline position errors increases by approximately 5 m for a 1° increase in the wave direction bias, but by less than 1 m for a 10% bias in the wave height.

The breaking wave angles obtained from the optimal corrected biases in this study generally agree well with the breaking wave angles obtained by propagating offshore wave conditions using the SWAN model. This comparison also demonstrated that the corrections to the mean wave direction are coherent with wave refraction processes in the nearshore zone, which are not taken into account in simple wave transformation models often used to estimate wave breaking conditions. Thus, the methodology presented in this paper is able to compensate for the lack of accurate breaking wave direction data by using available morphological observations.

Finally, this study highlights the need for high quality estimates of breaking wave conditions, and in particular, the wave breaking direction and its alongshore gradients, in longshore sediment transport models. Even when nearshore (e.g. 10 m depth) wave conditions are known, simple propagation methods like the approach of Larson et al. (2010) should be used with caution in areas with complex bathymetry, and the uncertainties associated with these simple modeling approaches should be evaluated.

CRediT authorship contribution statement

T. Chataigner: Conceptualization, Data curation, Formal analysis, Investigation, Methodology, Resources, Software, Validation, Visualization, Writing – original draft, Writing – review & editing. **M.L. Yates:** Conceptualization, Funding acquisition, Investigation, Methodology,

Project administration, Supervision, Visualization, Writing – original draft, Writing – review & editing. **N. Le Dantec:** Conceptualization, Funding acquisition, Methodology, Project administration, Resources, Supervision, Visualization, Writing – original draft, Writing – review & editing. **M.D. Harley:** Conceptualization, Data curation, Resources, Writing – original draft, Writing – review & editing. **K.D. Splinter:** Conceptualization, Supervision, Writing – original draft, Writing – review & editing. **N. Goutal:** Supervision, Funding acquisition, Project administration.

Declaration of competing interest

The authors declare that they have no known competing financial interests or personal relationships that could have appeared to influence the work reported in this paper.

Acknowledgment

Teddy Chataigner's thesis is financed by the *Agence de l'Innovation de Défense* (AID) program of the *Direction Générale de l'Armement* (DGA), the Cerema, and the Ecole des Ponts ParisTech.

References

- Anderson, D., Ruggiero, P., Antolínez, J.A., Méndez, F.J., Allan, J., 2018. A climate index optimized for longshore sediment transport reveals interannual and multidecadal littoral cell rotations. *J. Geophys. Res.: Earth Surf.* 123 (8), 1958–1981.
- Antolínez, J.A., Méndez, F.J., Anderson, D., Ruggiero, P., Kaminsky, G.M., 2019. Predicting climate-Driven Coastlines with a simple and efficient multiscale model. *J. Geophys. Res.: Earth Surf.* 124 (6), 1596–1624.
- Arduin, F., Roland, A., 2013. The development of spectral wave models: Coastal and coupled aspects. In: *Proceedings of Coastal Dynamics 2013: 7th International Conference on Coastal Dynamics*.
- Ashton, A.D., Murray, A.B., 2006. High-angle wave instability and emergent shoreline shapes: 1. Modeling of sand waves, flying spits, and capes. *J. Geophys. Res.: Earth Surf.* 111 (F4).
- Athanasiou, P., Van Dongeren, A.R., Giardino, A., Voudoukas, M.I., Ranasinghe, R., Kwadijk, J., 2020. Uncertainties in projections of sandy beach erosion due to sea level rise: An analysis at the European scale. *Sci. Rep.* 10.
- Barstow, S.F., Bidlot, J.R., Cairns, S., Donelan, M.A., Drennan, W.M., Dupuis, H., Graber, H.C., Green, J.J., Gronlie, O., Guérin, C., Gurgel, K.-W., Günther, H., Hauser, D., Hayes, K., Hessner, K., Hoja, D., Icard, D., Kahma, K.K., Keller, W.C., Krogstad, H.E., Lefevre, J.-M., Lehner, S., Magnusson, A.K., Monbaliu, J., Nieto Borge, J.C., Pettersson, H., Plant, W.J., Quentin, C.G., Reichert, K., Reistad, M., Rosenthal, W., Saetra, O., Schulz-Stellenfleth, J., Walsh, E.J., Weill, A., Wolf, J., Wright, C.W., Wyatt, L.R., 2005. In: Hauser, D., Kahma, K., Krogstad, H., Monbaliu, S., et al. Wyatt, S.L. (Eds.), *Measuring and Analysing the Directional Spectrum of Ocean Waves*. In: COST 714; EUR 21367, COST Office, p. 465.
- Bayram, A., Larson, M., Miller, H.C., Kraus, N.C., 2001. Cross-shore distribution of longshore sediment transport: comparison between predictive formulas and field measurements. In: *Coastal Engineering 2000*. American Society of Civil Engineers, pp. 3114–3127.
- Bergillos, R., López-Ruiz, A., Principal-Gómez, D., Ortega-Sánchez, M., 2018. An integrated methodology to forecast the efficiency of nourishment strategies in eroding deltas. *Sci. Total Environ.* 613–614, 1175–1184.
- Bouchette, F., Manna, M., Montalvo, P., Nutz, A., Schuster, M., Ghienne, J.-F., 2014. Growth of cusped spits. *J. Coast. Res.* 47–52.
- Cavaleri, L., Abdalla, S., Benetazzo, A., Bertotti, L., Bidlot, J., Breivik, O., Carniel, S., Jensen, R., Portilla-Yandun, J., Rogers, W., Roland, A., Sanchez-Arcilla, A., Smith, J., Staneva, J., Toledo, Y., Vledder, G., Westhuysen, A., 2018. Wave modelling in coastal and inner seas. *Prog. Oceanogr.* 167.
- D'Anna, M., Castelle, B., Idier, D., Rohmer, J., Le Cozannet, G., Thieblemont, R., Bricheno, L., 2021. Uncertainties in shoreline projections to 2100 at Truc Vert beach (France): Role of sea-level rise and equilibrium model assumptions. *J. Geophys. Res.: Earth Surf.*
- D'Anna, M., Idier, D., Castelle, B., Le Cozannet, G., Rohmer, J., Robinet, A., 2020. Impact of model free parameters and sea-level rise uncertainties on 20-years shoreline hindcast: the case of Truc Vert beach (SW France). *Earth Surf. Process. Landf.* 45 (8), 1895–1907.
- Davidson, M., Splinter, K., Turner, I., 2013. A simple equilibrium model for predicting shoreline change. *Coast. Eng.* 73, 191–202.
- Davidson, M.A., Turner, I.L., Splinter, K.D., Harley, M.D., 2017. Annual prediction of shoreline erosion and subsequent recovery. *Coast. Eng.* 130, 14–25.
- Delft Hydraulics, W., 1994. UNIBEST, A Software Suite for the Simulation of Sediment Transport Processes and Related Morphodynamics of Beach Profiles and Coastline Evolution.
- Durrant, T., Greenslade, D., Hemer, M., Trenham, C., 2014. A Global Wave Hindcast Focused on the Central and South Pacific. Technical report, CAWCR Technical Report No. 070.
- French, J., Payo, A., Murray, B., Orford, J., Eliot, M., Cowell, P., 2016. Appropriate complexity for the prediction of coastal and estuarine geomorphic behaviour at decadal to centennial scales. *Geomorphology* 256, 3–16.
- George, J., Sanil Kumar, V., Victor, G., Gowthaman, R., 2019. Variability of the local wave regime and the wave-induced sediment transport along the ganpatipule coast, eastern arabian sea. *Regional Stud. Mar. Sci.* 31.
- Hallermeier, R.J., 1983. Sand transport limits in coastal structure design. *Proc. Coast. Struct. '83, Am. Soc. Civ. Eng.* 703–716.
- Hanson, H., 1989. Genesis: A generalized shoreline change numerical model. *J. Coast. Res.* 5 (1), 1–27.
- Harley, M., Andriolo, U., Armaroli, C., Ciavola, P., 2014. Shoreline rotation and response to nourishment of a gravel embayed beach using a low-cost video monitoring technique: San Michele-Sassi Neri, central Italy. *J. Coast. Conserv.* 18, 551–565.
- Harley, M.D., Turner, I.L., Short, A.D., 2015. New insights into embayed beach rotation: The importance of wave exposure and cross-shore processes. *J. Geophys. Res.: Earth Surf.* 120 (8), 1470–1484.
- Harley, M.D., Turner, I.L., Short, A.D., Ranasinghe, R., 2010. Interannual variability and controls of the sydney wave climate. *Int. J. Climatol.* 30 (9), 1322–1335.
- Harley, M.D., Turner, I.L., Short, A.D., Ranasinghe, R., 2011. A reevaluation of coastal embayment rotation: The dominance of cross-shore versus alongshore sediment transport processes, Collaroy-Narrabeen beach, southeast Australia. *J. Geophys. Res.: Earth Surf.* 116 (F4).
- Jaramillo, C., González, M., Medina, R., Turki, I., 2021. An equilibrium-based shoreline rotation model. *Coast. Eng.* 163, 103789.
- Kamphuis, J., Davies, M., Nairn, R., Sayao, O., 1986. Calculation of littoral sand transport rate. *Coast. Eng.* 10 (1), 1–21.
- Komen, G.J., Cavaleri, L., Donelan, M., Hasselmann, K., Hasselmann, S., Janssen, P.A.E.M., 1996. *Dynamics and Modelling of Ocean Waves*.
- Kroon, A., De Schipper, M., Gelder, P., Aarninkhof, S., 2020. Ranking uncertainty: Wave climate variability versus model uncertainty in probabilistic assessment of coastline change. *Coast. Eng.* 158, 103673.
- Larson, M., Hanson, H., Kraus, N.C., 1997. Analytical solutions of one-line model for shoreline change near coastal structures. *J. Waterw. Port Coast. Ocean Eng.* 123 (4), 180–191.
- Larson, M., Hoan, L., Hanson, H., 2010. Direct formula to compute wave height and angle at incipient breaking. *J. Waterw. Port Coast. Ocean Eng.* 136.
- Le Cozannet, G., Bulteau, T., Castelle, B., Ranasinghe, R., Wöppelmann, G., Rohmer, J., Bernon, N., Idier, D., Louisor, J., Salas-Y-Méla, D., 2019. Quantifying uncertainties of sandy shoreline change projections as sea level rises. *Sci. Rep.* 9 (1), 42.
- Miller, J.K., Dean, R.G., 2004. A simple new shoreline change model. *Coast. Eng.* 51 (7), 531–556.
- Montaño, J., Coco, G., Antolínez, J.A.A., Beuzen, T., Bryan, K.R., Cagigal, L., Castelle, B., Davidson, M.A., Goldstein, E.B., Ibaceta, R., Idier, D., Ludka, B.C., Masoud-Ansari, S., Méndez, F.J., Murray, A.B., Plant, N.G., Ratliff, K.M., Robinet, A., Rueda, A., Sénéchal, N., Simmons, J.A., Splinter, K.D., Stephens, S., Townend, I., Vitousek, S., Vos, K., 2020. Blind testing of shoreline evolution models. *Sci. Rep.* 10.
- Murray, A.B., 2007. Reducing model complexity for explanation and prediction. *Geomorphology* 90 (3), 178–191. Reduced-Complexity Geomorphological Modelling for River and Catchment Management.
- Pelnaud-Considère, R., 1956. Essai de théorie de l'évolution des formes de rivages en plages de sable et de galets. *Houille Blanche* 289–301.
- Pilkey, O., Cooper, A., 2002. Longshore transport volumes: A critical view. *J. Coast. Res.* 36, 572–580.
- Ranasinghe, R., Callaghan, R.D., 2013. Does a more sophisticated storm erosion model improve probabilistic erosion estimates? *Coastal Dynamic*.
- Reeve, D., Pedrozo-Acuña, A., Spivack, M., 2014. Beach memory and ensemble prediction of shoreline evolution near a groyne. *Coast. Eng.* 86, 77–87.
- Robinet, A., Castelle, B., Idier, D., Harley, M., Splinter, K., 2020. Controls of local geology and cross-shore/longshore processes on embayed beach shoreline variability. *Mar. Geol.* 422, 106118.
- Robinet, A., Idier, D., Castelle, B., Marieu, V., 2018. A reduced-complexity shoreline change model combining longshore and cross-shore processes: The LX-shore model. *Environ. Model. Softw.* 109, 1–16.
- Roelvink, J., Banning, G., 1995. Design and development of DELFT3D and application to coastal morphodynamics. *Oceanograph. Lit. Rev.* 11, 925.
- Roelvink, D., Reniers, A., Van Dongeren, A., van Thiel de Vries, J., McCall, R., Lescinski, J., 2009. Modelling storm impacts on beaches, dunes and barrier islands. *Coast. Eng.* 56 (11), 1133–1152.
- Ruggiero, P., Buijsman, M., Kaminsky, G., Gelfenbaum, G., 2010. Modeling the effects of wave climate and sediment supply variability on large-scale shoreline change. *Mar. Geol.* 273, 127–140.

- Safak, I., List, J., Warner, J., Kumar, N., 2017. Observations and 3D hydrodynamics-based modeling of decadal-scale shoreline change along the Outer Banks, North Carolina. *Coast. Eng.* 120, 78–92.
- Splinter, K.D., Turner, I.L., Davidson, M.A., Barnard, P., Castelle, B., Oltman-Shay, J., 2014. A generalized equilibrium model for predicting daily to interannual shoreline response. *J. Geophys. Res.: Earth Surf.* 119 (9), 1936–1958.
- Toimil, A., Camus, P., Losada, I., Le Cozannet, G., Nicholls, R., Idier, D., Maspataud, A., 2020. Climate change-driven coastal erosion modelling in temperate sandy beaches: Methods and uncertainty treatment. *Earth-Sci. Rev.* 202, 103110.
- Tran, Y.H., Barthélemy, E., 2020. Combined longshore and cross-shore shoreline model for closed embayed beaches. *Coast. Eng.* 158, 103692.
- Turki, I., Medina, R., Coco, G., González, M., 2013. An equilibrium model to predict shoreline rotation of pocket beaches. *Mar. Geol.* 346, 220–232.
- Turner, I., Harley, M., Short, A., Simmons, J., Bracs, M., Phillips, M., Splinter, K., 2016. A multi-decade dataset of monthly beach profile surveys and inshore wave forcing at Narrabeen, Australia. *Scientific Data* 3.
- USACE, 1984. Shore Protection Manual. Technical report, U.S. Army Corps of Engineers, Vicksburg, Mississippi.
- Valiente, N.G., Masselink, G., Scott, T., Conley, D., McCarroll, R.J., 2019. Role of waves and tides on depth of closure and potential for headland bypassing. *Mar. Geol.* 407, 60–75.
- Vitousek, S., Barnard, P.L., Limber, P., Erikson, L., Cole, B., 2017. A model integrating longshore and cross-shore processes for predicting long-term shoreline response to climate change. *J. Geophys. Res.: Earth Surf.* 122 (4), 782–806.
- Wang, B., Reeve, D., 2010. Probabilistic modelling of long-term beach evolution near segmented shore-parallel breakwaters. *Coast. Eng.* 57 (8), 732–744.
- Warren, I., Bach, H., 1992. MIKE 21: A modelling system for estuaries, coastal waters and seas. *Environ. Softw.* 7 (4), 229–240, 3rd International Software Exhibition for Environmental Science and Engineering.
- Wright, L.D., Short, A.D., 1984. Morphodynamic variability of surf zones and beaches: A synthesis. *Mar. Geol.* 56, 93–118.
- Yates, M.L., Guza, R.T., O'Reilly, W.C., 2009. Equilibrium shoreline response: Observations and modeling. *J. Geophys. Res.* 114 (C09014).

Chapter V

Combined modeling

Ce chapitre détaille la combinaison des modèles cross-shore et longshore présentés dans les chapitres 3 et 4, et auxquels est ajouté un terme de tendance linéaire. Cette combinaison est effectuée en examinant différents degrés de couplage entre les 3 composants. Les hypothèses de couplage, ainsi que les formulations qui en résultent, sont décrits. Ainsi, 7 modèles combinés sont appliqués à la plage de Narrabeen et leurs performances sont analysées à l'aide de 3 critères pour évaluer leurs capacités à différentes échelles de temps: à court terme (horaire à mensuel), à moyen terme (saisonnier à infra-annuel) et à long terme (pluriannuel à decennal). Des hypothèses sont utilisées pour réduire le nombre de paramètres libres optimisés lors de l'application du modèle. Ainsi, un seul ensemble de coefficients pour le modèle cross-shore et une seule valeur de coefficient de flux longshore sont utilisés pour l'ensemble de la plage. Les performances de chaque modèle combiné sont discutées en tenant compte de leurs formulations et des hypothèses de couplage. Les résultats pour le site de Narrabeen montrent tout d'abord que la prise en compte des processus longshore dans l'approche combinée améliore toujours les performances par rapport au modèle cross-shore seul. L'intégration d'un terme linéaire améliore la capacité de reproduction du modèle, à moyen et long terme, davantage que la composante longshore, sur la majeure partie de la plage de Narrabeen. Les approches combinées, intégrant à la fois le terme linéaire et la composante longshore, présentent une meilleure capacité à reproduire les variations à long terme par rapport aux approches avec uniquement la composante longshore. Les différences sont moins importantes concernant les performances à reproduire les variations à moyen terme car le modèle longshore reproduit une partie de la variabilité aux extrémités des plages à ces échelles de temps. L'analyse de la performance du modèle en fonction du degré de couplage montre que les formulations indépendantes et faiblement couplées ont des performances équivalentes à toutes les échelles de temps, tandis que les approches fortement couplées sont moins performantes pour reproduire la variabilité à long terme. Finalement, les modèles avec les meilleures performances globales à Narrabeen sont le modèle cross-shore avec un terme linéaire intégré, le modèle hybride avec un terme linéaire et le modèle faiblement couplé avec un terme linéaire. Aucune différence significative n'est observée entre ces approches. Cependant, les résultats obtenus pour la plage de Narrabeen devront être validés sur d'autres sites avant d'être généralisés.

Chapter V

Combined modeling

In this chapter, the difficulty arising from accounting for both longshore and cross-shore processes in an empirical shoreline change model are presented, and the different approaches used to combine or couple the two models, the resulting model formulations, and their respective hypotheses are described and illustrated.

Then, the different model formulations are applied at Narrabeen Beach to compare their performance in reproducing the shoreline position evolution, using three different criteria to evaluate the model performance at different times scales.

V.1 Introduction to combined modeling

The need to represent both cross-shore and longshore processes is explained by variations in the relative importance of each process at different sites due to the existing diversity of morphological and hydrodynamical conditions. This relative predominance of one process can even potentially vary within the same site as a function of time and space.

Indeed, shoreline changes due to cross-shore processes are occurring either at short to medium term encompassing for example rapid changes during a single storm event, to seasonal/intra-annual shoreline oscillations generated from example by the seasonality of the wave height.

Shoreline changes from longshore processes depend on the gradient of the longshore sediment flux, thus the time scale of longshore shoreline evolution is related to all processes affecting the longshore sediment transport intensity or direction, such as changes in the forcing wave climate at pluriannual scales, changes in sediment availability, or human interventions like building of a groyne or detached breakwater. However, longshore processes can also generate shoreline changes on short time scales, for example for a storm event in particular near a groyne, where alongshore sediment transport is interrupted (Kamphuis 2000).

Hence, processes responsible for alongshore gradients in sediment fluxes generally occur at longer time scales than processes generating cross-shore sediment transport.

Thus, to manage the reproduction of complex coastal system evolution when considering large spatial scales and long temporal scales, it is necessary to consider both cross-shore and longshore processes. In the 2 previous chapters, empirical approaches that represent complex morphodynamical processes in a simplified manner were described. These approaches are formulated with strong hypotheses, since they both consider that the only process that affects the shoreline is the process they reproduce.

Thus, when trying to combine these 2 approaches, there are different potential degrees of interac-

tion and coupling possible, depending on the hypothesis taken concerning the independency of the component, thereby it result in different model numerical implementation.

Additionally, in order to account for other unresolved processes, a linear term may also be added to these 2 components. This term can be found in other combined models in the literature (e.g. [Long & Plant \(2012\)](#), [Jaramillo et al. \(2019\)](#) or [Vitousek et al. \(2017\)](#)) to account for changes in Mean Sea Level, or sediment sources or sinks not represented in the longshore or cross-shore models, such as eolian transport, beach nourishment, fluvial sediment input or sediment transport offshore.

One of the main difficulties in assessing the performance of these combined models is that the respective contributions of cross-shore and longshore processes to observed shoreline changes remains a challenge to distinguish and to quantify.

Overall, cross-shore and longshore process contributions are intertwine in the observations. In previous studies, trials were made to compare the Empirical Orthogonal Function analysis (EOF) from the observations and from the combined model to look for the variance explained by each model component, thus permitting one to evaluate that the mode reproduced by the cross-shore component could correspond to cross-shore processes ([Antolínez et al. 2019](#), [Robinet et al. 2020](#)). However, this is a strong hypothesis, as the EOF analysis is not directly separating the processes in the different modes but rather highlighting existing spatio-temporal correlations. This correlation can account for different processes contributing to the same mode as shown by [Harley et al. \(2015\)](#) for the rotation at Narrabeen that includes both longshore and cross-shore processes. Even from a modeling perspective, understanding the contributions of a particular component in the total combined approach performance is complex, in particular in coupled models with feedback between the different components.

Thus, a method based on the utilisation of 3 criteria, each qualifying the model performance at a particular time scale is presented here, to evaluate the differences in the combined model performance depending on the formulation used, and to highlight the different cross-shore and longshore component contributions.

V.2 Model combinations

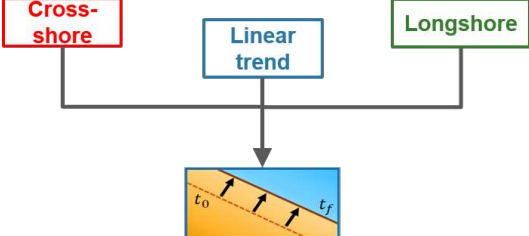
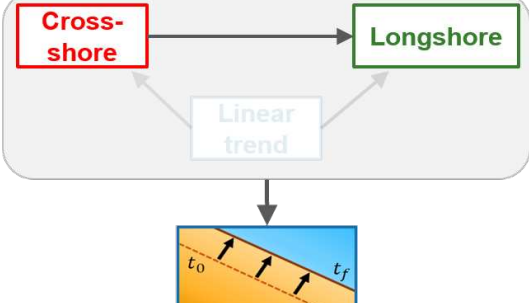
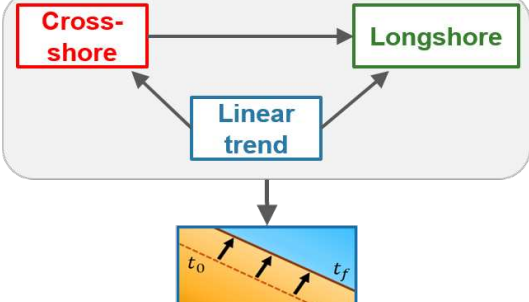
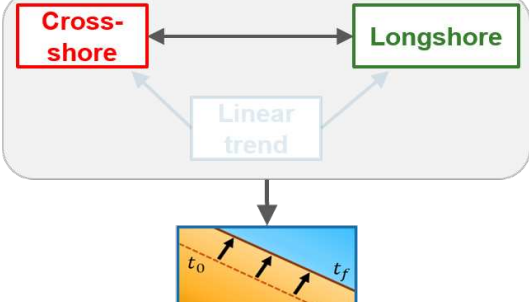
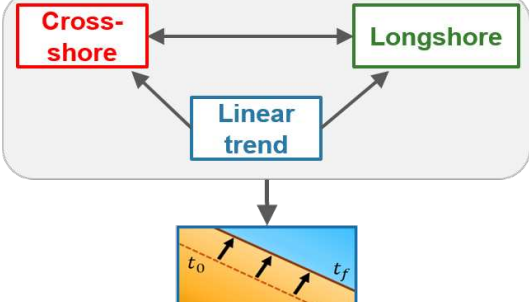
This section presents the different model combinations using the cross-shore empirical shoreline model (from Chapter III), a longshore one-line model (from Chapter IV), and potentially incorporating a linear term, and it describes how these components interact in the model with synthetic cases as illustrations (Table V.1).

First, 2 approaches based only on a cross-shore model incorporating a linear trend term will be presented, then 2 combined approaches will be introduced, using as component both the cross-shore, the longshore model and one with the linear term, but without interactions between these components. Finally, 4 combined approaches, with varying degrees of coupling between the components, will be described: 2 using only the longshore and cross-shore models, and 2 using the 3

components (Table V.1). The variable of interest, the shoreline position S , will be described using the model abbreviation name, listed in Table V.1, for example S_H for the hybrid model shoreline position.

Table V.1: Synthesis of the models presented in this chapter, their abbreviations, components, interactions, and free parameters.

Considered Models			
abbreviation	Model name	Components and interactions	Free parameter
CS	Cross-shore		$a, b, C+, C-$
LS	Longshore		K
CSL	Cross-shore plus linear term		$a, b, C+, C-, trd$
$CSLEEF$	Cross-shore integrating a linear term		$a, b, C+, C-, trd$
H	Hybrid		$a, b, C+, C-, K$

<p><i>HL</i></p>	<p>Hybrid plus linear term</p>		<p>$a, b, C+, C-, trd, K$</p>
<p><i>W</i></p>	<p>Weakly Coupled</p>		<p>$a, b, C+, C-, K$</p>
<p><i>WL</i></p>	<p>Weakly Coupled with linear term</p>		<p>$a, b, C+, C-, trd, K$</p>
<p><i>F</i></p>	<p>Fully Coupled</p>		<p>$a, b, C+, C-, K$</p>
<p><i>FL</i></p>	<p>Fully Coupled with linear term</p>		<p>$a, b, C+, C-, trd, K$</p>

V.2.1 Cross-shore model with a linear term

The first combination simply consists of the cross-shore empirical shoreline model and a linear trend term, thus these approaches don't integrate the longshore model. They assume that longshore processes may be simply approximated as a linear trend.

From this definition, 2 approaches were identified in the literature, one simply adding a linear term to the shoreline change estimate by the *CS* model (based on Long & Plant 2012), and the second integrating the linear trend term inside the equilibrium equation of the *CS* model (from Jaramillo et al. 2019), as described in more detail in the following sections.

CSL model

This first approach adds a linear trend term to the calculated cross-shore shoreline position, and is named *CSL* (table V.1 line 3). Here, the *CS* model doesn't interact with the linear term in time. So the model is written as :

$$S_{CSL}(t) = S_{CS}(t) + trd.t \quad (V.1)$$

with

$$S_{CS}(t) = S_{CS}(t-1) + \frac{dS_{CS}}{dt} \Delta t \quad (V.2)$$

and the cross-shore model as in eq III.1

$$\frac{dS_{CS}}{dt} = C^{\pm} E^{1/2} (E - (aS_{CS} + b)) \quad (V.3)$$

In this formulation, the linear trend term $trd.t$ is added to the *CS* model shoreline position $S_{CS}(t)$ to form the model shoreline position $S_{CSL}(t)$, thus the linear term doesn't impact the *CS* model calculation, because if the linear term were added in eq V.2, this formulation would force the cross-shore shoreline position S_{CS} to diverge more and more from the equilibrium position due to the linear term.

This modification of the shoreline disequilibrium would generate a progressive increase in amplitude of the *CS* model shoreline oscillations as the disequilibrium forces the shoreline position to return to the equilibrium position.

CSLEEF model from Jaramillo et al. (2019)

This combined approach is based on the approach proposed by Jaramillo et al. (2019), which integrates a linear term in the definition of the equilibrium energy in the *CS* model, as is named *CSLEEF* (table V.1 line 4). The trend parameter represents unresolved processes (for example a constant rate of sediment loss or gain) that induces a modification of the shoreline equilibrium position in time, thus inducing shoreline motion (retreat or advance).

The integration of the linear trend term in the equilibrium expression is performed, following the

Equilibrium Energy Function (EEF) defined by Jara et al. (2015), to enable the model to represent change of beach sediment volume over time, whereas the CS model alone considers a constant EEF and thus a constant sediment volume.

$$\frac{dS_{CSLEEF}}{dt} = C^{\pm} E^{1/2} (E - (a(S_{CSLEEF} - trd.t) + b)) \quad (V.4)$$

This formulation makes the equilibrium CS model to account for a linear adjustment of the beach equilibrium position.

The subtraction of the linear term in the equilibrium position is the equivalent of a constant change in the b parameter in time. This parameter controls the equilibrium shoreline position of the model, thus the linear change of b induces a linear variation of the equilibrium shoreline position and enabled this modified version of the CS model to reproduce long term linear trends.

When introduced in the equilibrium equation, this linear adjustment of the equilibrium accounts for the beach profile response to a change in the sediment budget, from either human activities like beach nourishment or infrastructure projects modifying longshore processes, or may represent unresolved processes like shoreline regression due to mean sea level change or shoreline change from longshore processes (Jaramillo et al. (2019)).

Comparing the CSL and $CSLEEF$ models

Using identical CS model coefficients and an identical linear term, different synthetic cases are proposed to compare the effects of adding (CSL) versus integrating ($CSLEEF$) the linear term in the CS model.

This synthetic test case was created using the forcing conditions of PF4 at Narrabeen Beach for a 9-year period (2005-2014) corresponding to the period presented in Chapter IV.

The initial shoreline position is set to 0 and the model is run using an hourly time step. The cross-shore coefficients are identical for both models using values similar to those obtained for Narrabeen Beach: $a=-0.25$, $b=5$, $C^+=-0.01$ and $C^-=-0.3$ (Fig. V.1 green curve).

Then two linear trend terms were chosen for two different tests: one generating an increase of ≈ 20 m of the shoreline position over 9 years $trd = 0.006$ m/day and a second creating a more important increase of ≈ 120 m with $trd = 0.04$ m/day.

The amplitude of the lower trend parameter was chosen to match over the 9 year period the amplitude of the CS model seasonal variation (≈ 20 m), and the second trend was chosen to generate a comparable amplitude of shoreline variations over a year or two.

This test shows that for a given set of cross-shore coefficients, there is almost no difference between the 2 modeled shoreline positions when using the small linear term coefficient compared to the cross-shore variation amplitude (Fig. V.1 red and dark blue curve). However, when the linear term coefficient increases, differences between the 2 model formulations arise from the influence of the linear term on the CS model equilibrium (Fig. V.1, compare the light blue and magenta curves).

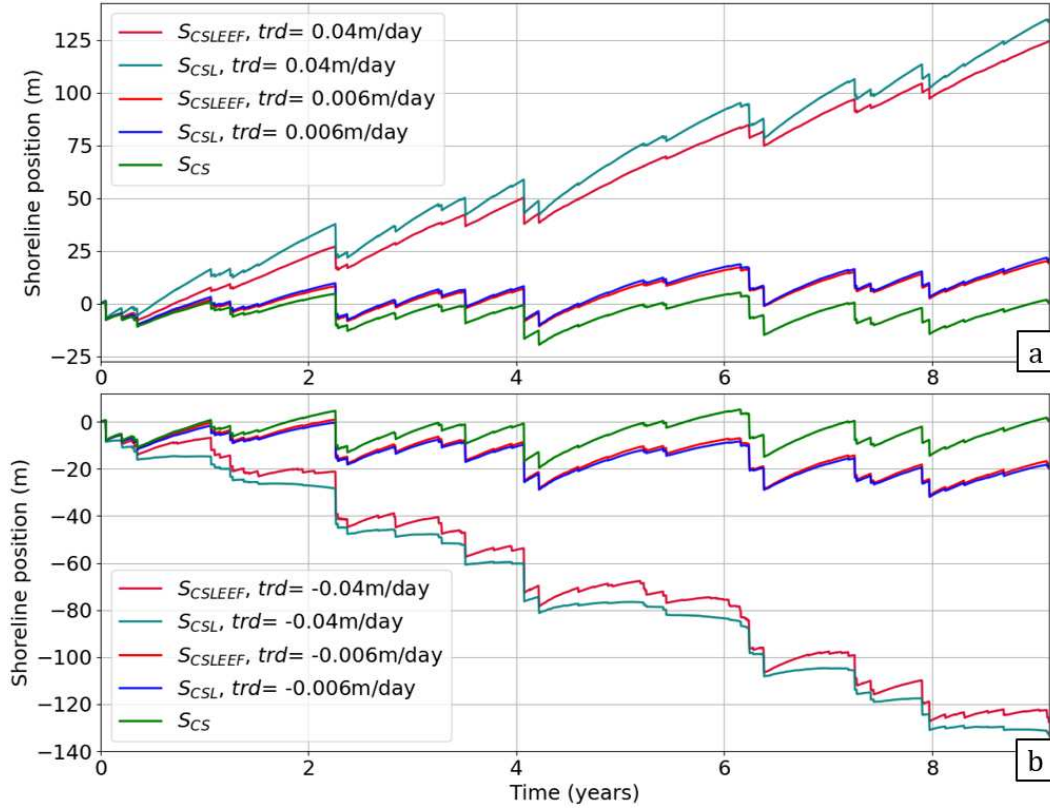


Figure V.1: Comparison of the linear term integration effects on model behavior for 2 different amplitudes of (a) positive linear trend, (b) negative linear trend. With S_{CSL} : model version with sum of the 2 independent components, and S_{CSLEEF} : model with the integration of the linear term in the equilibrium equation.

This difference depends on the convergence speed toward the equilibrium position of the equilibrium model.

In fact, in the [Jaramillo et al. \(2019\)](#) approach, the model reproduced a linear term trend because the equilibrium position of the CS model is shifted at every time step by the linear term. Thus the CS model tends toward this new equilibrium position at a certain rate that is equal to the shoreline disequilibrium multiply by the $aC^\pm E^{1/2}$ factor (eq. V.3). In this synthetic case, the converging speed is changing over time as $C^+ \neq C^-$ with $aC^+ < aC^-$.

It results in the model convergence rate toward equilibrium being higher during erosion events than during accretion events. Thus, for the positive trd values (Fig. V.1a), the influence of the linear term on the shoreline position is also more important during erosion events, and it results in a more reduced amplitude of the erosion event compared to the CS and CSL models (Fig. V.1, compare the light blue and the green curves with the magenta curve). During accretion events, accounting for a positive linear trend in the equilibrium already decreases the model disequilibrium, thereby the $CSLEEF$ model accretion rate is lower than the CSL accretion rate.

An identical comparison is performed with negative trd values (Fig. V.1b) of $trd = -0.006 \text{ m/day}$

and $trd = -0.04 \text{ m/day}$. For this negative trd values, the largest value of trd induced an increase of the amplitude of accretion events in the *CSLEEF* due to the modification of the equilibrium position by the trd term increasing the disequilibrium. While for erosion events, the erosion amplitude of the *CSLEEF* is increased due to linear term and the the model converging rate from the disequilibrium being of the same sign.

To summarize, when the amplitude of the linear trend term generates shoreline variations of comparable amplitude with the CS model variation, then compared to the *CSL* model: for a positive trd value, the *CSLEEF* model presents a smaller accretion rate but also a smaller amplitude of erosion events, while it shows higher accretion rates and higher amplitudes of erosion events for negative trd values.

However, when the trd value induces small shoreline variations compared to the CS model oscillations, the *CSL* and *CSLEEF* models present nearly identical modeled shoreline positions.

V.2.2 Hybrid models

This first approach combining both the empirical cross-shore shoreline change model and the one-line longshore model is called here the hybrid model, H (table V.1 line 5), based on the name used in Vitousek et al. (2017) to describe the CoSMoS-COAST model. The H model is inspired by the Vitousek et al. (2017) model, but is a simplification without the Bruun rule term and the extended Kalman filter.

The hybrid model formulation is

$$S_H(t) = S_{CS}(t) + \int_0^t \frac{dS_{LS}}{dt} dt \quad (\text{V.5})$$

with the cross-shore contribution evaluated from eq III.1

$$\frac{dS_{CS}}{dt} = C^\pm E^{1/2}(E - (aS_{CS} + b)) \quad (\text{V.6})$$

and the longshore component from eq IV.1

$$\frac{dS_{LS}}{dt} = -\frac{1}{Dc} \frac{dQ}{dx}. \quad (\text{V.7})$$

In this model, the 2 components are simply added together at the end of the simulation with the initial shoreline position. They are calculated independently such that there are no interactions in the calculation of the shoreline evolution dS_{LS} and dS_{CS} evaluated by the *LS* and *CS* models during the simulation.

Assuming total independence between the model components is possible if cross-shore and longshore processes are assumed to be the dominant processes responsible for shoreline changes on the beach at 2 different time scale. As explained by Long & Plant (2012) and Vitousek et al. (2017),

with their separation of the model shoreline variation in short term and long term components, on shorter time scales, the *CS* model is assumed to be dominant while at longer time scales, the *LS* model became progressively dominant.

However, this independence implies that at every time step the change in shoreline position in the *CS* component is not accounted for in the *LS* component and conversely.

Then, following the Vitousek et al. (2017) model, the introduction of an additional component, a linear trend term, is also performed by adding the term in the equation as follows to formed the hybrid linear, *HL* (table V.1 line 6), model:

$$S_{HL}(t) = S_{CS}(t) + \int_0^t \frac{dS_{LS}}{dt} + trd.t \quad (V.8)$$

V.2.3 Coupled models

The coupled models are combined models that enable interactions and feedbacks between the *LS* and *CS* components and potentially a linear term. From this definition, 2 variants of the coupled approach were implemented: the weakly coupled model, *W* (table V.1 line 7), where it's assumed that the *CS* model is not accounting for shoreline variations generated by the *LS* component, thus the equilibrium is written $Eq(t) = a(S_W(t) - S_{LS}(t)) + b$, and the fully coupled model, *F* (table V.1 line 9), where the equilibrium model accounts for this variation with $Eq(t) = aS_F(t) + b$. Hence, both coupled models are solving:

$$\frac{dS_{coupled}}{dt} = \frac{dS_{CS}}{dt} + \frac{dS_{LS}}{dt} \quad (V.9)$$

where $dS_{coupled}$ is either S_W or S_F depending on the considered coupled model approach, dS_{CS}/dt refers to shoreline changes from cross-shore processes (eq V.10 and eq V.11), and dS_{LS}/dt refers to shoreline changes from longshore processes (eq IV.1). With the cross-shore component contribution expressed in the *W* model as

$$\frac{dS_{CS}}{dt} = C^\pm E^{1/2}(E - (a(S_W - S_{LS}) + b)) \quad (V.10)$$

and in the *F* model as

$$\frac{dS_{CS}}{dt} = C^\pm E^{1/2}(E - (aS_F + b)) \quad (V.11)$$

Then, in both coupled approaches, the longshore model is

$$\frac{dS_{LS}}{dt} = -\frac{1}{Dc} \frac{dQ}{dx} \quad (V.12)$$

with the longshore flux Q calculated as

$$Q = Q_0 \sin(\alpha_{shore} - \alpha_{wave}), \quad (V.13)$$

where α_{wave} is the wave angle, and α_{shore} is the coastline angle calculated as

$$\alpha_{shore} = \arctan\left(\frac{dx_{coupled}(t)}{dy_{coupled}(t)}\right) \quad (V.14)$$

with $x_{coupled}(t)$ and $y_{coupled}(t)$ computed as

$$x_{coupled}(t) = x_{coupled}(t-1) + \frac{dS_{coupled}}{dt} \cos(\Phi) \quad (V.15)$$

and

$$y_{coupled}(t) = y_{coupled}(t-1) + \frac{dS_{coupled}}{dt} \sin(\Phi) \quad (V.16)$$

Here, $x_{coupled}$ and $y_{coupled}$ are the position of the coastline in the coupled model, and Φ is the transect angle. Therefore, the contributions of cross-shore processes and the linear trend term are taken into account in calculating the coastline angle. Thus changes in the coastline orientation from alongshore gradients in cross-shore changes or in the linear term shoreline change can modify the flux calculation of the LS component.

Contrary to the H model, the coupled approach assumes that cross-shore and longshore processes are interacting and thus they should not be considered independently. In the weakly coupled approach W , only cross-shore processes are assumed to have an impact on longshore processes, assuming that short time scales have an impact at longer time scales, whereas in the fully coupled approach F , both components are assumed to interact, thus implying that the two components are assumed to act at the same time scales in this model.

Similarly to the HL model, both coupled models W and F can integrate a linear trend term, and thus are named respectively WL (table V.1 line 8) and FL (table V.1 line 10). The linear term is integrated in both models as:

$$\frac{dS_{coupled}}{dt} = \frac{dS_{CS}}{dt} + \frac{dS_{LS}}{dt} + trd.t \quad (V.17)$$

then for the WL model, it's included in the cross-shore component:

$$\frac{dS_{CS}}{dt} = C^\pm E^{1/2} (E - (a(S_W - S_{LS} - trd.t) + b)) \quad (V.18)$$

Whereas the cross-shore component in the FL model is unchanged:

$$\frac{dS_{CS}}{dt} = C^\pm E^{1/2} (E - (aS_F + b)) \quad (V.19)$$

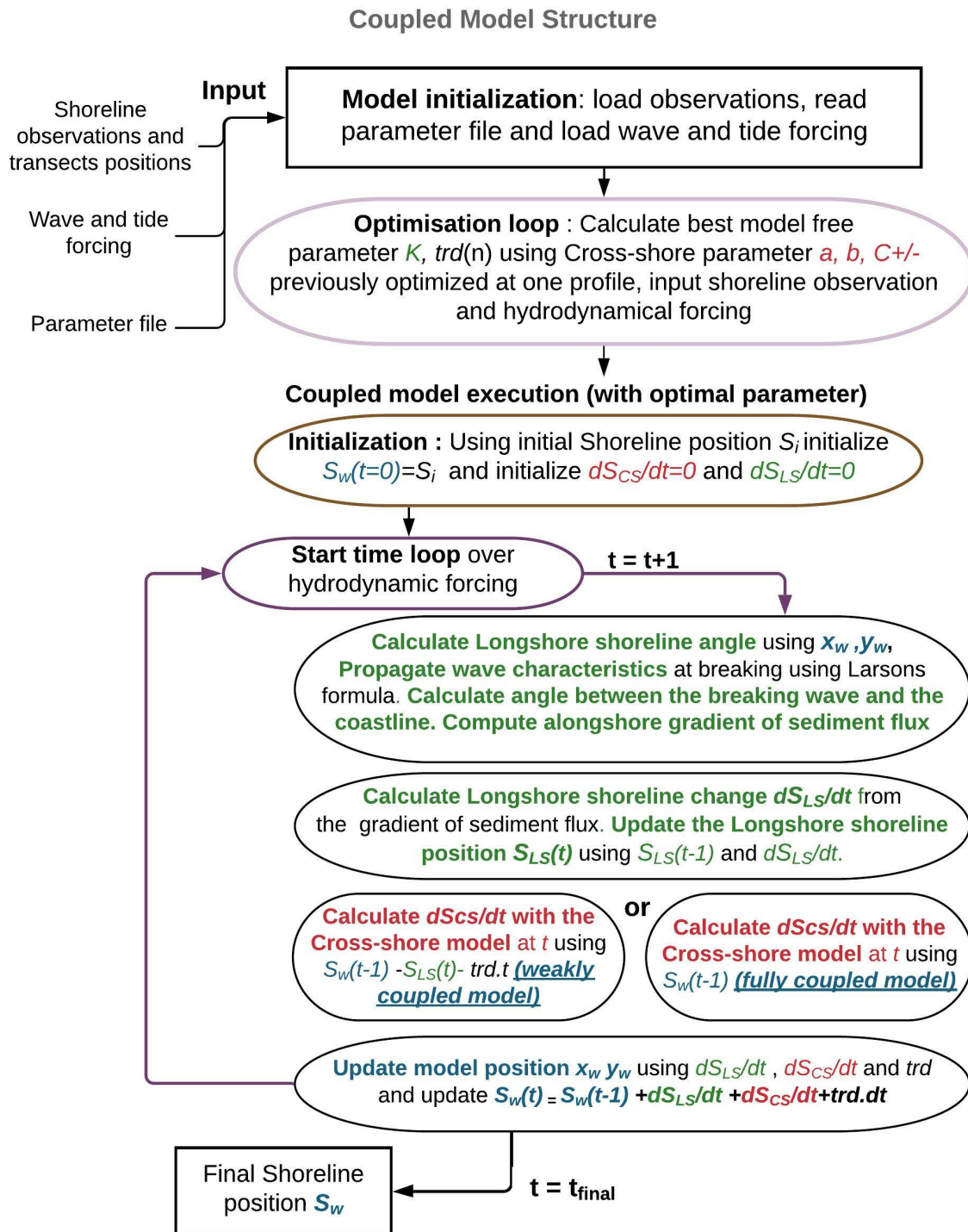


Figure V.2: Scheme of the weakly coupled model (*W*) functioning with illustration of the difference with the fully coupled approach (*F*). The text color refers to the cross-shore component in red, the longshore component in green, and the coupled model aspects in blue.

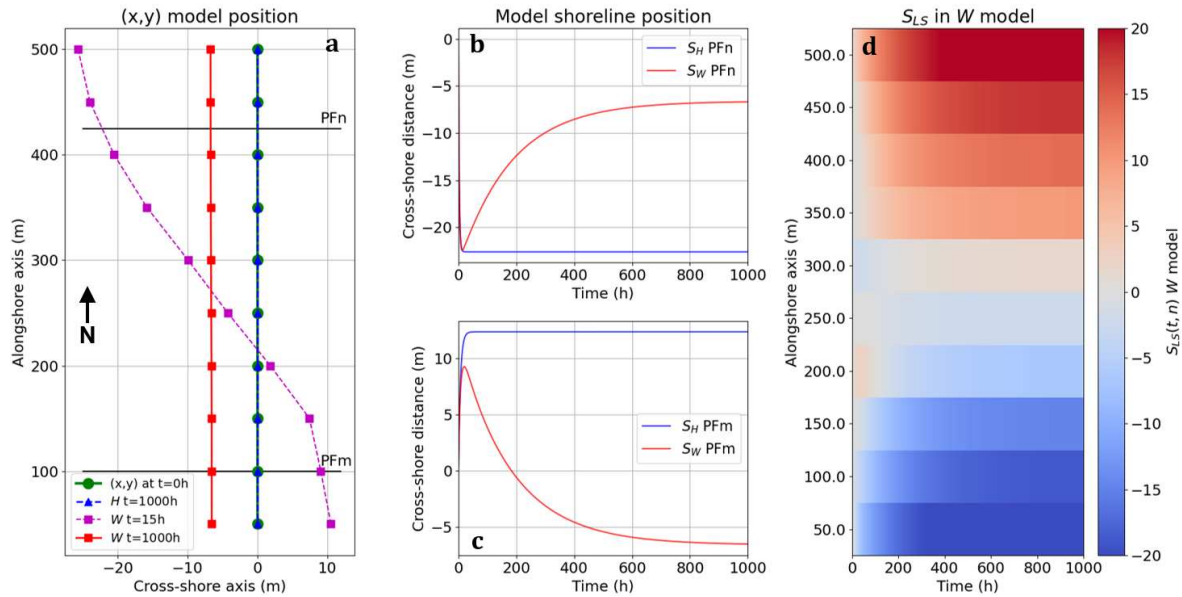
Comparing the H , W and F models

Figure V.3: Synthetic test case to illustrate the effects of the weak coupling between the longshore and cross-shore models: (a) model x , y position at $t=0$, $t=15$ h and $t=1000$ for W model and H model. (b-c) Model shoreline position for the W model S_W (red) and H model S_H (blue) at 2 locations, and (d) longshore model shoreline position S_{LS} in the W model in time at each transect position.

The coupling between the CS and the LS components is first evaluated and validated with a synthetic test case. This test is designed to compare the response of the W and H models to alongshore gradients in cross-shore shoreline changes.

The initial coastline is straight (Fig. V.3a in green at $t = 0$), and the model is forced with shore normal incident waves with a constant wave height in time, but with an alongshore gradient in space (with the wave height decreasing, from north to south, from 4m height to 1m height). The shoreline is discretized in 10 alongshore transects spaced by 50m uniformly. Two profiles, PFn and PFm were arbitrary defined and extracted at $x=100$ m and $x=425$ m to observe the evolution of the shoreline position in each model.

This test case was designed so that the alongshore gradient of sediment flux in the one-line model is equal to zero due to the initial planform and the wave conditions correspond to a cross-shore oriented wave direction, such that the LS component predicts no shoreline changes (Fig. V.3, H at $t = 1000$ h).

By using constant wave height conditions, the CS component converges toward an equilibrium position that depends on the model coefficients. Here, a set of coefficients that generates accretion in the southern lower energy part of the beach and erosion in the northern higher energy part of the beach are used, by prescribing the cross-shore coefficients: $a=-0.25$, $b=5$, $C^+=C^-=-0.4$. The K value is set to a relatively low value of $K=0.003$ to enhance the difference in time response between the cross-shore and the longshore components.

The constant wave conditions and the CS component coefficient choice results in the rapid convergence of the shoreline position S_H in the H model, as observed in Fig. V.3b,c (in blue), and it shows that the S_H stabilized at approximately -23m for PFn and +13m for PFM after about 20h of simulation. This evolution is due to the particular choice of cross-shore coefficients to permit such a fast convergence toward the equilibrium position. No modification of the (x, y) model position used in the LS component are observed (in Fig. V.3a, in blue), since there's no interaction between the CS and LS components in the H model.

Then, in the W model, the evolution of S_W shows the cross-shore component evolution and also its influence, from the coupling, on the (x, y) model position (as illustrated in Fig. V.3a at $t=15h$) used in the longshore component. This change in the coastline shape modifies the angles between the waves and the coastline, generating alongshore sediment fluxes in the longshore component of the W model. This results in an adjustment of the coastline planform by the LS component in response to the disequilibrium between the wave angle and the new coastline orientation generated by the CS component (Fig. V.3d and Fig. V.3a, coupled at $t=1000h$).

The feedback of the longshore component is also illustrated in the shoreline position, S_W , (in Fig. V.3b,c in red) converging to a new shoreline position where the coastline orientation is again in equilibrium with the incident wave direction.

Thus in the W model, the CS component converges toward its equilibrium position first (at $t \approx 20h$) due to its response time being shorter than that of the LS component. Then, the CS component generates a change in the planform orientation that creates an angle between the wave and the shoreline, so the LS component begins to redistribute the sediment to generate a planform shape that is in equilibrium with the wave angle (in Fig. V.3a,b,c in red, at $t=1000h$).

Using the same configuration, the fully coupled model, F , is applied and compared to the W model to evaluate the coupling effects (Fig. V.4). The (x, y) model position in the F model at $t=15h$, is similar to the W model with accretion at the southern extremity and erosion at the northern extremity. However, this shape is conserved in time in the F model, while the alongshore gradient in the LS component redistributes the sediment to reform a linear coastline at $t=1000h$ in the W model.

This is also observed in the shoreline position S_F (Fig. V.4)b,c in blue) that shows only a shoreline position converging toward the cross-shore equilibrium position at the start of the simulation, and then, a constant model shoreline position. Yet, the S_{LS} of the F model, represented in Fig. V.4d, shows important evolution of the longshore shoreline position.

In fact, due to the assumptions and formulation of the coupling in the F model, which accounts for the longshore shoreline evolution in the cross-shore equilibrium equation (eq V.11), the evolution of S_{LS} has created an opposite reaction of the cross-shore component S_{CS} , as illustrated in Fig. V.4e. The CS component has a faster time response than the LS component, in particular in this synthetic case where the chosen CS coefficients enhanced this effect.

Thus, accounting for the longshore shoreline evolution in the cross-shore equilibrium equation induced a compensation by the cross-shore equilibrium model with a time response faster than the LS component shoreline evolution. This results in the disappearance of the LS component contribution in S_F and (x_F, y_F) .

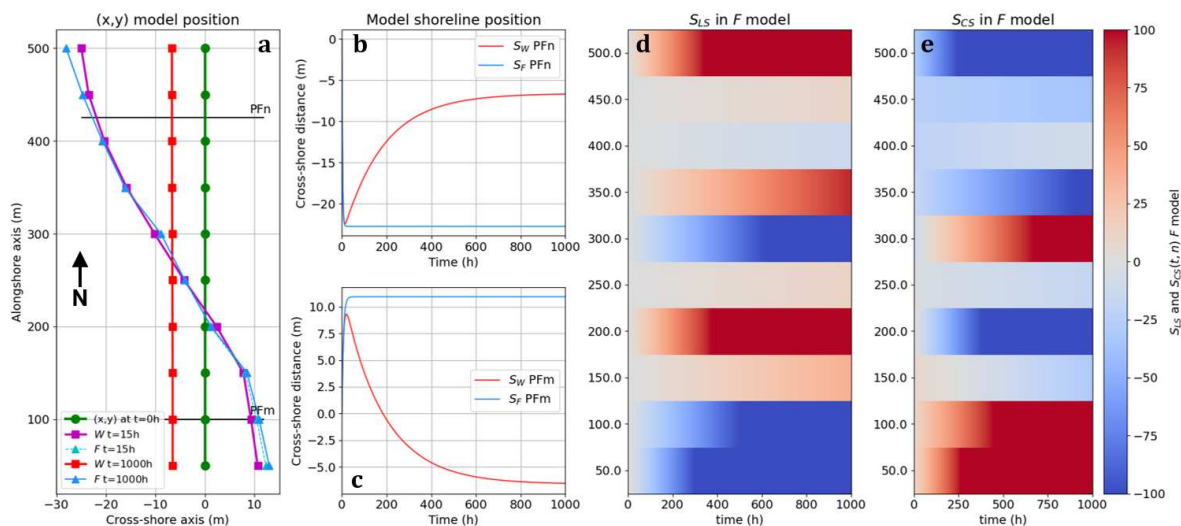


Figure V.4: Synthetic test case to illustrate the difference between the weakly coupled W and the fully coupled F models: (a) model x, y position at $t=0$, $t=15h$ and $t=1000$. (b-c) Model shoreline positions S_W (red) and S_F (light blue) at 2 locations, (d) longshore model shoreline position S_{LS} in the F model, and (e) cross-shore model shoreline position S_{CS} in the F model as a function of time at each transect position.

To conclude, this test case points out that, in the F model, the feedback of the LS component to the cross-shore equilibrium equation can erase the LS component contribution to the S_F when the time response of the CS is faster than that of the LS . Thus, the F approach should be more appropriate to apply in longshore dominated environments.

The 7 combined model approaches presented here are then applied at Narrabeen Beach for evaluation of their respective skill and analysis of their behavior at a real site.

V.3 Model performance at Narrabeen Beach

This section presents the application of the 9 models at Narrabeen Beach. Firstly, the model configuration for Narrabeen Beach is described, and secondly, the criteria used to evaluate the models performance are introduced. Then, the approach used to obtain the optimal model coefficients for each model is explained. Finally, the comparison of the behavior and performance of each model formulation is described.

V.3.1 Model configuration at Narrabeen Beach

The model configuration (e.g. domain, number of transects, boundary conditions, etc.) used to apply the combined model at Narrabeen is the same as described in Chapter IV. The models are applied at Narrabeen Beach at 15 cross-shore transects distributed uniformly every 250m along the Mean Sea Level contour (Fig. V.5) defined using observations from 2005.

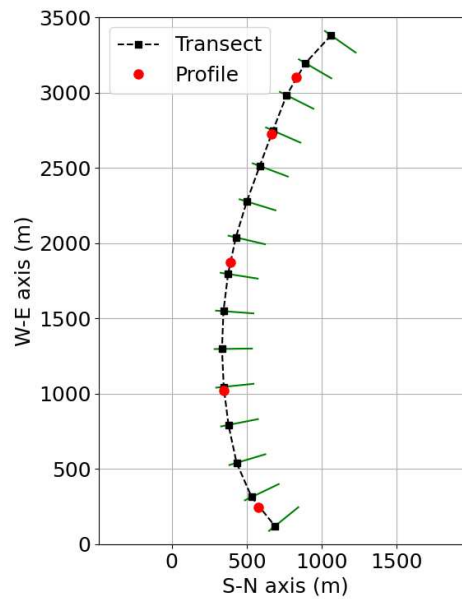


Figure V.5: Narrabeen model configuration showing the 15 cross-shore transects (green lines) used to discretize the model, with the initial shoreline position indicated for each transect (black squares) and cross-shore profile (red circles).

For the *CS* component, the wave conditions are interpolated at each transect, with a quadratic interpolation, using the 10m depth wave data available offshore of the 5 cross-shore profiles. Zero-flux boundary conditions are set in the one-line *LS* model. The depth of closure D_c is estimated using the formula proposed by Hallermeier (1983), and an alongshore mean value of 12 m is used for all transects (value supported by bathymetric data from Turner et al. (2016)). The choice of an alongshore homogeneous value of D_c is discussed in Chapter IV.2.

For the *LS* model, the 10m depth wave conditions were interpolated at the middle of every transect using the 5 available 10m depth wave condition located in front of each profile. The choice of the different model coefficient is described in the section V.3.3. Wave time series are unavailable at the 2 boundary transects, so the wave conditions at these locations are assumed to be the same as those of the nearest profiles.

Nine different models are applied over a 10-year time period (from 2005 to 2015), with a constant, hourly time step in the model. The year 2005 was chosen as it corresponds to a period with more

intense 2D surveying of the beach (Harley et al. 2015, Turner et al. 2016) to allow a comparison with observations outside of the 5 historical profiles. The simulation stops in 2015, as it corresponds to the end of the 10m depth wave time series available online.

V.3.2 Model performance

To understand and evaluate the model skill, and highlight the existing differences in model performance depending on the combination of the 3 components, 3 criteria were defined to assess the model skill at various time scales: at short (hourly to monthly), medium (seasonal to intra-annual), and long (inter-annual to decadal) term.

To evaluate the short-term variability reproduced by the model, which corresponds here to periods of the order of magnitude of the average frequency of observations (monthly), the percentage of time where the sign of dS/dt agrees between the simulations and the observations (*ISP* for Identical Sign of dS/dt Percentage) is computed (Fig. V.6). This metric quantifies the percentage of time during which the model reproduced correctly accretion (+ symbols in Fig. V.6) or erosion (– symbols in Fig. V.6).

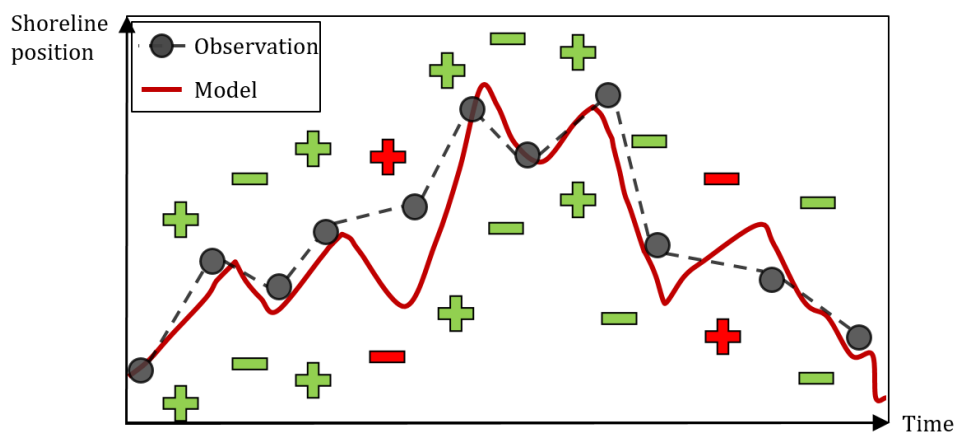


Figure V.6: Short term criterion conceptual scheme representing the observations and the model variations and their respective sign (+ or –) between 2 consecutive observations, with both signs in green indicating agreement between the model and observations, and in red indicating disagreement.

The Brier skill score (*BSS*, eq III.6) was used to quantify the medium term performance of the model, which corresponds to seasonal to interannual time scales. The *BSS* estimates a weighted difference between the model and the observations using a pre-defined baseline, which here was defined as the linear regression of the model (Fig. V.7). By using a linear regression as the baseline, the *BSS* evaluates the capacity of the model to reproduce the seasonal variability (shaded blue area in Fig. V.7) that is not associated with the long-term trend (green line in Fig. V.7). In particular, by using the model linear regression, this calculation enhances the importance of the seasonal variations reproduced by the model, neglecting differences between the simulated and observed linear

trends.

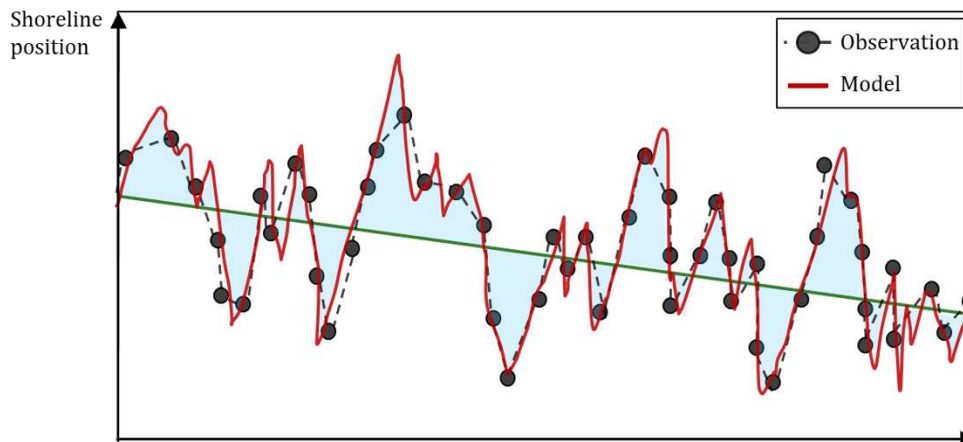


Figure V.7: Medium term criterion conceptual scheme representing the BSS calculation with the observations, the model, and the linear regression of the model (the baseline). The blue area corresponds to the model improvement compared to the baseline, assumed here mainly to account for the reproduced seasonal and intra-annual scales.

Finally, to evaluate the performance of the model at long time scales, the difference in slope between the linear regression of the model and the observations is estimated (Linear Slope Error, LSE). This criteria represents the ability of the model to reproduce long-term linear trends (Fig. V.8).

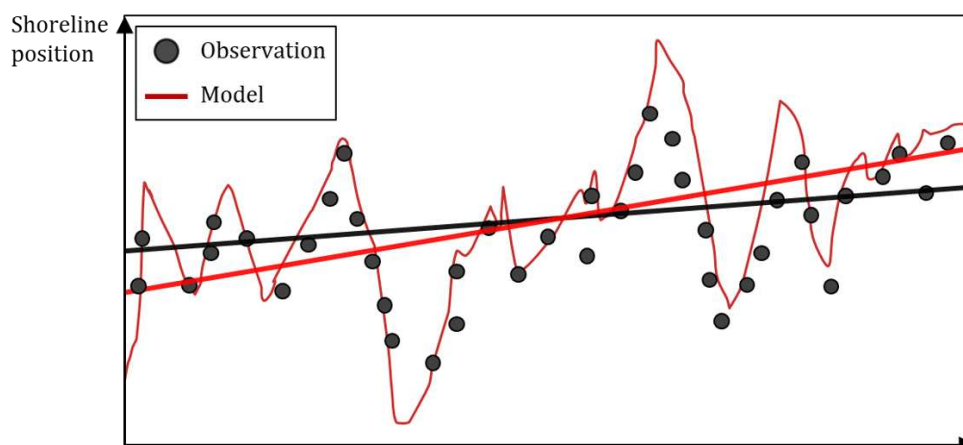


Figure V.8: Long term criterion conceptual scheme representing the observations, the model shoreline position, and their respective linear regressions in black and red, highlighting the difference in slope between the 2 regressions used as criteria.

The 3 criteria and their associated time scales and representative variables are summarized in Table V.2. The RMSE is also used as a global performance criteria, in fact, the RSME value accounts for the model performance of the dominant time scale of the profile.

For example, on a profile with a predominant long term trend not well reproduced by the model, it heavily impacts the RMSE value. Whereas, for a profile with no long term trend, the RMSE is more

impacted by the medium term model skill.

Table V.2: Performance criteria based on the time scale of reproduced shoreline variability

Time scale	Short term	Medium term	Long term
Corresponding period	~ Monthly	Seasonal to intra-annual	Inter-annual to decennial
Criteria	Percentage of time of agreement of dS/dt sign in model and observation	Brier skill score	Model and observation linear regression slopes error
Criteria variable	<i>ISP Identical Sign of dS/dt Percentage</i>	<i>BSS Brier Skill Score</i>	<i>LSE Linear Slope Error</i>

V.3.3 Model optimization

Before applying the different model formulations at Narrabeen Beach, the model free coefficients must be determined for the cross-shore, longshore, and linear trend components. The approach is described in the following.

In a first step, the CS model coefficients a , b , C^+ and C^- were calibrated at PF4 for the 10-year period from 2005 to 2015. This profile was selected assuming that PF4 is the profile most dominated by cross-shore processes of the 5 historically surveyed profiles.

This hypothesis is in agreement with previous studies performing an EOF analysis of the beach (Harley et al. 2015, 2011, Robinet et al. 2020), and the central location in the embayment of the profile. Hence this profile is less affected by longshore processes in particular those generating shoreline rotation responsible to more important shoreline change at the beach extremity.

Table V.3: Optimum set of cross-shore coefficients obtained for PF4, which are subsequently applied for all profiles.

Coefficient	a	b	C^+	C^-
Optimized value	-0.24	6.4	-0.01	-0.8

Then, the set of coefficients optimized at PF4 (Table V.3) is used for all the transects of the beach, in every model using the CS component. This assumption, that one set of cross-shore coefficients can be applied for the entire beach, is supported by the grain size at Narrabeen being alongshore homogeneous. Thus the alongshore variations in beach slope are primarily related to changes in beach morphology due to alongshore variability in wave height caused by sheltering effects from the rocky headland at the southern end of the beach Turner et al. (2016).

The alongshore variability in the wave conditions is explicitly calculated by the \sqrt{E} term in the model (eq V.3) and is assumed not to impact the model coefficients.

Among the CS coefficients, the b value is expected to vary from one profile to another. The b value determines the E_{eq} for $S = 0$, the position of the linear regression representing the limit

between erosion and accretion. Thus, the presence of a trend in the demeaned shoreline observations influences the b value, which adapts the position of the linear equilibrium relation ($E_{eq} = aS(t) + b$). The b value thus depends on the time period over which the mean is calculated since trends in the observations also vary in time. Therefore, the variation of the b value with the profile was estimated by removing the linear trend of the shoreline observations before subtracting the mean of the observations, thus enabling using a single value of b for all profiles of the beach.

In a second step, the optimization of the combined models that integrate a linear term (trd) and/or the one-line model (LS) are completed using the set of cross-shore coefficients optimized in the first step for PF4.

Then, for the LS component, a single value of K (eq IV.1)(constant alongshore) is searched for using the simulated annealing algorithm, for each model formulation. For the models containing a linear trend term, N values of trd are optimized at the same time as K with the simulated annealing algorithm for each of the N considered transects.

This methodology reduces the number of coefficients from potentially one set of $a, b, C+, C-, K, trd$ per transect of the beach to a single set of $a, b, C+, C-$ (Table V.3), and K values for all transects and one trd value for each transect (see Fig. V.9).

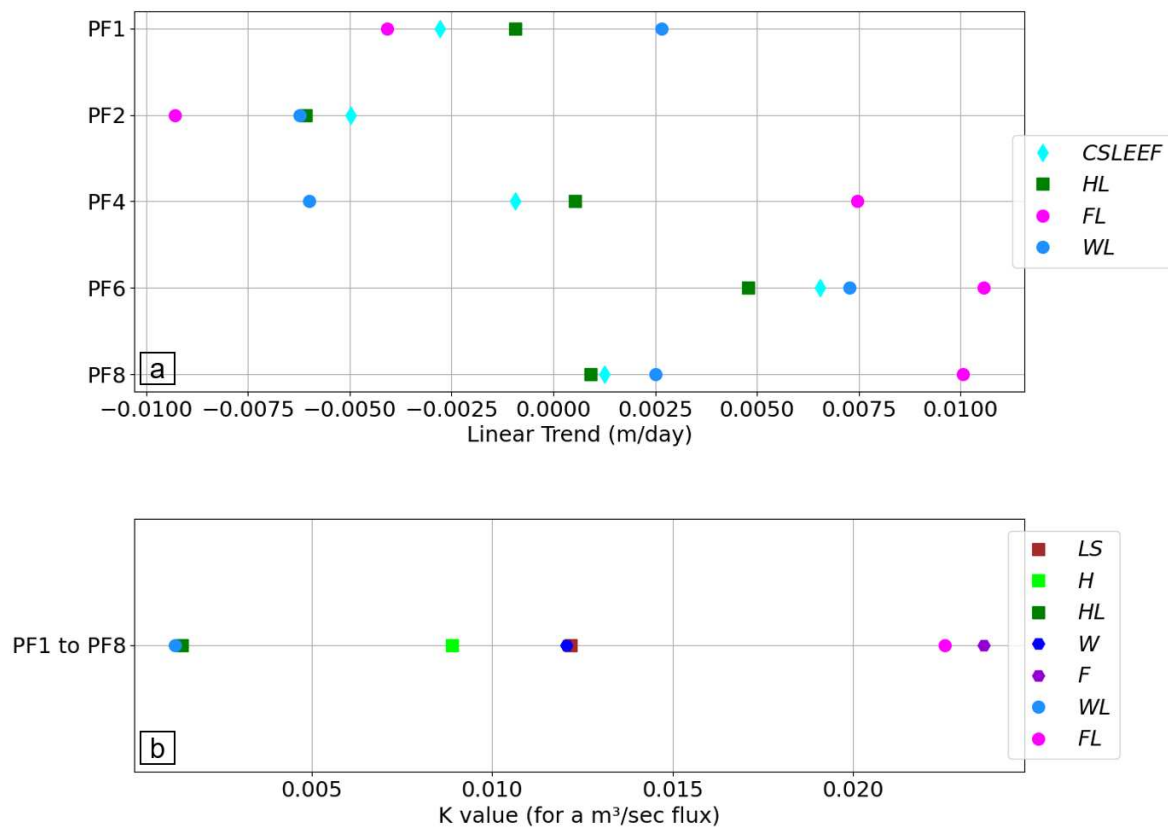


Figure V.9: Optimized values of (a) trd (linear trend term) and (b) K (longshore model coefficient, constant for all profiles) at Narrabeen Beach for each model formulation.

V.3.4 Comparison of model performance

Using the optimal coefficients defined in the previous section (section V.3.3), each of the 9 model formulations is applied at Narrabeen Beach, and the model performance is compared, using the 3 criteria defined in section V.3.2, the R^2 (eq III.5), and the RMSE (eq III.4).

First, a global description of the model behavior at each profile is presented. Then, the relative mean performance of each model is evaluated using the pre-defined criteria and the RMSE. The models are then ranked based on these 5 criteria from the best to worst performance.

Behavior of model shoreline time series

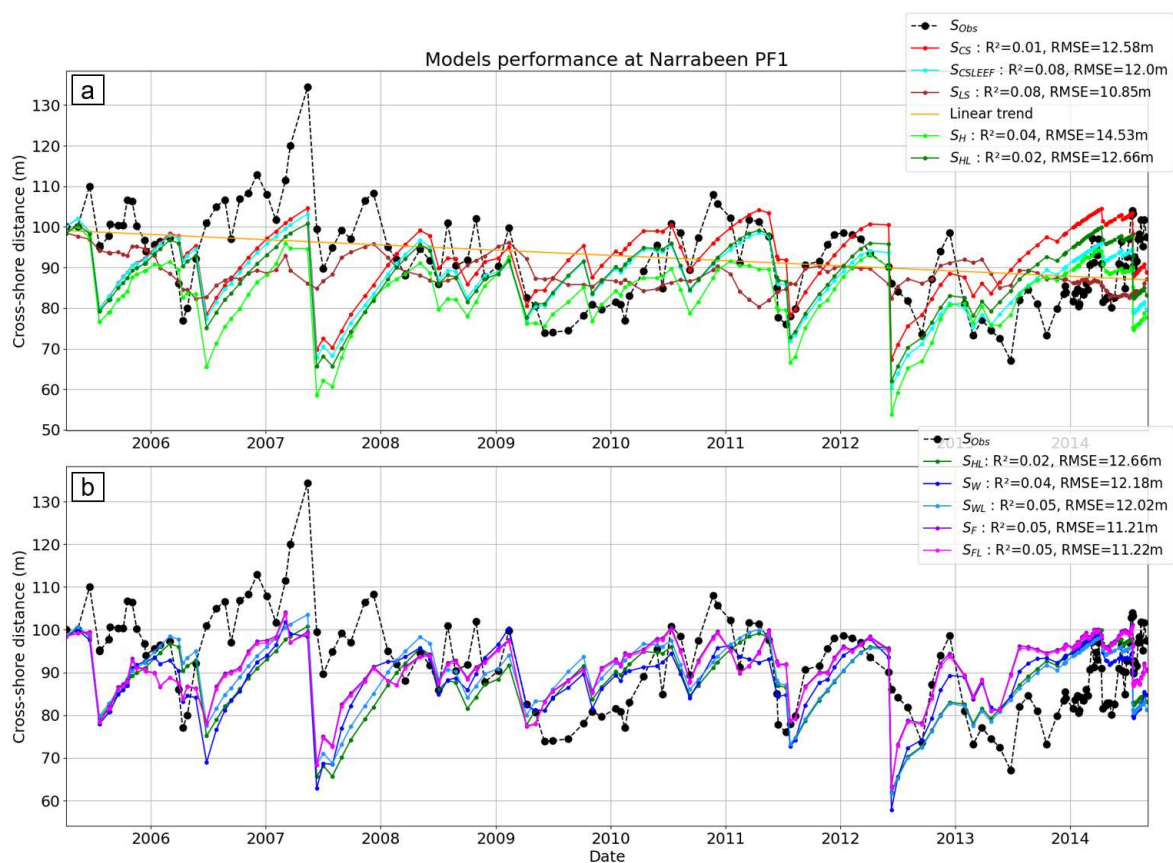


Figure V.10: Observed (black dashed line) and modeled (colored lines, see legend to identify each model) shoreline position time series for PF1 at Narrabeen Beach.

PF1 at Narrabeen Beach is located at the northern extremity of the beach and experiences high wave energy since it's exposed to large waves originating from the Southeast. However, reefs are located around 5 to 10 m depth along this profile, which may potentially dissipate some of the wave energy.

On this profile, the observed shoreline position shows only a small erosion trend during the simulation period (approximately 10m of erosion between 2005 and 2015). This profile shows important

seasonal and inter-annual shoreline variability, with a range of 50m between the most accreted and eroded shoreline positions during this period.

Looking at the modeled shoreline position, the *LS* model reproduced relatively well the small long-term trend of erosion in the observations, but simulated only a few meters of seasonal and inter-annual variability (Fig. V.10a).

The *CS* model did not reproduce well the long-term trend of the observations (Fig. V.10a), underestimating the shoreline position in the first third of the simulation (in particular between 2006 and 2008), and overestimating the shoreline position at the end of the simulation (in the 2 last years). The *CS* model also missed some seasonal variation of erosion occurring at the end of the year, after an accretion periods, like observed at the end of 2005, 2006, 2007 and 2010. Overall, the *CS* model almost always underestimates the rate of accretion.

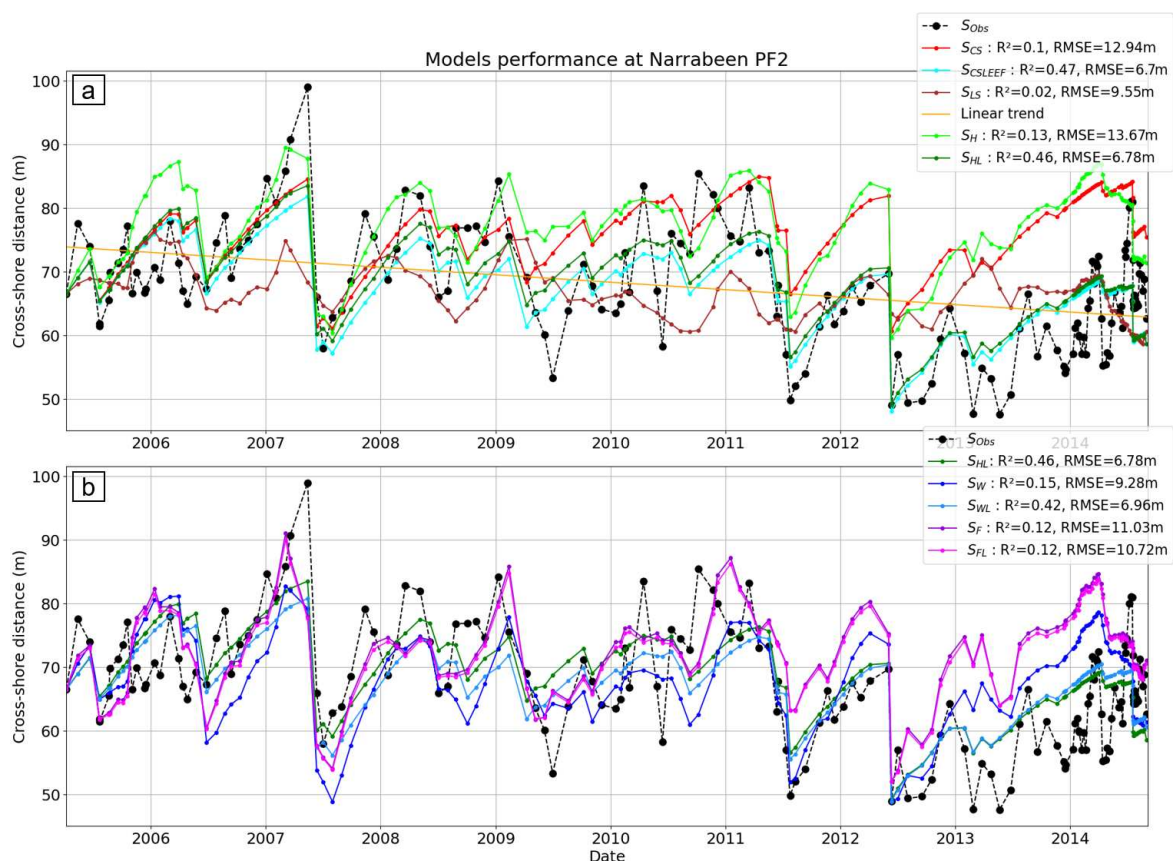


Figure V.11: Shoreline position time series for PF2 at Narrabeen Beach (same legend as Fig. V.10).

At PF1, all of the combined models underestimated the shoreline position during 2006-2008 (Fig. V.10). However, the overestimation in the last year of simulation is slightly less pronounced for the *CSLEEF* model and for the *H* model than for the other combined models but this is due to the *H* approach global underestimation and the effect of the linear trend for the *CSLEEF* (PF1 on Fig. V.9a).

The *F* and *FL* formulation reproduced some seasonal events of accretion and erosion better than

the other combined models, for example at the start of 2011 and 2013 (Fig. V.10b). This is assumed to be caused by the *LS* component reproducing more variability due to an higher *K* value for these 2 models (Fig. V.9b). Overall, PF1 shows the lowest global model performance of all profiles with $\max(R^2) < 0.1$.

PF2 is located approximately 400m south of PF1, and also experiences a small erosion trend with approximately 10m of erosion during the 10-year period. The amplitude of shoreline variations at PF2 is also similar to that observed at PF1.

At PF2, the *LS* model reproduced well the observed trend and part of the seasonal variability, including accretion events in 2007 and at the beginning of 2009 (Fig. V.11a). On the contrary, the *CS* model reproduced seasonal variations comparable to the observations, but was unable to simulate the long-term trend, thus overestimating the shoreline position during the last 4 years of the simulation.

The *CSLEEF* (Fig. V.11a), *HL*, *W* and *WL* (Fig. V.11b) model reproduced well both the seasonal variations and the observed long-term trend, with $RMSE < 10m$. The *H* model (Fig. V.11a), the *F* and *FL* model (Fig. V.11b) reproduced larger seasonal shoreline variability than the *CS* model alone, but even more than the previous models, they overestimated the shoreline position during the last 4 years of the simulation period, with $RMSE > 10m$ (Fig. V.11).

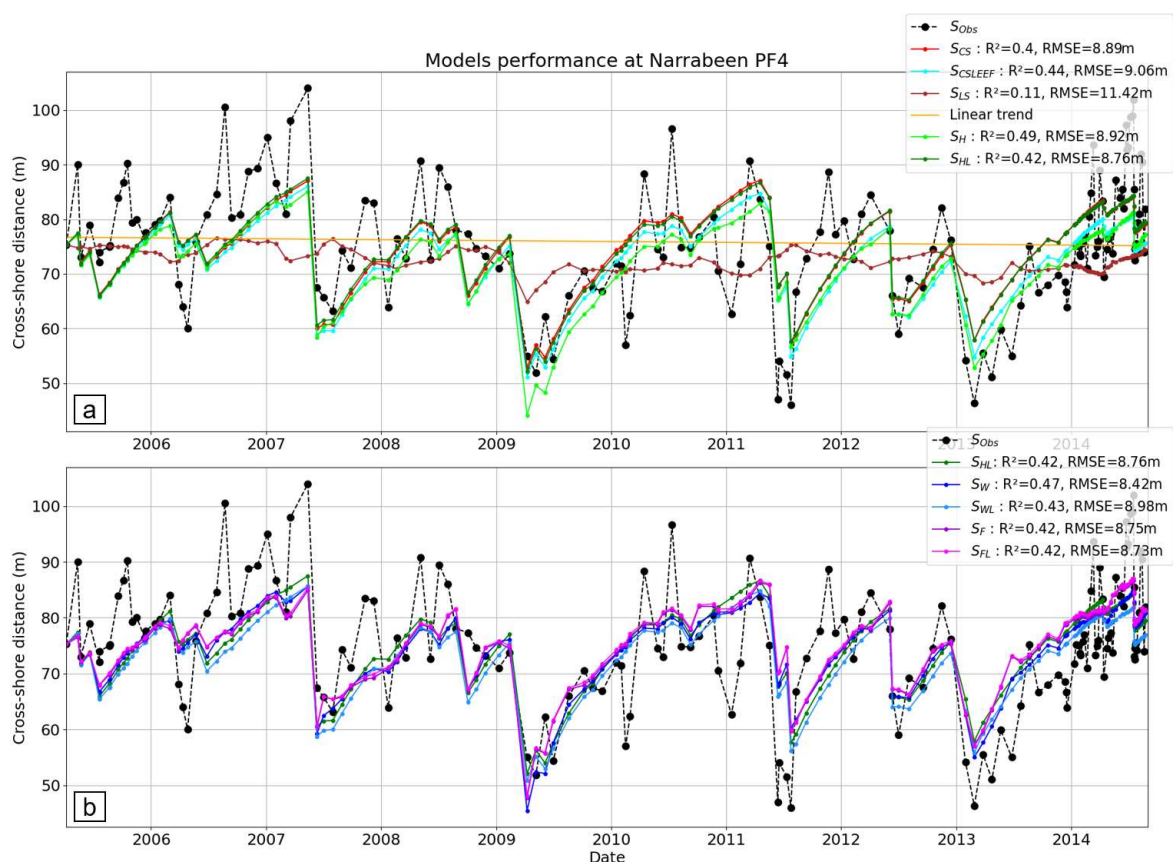


Figure V.12: Shoreline position time series for PF4 at Narrabeen Beach (same legend as Fig. V.10)

PF4 is located approximately in the middle of the beach, and as previously mentioned, cross-shore processes are dominant at this profile. The observations show almost no long-term trend, and similar to the 2 previous profiles, the seasonal variation of the shoreline position reaches up to 40m. At this profile, the *LS* model reproduced almost no seasonal variations (Fig. V.12a), as expected. The *CS* model reproduced well the seasonal and inter-annual variability (with $R^2 = 0.4$), but was still unable to reproduce or underestimated some accretion and erosion events occurring in 2006, 2008 and 2010 (Fig. V.12a).

Here, all combined models behave similar to the *CS* only model, with R^2 varying from $R^2 = 0.42$ and $R^2 = 0.49$ due to the *LS* component and the linear term contribution being negligible.

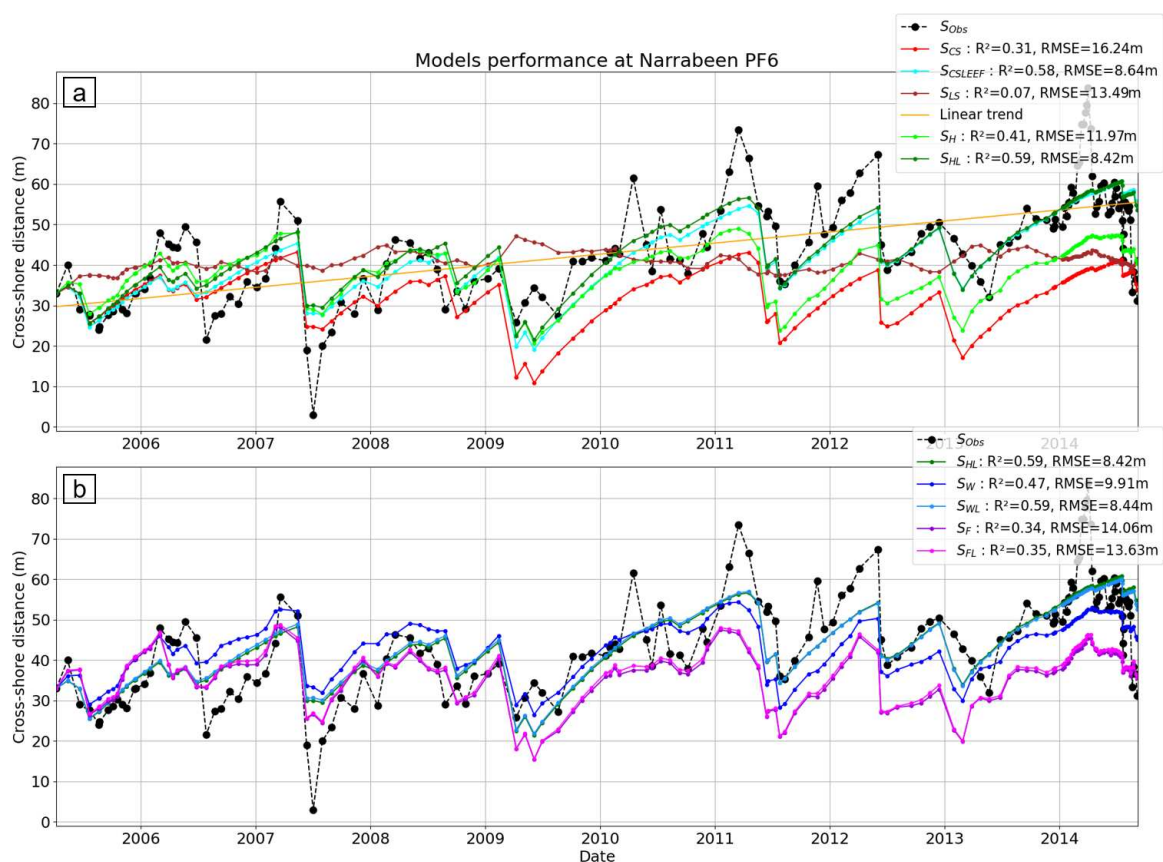


Figure V.13: Shoreline position time series for PF6 at Narrabeen Beach (same legend as Fig. V.10)

At PF6, the shoreline position shows a larger positive long-term trend than at the previous profiles, with an increase of the mean shoreline position of nearly 25m during the 10-year period.

At this profile, the *LS* model is unable to reproduce well the long-term trend: it overestimates the shoreline position during the first half of the simulation and underestimates it in the second half of the simulation (Fig. V.13a). This is due to the *LS* model being sensitive to the forcing condition for long term trend reproduction (cf. section IV.2), thus the long term shoreline position predict by the *LS* are not perfectly consistent with the observations.

The *CS* model, *H* model, *F* and *FL* models also are unable to reproduce well the long-term trend

and thus underestimate the shoreline position in the second half of the simulation. This is caused by the equilibrium approach not reproducing long term trend for the *CS* model, the *LS* component not reproducing well the long term trend for the *H* and *F* model and the linear trend term not impacting the model shoreline position in the *FL* approach (only slight difference between *F* and *FL* in Fig. V.13b).

However, the *CSLEEF*, the *HL*, *W* and *WL* models reproduce well the observed seasonal variations and long-term trends (Fig. V.13b), with R^2 in the range of $R^2 = 0.59$.

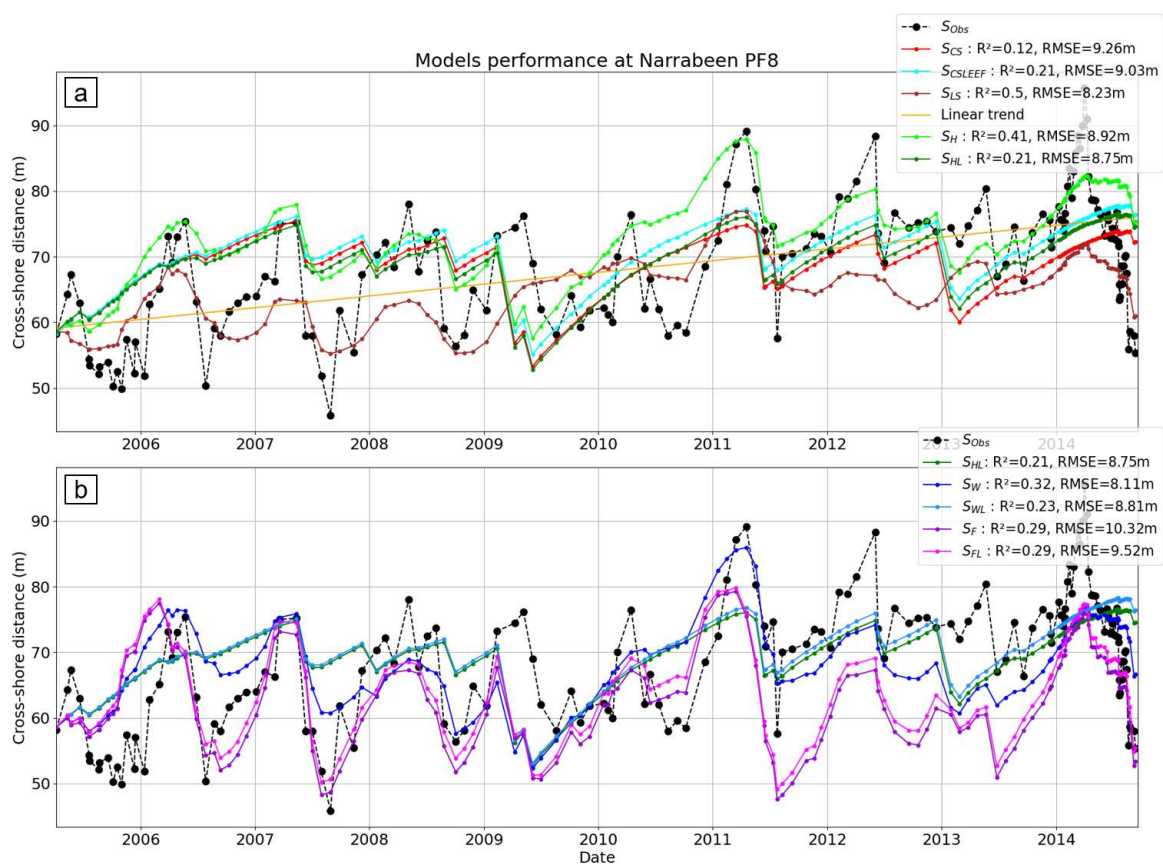


Figure V.14: Shoreline position time series for PF8 at Narrabeen Beach (same legend as Fig. V.10)

PF8, located at the southern extremity of the beach, is less exposed to waves originating in the southwest due to sheltering effects from the rocky headland at the southern end of the bay.

The observations show an accretion trend with approximately 16m of accretion over the 10-year period. Seasonal shoreline changes still reach up to 30m in amplitude.

Here, the *LS* model underestimates the shoreline position during the last 3 years of the simulation, while it reproduces well a part of the seasonal variability ($R^2 = 0.5$), but underestimates its magnitude (Fig. V.14a). At this profile, the *CS* model is unable to reproduce well the observed seasonal variability, in particular from 2006 to 2010. Furthermore, it overestimates the mean shoreline position in the first half of the simulation, and underestimates it in the second half of the simulation (Fig. V.14a). Yet, the poor performance of the *CS* model on this profile are expected, as this profile

is assumed to be more longshore dominate.

The *CSLEEF*, *HL* and *WL* models present almost the same behavior as the cross-shore only model with $R^2 \approx 0.2$ (Fig. V.14). Both the *H* and *W* models reproduce more seasonal variations than the cross-shore only model, and they don't underestimate the shoreline position in the second half of the simulation ($R^2 = 0.4$ and $R^2 = 0.3$ respectively). Finally, the *F* and *FL* models reproduced well the observed seasonal variations, but they underestimated the shoreline position in the last 3 years of simulation ($R^2 = 0.29$, Fig. V.14b).

Model relative mean performance at each time scale

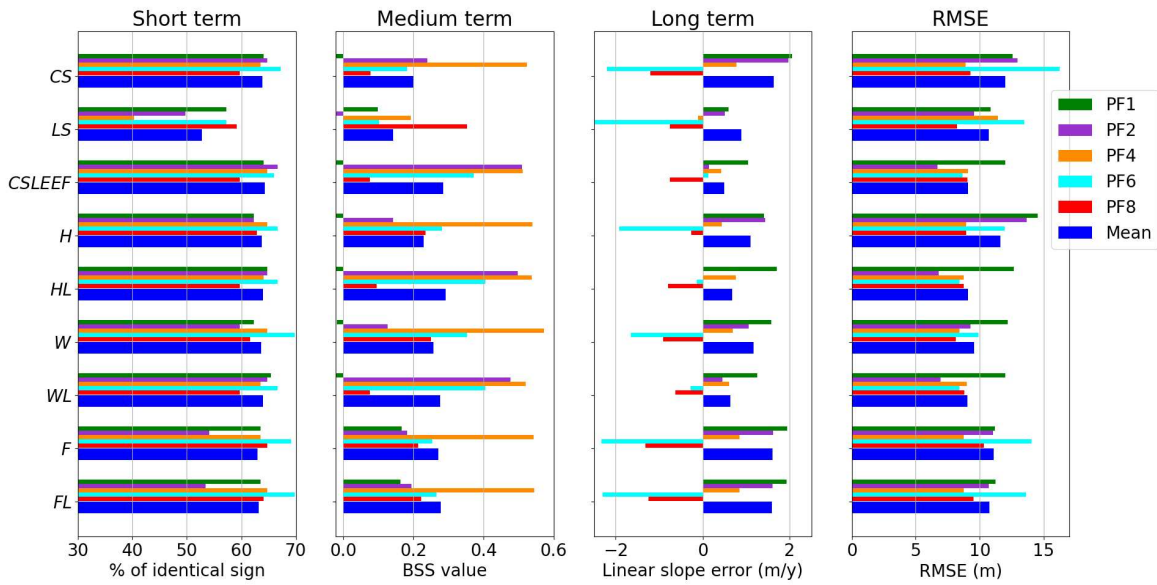


Figure V.15: Criteria value for every model at short term, medium term and long term for the 5 profile and mean value over all profile, and RMSE

In this section, a comparison of the models performance is completed by ranking, in decreasing order, the model performance for each criteria and based on the RMSE. This ranking uses the mean value of the criteria ζ (e.g. for the RMSE in eq V.20) defined for each of the 5 profiles (blue bar in Fig. V.15).

$$\zeta = \frac{\sum_{i=PF1}^{PF8} RMSE(i)}{N_{Profile}} \quad (V.20)$$

The relative difference between the mean model performance at each time scale described in this ranking are synthesized in the Fig. V.16, where all the mean criteria value are normalized using the minimum and maximum value of all model for each time scale. Thus the model with the highest performance have a normalized value of 1, and the model with the lowest performance a normalized value of 0. This representation highlights better the relative difference between the different model performance.

Based on mean over all 5 profiles RMSE, the models with the higher performance at reproducing

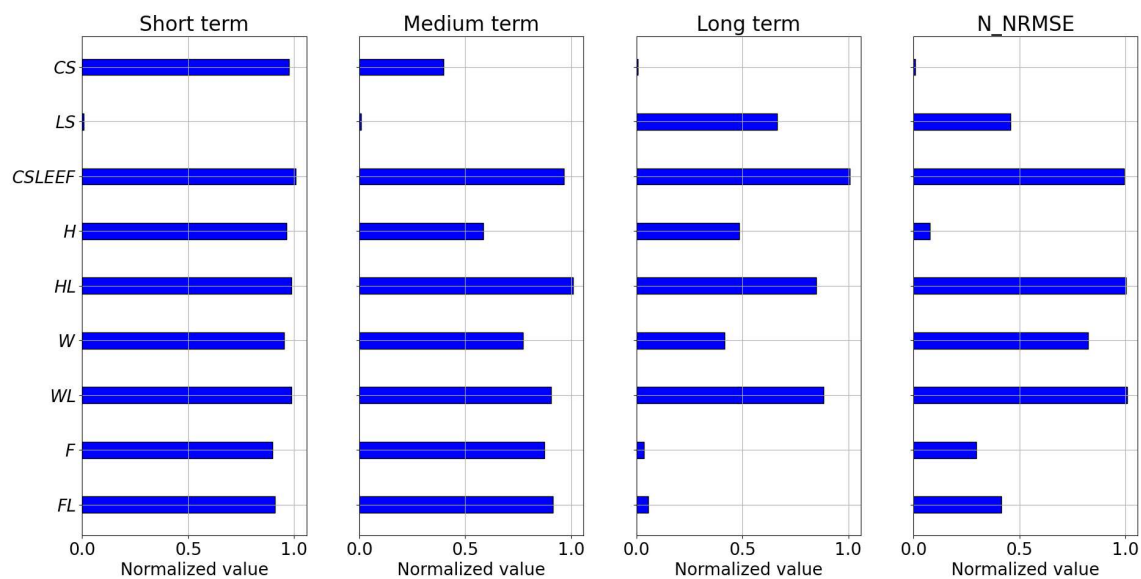


Figure V.16: Normalized Criteria for every model for short term, medium term, long term and RMSE based on mean value other all profile criteria and normalized using the lower and higher mean criteria value

the shoreline position on Narrabeen Beach are the 3 ex aequo following models: the *CSLEEF*, the *HL* and the *WL*, with a mean RMSE of 9.0m (Fig. V.15 and Fig. V.16). Then with a decreasing performance, there are the *W* model with RMSE = 9.5 m, followed by 2 ex aequo models: the *LS* and the *FL* with RMSE = 10.7 m, then the *F* model with RMSE = 11.0 m, the *H* RMSE=11.6 m, and finally, the *CS* model with RMSE = 12.0 m.

With respect to the long-term model performance, based on the mean over all profiles *LSE*, the best model is the *CSLEEF* with a mean slope error of 0.5m/y (Fig. V.15). Then, with almost identical performance there are the *WL* model with 0.64m/y and the *HL* model with 0.68m/y. Next, the *LS* model with 0.89m/y, then with similar performance: the *H* model with 1.1m/y and the *W* model with 1.17m/y. The 3 next model show similar and highest value of linear slope error: the *FL* with 1.59m/y, the *F* with 1.6m/y and finally the *CS* model with a mean slope error of 1.64m/y (Fig. V.16).

At medium time scales, the model skill, based on the mean *BSS*, is the highest for the *HL* with *BSS*=0.29, and the cross-shore linear *BSS*=0.28. Then both the *WL*, *FL* and *F* present similar performance with *BSS*=0.27 (Fig. V.15).

Next the *F* show slightly lower skill *BSS*=0.26. And the *H*, *BSS*=0.23. The *CS* model have even lower with *BSS*=0.2. But the model with the lowest performance at medium term is the *LS* model with mean *BSS*=0.15 (Fig. V.15). Overall the difference in medium term skill are small between the different model (Fig. V.16) as the mean *BSS* value are all below 0.3.

The short term model skill, based on the mean over all profiles *ISP*, shows that with the exception of the *LS* model with a mean agreement of 52.7%, all the combined models present similar

performance at this time scale as the *CS* model with percent of agreement between 63% to 64% (Fig. V.15 and Fig. V.16).

Comparing in detail the respective estimates for only accretion or erosion events shows that the *CS* model correctly reproduced most accretion event compare to erosion event, while for the *LS* model the distribution of the percentage of correctly reproduced accretion and erosion event is balanced. However, the mean *LS* model value of 52.7% indicates that the *LS* model predicts the correct sign of shoreline position change (dS/dt) only 2.7% more frequently than a random guess of the shoreline change (e.g. 50%).

V.3.5 Analysis and discussion of model performance

Profile dependency of model performance

The selected method of calibration of the model coefficients is such that the set of *CS* model coefficients are unique for all model formulations.

Thus, the contribution of the other components and/or the approach used to couple the cross-shore, longshore, and linear trend contributions are mainly responsible for change in the model performance from one profile to another.

Hence, profiles showing changes in the performance between different coupling approaches can be used to understand better the differences in the model skill based in the specificity of each profile.

The PF1 presents the lowest medium term skill of all profile with negative *BSS* with exception of the *LS* model where $BSS=0.1$ and the *F* and *FL* model with $BSS=0.18$, suggesting that even if the *BSS* value is really low, the *LS* component increases the medium term skill on this profile (Fig. V.15).

The *LS* component also increase the model skill at long time scales, since the *LS* model has the best long term performance on this profile, better even than the *CSLEEF* model. This is also verified by comparing the RMSE. At PF1, the models with the lowest RMSE are the *LS* model, the *F*, and the *FL* model. They are the 2 combined models with the highest optimized value of *K*, thus the relative importance of the *LS* component is the highest for these 2 models.

PF2 and PF6 show important increases in the medium term performance when a linear trend term is added to the *CS* model with exception of the *FL* (Fig. V.15). While the model skill decreased when combined with only the *LS* component.

The long term skill is also highly increased by the linear term on this 2 profiles compare to the *LS* component. However this effect is more expected, due to the method of calculation of the long term criteria, using the *LSE* between the model and the observation, this metric is more influenced by the integration of an optimized linear trend term in the model than a *LS* component.

PF4 shows at medium time scales and based on RMSE that all combined models have similar performance, with values close to the *CS* model skill.

However, the *LS* model presented lower performance. This illustrates that, as supposed based on

previous study, the cross-shore processes dominate on that profile (Fig. V.15).

PF8 shows interesting results at medium time scales. At this profile, the model with the highest medium term skill is the *LS* model (Fig. V.15, Fig. V.16).

Then all combined models that have an optimal high *K* value (Fig. V.9b) have a higher performance compared to models with low *K* values (*HL* and *WL* models) or models that don't represent long-shore process (*CS* and *CSLEEF*). However, this is not observed in the RMSE, but can be found in the short term model skill results, but in the latter, the differences are more subtle than for medium time scales (Fig. V.15 and Fig. V.16).

Synthesis of model skill based on time scale and formulation

Here, each model is analyzed by using the observed model behavior and the calculate skill criteria, and by taking into account the different hypotheses of each model formulation, to explain and discuss the model skill at each time scale.

- *CS* model: the *CS* model uses here only one set of coefficients for the whole beach, which were calibrated for PF4 (the profile most strongly dominated by cross-shore processes). The model skill at medium time scales and based on RMSE is close to the highest of all models on this profile.

The performance of the model decreases at medium time scales, closer to the extremities of the beach, likely caused by the relative importance of longshore processes moving away from PF4. In terms of relative performance, the *CS* model show the second worst model skill at medium term, and the worst model skill at long term. Based on the RMSE, the *CS* model skill is also ranked last of all approaches.

The *CS* model can't reproduce long term trends of the shoreline position, with exception of an existing long term trend in the forcing wave energy that would modify the equilibrium shoreline position. It impact the model skill at long term, as the forcing wave Energy on Narrabeen show no long term trend, it also increase the RMSE on all profile with long term trend.

- *LS* model: The *LS* model is using a single *K* parameter for the whole beach. When optimized alone, the *LS* model *K* parameter shows a higher value compared to the value obtained with both the *H* or both *W* and *WL* approaches (Fig. V.9). This is not surprising since the optimal model coefficient can potentially try to account for more shoreline variability in the *LS* model when cross-shore process are not represented. The *LS* model has the worst model skill at reproducing short term and medium term variability. However, this is expected since processes that dominate the shoreline variability at these time scales are cross-shore processes. The *LS* model has the highest *BSS* value of all models at PF8 (*BSS*=0.32) at medium time scales, thus illustrating the relative importance of longshore processes at the southern end of the beach. For long-term criteria, the *LS* model is ranked 4th highest skill of all 9 approaches just behind

the models integrating a linear trend term. Moreover, the trend is underestimated by the *LS* model at PF6, and this strongly decreases the mean model performance. Otherwise, the *LS* model long-term skill at the others profiles (Fig. V.15) is closer to the best of the 9 models skills.

Finally, based on the RMSE, the *LS* is ranked 5th (behind the *CSLEEF*, *HL*, *W* and *WL*) but shows the lowest RMSE on PF1 and PF8 among all models, thus the RMSE also supports the relative importance of longshore processes at the extremities of the beach, as observed with the medium term skill.

- *CSLEEF* model: In the model skill analysis, the *CSLEEF* following (Jaramillo et al. 2019) was treated, however, as illustrated in a synthetic case before in section V.2.1, using an additional linear term (CSL model) gives identical results since the linear term slope are small compared to the cross-shore variability at Narrabeen.

In terms of model skill, this simple approach is among the best of all model versions. At medium time scales, this model ranked 2nd, just behind the *HL* model. At long time scales, this approach has the best performance of all models due to the importance of the optimized linear trend term in the model variability and in the long-term model skill.

Based on the RMSE, the *CSLEEF* model is best model *ax-eaquo* with the *HL* model and the *WL* model, showing nearly identical skill at each profile as those 2 models.

These results illustrate well that the shoreline variability at Narrabeen Beach is mostly dominated by cross-shore processes and that longshore processes can be accounted for well by a simple linear trend approximation in most parts of the beach. However, the *CSLEEF* presents lower performance at medium time scales and based on the RMSE compared to the *LS* model at both beach extremity (PF1 and PF8 Fig. V.15) .

- *H* and *HL* models: The simple addition of the *CS* model (with the optimum set of coefficients from PF4) and the *LS* model gives rather average model skill at medium and long time scales, and poor skill with respect to the RMSE, compared to other combined approaches. This is mainly due to the *H* model shoreline position being slightly shifted away from the observations mean position, either from the sum of components overestimating (e.g. PF2 and PF8, Fig. V.11 and Fig. V.14, respectively) or underestimating (e.g. PF1 and PF6, Fig. V.10 and Fig. V.13, respectively) the mean shoreline position. Hence the *H* model is ranked 7th based on medium-term skill, 5th based on long-term skill and second to last based on the RMSE, ahead only of the *CS* model.

The addition of the linear term improves the model at all time scales, improving the ability of the model to reproduce well the long-term trend, which corrects the *H* model's underestimation/overestimation of the mean shoreline position. However, the optimal *K* value for the *HL* is 3 times smaller than that of the *H* model. Thus, the variability reproduced by the *LS* model is less important relative to the *CS* model when the linear trend term is added.

The model behavior tends toward the *CSLEEF* behavior with similar criteria performance:

the *HL* model is ranked first for medium time scales and based on the RMSE, where it's ex-aequo with the *WL* model and ranks 3rd based on long-term skill.

- The *W* and *WL* approaches: This approach is a weak coupling between the *CS* and *LS* models by not taking into account shoreline change from the linear term and from the *LS* component in the *CS* equilibrium equation. However, this combined model allows feedback of *CS* shoreline changes in the *LS* component by modifying the local shoreline angle. Thus the *LS* component can potentially account for shoreline variations that are not represented in the *H* model, while the *CS* component is identical in both the *W* and *H* model.

During the optimization, it was observed that the optimal value of K is small and that the linear term adjusting the long-term variability, result in smaller RMSE, as with the *HL* model. The decrease in RMSE is more important when optimizing the long-term trend with a linear term, than when increasing the variability reproduced by the longshore component (with a larger K). Thus, the model behavior and associated skill at all time scales are similar to those of the *HL* model (Fig. V.15 and Fig. V.16).

- The *F* and *FL* approach: This approach assumes that the *CS* model equilibrium equation should account for shoreline changes caused by the *LS* or long-term trend model components. Thus, this formulation assumes that all the model shoreline position changes are varying at the same timescales and that their interactions must be taken into account.

At Narrabeen Beach, the shoreline changes from the *CS* model evolve at a higher rate than the variation generated by the *LS* model or the linear trend term at most profile (see Fig. V.10, V.11, V.12, V.13). Thus, in this model, the *CS* model equilibrium integrates the *LS* and linear term contributions in the S_F and compensates for the variations produced by the 2 other components. However, this compensation of the long-term trend of the *LS* component and the linear trend term generates a trend in the S_{CS} (see S_{CS} component in PF2 and PF8 in Fig. V.17). Yet, due to the coupling, the shoreline variations from the *CS* component affect the *LS* component. Thus the trend created in the *CS* component can create a long-term trend on the *LS* components (see S_{LS} component in PF2 and PF8 in Fig. V.17), and by feedback the trend of the *CS* component will also increase so that the S_F remains at the same equilibrium position (Fig. V.17).

Thereby, despite the important long-term trend observed in the *LS* and *CS* contributions of the *F* models, this approach can't reproduce a long-term trend on this beach, as the *CS* component compensates the trend from the 2 others components (Fig. V.17). This formulation could only reproduce a long term trend if the shoreline variation from the *LS* or the linear trend change at a higher rate than the *CS* shoreline variation as observed in synthetical test case. However the optimized K parameter is the largest for these 2 models (Fig. V.9), meaning that this model accounts for the most longshore variability of all the models. This is observed at PF8 (Fig. V.14), especially in the first 3 years of the simulation.

To conclude, this approach, while showing interesting skill at reproducing medium time scales

and longshore variability, presents the lowest skill of all combined models at long time scales due to the equilibrium compensating for shoreline trend reproduction from longshore and linear term component.

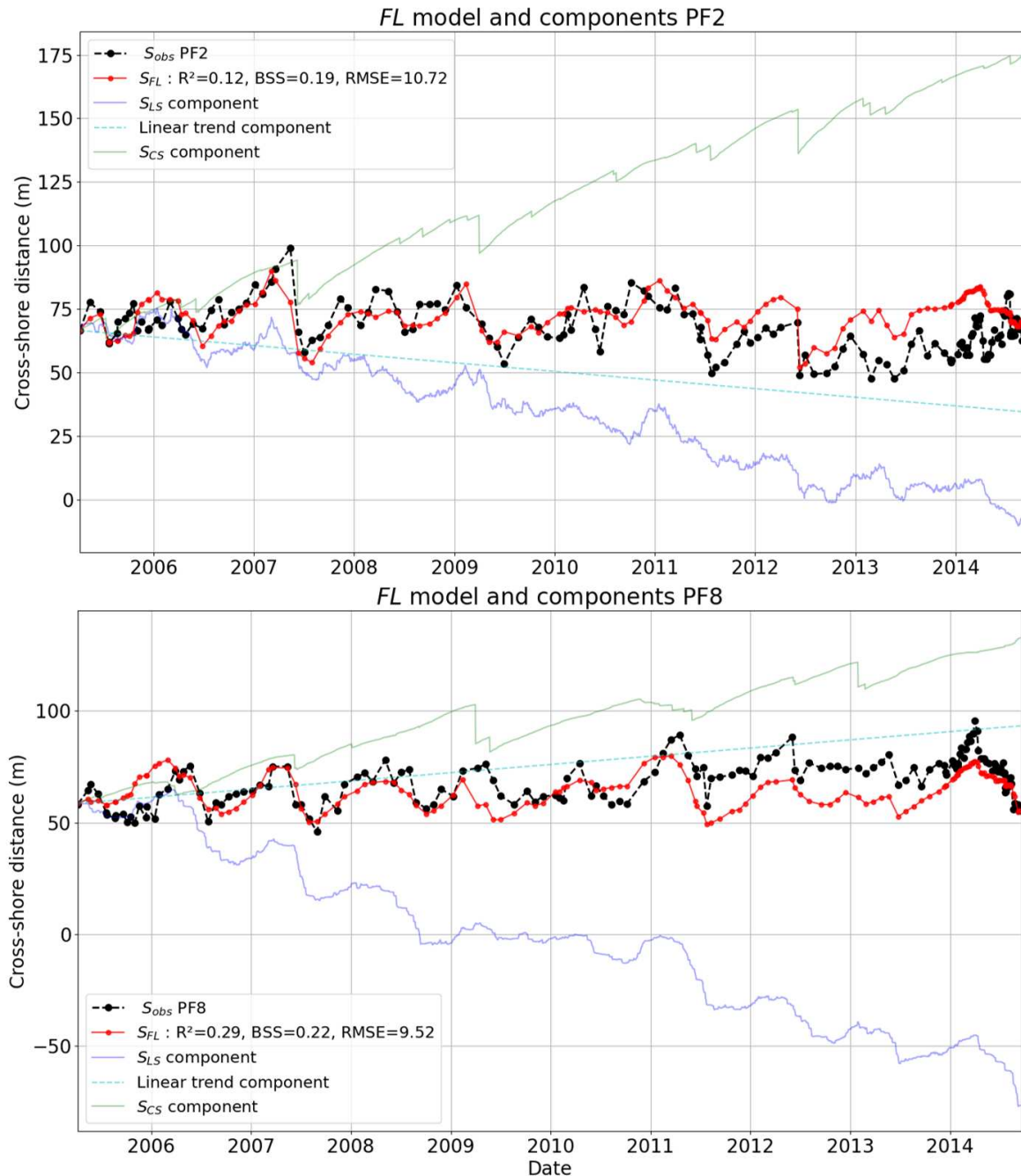


Figure V.17: Fully coupled model, FL shoreline position time series at PF2 and PF8 with the cross-shore S_{CS} , longshore S_{LS} and linear trend term component contribution.

V.3.6 Conclusion

The application of 7 different combined modeling approaches at Narrabeen Beach, and the analysis of the skill of each model has emphasized that accounting for longshore processes improves upon the *CS* only model performance (Fig. V.16).

However, at Narrabeen, the incorporation of a simple linear term increases the model skill at medium and long time scales better than the incorporation of the *LS* component along most of the beach (Fig. V.15, Fig. V.16).

The short term criteria shows that all combined approaches present similar skill, which is attributed to the *CS* model, this is expected due to the cross-shore processes dominating at this time scale and being used here with identical coefficients in all combined models.

As expected, the combined approaches integrating both the linear term and the *LS* component (*HL*, *WL*, *FL*) have higher skill at long time scales than the approaches with only the *LS* component (*H*, *W*, *F*). However, the differences are less significant for medium term skill due to the *LS* model accounting for part of the medium term variability at the beach extremities.

In terms of model skill as a function of the coupling approach, the analyzed criteria show that both independent (*H*) and weakly coupled (*W*) approaches have equivalent model skill at all time scales. Whereas the fully coupled (*F*) approaches are less efficient at reproducing long term variability due to the *CS* component equilibrium time response being faster than the other component and constraining the fully coupled model position to evolve around an equilibrium position.

To conclude, the models showing the overall best performance at reproducing the shoreline position at Narrabeen are the *CSLEEF*, the *HL* and the *WL* models, without significant differences observed between these approaches, however the *HL* and the *WL* models represent explicitly the longshore process contrary to the linear approximation used in the *CSLEEF*. Though, it should be noted that even these 3 better performing approaches reproduce at best, less than 60% of the shoreline variance (based on R^2 value) at Narrabeen. This is due to both these approaches accounting for cross-shore and longshore processes in a too simplistic manner. Other combined model were applied at Narrabeen Beach, for example, with LX-Shore model Robinet et al. (2020) have reproduced in the 2006-2010 period up to 80% of shoreline variance at PF1 and PF4 (with respectively $RMSE=6.38$ m and $RMSE=7.4$ m), but still only 40% on PF8 ($RMSE=6.9$ m).

Tran & Barthélemy (2020) also used the $RMSE$ to quantify their model skill, they obtained for the period 2005-2013, the combined model skill of $RMSE=7.7$ m at PF1, $RMSE=7.8$ m at PF4, and $RMSE=6.1$ m at PF8.

Thus, even if the different time periods of model application limit the direct comparison of the $RMSE$ values, these 2 combined approaches appear to show slightly better skill at Narrabeen Beach than the combined model presented in this chapter.

However, it should be noted that the cross-shore model used in Robinet et al. (2020) and Tran & Barthélemy (2020), the ShoreFor model, presented higher skill (lower $RMSE$) when applied alone

at Narrabeen Beach than the (Yates et al. 2009) model, and this contributes to the observed differences between the combined approach skill.

To generalize the model application, the results obtained here from the calibration at one particular site should be interpreted cautiously. For example, assuming a linear trend represents longshore processes, as in the *CSLEEF*, might be limiting at sites with more complex longshore dynamics. Furthermore, even if the *HL* and the *WL* models present nearly identical model performance, the hypothesis that longshore processes should be taken into account in the cross-shore model evolution in the *WL* approach should be tested further on additional natural sites where longshore processes are more dominant relative to cross-shore processes than at Narrabeen to assess the importance of accounting for these feedbacks.

Chapter VI

Long term modeling

Ce chapitre est consacré aux problématiques de prévisions à long terme de l'évolution du trait de côte. Une méthode statistique (Banno et Kuriyama, 2014) qui génère des projections de vagues incluant les effets du changement climatique à travers différents scénarios RCP a été appliquée à la plage du Vougot pour évaluer les performances à long terme (10-100 ans) du modèle cross-shore, et la sensibilité de 2 autres approches simples déjà existantes a été évaluée, ainsi que les incertitudes associées. La capacité du modèle cross-shore, présenté en chapitre 3, à fournir des prédictions de la position du trait de côte jusqu'en 2100, a été explorée en utilisant ces différentes séries temporelles de vagues projetées sur cette période future, sans tenir compte des effets possibles des scénarios RCP sur les changements du niveau d'eau moyen. Les résultats montrent qu'une légère modification des caractéristiques des conditions de vagues génère de petites différences dans la position prédite du trait de côte. Comme cette application ne tient compte que du changement du climat des vagues, il serait intéressant de développer une approche pour tenir compte des effets du changement du niveau moyen de la mer dans le modèle cross-shore. En parallèle, 2 approches alternatives simples existantes, largement utilisées pour prédire la position future du trait de côte, ont été appliquées à la plage du Vougot : la loi de Bruun et l'extrapolation linéaire des tendances historiques. Leur application confirme la sensibilité inhérente connue de ces approches, due à l'estimation des paramètres pour la loi de Bruun, et à l'exactitude des données actuelles pour l'extrapolation linéaire. Elle met aussi en évidence les incertitudes attendues lors de la prévision des changements du trait de côte à l'échelle centennale.

Chapter VI

Long term modeling

VI.1 Introduction

In this thesis work, the morphological model has been applied to reproduce past shoreline evolution (hindcasts) in comparison with observations. These data-based models can also be calibrated using past observations, and then be applied during both the training period and an additional period not used for the calibration (forecasts), but still corresponding to the observation period to evaluate the forecast model performance. This is an alternative model performance evaluation that should be completed in the future.

However, this chapter aims to focus on the problem of long-term shoreline forecasting by investigating the particular difficulties and the existing methods used to make 10 year to 100 year shoreline forecasts.

The first obvious problem when dealing with future shoreline evolution is that evaluating the precision of the model prediction is complex since, by definition, no future observations of the shoreline position exist for comparison.

The second difficulty in making future shoreline predictions is that the previously presented process-based models need forcing conditions to run, thus requiring a method to generate future wave climates and water level predictions, before being able to apply the morphological model.

The third difficulty arises from the previous one: the exact future trend of evolution of the hydrodynamical forcing conditions is also unknown, but there is evidence, in particular due to predicted climate changes, that future wave climates and water levels will be different from the current and past ones.

Thus, it is necessary to understand the potential evolution of current hydrodynamical conditions to better account for this when generating the future forcing conditions.

Lastly, the morphological modeling approaches presented in the previous chapters represent cross-shore and longshore processes, however the relevancy of these models can be questioned for applications at long time scales, such as a one hundred year period in particular the choice of the coefficients used to model these processes. In fact, cross-shore equilibrium models are usually applied to reproduce shoreline changes at seasonal to pluriannual time scales, and even the equilibrium theory is based on some hypotheses that could be questioned for model applications at centennial scales. For example, in the cross-shore model of [Yates et al. \(2009\)](#), the model coefficients (a , b , C^+ , C^-) are assumed constant in time. It should be note that in the CoSMoS-COAST model, [Vitousek et al. \(2017\)](#) used a Kalman filter approach for data assimilation enabling the model coefficient to

evolve in time during the assimilation process.

Furthermore, the presented approaches only include the effects of waves on the beach morphology, and currently, there exist few approaches that can reproduce accurately both the effects of the waves and changes in the mean sea level at these time scales (for example [Banno & Kuriyama 2014](#)).

The evaluation of sea level rise is now a globally studied problem due to the increasing need to estimate climate change impacts ([Oppenheimer et al. 2019](#)) for coastal management. Different projections of changes in mean sea level have been made worldwide, based on different emissions scenarios that control the global warming intensity and effects (Intergovernmental Panel on Climate Change (IPCC) Representative Concentration Pathways (RCPs) scenarios) ([Oppenheimer et al. 2019](#)).

To make long term shoreline predictions that include the impacts of sea level rise, 2 different kinds of approaches have been used historically: one based on observations (data-based) and one based on modeling approaches ([Le Cozannet et al. 2014](#)).

Data-based approaches use observations to search for relations between sea level rise rates and shoreline variability by comparing either similar site subjected to different magnitudes of sea level rise (spatial approach), or by investigating the link between shoreline and sea level evolution in time (temporal approach).

The application of these 2 approaches has shown that the shoreline response to sea level rise is highly influenced by local coastal factors, and that the observed shoreline evolution is well correlate with the sea level rise intensity at global scale ([Le Cozannet et al. 2014](#)).

Modeling approaches are applied to identify the impacts of sea level rise on shoreline variations by reproducing the other components of shoreline evolution to isolate sea level rise contribution. These models can be regrouped in 2 categories: those representing only sea level variations without modification of the morphology (i.e. submersion model), and the models that are trying to reproduce the morphological response to sea level rise.

In both approaches, an important limitation resides in the lack of available data to evaluate accurately the impacts of sea level rise, because the data is too scarce or covers too short of a time period or is not well-distributed spatially and often not accurate or reliable enough ([Le Cozannet et al. 2014](#)).

Climate change also has an impact on the wave climate by modifying the wave height distribution or the wave direction, due to changes in the wind climate, as shown by [Hemer et al. \(2010\)](#), [Hemer, Fan, Mori, Semedo & Xiaolan \(2013\)](#), [Hemer, Katzfey & Trenham \(2013\)](#), [Mori et al. \(2010\)](#). However, these studies point out the effects of the different RCP scenarios on the wave spectra. Thus, for individual coastal applications, approaches have been developed to account for these modifications to the wave spectra by generating future wave conditions with statistical approaches, such as [Banno & Kuriyama \(2014\)](#).

Using a probabilistic method with past wave observations, more complex methods were also developed to generate future storm sequences like the Joint probability method (JPM) used in the Probabilistic Coastline Recession (PCR) Model ([Callaghan et al. 2008](#), [Ranasinghe et al. 2012](#)).

In this chapter, the first section will introduce existing methods used to generate future wave conditions and the application of the approach of [Banno & Kuriyama \(2014\)](#) to generate wave time series projections at Vougot Beach.

Then 2 simple existing morphological change approaches will be presented and applied at Vougot Beach to illustrate the large uncertainties associated with future shoreline predictions. The first is based on an idealized modeling approach of shoreline retreat caused by sea level rise, called the Bruun rule ([Bruun 1962](#)), and the second is based on estimating future shoreline change based on the extrapolation of a linear trend calculated from past observations.

Finally, using wave time series generated with the [Banno & Kuriyama \(2014\)](#) approach, the empirical shoreline change model of [Yates et al. \(2009\)](#) will be applied to estimate future shoreline evolution (induced by cross-shore processes only) at Vougot Beach under different wave climate scenarios.

The methods and results presented in this chapter were obtained during 2 internships that I co-supervised and the work completed following their internships: Corentin Petton : "Empirical modeling of long term beach morphological evolution: impacts of wave climate change" and Nicolas Cailler: "Sea level rise impact on an empirical equilibrium model for beach morphological evolution".

VI.2 Generation of future wave time series

The generation of future wave time series can be performed using a global or a regional scale (e.g. the North Atlantic Ocean) wave model forced by wind projections generated by a global general circulation model (GCM) that simulates the climate based on different RCP scenarios. However, the evaluation of the hydrodynamic forcing conditions for a local coastal system is more complex, due to locally variable bathymetry, and is subject to important uncertainties, thus probabilistic approaches should be used ([Church et al. 2013](#)).

Nearshore wave conditions can be obtained using GCM downscaling to generate local winds as forcing boundary conditions for a wave model, but this method is computationally expensive ([Ranasinghe 2020](#)) and is thus difficult to apply at all coastlines.

For coastlines where fine resolution wind and wave projections can't be obtained accurately by these modeling approaches, a statistical approach was developed by [Banno & Kuriyama \(2014\)](#). They used historical local wave conditions to generate wave projections from historical wave conditions modified by predicted changes in the wave statistics (mean, standard deviation, log normal distribution) calculated for different RCP scenarios.

Their approach can be summarized as follows:

1. compute the histogram of the historical wave height
2. fit a log normal law to the historical wave height distribution
3. adjust the shape of this distribution using the projection of future change of wave statistics

(mean and standard deviation).

4. adjust the historical wave height time series according to the future wave distribution to create future wave condition.

With this approach, the impact on the future wave statistics of the different RCP scenarios is represented by modifying the historical wave statistics (mean and standard deviation) according to the future statistics. This future statistics are obtained for the different scenario using GCM simulations, that account for the different RCP scenarios effects, as forcing conditions of wave model.

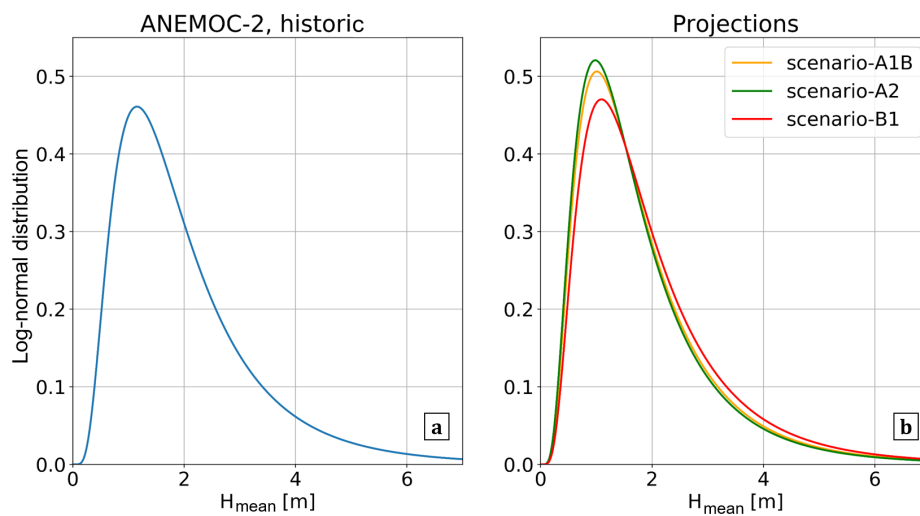


Figure VI.1: Calculation of the wave height distribution following the [Banno & Kuriyama \(2014\)](#) approach to account for RCP scenarios impacts.

The approach of [Banno & Kuriyama \(2014\)](#) has been applied to generate wave projections for Vougot Beach up to 2100.

In their approach, [Banno & Kuriyama \(2014\)](#) repeated 4 times 20 years of historical wave data to generate the total future time series. This time series was then corrected using the future wave statistics, by adapting wave by wave the historical wave height based on their probability distribution in comparison to the projected future wave height probability distribution.

In this application at Vougot Beach, the approach of [Banno & Kuriyama \(2014\)](#) was modified to generate the wave time series using annually segmented wave time series obtained from the historical 40 year long wave height time series (1961-2000) from the ANEMOC database (see [Laugel 2013](#), for more detail) generated using TOMAWAC spectral wave model ([Benoit et al. 1997](#)), that then were randomly drawn from a uniform distribution, and assembled to form the complete projected wave time series from 2017 to 2100.

The annual wave time series were made by cutting the total 40 years of historical wave time series from one summer to another, because of the more calm wave conditions in summer to avoid abrupt transitions in the constructed wave height time series.

With this methodology, the seasonality, the alternation of calm and energetic periods, the storm duration are preserved without repeating the 40 years of identical wave chronology whereas the variability at longer periods, for example from variation of the North Atlantic Oscillation index, is not accounted for. These wave projection time series were then modified to account for evolution of wave statistics (mean and standard deviation) following the RCP scenarios A1B, A2 and B1 (IPCC 2014) (Fig. VI.1b) by adjusting the shape of the fitted log normal distribution (Fig. VI.1a).

To account for the effects of the random sampling of the annual time series, this process was repeated and 200 projected time series were generated for each RCP scenario to be analyzed in a probabilistic manner.

VI.3 Existing methods for long term shoreline change predictions

Two existing approaches are described, the first one is the Bruun rule (Bruun 1962), an idealized modeling approach that accounts for the impact of sea level rise.

The second is the linear extrapolation, this method represent shoreline change trends based on the extrapolation of a linear trend calculated from observations, thus this method is accounting for both the impact of the wave and the sea level change but assuming with the linear extrapolation that past trend and future trend in the wave climate and sea level rise are identical.

VI.3.1 Bruun rule

The Bruun rule is an idealized modeling approach that predicts shoreline changes caused by sea level rise. The retreat is estimated as a simple shoreward translation of the beach profile (Bruun 1962).

This approach has been largely applied due to the simplicity of its formulation to obtain rapidly an estimate of the shoreline retreat due to the sea level rise:

$$R = \frac{LSlr}{B + h}, \quad (\text{VI.1})$$

where R is the predicted shoreline retreat (in m), L is the horizontal distance between the shoreline position and the depth of closure (h), Slr here represents the sea level change, B is the eroded berm or front dune height (Fig. VI.2).

This approach makes the hypothesis that the cross-shore sediment volume is conserved in the considered beach profile such that the eroded sediment is redistributed along the profile between the front dune height and the depth of closure, thus neglecting the potential impacts of longshore processes.

This approach has been included in process-based models to account for the impacts of long term sea level rise, such as in the CoSMoS-Coast model of Vitousek et al. (2017), or more recently LX-Shore of Robinet et al. (2018).

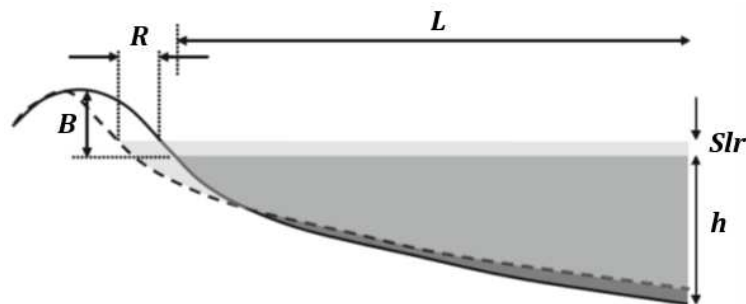


Figure VI.2: Bruun rule conceptual scheme, from [Ranasinghe et al. \(2012\)](#).

In recent decades, this approach was largely criticized as being too simplistic ([Cooper & Pilkey 2004](#)), as well as giving inaccurate and overestimated results, and also being unsuitable for coastlines dominated by longshore processes. This model is also highly sensitive to the value of the parameters used for the shoreline retreat calculation.

There are large uncertainties in the estimation of some of these parameters, for example the determination of the depth of closure is still a conceptual problem. However, this approach continues to be used widely due to its simplicity for coastal managers and the lack of easy alternatives ([Cooper & Pilkey 2004](#)).

Thus, it's interesting to evaluate the shoreline retreat prediction of this model compared to other methods, including the uncertainties and sensitivity associated when applied at Vougot Beach.

The Bruun rule was applied at Vougot Beach using 2 different sources of data for the sea level elevation Slr :

- The mean IPCC estimation ([Church et al. 2013](#)) of the global sea level rise, based on the different scenarios (RCP2.6, RCP4.5, RCP6.0 and RCP8.5) between 2000 and 2100 (blue curves in Fig. VI.3a).
- A local linear extrapolation of the sea level based on tide gauge data of Brest harbour, using data from 1953 to 2017 (tide gauge data from PSMSL, orange curve in Fig. VI.3a).

Using a linearly extrapolated sea level time series is an important simplification since the sea level rise is expected to increase exponentially according to the IPCC predictions (Fig. VI.3a).

In the Bruun Rule, the B parameter was taken as the dune height using the observations. For profile 6, presented in Fig. VI.3b, $B = 11.6 \text{ m}$.

The depth of closure, h , was calculated with the [Hallermeier \(1980\)](#) formula: $h = 8.9\bar{H}_s$ where \bar{H}_s represents the mean annual wave height using the wave data from the more offshore Homere node point (located -4.1358N, 4.8684W) presented in Chapter III, and a value of $h = 16.2 \text{ m}$ was found. Finally, using the bathymetric data available together with the nautical chart from the SHOM, the distance between the shoreline and the depth of closure was estimated as approximately $L = 2250 \text{ m}$.

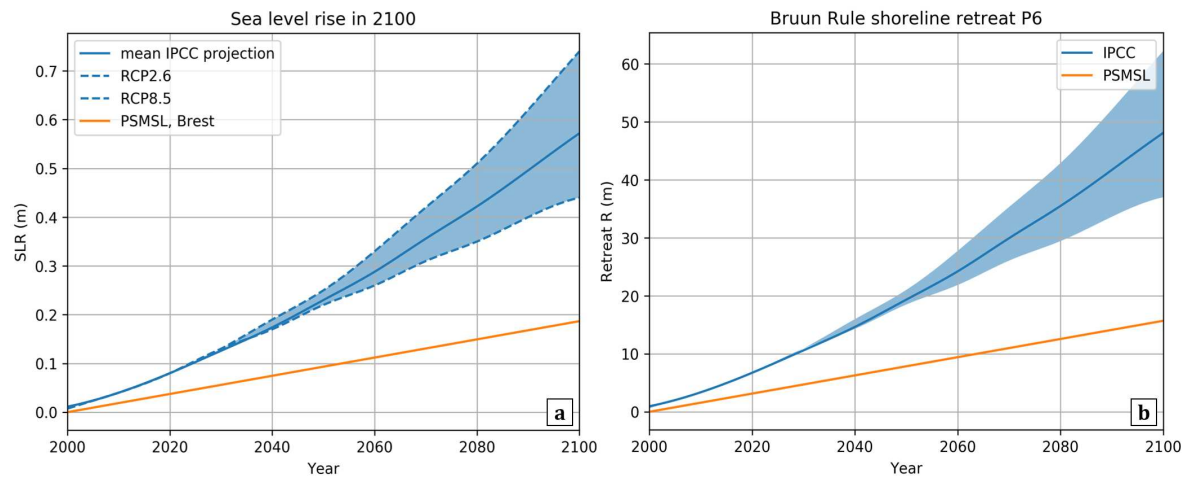


Figure VI.3: Bruun rule application: (a) sea level elevation used in the Bruun rule application at Vougot Beach, and (b) shoreline retreat estimated with the Bruun rule using 2 sea level rise estimates.

The results of the Bruun rule application (Fig. VI.3b) show that the estimated shoreline retreat by the year 2100 ranges between 37 m and 62 m for the different RCP scenarios (in blue), and is approximately 15 m with the linear extrapolation of the historical PSMSL data (in orange). This important difference between the shoreline retreat obtained for the 2 different sources of sea level rise projections highlights the influence of the approach used to estimate Slr , and the sensitivity of the Bruun rule to the parameter estimation.

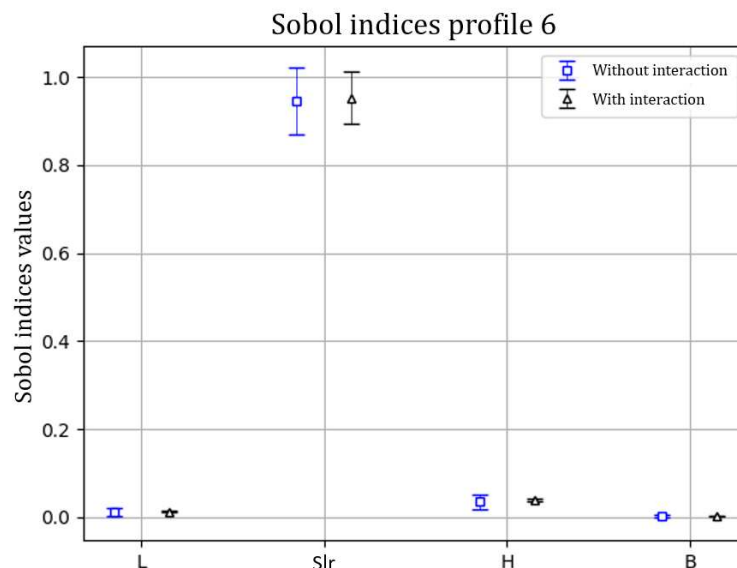


Figure VI.4: Sobol indices for Bruun rule at profile 6 (Cailler 2019) representing the contribution of each parameter to the variance of R with or without accounting for the interaction and compensation effect between the parameter (figure from Cailler (2019)).

To further explore the Bruun rule’s dependency on the parameter values, a sensitivity analysis

using Sobol indices (Sobol 2001). This indices estimates the weight of the different parameters in the shoreline retreat (R) variance calculated by the Bruun rule by repeating the R calculation while testing different parameter value to analyzed the influence of each parameter on R .

Cailler (2019) showed that Slr is the most important parameter in the Bruun rule estimate of shoreline retreat (about 85% of the R variance). The second most important parameter is L (with about 10% of the R variance), and finally h and B explaining less than 5% of the variance (as can be seen in Fig. VI.4). However, L is determined using the value of the depth of closure h , whose concept and calculation are still questionable. Furthermore, the practical estimation of L could become more inaccurate with a lack of or coarse resolution bathymetric data.

VI.3.2 Linear extrapolation

The linear extrapolation method is a data-based approach used to estimate future shoreline evolution by performing a linear regression of historical observations (Fig. VI.5a) that is then extrapolated into the future to make shoreline change predictions. The simplicity of application makes it a popular approach for estimating rapidly shoreline evolution in coastal engineering projects or for coastal management.

Yet, this approach is highly sensitive to the data quantity and quality, as well as the time period used to calculate the regression, with additional problems such as seasonal and inter-annual oscillations that influence the slope of the regression in the case of short or sparse time series.

Extrapolating the linear trend also assumes that the wave climate statistics are stationary in time, which is now known to be potentially inexact.

When applied to a site with observations of contour position along the intertidal zone, such as Vougot Beach, an additional problem appears with the choice of the reference level at which to estimate and apply the linear extrapolation.

Analysis of the time series of shoreline position at different altitudes shows that, for the same profile, the slope of the linear regression can vary significantly. This is assumed to be due to the differences in morphological response of the different parts of the beach to cross-shore and longshore processes, as well as impact of sediment depletion locally on the cross-shore profile (hard ground) limiting the morphological change.

Consequently, the shoreline position predictions from the linear extrapolation method vary depending on the selected altitude, as illustrated in Fig. VI.5b. For profile 6, extrapolated shoreline changes at MSL, MHWN and MHWS are respectively 75 m, 135 m and 95 m.

To compare with the Bruun rule, the linear extrapolation was also applied at different elevations corresponding to the approximate location of the dune toe (between 6.4m and 7.0m with increment of 0.2m) for all 6 profiles at Vougot Beach. The results (not shown here) show large variability of the predicted shoreline retreat depending on the profile, with variations between 6.4m and 7.0m elevation ranging from 40 m of retreat, estimated for profile 4, to 20 m of accretion, predicted for profile 6. The sensitivity of the approach was also observed here, as important variability in the

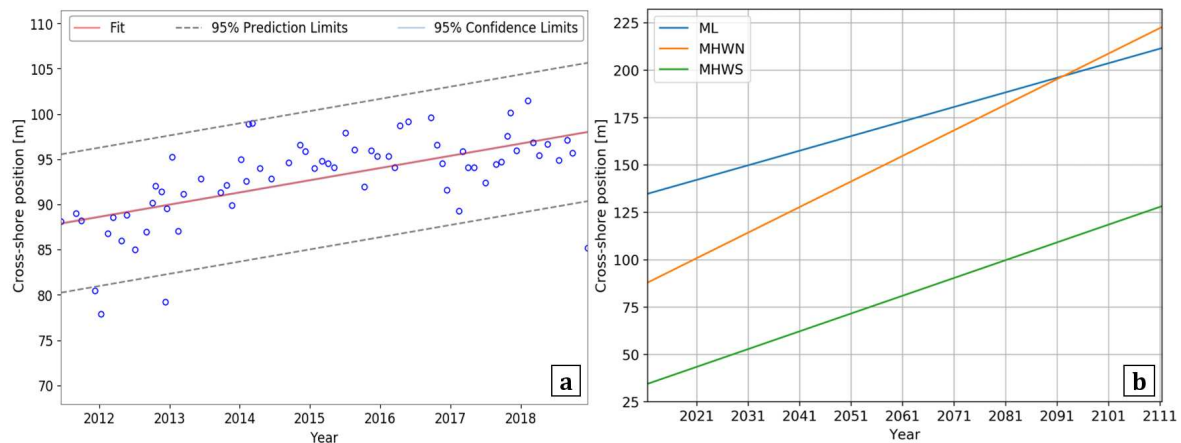


Figure VI.5: Linear extrapolation method applied to profile 6 at Vougot Beach: (a) Example calculated linear regression (in red) of the shoreline position observations (blue points) at MHWN elevation. (b) Linear extrapolation of the shoreline position at MSL, MHWN and MHWS elevations from the present to the year 2100 (figure from Cailler (2019)).

predicted shoreline retreat was found along the same profile, even though the 4 altitudes used are located close to each other (within a 0.6 m vertical range).

VI.3.3 Empirical cross-shore model

Using the projected wave time series obtained from the adapted approach of Banno & Kuriyama (2014), the impacts of the different RCP scenarios and the associated changes in the wave height on shoreline evolution were evaluated at Vougot Beach using the empirical shoreline change model of Yates et al. (2009). In this application, the impacts of changes in mean sea level are not represented since the future water levels are generated using only astronomical tide predictions, which are accounted for in the model following Lemos et al. (2018), as presented in Chapter III.

The model was applied at profile 6 at the Mean Sea Level elevation ($z = 0.5 \text{ m NGF}$) (Fig. VI.6 and Fig. VI.7a,b) using 200 time series generated for each RCP scenario, covering the time period 2017 to 2100, after a calibration period from 2011 to 2017 (red area in Fig. VI.6 and Fig. VI.7a). The mean of the predicted shoreline positions is calculated from the 200 realizations for each RCP scenario, and the global shoreline position envelope (minimum and maximum of all realizations) is also shown (in color representing each RCP scenario and in grey in Fig. VI.6 and Fig. VI.7a,b).

The mean and the envelope of the shoreline position obtained for the different scenarios shows a rather constant mean shoreline position over time, with small shoreline position differences between the 3 scenarios. This is coherent with the difference between the wave projections following the 3 scenarios being relatively small (Fig. VI.1b). Shoreline positions obtained with the A2 projection are slightly more eroded, while the B1 projections are slightly more accreted (Fig. VI.7a,b).

The overall differences are small, indicating that the impact of the predicted variations of the wave height characteristics on the shoreline response is small with this modeling approach.

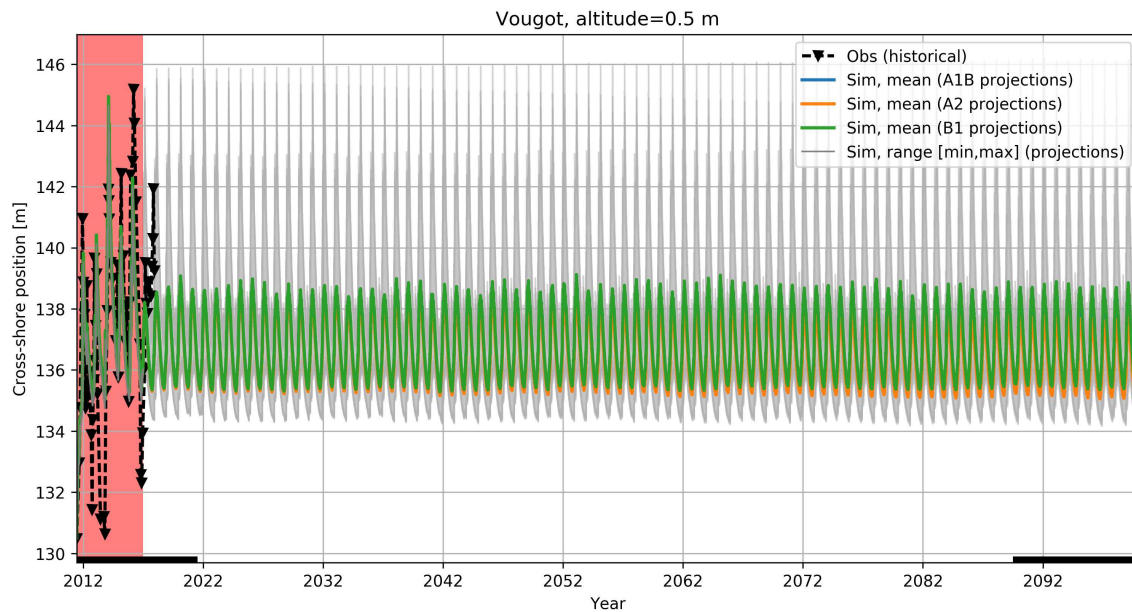


Figure VI.6: Empirical cross-shore model application at Profile 6 of Vougot Beach at MSL ($z=0.5\text{m}$) from 2011 to 2100, using the projected wave time series from different RCP scenarios generated following the approach of [Banno & Kuriyama \(2014\)](#). The shaded red zone indicates the model calibration period.

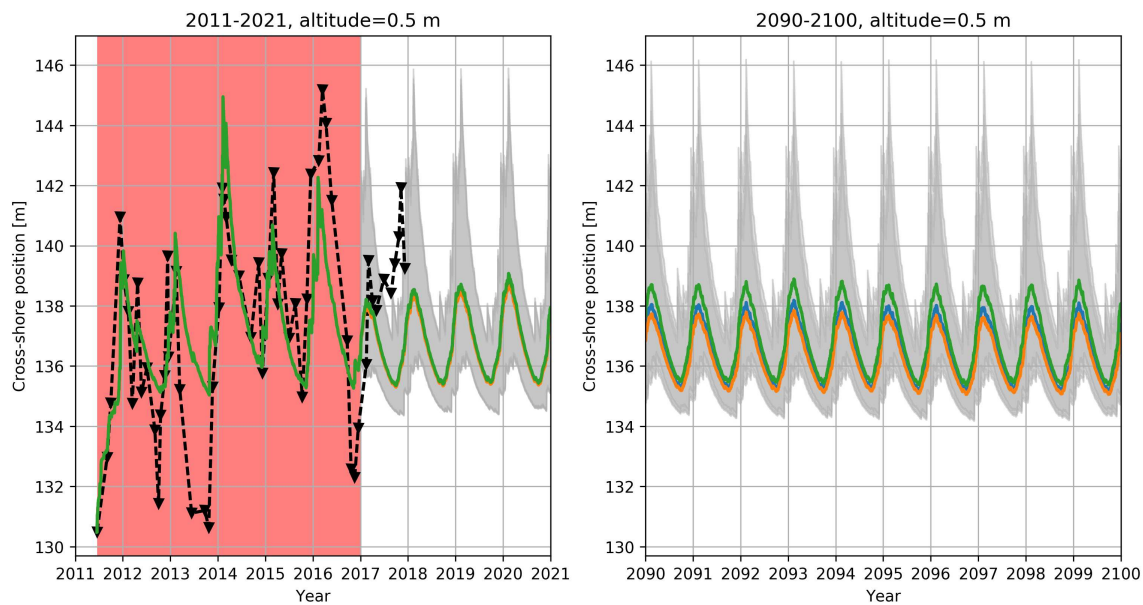


Figure VI.7: Empirical cross-shore model application at profile 6 of Vougot Beach at MSL ($z=0.5\text{m}$), using the projected wave time series from different RCP scenarios generate following the approach of [Banno & Kuriyama \(2014\)](#) (same color legend as Fig. VI.6): zooms of (a) the first 10 years (showing the calibration period in the shaded red zone) and (b) the last 10 years of the simulation period.

However, as mentioned in the introduction of this chapter, the relevance of a cross-shore equilibrium model to make a 100 year long shoreline projection can be discussed. For example, the absence of long term trends of shoreline retreat or accretion observed with the generated wave projections in Fig. VI.6 is expected to be due to the model coefficients because they define the equilibrium position and the model response to change in the wave characteristics.

This application shows that the equilibrium cross-shore model could easily be applied to make long term shoreline predictions using, for example, wave projections generated following the approach of [Banno & Kuriyama \(2014\)](#). Yet, in its current formulation, the cross-shore model does not account for changes in the mean sea level. Hence, further developments are needed to better account for variations of the mean water level and its impact on the beach morphological changes.

Conclusion

This chapter was dedicated to long term shoreline predictions, and the preliminary work presented here allowed pointing out the inherent difficulties of this objective. The interest in modeling future shoreline evolution, and in particular, accounting for climate change impacts is growing. However, it requires the generation of wave climate and water level projections that accurately include the different possible climate change effects. Thus probabilistic approaches are necessary. Here, the statistical approach of [Banno & Kuriyama \(2014\)](#) has been applied to Vougot Beach to generate nearshore wave predictions from the historical wave conditions and offshore wave projections of the future wave climate.

Furthermore, 2 existing simple approaches, the Bruun rule and linear extrapolation of historical rates of change, the two most commonly used methods for predicting shoreline evolution, have been applied at Vougot Beach to predict shoreline changes until the year 2100. Both methods show, due to their deterministic nature, significant sensitivity to the data availability and quality for the linear extrapolation approach, and to the estimation of the model parameters for the Bruun rule. They both highlight that large uncertainties and variability in predictions can be observed for a site depending on the choice of altitude, the profile data used to estimate the historical change rate for linear extrapolation approach, or on the water level projections selected for the Bruun rule.

Finally, an equilibrium shoreline change model has been applied until the year 2100 using wave projections generated following the approach of [Banno & Kuriyama \(2014\)](#) and predictions of the astronomical tide. The model results show that, while only accounting for climate change impacts via changes in the wave climate, the predicted shoreline evolution shows almost no long term trend at the applied elevation and small variations of the equilibrium position between the different RCP scenarios. This application highlights the necessity to develop a method to account for the impacts of mean sea level variations in equilibrium-based models.

Conclusions and future work

Cette thèse a pour objectif l'amélioration d'un modèle d'équilibre empirique reproduisant l'évolution du trait de côte due au processus hydro-sédimentaires cross-shore. La capacité du modèle à été évaluée sur la plage de Vougot, un site où l'évolution morphologique est provoquée par des processus cross-shore mais aussi longshore. Cette application montre que la performance du modèle est relativement bonne sur ce site macrotidal mais diminue lorsque l'importance des processus longshore augmente. Ainsi, pour ajouter la composante longshore au modèle cross-shore, une approche one-line a été implémentée, testée et validée sur la plage de Narrabeen. Une étude de sensibilité aux conditions de vagues utilisées en forçage, a été réalisée à Narrabeen, et montre que le modèle one-line est très sensible aux biais dans la direction des vagues. A Narrabeen et sur d'autre site, l'approche one-line peut produire une réorientation de la côte qui n'est pas observée. En supposant qu'elle provient de biais dans la direction des vagues, une méthode est proposée, utilisant un processus de Monte-Carlo, qui permet d'obtenir un ensemble de biais dans la direction des vagues qui corrige ce phénomène. En utilisant le modèle cross-shore, le modèle one-line et un terme linéaire, 7 modèles combinant ces 3 composantes de manière plus ou moins couplée sont définis, implémentés et testés sur la plage de Narrabeen. Leurs performances sont ensuite comparées en utilisant 3 critères évaluant la capacité du modèle à reproduire la variabilité du trait de côte à différentes échelles de temps: à court terme (mensuel), à moyen terme (saisonnier) et à long terme (pluriannuel). Cette analyse montre que l'ajout d'une composante longshore améliore le modèle cross-shore à toutes les échelles de temps, mais que, à Narrabeen, l'ajout d'un terme linéaire seul est plus efficace que l'ajout d'un terme longshore seul pour les performances à long terme. Les approches qui montrent les meilleures performances intègrent à la fois le terme linéaire et le terme longshore. L'augmentation du degré de couplage n'augmente pas la performance du modèle à Narrabeen, ainsi l'approche couplant faiblement les modèles longshore et longshore et l'approche où ils sont indépendants obtiennent des performance égales, et de meilleure performance que l'approche couplée. Pour évaluer les performances à long terme (10-100 ans) du modèle cross-shore, une approche statistique qui génère des projections de vagues incluant les effets du changement climatique à travers différents scénarios RCP, a été appliquée à la plage du Vougot et utilisée pour forcer le modèle cross-shore. En parallèle, 2 approches simples existantes, très utilisées pour prédire la position future du trait de côte, ont été appliquées: la loi de Bruun et l'extrapolation linéaire des tendances historiques. Leur application sur la plage de Vougot confirme leur sensibilité aux données et paramètres utilisés, qui est connue pour ces

approches. Cette dernière application pointe les incertitudes attendues lors de la prévision des changements du trait de côte aux échelles décennale à centennale.

Suite à ces travaux de thèse, il sera nécessaire d'appliquer sur d'autres sites, aux conditions hydrodynamiques et aux morphologies variées, les différentes approches combinées pour valider et pouvoir ensuite généraliser les conclusions obtenues à Narrabeen. Pour une application sur des environnements plus variés, plusieurs implémentations du modèle sont à envisager comme la gestion des structures de défense côtière ou de zone non érodable ainsi qu'une meilleure prise en compte des hauteurs d'eau à long terme. Ces applications à d'autres sites sont une étape vers la sélection de la meilleure approche et la généralisation des coefficients permettant l'application du modèle sur des sites où moins de données d'observation sont disponibles.

Conclusions and future work

Summary

To understand shoreline evolution and prevent coastal risks such as coastal erosion or marine flooding, numerical models able to represent accurately shoreline evolution on large spatial scales (site to regional) and at medium to long temporal scales (seasonal to decennial) are required, and they are still lacking.

Process-based approaches perform well at these scales, and are a viable alternative to computationally expensive, physics-based models as tools for operational and management purposes.

The goal of this thesis work was to improve the performance of the shoreline change modeling tools by extending an existing empirical equilibrium shoreline change model. These kinds of approaches aim to reproduce the evolution of the cross-shore position of an altitude on a beach based on equilibrium beach profile theory. These approaches are relatively simple and their computational cost are low, thus they can be easily applied at operational spatio-temporal scales, even on a personal computer.

Nevertheless, they have several limitations.

First, they only account for cross-shore processes, while the relative importance of other processes, like longshore processes, can increase and dominate depending on the time scales of application, the forcing conditions and the studied site.

Second, these approaches are data-based and need morphological observations to calibrate their coefficients, as well as time-series of wave forcing conditions. Thus, the model performance depends on the quality and quantity of available data.

Thus, this thesis work aimed to answer the following questions:

Firstly, the goal is to further evaluate the empirical equilibrium cross-shore model skills and limitations, in particular by asking, how well does the model reproduce contour changes in complex macrotidal environments influenced by both cross-shore and longshore processes? What are its limitations? In addition, what is its applicability for making long-term predictions that include climate change impacts?

Secondly, this thesis work was focused on representing longshore processes coupled with empirical cross-shore modeling. Thus, a one-line approach was implemented to maintain the efficiency and simplicity of application of the model. Hence, what are the expected uncertainties and limitations of the longshore approach?

Thirdly, how can cross-shore and longshore models be coupled? And how do the different coupling approaches impact the model performance at different time scales of application?

To address these different issues, an empirical equilibrium shoreline change model (from [Yates et al. \(2009\)](#), modified by [Castelle et al. \(2014\)](#) and [Lemos et al. \(2018\)](#)) was applied at the complex macrotidal environment of Vougot Beach to evaluate the model performance and limitations along 6 cross-shore profiles of this beach where both cross-shore and longshore processes have an important role in controlling the beach morphodynamics (in Chapter III).

The model application at different elevations along 6 profiles of the beach shows vertical and alongshore variability of the empirical shoreline change model performance. Along the beach profile, the model reproduced well altitudes located in the intertidal zone and below the dune toe, but had lower skill around the MHWN contour, corresponding to the transition zone between the reflective and dissipative parts of the profile. The dynamics in this zone are too complex to be represented with a simple empirical equilibrium shoreline change model, since they are determined by the total profile shape. In the alongshore direction, the model shows better performance at the western end of the beach than at the eastern end, where the influence of longshore processes appears to be more significant in the beach morphological evolution.

In the case of long-term trends in the shoreline position, the optimization algorithm that is used to determine the model free coefficients identified minima corresponding to sets of coefficients that enable the equilibrium-based cross-shore model to produce long-term trends (pluriannual) at the expense of reproducing the seasonal variability. This result highlights the potential model improvement in integrating processes responsible for long-term trends in the model formulation.

Thus, based on the reported model difficulties in the presence of longshore processes, a longshore model has been implemented. This model has been validated with synthetic and analytical test cases and then applied at Narrabeen Beach, where 10m depth wave data are available at 5 positions alongshore, to validate its performance at a natural site.

Then, the model sensitivity to the wave forcing conditions, in particular the wave direction, has been investigated and a method correcting for a coastline reorientation that was predicted by the model but not present in the observations, has been proposed (in Chapter IV).

From the state of art, a simple one-line model (based on the approach of [Pelnard-Considére \(1956\)](#)) was implemented to represent longshore processes. This approach is used widely as an operational tool due to its simplicity and low computational cost. However, the approach's simplicity has also been criticized, in particular regarding the evaluation and calibration of the longshore sediment flux. Previous applications of the one-line model at Narrabeen Beach in other studies, and the application of the model in this thesis work, showed that the one-line model can generate a change in the shoreline planform orientation that is not present in the observations. Thus, by assuming that this planform reorientation is produced by biases in the input wave direction, a method based on a Monte-Carlo approach has been proposed that efficiently corrects for changes in the orientation of the modeled shoreline planform.

A sensitivity analysis was also conducted on the impacts of biases in the 10m depth wave height and direction forcing the model. Results showed that small biases in the breaking wave direction

may have important impacts on the model shoreline position, which can be larger than the effects of biases in the breaking wave height.

Next, a range of combinations of the empirical cross-shore model, the longshore one-line model, and a linear trend term have been explored by implementing different coupling methods and applying the models at Narrabeen Beach.

The skill of each combined model is analyzed and discussed using three time-scale based performance criteria to highlight the relative contributions of each model component depending on the model formulation (in Chapter V).

By testing different approaches for coupling the 3 following components: the cross-shore empirical shoreline change model, the one-line model and a linear term, 7 combined models were implemented and tested on synthetic cases and applied at Narrabeen Beach.

An optimization methodology has been adopted that reduces the number of optimized free parameters in the model application by using only one set of cross-shore model coefficients (a , b , C^+ , C^-) and one value of longshore flux rate coefficient (K) for the whole beach. The comparison of the different model combinations was made using time-scale based skill criteria evaluating the short-term (monthly), medium-term (seasonal), and long-term (pluriannual) performance of the model.

It shows, first, that accounting for longshore processes in the combined approach always improves upon the cross-shore model skill alone.

Secondly, the incorporation of a simple linear term increases the model skill at medium and long time scales better than with the longshore component along most of Narrabeen Beach. At short time scales, the corresponding skill criteria shows that all combined approaches present similar performance, due to the cross-shore processes dominating at this time scale, and using identical cross-shore coefficients in all combined models.

Third, the combined approaches integrating both the linear term and the longshore component have higher skill at long time scales than the approaches with only the longshore component, but the differences are less significant for medium-term skill due to the longshore model accounting for part of the medium-term variability at the beach extremities.

Fourth, in terms of model performance as a function of the coupling approach, the criteria show that both the hybrid *HL* and weakly-coupled *WL* approaches have equivalent model skill at all time scales whereas fully-coupled approaches are less efficient at reproducing long-term variability.

To conclude, the models showing the overall best performance at reproducing the shoreline position at Narrabeen are the cross-shore with an integrated linear term model, the hybrid linear model and the weakly-coupled plus linear term model, without significant differences observed between these approaches. However, the results obtained here from the calibration at one particular site should be interpreted with caution and not generalized before validation at other sites.

Finally, long-term predictions were investigated at Vougot Beach, using a statistical method generating wave projections that included the impacts of different RCP scenarios, and exploring the

sensitivity and uncertainty of simple existing approaches. The cross-shore model skill for making long-term shoreline predictions using different future projections of wave time-series was also explored (in Chapter VI).

The [Banno & Kuriyama \(2014\)](#) approach was modified and applied at Vougot Beach to generate projections of wave height time series that integrate the impacts of the different RCP scenarios on the wave height characteristics (e.g. mean, standard deviation). Using these projected wave forcing conditions, the empirical cross-shore model was applied to predict shoreline evolution up to 2100 but without considering the different RCP scenarios impacts on changes in the mean water level. It showed that when using this approach, small differences in the wave field characteristics induced small differences in the predicted shoreline position. This application only accounts for changes in the wave climate. Therefore, there is a necessity to develop an approach to account for the effects of mean sea-level changes in the model.

Two existing simple alternative approaches, which are used widely to predict the future shoreline position, were applied at Vougot Beach: the Bruun rule and linear extrapolation of historical trends. Their application confirms the known inherent sensitivity of these approaches to the parameter estimation and the data quality, respectively, and highlight the expected range of uncertainty when predicting centennial scale shoreline changes.

Perspectives

The implementation and comparison of the different combined models presented in this thesis work have pointed out differences in model skill, showing that a ranking can be made for each produced time scale and overall model performance.

However, this ranking was obtained for Narrabeen Beach, and before further exploitation of the different combined approaches, validation at other sites with different geomorphological and hydrodynamical conditions should be conducted to verify the wider relevance of the model rating. This validation phase could also integrate an evaluation of the blind shoreline forecasting skill (e.g. [Montaño et al. 2020](#)) and not only use hindcast results, as presented in this work.

To apply the combined models at a larger range of coastal environments, the implementation of a module to account for coastal structures (e.g. groin, jetty, breakwater) and their impacts on the longshore sediment transport should be completed such as in formerly developed one-line models for engineering (e.g. GENESIS model ([Hanson 1989](#))).

In addition, it will be necessary to account for non-erodible areas (e.g. rocky substrate), along all or part of a profile, that would limit the retreat of the shoreline position in the cross-shore model (as implemented in [Doria et al. \(2016\)](#)), or affect the sediment availability in the longshore sediment flux calculation.

The representation of these effects would enable the model application to beaches with anthropogenic development (e.g. groins, breakwaters) such as the Japanese beaches of Hasaki and Omote-

hama, for which observational data were obtained from a collaboration with the Port and Airport Research Institute (PARI), Japan (PHC Sakura funding, 2018-2020, on accounting for climate change impact in long-term shoreline prediction) in which I was able to participate during this thesis work. The representation of these structures also concerns the combined model application at Vougot Beach, which features a jetty at the eastern limit, a tombolo formed from a rocky outcrop at the center (that could be assimilated to a breakwater in a preliminary approach), and many patches of rocky substrate underneath a thin sand layer in the lower intertidal zone.

The validation of the conclusions of this thesis work on other beaches is a necessary step to select the best combined model to be applied on a large variety of beaches with varying morphological and hydrodynamical settings, in order to derive a generalization of the model coefficients.

As was done by [Splinter et al. \(2014\)](#) with the ShoreFor cross-shore model, the goal of this generalization is to find relations between the optimum coefficients (a , b , C^- , C^+ , K) obtained with available observations and the beach characteristics to would then enable the application of the combined model at sites without sufficient data availability.

During this thesis work, the sensitivity of the cross-shore model to changes in the forcing wave conditions and the quantification of the longshore model sensitivity to errors in the wave direction and height have been performed. However, additional work is needed to test the sensitivity of the combined model to the length and frequency of the morphological observations used to calibrate the model, similar to the study done with the cross-shore model in [Yates et al. \(2009\)](#).

Similarly, the sensitivity of the combined model performance to the length of observations used to calibrate the model for long-term shoreline modeling should also be investigated. These analyses would contribute to answering the question: what are the time scales that need to be represented in the observations so as to predict correctly shoreline evolution at long time scales?

Finally, given the conclusions of the cross-shore model application at the macrotidal Vougot Beach, the potentially increasing importance of the sea-level variations in long-term shoreline modeling, and also the perspective of a generalization of the model coefficients, it is necessary to improve the approaches used to take into account mean water level variations and their effects on beach morphological evolution. This additional element in the model will improve the combined model performance at long time-scale and for cases with significant sea-level change.

The current cross-shore model integrates the modification proposed by [Lemos et al. \(2018\)](#) that uses a binary approach to account for the impacts of the tidal level. The method consists in a threshold based on instantaneous wave height and water level that enables or prevents the shoreline evolution in the model, yet this formulation cannot represent the effects of a temporal variation of the mean sea-level, which needs to be improved.

Thus, a method still has to be implemented to account for the water level effects in both the cross-shore and longshore components of the combined approach.

Bibliography

- Aagaard, T., Greenwood, B. & Nielsen, J. (1997), 'Mean currents and sediment transport in a rip channel', *Marine Geology* **140**(1), 25–45.
- Antolínez, J. A. A., Méndez, F. J., Anderson, D., Ruggiero, P. & Kaminsky, G. M. (2019), 'Predicting climate-driven coastlines with a simple and efficient multiscale model', *Journal of Geophysical Research: Earth Surface* **124**(6), 1596–1624.
- Arriaga, J., Rutten, J., Ribas, F., Falques, A. & Ruessink, B. (2017), 'Modeling the long-term diffusion and feeding capability of a mega-nourishment', *Coastal engineering* **121**, 1–13.
- Ashton, A. D. & Murray, A. B. (2006), 'High-angle wave instability and emergent shoreline shapes: 1. modeling of sand waves, flying spits, and capes', *Journal of Geophysical Research: Earth Surface* **111**(F4).
- Ashton, A., Murray, A. B. & Arnoult, O. (2001), 'Formation of coastline features by large-scale instabilities induced by high-angle waves', *Nature* **414**, 296–300.
- Banno, M. & Kuriyama, Y. (2014), 'Prediction of future shoreline change with sea-level rise and wave climate change at Hasaki, Japan', *Coastal Engineering Proceedings* **1**(34), 56.
- Bascom, W. N. (1951), 'The relationship between sand size and beach-face slope', *Transactions, American Geophysical Union* **32**(6), 866–874.
- Battjes, J. (1974), 'Surf similarity', *Coastal Engineering Proceedings* **1**(14), 26.
- Benoit, M., Marcos, F. & Becq, F. (1997), Development of a third generation shallow-water wave model with unstructured spatial meshing, Proc. 25th Int. Conf. on Coast. Eng.
- Blaise, E., Suanez, S., Stéphan, P., Fichaut, B., David, L., Cuq, V., Autret, R., Houron, J., Rouan, M., Floc'h, F., Arduin, F., Cancouët, R., Davidson, R., S., C. & Delacourt, C. (2015), 'Bilan des tempêtes de l'hiver 2013-2014 sur la dynamique de recul du trait de côte en Bretagne', *Géomorphologie: relief, processus, environnement* **21**(3), 267–292.
- Bodge, K. & Kraus, N. (1991), Critical examination of longshore transport rate magnitude.

- Booij, N., Ris, R. C. & Holthuijsen, L. H. (1999), 'A third-generation wave model for coastal regions: 1. model description and validation', *Journal of Geophysical Research: Oceans* **104**(C4), 7649–7666.
- Boudière, E., Maisondieu, C., Arduin, F., Accensi, M., Pineau-Guillou, L. & Lepasqueur, J. (2013), 'A suitable metocean hindcast database for the design of marine energy converters', *International Journal of Marine Energy* **3-4**, e40–e52. Special Issue – Selected Papers - EWTEC2013.
- Bruun, P. (1962), 'Sea-level rise as a cause of shoreline erosion', *J. Waterways and Harbours Division* **88**(1-3), 117–130.
- Cailler, N. (2019), Sea level rise impact on an empirical equilibrium model for beach morphological evolution, Master's thesis, ENSTA Bretagne.
- Callaghan, D., Nielsen, P., AD, S. & Ranasinghe, R. (2008), 'Statistical simulation of wave climate and extreme beach erosion', *Coastal Engineering* **55**, 375–390.
- Camus, P., Mendez, F. J. & Medina, R. (2011), 'A hybrid efficient method to downscale wave climate to coastal areas', *Coastal Engineering* **58**(9), 851–862.
- Castelle, B., Marieu, V., Bujan, S., Ferreira, S., Parisot, J.-P., Capo, S., Sénéchal, N. & Chouzenoux, T. (2014), 'Equilibrium shoreline modelling of a high-energy meso-macrotidal multiple-barred beach', *Marine Geology* **347**, 85–94.
- Chamley, H. (2002), *Geosciences, Environment and Man*, Elsevier.
- Chapell, J. (1974), 'Geology of Coral Terraces, Huon Peninsula, New Guinea: A Study of Quaternary Tectonic Movements and Sea-Level Changes', *GSA Bulletin* **85**(4), 553–570.
- Charniak, E. (1991), 'Bayesian networks without tears', *AI Magazine* **12**(4), 50–63.
- Church, J., Clark, P., Cazenave, A., Gregory, J., Jevrejeva, S., Levermann, A., Merrifield, M., Milne, G., Nerem, R., Nunn, P., Payne, A., Pfeffer, W., Stammer, D. & Unnikrishnan, A. (2013), *Sea Level Change*, Cambridge University Press, Cambridge, United Kingdom and New York, NY, USA, book section 13, p. 1137–1216.
- Cooper, J. A. G. & Pilkey, O. H. (2004), 'Sea-level rise and shoreline retreat: time to abandon the bruun rule', *Global and Planetary Change* **43**(3), 157–171.
- Cowell, P. J., Roy, P. S. & Jones, R. A. (1995), 'Simulation of large-scale coastal change using a morphological behaviour model', *Mar. Geol.* **126**, 45–61.
- Davidson, M., Lewis, R. & Turner, I. (2010), 'Forecasting seasonal to multi-year shoreline change', *Coastal Engineering* **57**(6), 620–629.
- Davidson, M., Splinter, K. & Turner, I. (2013), 'A simple equilibrium model for predicting shoreline change', *Coastal Engineering* **73**, 191–202.

- Davidson, M. & Turner, I. (2009), 'A behavioral template beach profile model for predicting seasonal to interannual shoreline evolution', *Journal of Geophysical Research: Earth Surface* **114**(F1).
- Davies, J. L. (1964), 'A morphogenic approach to world shorelines', *Zeitschrift fur Geomorphologie* **8**, 127–142.
- Dean, R. G. (1977), *Equilibrium beach profiles: US Atlantic and Gulf coasts*, Department of Civil Engineering and College of Marine Studies, University of Delaware.
- Dean, R. G. & Dalrymple, R. (1991), *Water Wave Mechanics for Engineers and Scientists*, World Scientific Publishing.
- De'ath, G. & Fabricius, K. E. (2000), 'Classification and regression trees: A powerful yet simple technique for ecological data analysis', *Ecology* **81**(11), 3178–3192.
- Delft Hydraulics, W. (1994), *UNIBEST, A software suite for the simulation of sediment transport processes and related morphodynamics of beach profiles and coastline evolution*.
- Doria, A., Guza, R. T., O'Reilly, W. C. & Yates, M. L. (2016), 'Observations and modeling of San Diego beaches during El Niño', *Cont. Shelf Res.* **124**, 153–164.
- Durrant T., Greenslade D., H. M. & C., T. (2014), A global wave hindcast focussed on the central and south pacific, Technical report, CAWCR Technical Report No. 070.
- Elgar, S. & Guza, R. T. (1985), 'Observations of bispectra of shoaling surface gravity waves', *Journal of Fluid Mechanics* **161**, 425–448.
- Falqués, A. & Calvete, D. (2005), 'Large-scale dynamics of sandy coastlines: Diffusivity and instability', *Journal of Geophysical Research Atmospheres* **110**.
- French, J., Payo, A., Murray, B., Orford, J., Eliot, M. & Cowell, P. (2016), 'Appropriate complexity for the prediction of coastal and estuarine geomorphic behaviour at decadal to centennial scales', *Geomorphology* **256**, 3 – 16.
- Goldstein, E., Coco, G. & Plant, N. G. (2018), 'A review of machine learning applications to coastal sediment transport and morphodynamics', *EarthArXiv online* p. 43.
- Guilcher, A. (1954), *Morphologie littorale et sous- marine*, Orbis.
- Hallermeier, R. J. (1980), 'A profile zonation for seasonal sand beaches from wave climate', *Coastal Engineering* **4**, 253 – 277.
- Hallermeier, R. J. (1983), 'Sand transport limits in coastal structure design', *Proceedings, Coastal Structures '83, American Society of Civil Engineers* pp. pp. 703–716.
- Hanson, H. (1989), 'Genesis: A generalized shoreline change numerical model', *Journal of Coastal Research* **5**(1), 1–27.

- Hanson, H., Gravens, M. B. & Kraus, N. C. (1988), *Prototype Applications of a Generalized Shoreline Change Numerical Model*, ASCE, pp. 1265–1279.
- Hanson, H. & Kraus, N. C. (1985), 'Seawall constraint in shoreline numerical model', *Journal of Waterway, Port, Coastal, and Ocean Engineering* **111**(6), 1079–1083.
- Harley, M. D., Turner, I. L. & Short, A. D. (2015), 'New insights into embayed beach rotation: The importance of wave exposure and cross-shore processes', *Journal of Geophysical Research: Earth Surface* **120**(8), 1470–1484.
- Harley, M. D., Turner, I. L., Short, A. D. & Ranasinghe, R. (2010), 'Interannual variability and controls of the sydney wave climate', *International Journal of Climatology* **30**(9), 1322–1335.
- Harley, M. D., Turner, I. L., Short, A. D. & Ranasinghe, R. (2011), 'A reevaluation of coastal embayment rotation: The dominance of cross-shore versus alongshore sediment transport processes, collaroy-narrabeen beach, southeast australia', *Journal of Geophysical Research: Earth Surface* **116**(F4).
- Hasselmann, K. (1962), 'On the non-linear energy transfer in a gravity-wave spectrum part 1. general theory', *Journal of Fluid Mechanics* **12**(4), 481–500.
- Hemer, M. A., Church, J. A. & Hunter, J. R. (2010), 'Variability and trends in the directional wave climate of the southern hemisphere', *International Journal of Climatology* **30**(4), 475–491.
- Hemer, M. A., Fan, Y., Mori, N., Semedo, A. W. & Xiaolan, L. (2013), 'Projected changes in wave climate from a multi-model ensemble', *Nature Climate Change* **3**, 471–476.
- Hemer, M. A., Katzfey, J. & Trenham, C. E. (2013), 'Global dynamical projections of surface ocean wave climate for a future high greenhouse gas emission scenario', *Ocean Modelling* **70**, 221–245. Ocean Surface Waves.
- Hesp, P. A. (1989), 'A review of biological and geomorphological processes involved in the initiation and development of incipient foredunes', *Proceedings of the Royal Society of Edinburgh. Section B. Biological Sciences* **96**, 181–201.
- Holland, J. H. et al. (1992), *Adaptation in natural and artificial systems: an introductory analysis with applications to biology, control, and artificial intelligence*, MIT press.
- Horikawa, K. (1988), *Nearshore Dynamics and Coastal Processes*, University of Tokyo Press, Tokyo.
- Hurst, M. D., Barkwith, A., Ellis, M. A., Thomas, C. W. & Murray, A. B. (2015), 'Exploring the sensitivities of crenulate bay shorelines to wave climates using a new vector-based one-line model', *Journal of Geophysical Research: Earth Surface* **120**(12), 2586–2608.

- IPCC (2014), *Climate Change 2014: Synthesis Report. Contribution of Working Groups I, II and III to the Fifth Assessment Report of the Intergovernmental Panel on Climate Change*, Technical report, IPCC, Geneva, Switzerland.
- Jara, M., González, M. & Medina, R. (2015), 'Shoreline evolution model from a dynamic equilibrium beach profile', *Coastal Engineering* **99**.
- Jaramillo, C., González, M., Medina, R. & Turki, I. (2021), 'An equilibrium-based shoreline rotation model', *Coastal Engineering* **163**, 103789.
- Jaramillo, C., Jara, M.-S., González, M. & Medina, R. (2019), 'A shoreline evolution model considering the temporal variability of the beach profile sediment volume (sediment gain / loss)', *Coastal Engineering* **156**, 103612.
- Kaergaard, K. & Fredsoe, J. (2013), 'Numerical modeling of shoreline undulations part 2: Varying wave climate and comparison with observations', *Coastal Engineering* **75**, 77–90.
- Kamphuis, J. W. (1991), 'Alongshore sediment transport rate', *Journal of Waterway, Port, Coastal, and Ocean Engineering* **117**(6), 624–640.
- Kamphuis, J. W. (2000), *Introduction to Coastal Engineering and Management*, 1st edn, World Scientific.
- Keijsers, J., De Groot, A. & Riksen, M. (2015), 'Vegetation and sedimentation on coastal foredunes', *Geomorphology* **228**, 723–734.
- Kirkpatrick, S., Gelatt, C. & Vecchi, M. (1983), 'Optimization by simulated annealing', *Science (New York, N.Y.)* **220**, 671–80.
- Komar, P. D. & Inman, D. L. (1970), 'Longshore sand transport on beaches', *J. Geophys. Res.* **75**, 5914–5927.
- Koza, J. R. & Koza, J. R. (1992), *Genetic programming: on the programming of computers by means of natural selection*, Vol. 1, MIT press.
- Kraus, N. C. (2001), *On Equilibrium Properties in Predictive Modeling of Coastal Morphology Change*, ASCE, pp. 1–15.
- Kriebel, D. L. & Dean, R. G. (1993), 'Convolution method for time-dependent beach profile response', *J. Waterw. Port Coastal Ocean Eng.* **119**, 204–226.
- Larson, M., Hoan, L. & Hanson, H. (2010), 'Direct formula to compute wave height and angle at incipient breaking', *Journal of Waterway Port Coastal and Ocean Engineering* **136**.
- Laugel, A. (2013), *Climatologie des états de mer en Atlantique nord-est : analyse du climat actuel et des évolutions futures sous scénarios de changement climatique par descente d'échelle dynamique et statistique*, Theses, Université Paris-Est.

- Le Cozannet, G., Garcin, M., Yates, M., Idier, D. & Meyssignac, B. (2014), 'Approaches to evaluate the recent impacts of sea-level rise on shoreline changes', *Earth Science Reviews* **138**, 47–60.
- LeCun, Y., Bengio, Y. & Hinton, G. (2015), 'Deep learning', *Nature* **521**.
- Lemos, C., Floc'h, F., Yates, M. L., Le Dantec, N., Marieu, V., Hamon, K., Cuq, V., Suanez, S. & Delacourt, C. (2018), 'Equilibrium modeling of the beach profile on a macrotidal embayed Low Tide Terrace beach', *Ocean Dynamics*.
- Limber, P. W., Adams, P. N. & Murray, A. B. (2017), 'Modeling large-scale shoreline change caused by complex bathymetry in low-angle wave climates', *Marine Geology* **383**(C), 55–64.
- Long, J. W. & Plant, N. G. (2012), 'Extended Kalman Filter framework for forecasting shoreline evolution', *Geophysical Research Letters* **39**(13).
- Luijendijk, A., Hagenaars, G., Ranasinghe, R., Baart, F., Donchyts, G. & Aarninkhof, S. (2018), 'The state of the world's beaches', *Scientific Reports* **8**.
- Masselink, G., Castelle, B., Scott, T., Dodet, G., Suanez, S., Jackson, D. & Floc'h, F. (2016), 'Extreme wave activity during 2013/2014 winter and morphological impacts along the Atlantic coast of Europe', *Geophysical Research Letters* **43**(5), 2135–2143.
- Masselink, G. & Short, A. D. (1993), 'The effect of tide range on beach morphodynamics and morphology: a conceptual beach model', *Journal of Coastal Research* pp. 785–800.
- Miller, J. K. & Dean, R. G. (2004), 'A simple new shoreline change model', *Coastal Engineering* **51**(7), 531–556.
- Montaño, J., Coco, G., Antolínez, J. A. A., Beuzen, T., Bryan, K. R., Cagigal, L., Castelle, B., Davidson, M. A., Goldstein, E. B., Ibaceta, R., Idier, D., Ludka, B. C., Masoud-Ansari, S., Méndez, F. J., Murray, A. B., Plant, N. G., Ratliff, K. M., Robinet, A., Rueda, A., Sénéchal, N., Simmons, J. A., Splinter, K. D., Stephens, S., Townend, I., Vitousek, S. & Vos, K. (2020), 'Blind testing of shoreline evolution models', *Scientific Reports* **10**.
- Mori, N., Yasuda, T., Mase, H., Tom, T. & Oku, Y. (2010), 'Projection of extreme wave climate change under global warming', *Hydrological Research Letters* **4**, 15–19.
- Murray, A. B. (2007), 'Reducing model complexity for explanation and prediction', *Geomorphology* **90**(3), 178 – 191. Reduced-Complexity Geomorphological Modelling for River and Catchment Management.
- Neumann, B., Vafeidis, A. T., Zimmermann, J. & Nicholls, R. J. (2015), 'Future coastal population growth and exposure to sea-level rise and coastal flooding - a global assessment', *PLOS ONE* **10**(3), 1–34.

- Oppenheimer, M., Glavovic, B., Hinkel, J., van de Wal, R., Magnan, A., Abd-Elgawad, A., Cai, R., Cifuentes-Jara, M., DeConto, R., Ghosh, T., Hay, J., Isla, F., Marzeion, B., Meyssignac, B. & Sebesvari, Z. (2019), *IPCC Special Report on the Ocean and Cryosphere in a Changing Climate*, In press, chapter Sea Level Rise and Implications for Low-Lying Islands, Coasts and Communities, pp. 321–446.
- Ozasa, H. & Brampton, A. (1980), 'Mathematical modelling of beaches backed by seawalls', *Coastal Engineering* **4**, 47–63.
- Pelnard-Considère, R. (1956), 'Essai de théorie de l'évolution des formes de rivages en plages de sable et de galets', *La Houille Blanche* pp. 289–301.
- Peltier, W. R. (1998), 'Postglacial variations in the level of the sea: Implications for climate dynamics and solid-earth geophysics', *Reviews of Geophysics* **36**(4), 603–689.
- Pilkey, O. & Cooper, A. (2002), 'Longshore transport volumes: A critical view', *Journal of Coastal Research* **36**, 572–580.
- Ranasinghe, R. (2020), 'On the need for a new generation of coastal change models for the 21 century', *Scientific Reports* **10**.
- Ranasinghe R., Callaghan D., R. D. (2013), 'Does a more sophisticated storm erosion model improve probabilistic erosion estimates?', *Coastal Dynamic* .
- Ranasinghe, R., Callaghan, D. & Stive, M. J. F. (2012), 'Estimating coastal recession due to sea level rise: beyond the Bruun rule', *Climatic Change* **110**(3), 561–574.
- Ranasinghe, R., McLoughlin, R., Short, A. & Symonds, G. (2004), 'The southern oscillation index, wave climate, and beach rotation', *Marine Geology* **204**, 273–287.
- Robinet, A., Castelle, B., Idier, D., Harley, M. & Splinter, K. (2020), 'Controls of local geology and cross-shore/longshore processes on embayed beach shoreline variability', *Marine Geology* **422**, 106118.
- Robinet, A., Idier, D., Castelle, B. & Marieu, V. (2018), 'A reduced-complexity shoreline change model combining longshore and cross-shore processes: The lx-shore model', *Environmental Modelling & Software* **109**, 1 – 16.
- Roelvink, D., Reniers, A., van Dongeren, A., van Thiel de Vries, J., McCall, R. & Lescinski, J. (2009), 'Modelling storm impacts on beaches, dunes and barrier islands', *Coastal Engineering* **56**(11), 1133 – 1152.
- Roelvink, J. & Banning, G. (1995), 'Design and development of delft3d and application to coastal morphodynamics', *Oceanographic Literature Review* **11**, 925.
- Schoonees, J. & Theron, A. (1993), 'Review of the field-data base for longshore sediment transport', *Coastal Engineering* **19**, 1–25.

- Schoonees, J. & Theron, A. (1996), 'Improvement of the most accurate longshore transport formula', *25th International Conference on Coastal Engineering* **3**, 3652–3665.
- Short, A. (2007), *Beaches of the New South Wales Coast (2nd Edition)*, Sydney Univ. Press, Sydney, Australia.
- Simon, B. (2007), *Coastal tide*, Institut Oceanographique.
- Sobol, I. (2001), 'Global sensitivity indices for nonlinear mathematical models and their monte carlo estimates', *Mathematics and Computers in Simulation* **55**(1), 271–280. The Second IMACS Seminar on Monte Carlo Methods.
- Splinter, K. D., Turner, I. L., Davidson, M. A., Barnard, P., Castelle, B. & Oltman-Shay, J. (2014), 'A generalized equilibrium model for predicting daily to interannual shoreline response', *Journal of Geophysical Research: Earth Surface* **119**(9), 1936–1958.
- Stépanian, A. (2002), Evolution morphodynamique d'une plage macrotidale à barres : Omaha beach (Normandie), Theses, Université de Caen/Basse-Normandie.
- Suanez, S., Cancouët, R., Floc'h, F., Blaise, E., Arduin, F., Filipot, J.-F., Cariolet, J.-M. & Delacourt, C. (2015), 'Observations and predictions of wave runup, extreme water levels, and medium-term dune erosion during storm conditions', *Journal of Marine Science and Engineering* **3**(3), 674–698.
- Suanez, S., Cariolet, J.-M., Cancouët, R., Arduin, F. & Delacourt, C. (2012), 'Dune recovery after storm erosion on a high-energy beach: Vougot beach, brittany (france)', *Geomorphology* **139-140**, 16–33.
- Suanez, S., Cariolet, J.-M. & Fichaut, B. (2010), 'Monitoring of recent morphological changes of the dune of Vougot beach (Brittany, France) using differential GPS', *Shore and beach* **78**(1), 37–47.
- Suanez, S., Fichaut, B. & Sparfel, L. (2007), 'Assessment method of low coastal flooding hazard applied to vougot beach, guisseny (brittany)', *Geomorphologie-relief processus environnement* **4**, 319–334.
- Sutherland, J., Walstra, D., Chesher, T., van Rijn, L. & Southgate, H. (2004), 'Evaluation of coastal area modelling systems at an estuary mouth', *Coastal Engineering* **51**(2), 119 – 142.
- Tolman, H. (2009), 'User manual and system documentation of wavewatch iii version 3.14', *Analysis* **166**.
- Tran, Y. H. & Barthélemy, E. (2020), 'Combined longshore and cross-shore shoreline model for closed embayed beaches', *Coastal Engineering* **158**, 103692.
- Turki, I., Medina, R., Coco, G. & González, M. (2013), 'An equilibrium model to predict shoreline rotation of pocket beaches', *Marine Geology* **346**, 220–232.

- Turner, I., Harley, M., Short, A., Simmons, J., Bracs, M., Phillips, M. & Splinter, K. (2016), 'A multi-decade dataset of monthly beach profile surveys and inshore wave forcing at narrabeen, australia', *Scientific data* **3**.
- USACE (1984), Shore Protection Manual, Technical report, U.S. Army Corps of Engineers, Vicksburg, Mississippi.
- Valentini, E., Taramelli, A., Cappucci, S., Filippini, F. & Nguyen, X. A. (2020), 'Exploring the dunes: The correlations between vegetation cover pattern and morphology for sediment retention assessment using airborne multisensor acquisition.', *Remote Sensing* **12**.
- Van Den Berg, N., Falqués, A. & Ribas, F. (2011), 'Long-term evolution of nourished beaches under high angle wave conditions', *Journal of Marine Systems* **88**(1), 102–112.
- van Rijn, L. (1998), *Principles of coastal morphology*, Aqua Publications.
- van Rijn, L., Walstra, D., Grasmeijer, B., Sutherland, J., Pan, S. & Sierra, J. (2003), 'The predictability of cross-shore bed evolution of sandy beaches at the time scale of storms and seasons using process-based profile models', *Coastal Engineering* **47**(3), 295 – 327.
- Vitousek, S. & Barnard, P. L. (2015), *A nonlinear, implicit one-line model to predict long-term shoreline change*.
- Vitousek, S., Barnard, P. L., Limber, P., Erikson, L. & Cole, B. (2017), 'A model integrating longshore and cross-shore processes for predicting long-term shoreline response to climate change', *Journal of Geophysical Research: Earth Surface* **122**(4), 782–806.
- Wang, P., Kraus, N. C. & Davis Jr, R. A. (1998), 'Total longshore sediment transport rate in the surf zone: field measurements and empirical predictions', *Journal of Coastal research* pp. 269–282.
- Warren, I. & Bach, H. (1992), 'Mike 21: a modelling system for estuaries, coastal waters and seas', *Environmental Software* **7**(4), 229–240. 3rd International Software Exhibition for Environmental Science and Engineering.
- Warrick, J. A. & Mertes, L. A. (2009), 'Sediment yield from the tectonically active semiarid Western Transverse Ranges of California', *GSA Bulletin* **121**(7-8), 1054–1070.
- Wright, L. D., Kim, C. S., Hardaway, C. S., Kimball, S. M. & Green, M. O. (1987), Shoreface and beach dynamics of the coastal region from cape henry to false cape, virginia., Technical report, Virginia Institute of Marine Science.
- Wright, L. D. & Short, A. D. (1984), 'Morphodynamic variability of surf zones and beaches: A synthesis', *Mar. Geol.* **56**, 93–118.
- Yates, M. (2009), Seasonal Sand Level Changes on Southern California Beaches, PhD thesis, University of California, San Diego.

- Yates, M. L., Guza, R. T. & O'Reilly, W. C. (2009), 'Equilibrium shoreline response: Observations and modeling', *J. Geophys. Res.* **114**(C09014).
- Yates, M. L., Guza, R. T., O'Reilly, W. C., Hansen, J. E. & Barnard, P. L. (2011), 'Equilibrium shoreline response of a high wave energy beach', *J. Geophys. Res.* **116**(C04014).
- Zijlema, M., Stelling, G. S. & Smit, P. (2011), 'SWASH: An operational public domain code for simulating wave fields and rapidly varied flows in coastal waters', *Coast. Eng.* **58**, 992–1012.
- Černý, V. (1985), 'Thermodynamical approach to the traveling salesman problem: An efficient simulation algorithm', *Journal of Optimization Theory and Applications* **45**, 41–51.